Development of a high-throughput small-scale methodology for intensified cell culture processes

A thesis submitted for the degree of Doctor of Engineering to the University College London

by

Marie Dorn

University College London

Department of Biochemical Engineering

2025

I, Marie Dorn, confirm that the work presented in this thesis is my own. Where information has been derived from other sources, I confirm that this has been indicated in the thesis.

Signed: Date:

To my lovely Omi, who taught me to always be observant and curious!

Acknowledgements

It's almost to the day that I write these words that I received and accepted the offer for this EngD. Four years later, I find myself trying to properly express my gratitude—though I doubt any words could truly capture the depth of it.

First and foremost, I want to thank my UCL supervisors, Prof. Martina Micheletti and Dr. Duygu Dikicioglu. Martina, thank you so much for giving me a chance. Your guidance and support over these four years have meant the world to me. You've been the best supervisor I could have asked for, and I hope I've lived up to whatever it was you saw in me back then. Duygu, although the project took a slightly different direction than originally planned, I'm truly grateful for your open ear, fresh perspective, and sanity checks whenever I needed them.

This research was funded by the Engineering and Physical Sciences Research Council (EPSRC), whose support I deeply appreciate in making this project a reality. I'd also like to thank the UCL–AstraZeneca Centre of Excellence for their funding and collaboration, as well as their insight and support throughout the years. Special thanks to Kerensa Klottrup-Rees and Ken Lee as my industrial supervisors, to Christine Ferng for her additional supervision and scientific input, and to Diane Hatton for always reviewing my (many) PSO submissions for papers and this thesis.

A huge thank you to the Mixing Group—especially Andrea, Artemis, Gergana, and Jordan—for welcoming me with open arms and always having my back. To Delphine, for the many lab hours spent and the conference memories we made. To Felipe, Laia, and Cristina—for the seemingly endless weekends in the lab. To Matty—for always smiling during my CoE annual meeting presentations. To my friends back home—Sarah, Anni, Caro, Rosalie, and many more—for accepting my strange working hours and bearing with me as I talked endlessly about work instead of anything else.

To Ivano—I'm not always great at expressing myself, but I'll try to put into words just how much your support means to me. Thank you for seeing me, believing in me, and pushing me to be the best version of myself. Thank you for reminding me not to let a bad day affect my work, and to keep the standards high so all the hard work pays off. Thank you for never questioning all my

weekend work (I know you've been through it too), and for showing me that even when things get tough, I'm not alone. Thank you for being by my side!

And lastly, to my family—too many to name individually—thank you, and I'm sorry for all the little occasions I missed along the way. Mami, Papi, Omi, Felix, and Brita—I owe you the world and can never repay all that you've given me. Without your unwavering support, I would never have made it this far. Without your trust and faith in me, I doubt I would have had the courage to spontaneously move countries, pursue such a challenging path, and do so in a city and at an institution I had never even imagined myself in. Thank you for always having my back. Ich hab Euch lieb! – Marie

"Nothing in life is to be feared; it is only to be understood

Now is the time to understand more,

so we may fear less."

~Marie Curie

Abstract

This thesis describes the development and characterisation of a high-throughput and scalable scale-down model capable of mimicking key features of CHO perfusion processes. While well plates-based methodologies are well established for fed-batch operations and have been explored for perfusion-mimicking modes, a comprehensive understanding of their limitations and capabilities is still sought after - particularly in the context of early-stage process development (i.e. cell clone screening protocols). This work focuses on evaluating the ability of well plates to replicate perfusion-like conditions, with an emphasis on achieving and maintaining a stable culture environment.

The 24-well microwell plate (MWP) platform (V_W = 1.2 mL) was characterised for operation in semi-perfusion mode, using daily medium exchange and centrifugation-based cell retention. The approach enabled the cultivation of high-density cultures (up to 70×10^6 cells mL^{-1}) and supported "quasi steady-state" operation through implementing a cell bleed step.

The methodology was applied in a user case for cell clone screening. Two panels of antibody-producing CHO cell lines (comprising 14 clones) were evaluated under both fed-batch and semi-perfusion conditions in the MWP format. Clone performance was assessed in terms of growth, metabolism, and productivity, and two ranking strategies were compared: (i) a conventional single-parameter method based on cell-specific productivity, and (ii) a multi-parameter approach using a manufacturability index. Clone performance and ranking were shown to be influenced by operational mode and perfusion strategy, and the multi-parameter ranking yielded more robust results. The reproducibility of the results was confirmed by showing comparability in cell growth performance and ranking across two different cultivations runs.

Finally, the semi-perfusion methodology was miniaturised to a 96-well deepwell plate (V_W = 200 – 300 µL), commonly used in industry, confirming the method's transferability and the scalability to smaller volumes.

This work establishes a novel and versatile platform that enhances early-stage perfusion process development and accelerates reliable high-throughput clone screening for industrial bioprocessing.

Impact statement

This thesis contributes to the advancement of intensified and continuous bioprocess development through the evaluation of a scalable, high-throughput small-scale methodology based on well plate format. As the biopharmaceutical industry shifts toward continuous manufacturing to improve efficiency, enhance robustness and embed sustainability, the need for predictive, resource-efficient tools for early-stage process development becomes increasingly important. Traditional screening platforms such as shake flasks and spin tubes offer limited throughput, which can hinder the identification of optimal cell lines and process conditions.

To address this challenge, the work investigates the use of 24-well microwell plates (MWPs) operated in semi-perfusion mode, incorporating both total and partial media exchange strategies adopting a cell-specific perfusion rate (CSPR)-based approach. The methodology enables the cultivation of CHO cell cultures at "quasi steady-state" conditions in ultra-low working volumes (1.2 mL), providing a cost-effective and high-throughput platform for evaluating multiple perfusion strategies. The results obtained show consistent growth and productivity across a range of conditions, demonstrating its robustness and suitability for early-stage screening.

To validate scalability, the method was adapted to a 30 mL 6-well deepwell plate (DWP) format. This configuration mimics shake flask performance while offering automation compatibility and reduced material consumption. The DWP format serves as a bridge between high-throughput screening and larger-scale process development, supporting efficient and sustainable scale translation.

To demonstrate a practical application, the MWP methodology was applied to a CHO cell clone screening study, investigating how operational mode and perfusion rate strategies influence clone performance and ranking outcomes. The results reveal that clone behaviour under semi-perfusion conditions can differ significantly from that observed in traditional fed-batch processes, which remain the standard for early-stage screening. This discrepancy highlights the limitations of conventional selection methods as they may not reliably predict performance in continuous or intensified manufacturing environments. By comparing single-parameter and multi-parameter ranking approaches, the research demonstrates that incorporating a broader dataset yields more

robust and predictive clone selection outcomes. These findings highlight the importance of process-relevant screening strategies for aligning early development with the requirements of next-generation manufacturing.

In addition to the 24-well MWP and 6-well DWP formats, the methodology was further scaled down to 96-well DWP to assess its applicability to even higher-throughput settings. Key performance trends in cell growth, viability, and productivity were preserved, confirming the platform's adaptability to smaller scales. This miniaturisation enhances screening capacity while conserving reagents and materials, making it particularly useful for early-phase media optimisation and clone selection. Its compatibility with standard automated liquid handling systems further supports scalability, reproducibility, and integration into automated workflows, reinforcing the platform's value as a flexible tool for intensified bioprocess development.

Overall, this thesis establishes a scalable, automatable, and resource-efficient platform for high-throughput semi-perfusion screening. The combined use of microwell and deepwell plate formats supports both detailed parameter exploration and scalable process confirmation. The findings have direct implications for upstream bioprocess development and clone selection, contributing to more predictive, efficient, and sustainable workflows that are aligned with the future of continuous biomanufacturing in the biopharmaceutical industry.

Scientific Output

The research conducted in this thesis has resulted in multiple publications in peer-reviewed academic journals and has been presented at several international conferences through oral and poster presentations. A list of these scientific contributions is provided below.

Journal articles:

- Dorn, M., Ferng, C., Klottrup-Rees, K., Lee, K., & Micheletti, M. Working title: Miniaturization of established 24-well MWP-based semi-perfusion method to 96-well DWP for CHO cell culture. *In progress*.
- Dorn, M., Ferng, C., Klottrup-Rees, K., Lee, K., & Micheletti, M. Working Title: Improved Clone Selection Through Manufacturability Index in Scalable Small-Scale Screening Platforms. *In progress*.
- Dorn, M., Ferng, C., Klottrup-Rees, K., Lee, K., & Micheletti, M. Working title: High-throughput semi-perfusion screening of CHO clones using automated shaken deepwell plates. *In progress*.
- Dorn, M., Ferng, C., Klottrup-Rees, K., Lee, K., & Micheletti, M. (2025). Cell clone selection—Impact of operation modes and medium exchange strategies on clone ranking. Frontiers in Bioengineering and Biotechnology, 12. https://doi.org/10.3389/fbioe.2024.1479633
- Dorn, M., Lucas, C., Klottrup-Rees, K., Lee, K., & Micheletti, M. (2024). Platform development for high-throughput optimization of perfusion processes—Part II: Variation of perfusion rate strategies in microwell plates. Biotechnology and Bioengineering. https://doi.org/10.1002/bit.28685
- Dorn, M., Klottrup-Rees, K., Lee, K., & Micheletti, M. (2024). Platform development for high-throughput optimization of perfusion processes: Part I: Implementation of cell bleeds in microwell plates. Biotechnology and Bioengineering. https://doi.org/10.1002/bit.28682

Conferences contributions:

- Dorn, M., Ferng, C.; Klottrup-Rees, K., Lee, K., & Micheletti, M. (2025). Accelerating Cell Clone Selection with High-Throughput Screening for Perfusion Bioprocess Optimization. Talk presented at 7th HTPD meeting, Uppsala (Sweden)
- Dorn, M., Ferng, C.; Klottrup-Rees, K., Lee, K., & Micheletti, M. (2025). Transforming Bioprocess Development: Sustainable, Resource-efficient Perfusion Screening with Single-use Microwell plates. Poster presented at Single-Use Technology Conference VII, St. Julians (Malta)
- Dorn, M., Klottrup-Rees, K., Lee, K., & Micheletti, M. (2024). Early manufacturing insights and clone selection for perfusion process. Poster presented at Integrated Continuous Biomanufacturing VI, Leesburg, Virginia (US)
- Dorn, M., Klottrup-Rees, K., Lee, K., Micheletti, M. (2023). Ultra scale-down models in semi-perfusion: Exploration of cell bleeds and medium exchange regimes as tools for cell clone screening. Talk presented at ESACT Frontiers 2023, Brussels (Belgium)
- Dorn, M., Micheletti, M., Klottrup-Rees, K., Lee, K., (2023). Ultra scale-down models in semi-perfusion with cell bleeds and different medium exchange regimes. Poster presented at the 14th European Congress of Chemical Engineering and 7th European Congress of Applied Biotechnology, Berlin (Germany)
- Dorn, M., Klottrup-Rees, K., Lee, K., Micheletti, M. (2023). Ultra scale-down models in semi-perfusion with different medium exchange regimes. Poster presented at ESACT-UK 2023, Nottingham, (UK)
- Dorn, M., Klottrup-Rees, K., Lee, K., Micheletti, M., et al (2022). Exploring different medium exchange regimes in ultra scale-down models. Talk presented at Integrated Continuous Biomanufacturing V, Sitges (Spain).
- Dorn, M., Klottrup-Rees, K., Lee, K., Micheletti, M. (2022). Development of high throughput microscale methodologies for optimisation of perfusion processes. Poster presented at ChemEngDayUK 2022, London (UK)

The following awards were also received:

- Best Poster Prize at Integrated Continuous Biomanufacturing VI Conference, Oct 2024
- Poster Prize for the Best Technical Poster at Single Use Technology VII Conference, Mar 2025
- ACTIP Fellowship Award Sep 2025

Tables of Content

List of Tables

List of Figures

Nomenclature

Abbreviations

Amm	Ammonium
ATF	Alternating tangential flow filtration
B	Bleed rate
BHK	Baby hamster kidney cells
BR	Bioreactor
BSC	Biosafety cabinet
BSPR	Biomass specific perfusion rate
CCD	Conventional cell density
CD CHO	Chemically defines CHO media
CHO	Chinese Hamster Ovary cells
CLD	Cell line development
CM	Continuous manufacturing
CO_2	Carbon dioxide
CoE	Centre of Excellence
CRD	Cell retention device
CSPR	Cell specific perfusion rate
$CSPR_{min}$	Minimum cell specific perfusion rate
DFHR	Dihydrofolate reductase
DMSO	Dimethyl sulfoxide
DNA	Deoxyribonucleic acid
DO	Dissolved oxygen
DWP	Deepwell plate
ELISA	Enzyme-Linked Immunosorbent Assay
EMA	European Medicine Agency
FB	Fed-batch
FDA	Food and Drug Administration
g	Gravitational constant
Gln	Glutamine
Glu	Glutamate
Gluc	Glucose
H	Harvest rate
HCD	High cell density
HEK	Humen embryonic kidney cells
HILVOP	High intensity, low-volume perfusion
HIP	High intensity perfusion media
HPLC	High Performance Liquid Chromatography
HT	High throughput
HTPD	High throughput process development

ICB	Integrates continuous biomanufacturing
IVCC	Integrated viable cell concentration
LAC	Lactate
LN_2	Liquid nitrogen
MCB	Master cell bank
MG	Maximum growth
MI_{CL}	Manufacturability index
MSX	methionine sulfoximine
MTX	methotrexate
MWP	Microwell plate
Na_2HPO^4	disodium hydrogen phosphate
$NaH_2PO_4{\cdot}H_2O$	monosodium phosphate monohydrate
NS0, Sp2/0	Mouse myeloma cell lines
O2	Oxygen
OD	Orbital diameter
P	Perfusion rate
PAT	Process analytical technology
PBS	Phosphate Buffered Saline
q	Cell specific rate
q_P	Cell specific productivity
R&D	research and development
RPM	Revolutions per minute
RV	Reactor volume
SDM	Scale-down model
SF	Shake flask
SG	Stable growth
SP	Semi-perfusion
ST	Spin tube
STR	Stirred tank reactor
STY	Space-time-yield
SU	Single use
SUT	Single use technology
t	Time
TAFE	Targeted feeding
TCC	Total cell concentration
TFF	tangential flow filtration
tPA	Tissue plasminogen activator
UCL	University college London
VCC	Viable cell concentration
VP	Volumetric productivity
VVD	Vessel volume per day
Vw	Working volume
WCB	Working cell bank
Y	Yield

Chapter 1: Introduction

1.1 Context of the research

A new era for the biopharmaceutical industry began in 1982 with the approval of Humulin®, the first recombinant human insulin product. This milestone marked the regulatory acceptance of recombinant DNA (rDNA) technology for the production of biotherapeutics. While Humulin® was produced using the microorganism Escherichia coli (E. coli), subsequent commercialisation of therapeutic proteins and monoclonal antibodies (mAbs) increasingly relied on mammalian cell lines. That same year, the first recombinant protein product, tissue plasminogen activator (tPA), was approved and manufactured using Chinese Hamster Ovary (CHO) cells. This was followed in 1986 by the approval of the first monoclonal antibody, muromonab-CD3 (marketed as Orthoclone OKT3 by Janssen Cilag), produced in hybridoma cells.

Biopharmaceuticals are pharmaceutical drug products manufactured by biological organisms (i.e. bacteria, yeast or mammalian cells) using rDNA technology and cover a range of different products such as biomolecules (e.g. antibiotics), recombinant therapeutic proteins (e.g. mAbs), virus-based biopharmaceuticals (e.g. viral vectors, vaccines) and cell and gene therapies (Szkodny & Lee, 2022; Tripathi & Shrivastava, 2019; Zhang et al., 2017) to name a few. Biopharmaceuticals offer unique mechanisms of action and increased potency compared to small-molecule drugs, making them valuable tools for treating a variety of immunopathological diseases like cancer and autoimmune disorders. MAbs in particular have experienced a rapid growth as treatment due to their high affinity and specificity target binding. Despite new modalities gaining momentum, mAbs remain the dominant product class with a global market value of $401.5 billion in 2024 and are estimated to reach $609 billion by 2032 (Mordor, 2024; Szkodny & Lee, 2022; Walsh, 2018; Walsh & Walsh, 2022). Since 2014, 50% of all biopharmaceutical approvals were mAbs and as of October 2023 over 1100 antibody products, primarily for oncological application, are being investigated in clinical trials (Crescioli et al., 2024; Walsh & Walsh, 2022).

Different host cell systems are established to produce biopharmaceuticals among other bacteria, yeast, insect and mammalian cells. While bacterial systems were used to produce many early

biopharmaceuticals, they lack the ability to produce products with human-like post translational modifications (i.e. glycan patterns). However, post translational modifications are essential for the quality of the product and impact the serum half-life, efficacy and antigenicity of the recombinant protein. Yeast, insect and mammalian cells were engineered to safely and effectively produce biopharmaceuticals with human-like glycan patterns at high quantities. To date, mammalian cell lines are the production system of choice and are the dominating system of all approved recombinant protein products (Crescioli et al., 2024; Walsh & Walsh, 2022). Several cell lines are commercially used for the production of biopharmaceuticals. The majority (70 - 80%) of recombinant proteins on the market are produced in suspension CHO cell lines (Tripathi & Shrivastava, 2019; Wurm, 2004). However other cell lines were also approved for production of recombinant proteins such as mouse-myeloma derived NS0 and Sp2/0 cells, baby hamster kidney cells (BHK), and human embryonic kidney cells (HEK293). The latter is also widely used to produce virus-based biopharmaceuticals (e.g. viral vectors) (Malm et al., 2020; Tripathi & Shrivastava, 2019).

So far biomanufacturing has predominantly focused on conservative approaches like batch processing. The stringent quality and regulatory standards, combined with the need for rapid development and cost control, have heavily influenced industry practices. While economic benefits and process innovations have been realised, they have primarily been driven by product development rather than significant advancements in process engineering (Drobnjakovic et al., 2023; Warikoo et al., 2012). The biopharmaceutical industry is facing challenges maximizing the production throughput to cover the increasing demand for biopharmaceuticals, while reducing the high costs associated with the research and development (R&D) as well as manufacturing (Farid et al., 2020). Growing competition (e.g., expiring patents, biosimilars) and limitations in manufacturing capacity, as well as requirements for product quality, ensuring product safety and maintaining high product quality add to the list of challenges. Hence, more flexible, cost and time-efficient next-generation manufacturing platforms are required (Bielser et al., 2018; Mahal et al., 2021; Narayanan et al., 2022). To tackle these challenges, the biopharmaceutical industry, supported by regulatory agencies, is shifting towards continuous manufacturing (CM) with the long-term goal for end-to-end integrated continuous biomanufacturing (ICB). While a typical CM process comprises a continuously operated perfusion bioreactor followed by purification units operated in batch mode, the ICB process is characterised by an uninterrupted flow from upstream to downstream by eliminating intermediate hold steps in the downstream stage. CM and ICB processes offer various advantages such as increased yields and volumetric productivities as well as reduced facility sizes and production costs. However, so far CM processes have been applied solely to labile biopharmaceuticals (e.g. blood coagulation factors, fragile therapeutic proteins and

enzymes) and ICB processes remain in early stages of development with limited studies available at larger scales (Arnold et al., 2019; Drobnjakovic et al., 2023; Wong et al., 2021).

While continuous manufacturing processes have been shown to reduce overall production costs, their total R&D expenses remain significant, with approximately 17% allocated to clinical manufacturing and process development (Farid et al., 2020). When evaluating new technology platforms, it is essential to consider the potential reduction in manufacturing costs in conjunction with the associated impact on process development (Mahal et al., 2021). Consequently, the biopharmaceutical industry is increasingly adopting scale-down models (SDMs) and high-throughput (HT) approaches for screening experiments to streamline process development and optimisation. Utilising SDM allows to achieve process understanding of a multi-dimensional design space and an in-depth characterisation of process parameters. HT systems, such as multi-well plates and mini-bioreactors, are well established in industry for batch and fed-batch processes. However, complementary systems for the more complex perfusion process mode, which involves additional parameters (i.e. perfusion flow rates), remain limited. This adds to the critical bottleneck, that are the lengthy timelines of both product and process development timeline, contributing to overall development cycles of 10 to 15 year (Mahal et al., 2021; Singh et al., 2023). In addition to the parameter screening, SDMs are widely used in media development and for cell clone selection. Given the large number of cell clones requiring screening, small-scale methods are essential for maintaining cost efficiency and timeliness.

Due to the lack of robust perfusion-mimicking SDMs, cell clone screenings are still predominantly conducted in fed-batch mode. This may lead to the selection of clones optimised for fed-batch conditions but suboptimal for perfusion processes, as the transition between these modes exposes cells to markedly different environments. For instance, perfusion processes maintain a relatively stable culture environment with minimal fluctuations in nutrient and metabolite concentrations, whereas fed-batch systems are characterised by dynamic shifts that can result in variable cellular responses. These metabolic differences are only one aspect of the divergence between fed-batch and perfusion systems. Engineering parameters—such as cell density, oxygen transfer requirements, and mixing intensity—also differ significantly, with perfusion typically requiring higher turbulence and tighter environmental control to sustain high cell densities. As a result, developing a robust, reproducible, and scalable screening method tailored to perfusion processes is a critical element of upstream process development. Such methods should enable the identification of cell lines capable of achieving stable growth at high cell densities, high productivity, and consistent, controllable product quality. Moreover, the screening approach should be broadly applicable, supporting the evaluation of cell lines expressing a wide range of

heterologous proteins. A comprehensive understanding of cellular performance under perfusion-relevant conditions is therefore essential.

The motivation for this work stems from the need for suitable perfusion mimicking SDMs that can be automated and used during the critical step of cell clone screening. To this end, scientific knowledge and methods previously developed for optimisation of perfusion processes are leveraged and expanded to smaller scales with the aim to perform a systematic characterisation of well-plate-based SDM. The acquired knowledge on cellular, metabolic and production performance of a standard CHO cell line provides insights for the assessment of a cell clone screening and is the baseline to build a robust framework for perfusion specific clone screening method.

In the subsequent section, a comprehensive literature review is conducted, examining previous research on biomanufacturing in mammalian cells, process intensification, and scale-down models for process development. Based on this review, the projects aim, and objectives are articulated along with a detailed thesis outline in **Sections 1.4** and **1.5**.

1.2 Literature survey

The following literature review explores the historical development and contemporary trends in upstream bioprocessing, focusing on mammalian cell culture. It examines the evolution of cell culture operations, the recent advancements in continuous biomanufacturing and perfusion cell culture and the development of scale-down models and small-scale methods. Further, the review critically assesses the industrial applicability and limitations of these small-scale methods and scale-down models.

1.2.1 Mammalian cell lines for therapeutic protein production

Biopharmaceuticals designated for human use are predominantly produced in mammalian cell culture. The largest group of new products gaining regulatory approval are therapeutic proteins such as recombinant proteins, peptides and mAbs. For the manufacture of these, mammalian host systems are often preferred because they possess the ability to properly fold, assemble, and modify the produced proteins (i.e. post-translational modifications).

Depending on the process specification and the product of interest, the cell culture can either be anchorage-dependent (adherent) or in suspension. Although adherent growing cells have been widely used especially for production of virus-based biopharmaceuticals, biomanufacturing of therapeutic proteins and in early developmental stages for virus-based biopharmaceuticals has shifted towards the use of suspension cell culture (Genzel, 2015; Mertz, 2021). As high titres are required, the use of suspension cell culture is advantageous over static cell culture systems due to easier scale-up, the possibility of high cell density (HCD) cultivations and higher yields all while

utilising more space-efficient equipment (Pincus et al., 2018). Furthermore, these cultures are typically cultivated in serum-free, animal-component free or even in chemically-defined media, which lowers the risk of lot-to-lot inconsistencies and eliminates adventitious pathogens in the process. In this way biosafety is increased, thus facilitating regulatory approval (Moreira et al., 2020; Pincus et al., 2018).

Several mammalian cell lines are commercially used for the production of therapeutic proteins, including HEK293 cells, NS0 and Sp2/0 cells, as well as CHO cells. The latter is used for 70 – 80% of all therapeutic proteins on the market (Tripathi & Shrivastava, 2019; F. M. Wurm, 2004). A couple of factors contribute to the popularity of CHO cells in the industry. Firstly, CHO cells are relatively easy to transfect and are able to generate post-translational modifications, that are compatible and bioactive in humans (Wurm, 2013). Secondly, when provided with the optimal conditions, CHO cells are fast-growing, adaptable to suspension, grown in chemically-defined medium, and fit well within large-scale manufacturing processes. Thirdly, several powerful gene amplification tools are available for CHO cells and the long-track record as a safe host simplifies the approval processes with regulatory authorities (Wurm, 2013). It should be noted that, although often summarised under the term CHO cell line, each CHO clone designed for a specific application is technically a new CHO cell line (Genzel, 2015; Wurm, 2013).

1.2.1.1 CHO cell line development for stable expression of therapeutic proteins

The continuous CHO cell line is an epithelial cell line derived from ovary cells of a female Chinese Hamster (*Cricetulus griseus*) (Puck, 1957; Tjio & Puck, 1958). The primary ovary cells could be maintained for several months at stable growth rates. At an unknown time thereafter, the cells must have undergone spontaneous immortalisation together with a morphological change from fibroblast-like to epithelioid, building the original CHO cell line (CHO-ori) (Puck, 1957; Tjio & Puck, 1958; Wurm, 2013). CHO-ori cells were characterised as fast-growing in adherent cell culture with high cloning efficiency in serum containing medium even at low serum concentrations. Since then, numerous CHO-derived cell lines have been reported, the most popular being CHO-K1, CHO-DXB11 and CHO-DG44 (F. Wurm, 2013). The latter two were engineered to have single or double knockouts for the dihydrofolate reductase (DHFR) gene. The CHO-K1 and its suspension sub-cell line CHO-K1SV have increased in popularity due to their coupling with a glutamine synthetase (GS) selectable marker which was originally designed for NS0 cells. The utilisation of the genes DHFR and GS as metabolic markers together with respective inhibitors methotrexate (MTX) and methionine sulfoximine (MSX) made the clone selection process easier. The DFHR-mediated MTX-based and GS-mediated MSX-based selection systems have become the standard methods for stable transfection of CHO cells in industry. Simultaneously, MTX selection works as gene amplification system resulting in higher product

yields. It is assumed that a similar mechanism applies to the MSX selection as well (Kim & Eberwine, 2010; Lin et al., 2019; Wurm, 2013).

The systematic procedure to obtain a stable producing CHO cell line for therapeutic protein production begins with the transfection of the cells with a gene of interest encoding the targeted product in combination with a selection gene (i.e DHFR or GS) (T. K. Kim & Eberwine, 2010). The conventional method relies on random integration of the gene of interest into the host cell genome resulting in a cell pool with heterogenous transgene insertions. However, the integration site is impacting the transcription rate of the gene of interest, a phenomenon known as position effect, resulting in differences in transgene expression. This in turn influences the overall cellular growth and metabolic performance. As a consequence a single cell isolation and cloning from the heterogeneous cell pool is performed to identify high expressing clonal cells in subsequent screening steps (Frye et al., 2016; Kim & Eberwine, 2010).

1.2.2 Biomanufacturing

The demand for biopharmaceuticals has expanded significantly since its introduction in the early 1980s. In addition, the biopharmaceutical industry is facing a variety of challenges including growing competition from biosimilars due to expiring patents, increasing need to monitor more product quality attributes, increasing clinical pipelines and limitations in manufacturing capacity. The need for more flexible and cost-efficient manufacturing platforms is driving the industry towards CM with the long-term goal for end-to-end ICB. The CM process is characterised by a perfusion bioreactor operation in the upstream followed by downstream with units operated in batch mode. ICB represents a significant advancement in process development. It extends the continuous, steady-state processing downstream of the perfusion bioreactor to encompass the capture step (Warikoo et al., 2012). The introduction of ICB has led to a wide variety of platforms that extend the continuous processing beyond the capture step, culminating in an end-to-end ICB process that extends from bioreactor through to the final concentration step (Coffman et al., 2021). Both CM and ICB have demonstrated notable advantages including increased yields, volumetric productivities, product pipeline diversity, and reduced equipment size. These benefits contribute to a smaller manufacturing footprint, lower capital investment, and potential cost savings, ultimately resulting in a more economically viable process (Arnold et al., 2019; Mahal et al., 2021).

The development and adoption of single-use (SU) processing devices for continuous up- and downstream operations contribute to cost reductions and greater process flexibility (Samaras et al., 2022). Furthermore, a modular approach to manufacturing capacity can increase scalability without relying solely on volumetric scale-up, accommodating varying product volumes and demands. This vision of a future biomanufacturing facility, featuring a modular ballroom layout

with fully single-use, closed, and continuous processes, is gaining traction. Despite the promising potential of ICB processes, they remain in their early stages of development as the biopharmaceutical industry continues to rely on well-established batch and fed-batch processes (Mahal et al., 2021; Wong et al., 2021). Overcoming various technical challenges and addressing open questions remains crucial for the widespread adoption of ICB. Current research efforts are increasingly focused on long-term process performance, clonal stability, and manufacturing robustness (Drobnjakovic et al., 2023; Müller et al., 2022; Warikoo et al., 2012).

The recent process development advances have been accompanied by regulatory agencies (e.g. FDA, EMA) advocating the implementation of Quality by Design. This aims at designing and developing a process based on specific quality targets of the product. Therefore, critical quality attributes, that impact the clinical product performance, must be identified and correlated with influencing production parameter, so called critical process parameters. A well-implemented quality by design pipeline streamlines the production process, making it more cost-effective and flexible. By establishing a defined operating range, changes within this range can be implemented without requiring additional regulatory approval, reducing both time and costs (Drobnjakovic et al., 2023). To effectively implement a Quality by Design approach for continuous processes, real-time control of critical process parameters and monitoring of critical quality attributes are essential. This requires extensive research into novel control strategies, advanced process analytical technology (PAT), and mathematical modelling for process design and control (Drobnjakovic et al., 2023; Fisher et al., 2019). PAT innovation across all stages of bioprocessing, including upstream, downstream, and process development/validation, is essential for advancing the level of process control required for integrated continuous processes. Real-time assessment of product quality attributes through in-line, at-line, and on-line monitoring enables immediate feedback and feedforward decision-making (Drobnjakovic et al., 2023; Fisher et al., 2019). The integration of on-time monitoring with data-driven statistical and multi-scale mechanistic modelling facilitates the creation of a bioprocess digital twin, a virtual representation of the physical system's dynamics and behaviour. This digital twin can be leveraged for process monitoring, control, prediction of process outcomes, and risk assessment through simulation or by leveraging historical data. A robust digital twin can significantly contribute to the regulatory-mandated Quality by Design approach (Chen et al., 2020; Portela et al., 2021; Zobel-Roos et al., 2019). While these technologies are still in their early stages, they represent a crucial step towards the digitalisation of the biopharmaceutical industry.

1.2.2.1 Process intensification in mammalian upstream processing

The increasing demand for cell culture-derived biopharmaceuticals, coupled with growing economic and social pressures, necessitates significant advancements in their development and

manufacturing processes. Optimisation and intensification of manufacturing are crucial to enhance productivity, yields, and product quality at every stage (Radhakrishnan et al., 2018).

The upstream process faces unique challenges in maintaining product quality while ensuring safety and efficacy. Key targets for improvement include productivity, yields, and product quality. Microscale and macroscale strategies can be employed to address these challenges (Radhakrishnan et al., 2018). Microscale strategies target cellular and subcellular manipulation, such as metabolic or genetic engineering can be used to modify cellular processes, identify bottlenecks in protein folding and secretion and alter the quantity profile of the target product of interest. On the other hand, macrocellular strategies are implemented when cell line modifications are not feasible. These include, HCD cultivations under optimised process conditions, optimising the operation mode by transitioning to perfusion mode operation, and optimisation of medium composition with additives and supplements (Radhakrishnan et al., 2018; Tapia et al., 2016; Wu et al., 2021). Recent trends have focused on hybrid strategies that combine cell clone optimisation at the cellular level with selection for specific process strategies, such as perfusion operation modes. This approach aims to achieve a more targeted and efficient manufacturing process.

Biomanufacturing processes in the upstream process can be categorised into three modes of operation: batch, fed-batch and continuous perfusion. The batch mode is the simplest process operation mode, where the bioreactor operates as a closed system. The cells grow and produce the target product of interest until nutrient limitations cause cell concentration to decline. The simplest form of process intensification is the fed-batch mode, where a defined cocktail of highly concentrated nutrients is supplied in either a bolus or continuous feed. This helps prevent depletion of essential nutrients, extends cultivation time, allows for higher viable cell concentrations (VCCs), and increases final productivities and volumetric yields compared to batch mode. Fed-batch processes are currently the state-of-the-art technology in commercial biomanufacturing due to their scalability and robustness. However, the fed-batch mode is associated with the accumulation of inhibitory by-products and prolonged residence times of the product of interest, both of which can negatively impact cell growth, productivity, and product quality. To address the limitations of the fed-batch mode, continuous perfusion can be implemented. This mode involves the continuous removal of culture medium and the simultaneous addition of fresh medium. Cells are retained within the bioreactor using a cell retention device, allowing for various operational strategies (Bielser et al., 2018). It is important to note that a continuous process without cell retention is typically referred to as a chemostat.

1.2.2.2 Continuous perfusion culture in mammalian cell culture

Perfusion culture is not a new technique in cell culture. Since the early 1990s, perfusion processes have been used to produce labile biopharmaceuticals that benefit from short and consistent residence times. Examples include factor VIII (Kogenate-FS®, Bayer), alglucosidase alfa (Myozyme®, Genzyme), and infliximab (Remicade®, Janssen Biotech). While advancements in cell biology, expression systems, and media development have led to significant increases in cell-specific productivities in batch cultures, the growing demand for biopharmaceuticals and economic pressures have renewed interest in perfusion mode for stable biopharmaceuticals (Bielser et al., 2018; Croughan et al., 2015).

In many perfusion processes, especially for antibody production, the objective is to establish steady-state conditions to maintain a consistent and well-defined environment for the cells (Bielser et al., 2018; Narayanan et al., 2022). This involves growing the cells until a specific target cell concentration is reached and then maintaining that concentration (Chotteau, 2015). There are two main strategies for achieving this. The first strategy, known as 'cell bleeds', involves maintaining a steady-state cell concentration by keeping the cells in a growing stage while continuously discarding a fraction of cell broth. This strategy is commonly used in the perfusion field and in industrial processes that can run for several months. The second strategy involves maintaining a target cell concentration by slowing down or completely arresting cell growth through temperature adjustments or by using chemicals such as sodium butyrate. Depending on the cell line used, cell arrest has been associated with higher cell specific productivities (Chotteau, 2015).

1.2.2.2.1 Perfusion rate

Perfusion processes have some key features. One of them is the continuous renewal of culture medium that generates stable process conditions by providing constant metabolite levels and avoiding the accumulation of unwanted toxic by-products (Chotteau, 2015). The amount of medium exchanged depends on the perfusion rate, which must be determined and optimised for each process individually. Therefore, several concepts can be applied: (i) based on the cell-specific perfusion rate (CSPR), (ii) based on the concentration of the main substrate (e.g. glucose), (iii) based on the concentration of toxic by-products (e.g. lactate), or (iv) a combination of the items above. An ideal perfusion rate for bioreactors is approximately 1 reactor volume per day (RV d^{-1}) which balances high batch-like titres with minimal liquid throughput. When combined with HCD and superior product quality, this would substantially improve the economic feasibility of perfusion technology (Konstantinov et al., 2006). However, reducing the perfusion rate requires careful consideration of several factors including relationship between specific productivity and

specific perfusion rate, the medium formulation and cost, the half-life and residence time of the product of interest (Konstantinov et al., 2006).

The most commonly used strategy to control the medium exchange is a CSPR-based regime. Thereby, the perfusion rate is altered proportionally to the VCC resulting in a constant CSPR and metabolic environment over the entire cultivation time (Ozturk, 1996). This strategy minimises depletion of the main substrates and the accumulation of toxic by-products. Provided that the cellular activities do not change over time or with VCC and the CSPR is maintained constant, this perfusion regime allows for HCD at a constant medium composition, thus ensuring consistent production. This regime has been successfully implemented in various manually and automatically controlled perfusion processes at bench scale (Dowd et al., 2003; Konstantinov et al., 2006; Nikolay et al., 2020; Vazquez-Ramirez et al., 2018) and at pilot scale (Coolbaugh et al., 2021; Mayrhofer et al., 2021; Schwarz et al., 2022; Warikoo et al., 2012). There are different options to identify the CSPR with the highest productivity. A first option is to apply different combinations of cell concentration and perfusion rates (Chotteau, 2015). A second option is the "push-to-low" method where the perfusion rate is gradually reduced while maintaining a constant VCC (Konstantinov et al., 2006). In this approach, the cellular performance is evaluated at each step after reaching a steady metabolic state. This method is most suitable for optimising stable product production in highly monitored bioreactors, especially when residence time is not a critical factor (Konstantinov et al., 2006). A third option is to use a combination of high and low CSPRs in a high intensity, low-volume perfusion (HILVOP) process. In this strategy, a high CSPR is applied to support HCD, followed by a shift to low CSPR perfusion to increase productivity in the stationary phase (Gagnon et al., 2018). Generally, lower CSPRs are often preferred as they allow more cells to be sustained with a certain amount of medium, resulting in a reduction of the cost of goods manufactured. Furthermore, CSPRs close to the minimum cell-specific perfusion rate ($CSPR_{min}$) are associated with higher productivities. However, a CSPR that is too low leads to a reduction in cell concentration, viability, and productivity (Chotteau, 2015; Gagnon et al., 2018; Konstantinov et al., 2006).

The second and third concepts, metabolite-based medium exchange, determine the perfusion rate based on the concentrations of key metabolites. This approach considers changes in either substrate or inhibitory by-products. Both are good indicators for the overall metabolite consumption and secretion, providing valuable insights and allowing the control of the overall cellular metabolic state. By-products such as lactate and ammonium can significantly impact cell performance by altering the culture pH, inhibiting cell growth, and influencing the glycosylation of the product of interest. Maintaining low levels of these inhibitory by-products through medium exchange and metabolite dilution is crucial. A thorough understanding of cellular nutrient

demand is essential to prevent overfeeding or underfeeding (Chotteau, 2015). Additionally, more sophisticated approaches like metabolomics and transcriptomics can provide deeper insights into production and process performance (Bielser et al., 2018; Chotteau, 2015)

Recent studies have explored innovative perfusion strategies to enhance cell culture performance and product quality based on the above-named strategies. Building upon the CSPR-based strategy, recent advancements have focused on tailoring the perfusion rate to the viable cell volume (VCV) rather than solely the VCC. This approach addresses the limitation of assuming a constant relationship between cell number and nutrient demand. Studies have shown that cell size can influence nutrient consumption, emphasising the importance of biomass-specific perfusion rate (BSPR) strategies to ensure adequate nutrient supply (Caso et al., 2022; Leong et al., 2024). In addition to optimising nutrient delivery, perfusion strategies can also be used to target specific product quality attributes. The Targeted Feeding (TAFE) strategy involves adjusting the concentration of fed sugars to modify the glycosylation patterns of the product (Zhang et al., 2021).

1.2.2.2.2 Cell retention

Another key feature of perfusion processes is the cell retention that enables the achievement of HCD cultures. A well-designed cell retention device (CRD) is essential for preventing cell loss in the harvest stream while also meeting critical operational requirements such as avoiding product retention, scalability, and sufficiently long, reliable operation (Chotteau, 2015). The operation of a CRD is influenced by its perfusion rate capacity, cell density capacity, recirculation rate, mechanical stress, residence time, cell retention, and product retention (Bielser et al., 2018; Chotteau, 2015). Existing CRDs for mammalian cells in suspension primarily rely on either cell size or cell density separation principles. Common examples include cross-flow and hollow fibre filters, gravity and inclined settles, and acoustic wave separators. Tangential filtration systems, such as alternating tangential flow (ATF) and tangential flow filtration (TFF) hollow fibre systems, are among the most widely used CRDs (Bielser et al., 2018; Chotteau, 2015). Numerous studies have compared the performance of different CRDs in recombinant protein and virus-based biopharmaceutical production, emphasising the critical role of the CRD in the development of successful perfusion bioreactors (Chotteau, 2015; Granicher et al., 2020, 2021; Hein et al., 2021; Pappenreiter et al., 2024; Voisard et al., 2003).

1.2.2.2.3 Stable operation and product quality considerations

In perfusion bioreactors, the combination of continuous medium exchange, a CRD, and a well-controlled bleed flow rate enables the maintenance of a constant cell density. This “steady-state” operation creates a stable environment within the bioreactor, characterised by a consistent cell concentration and other physical parameters (Bielser et al., 2018). While the concept of “steady-

state" is often applied to systems governed by chemical reactions, its application to biological systems is more complex. Biological reaction rates can vary over time, especially during extended process durations. This dynamic behaviour can lead to a slow drift away from the ideal "steady-state" condition. It is crucial to use the term "steady-state" with caution when describing perfusion bioreactor operations. While most individual parameters may reach a steady state, certain biological events can still exhibit temporal variation (probably with minor macroscopic effect). Nonetheless, this could contribute to an overall system drift (Bielser et al., 2018; Nasr et al., 2017). Consequently, the term 'stable operation' can be defined as an operation that maintains critical process parameter and quality attributes in a well-defined range. Minor perturbations may cause temporary deviations from the setpoint, but effective control strategies can minimize their impact on product quality (Nasr et al., 2017).

The constant environment maintained within perfusion bioreactors has been demonstrated to mitigate product quality heterogeneity (Godawat et al., 2015; Karst, Scibona, et al., 2017; Karst, Steinebach, et al., 2017; Walther et al., 2019). A cornerstone of the Quality by Design initiative is identification of Critical Quality Attributes that are crucial for the efficacy and safety of a drug. These Critical Quality Attributes include protein modifications such as glycosylation pattern, charge variants, and limitations of product relates impurities such as aggregates, and fragmentation (Drobnjakovic et al., 2023; Fisher et al., 2019; Rathore et al., 2023). In batch and fed-batch processing the fluctuating metabolic environment can lead to alternating metabolism and uneven residence times of the secreted product of interest, resulting in a broad distribution of Critical Quality Attributes. In contrast, the stable environment of a continuous process with its constant product residence times enables to circumvent any drastic changes in glycosylation patterns and the occurrence of product relates impurities (i.e. aggregate formation, fragmentation).

Recent years have witnessed a surge in the development and popularity of novel protein product modalities, such as bispecific antibodies (bspAbs) (Bielser et al., 2019; Gomez et al., 2019; Sinharoy et al., 2020). Currently, over 85 bspAb products are in clinical testing (Hosseini et al., 2021; Labrijn et al., 2019). While these molecules hold great promise for treating numerous diseases, their production often faces challenges related to aggregate formation during traditional fed-batch manufacturing. Aggregates can elicit severe immunogenic responses in patients, necessitating strategies for their removal, which can reduce overall yield and increase manufacturing costs. Several studies have unequivocally demonstrated that the implementation of perfusion mode can effectively decrease aggregate formation, undesired clipping, and overall product heterogeneity, leading to a substantial increase in recoverable product (Bielser et al., 2019; Gomez et al., 2019; Qin et al., 2022; Sinharoy et al., 2020). This highlights the potential of

perfusion bioreactors to address the specific challenges associated with the production of complex protein therapeutics like bspAbs.

1.2.2.2.4 Challenges

Perfusion processes achieve HCD cultures with high cell viabilities by continuously exchanging medium and retaining cells. Compared to fed-batch, this method increases titres and yields without inhibitor accumulation or increase in bioreactor size. Additionally, cultivation time can be extended, while product residence time within the bioreactor can be reduced (depending on the retention device), enhancing product stability and quality. However, despite these advantages, batch and fed-batch operations remain predominant. This is due to the complexity of controlling multiple parameters such as perfusion rates, cell separation, and aeration at HCD, as well as technical and operational challenges that require special control strategies (Bielser et al., 2018; Chotteau, 2015; Croughan et al., 2015). These include the optimisation of several parameters for perfusion operations, specifically, to maximise the yields while maintaining quality (e.g., medium development: to minimise medium consumption and to allow operation at lower perfusion rates) (Bielser et al., 2018; Bielser, 2019). It needs to be considered, that technical failures are more likely to occur with prolonged operation times and the accumulation of large harvest volumes, requiring further downstream processing (Chotteau, 2015). Besides the technical and operational challenges, there are a couple of biological challenges that need further consideration. As continuous perfusion processes target long cultivation times and as the typical fed-batch processes do not last as long, little is known about the genetic stability and production performance of the cells in long-term cultivations (Croughan et al., 2015). Hence, these parameters must equally be considered in the early stages of cell clone screening. Furthermore, the product characteristics can influence certain process parameters. For example, lability may influence perfusion rate and overall product residence time. Addressing these challenges will be crucial for the wider adoption of perfusion processes in biopharmaceutical manufacturing.

In general, perfusion operations offer significant potential for producing various cell culture-derived biopharmaceuticals to meet increasing demand. The prospect of higher VCCs and productivities makes perfusion an attractive alternative. A well-designed perfusion process, considering volumetric productivity and equipment, can be more cost-effective, leading to more economical manufacturing (Chotteau, 2015).

1.2.3 Small-scale bioprocessing

Process development and clinical manufacturing are estimated to account for approximately 17% of total R&D expenditures (Farid et al., 2020). To reduce per-patient costs, increasing process efficiency and shortening development timelines are essential (Betts & Baganz, 2006). The use of small-scale models enables high-throughput optimisation and process development by allowing

multiple experiments to be conducted in parallel. This approach significantly reduces the time required for multi-parameter optimisation and minimises process volumes, leading to lower development costs. By running experiments in parallel makes it possible to simultaneously evaluate a broad range of variables, including cell lines, medium composition, pH, and temperature (Betts & Baganz, 2006).

The design and development of fed-batch processes benefitted from a variety of widely established small-scale bioprocessing systems, such as well plates and mini- and small-scale bioreactor systems (Bielser et al., 2019). In contrast, perfusion processes are more complex, requiring the optimisation of multiple parameters and small-scale systems mimicking perfusion have not yet been fully developed or widely adopted.

Ideally the small-scale process should behave as the pilot- and large-scale systems (Chotteau et al., 2023). However, challenges in accurately replicating medium exchange and cell retention at small-scales often necessitate the use of bench-scale bioreactors (5 - 10 L) for process development. This approach, while effective, demands substantial resources in terms of labour, media, consumables, and logistics (Bielser et al., 2018; Chotteau et al., 2023). For the development of competitive perfusion processes, a strategy was developed based on two systems for perfusion process development (Chotteau et al., 2023). Small-scale bioreactors incorporating CRDs offer a means to investigate perfusion dynamics, though the scalability of the CRD to large-scale operations may be limited. In tandem, small-scale (ideally) HT screening systems operated in semi-perfusion mode enable the efficient evaluation of a broad spectrum of process conditions. A combined approach, starting with HT screening, followed by small-scale bioreactor optimisation, and finally pilot-scale validation, can be employed to understand, predict, and optimise perfusion process parameters (Chotteau et al., 2023).

1.2.3.1 Small-scale high-throughput screening systems in semi-perfusion mode

To effectively develop perfusion processes for various purposes, it is often necessary to optimise multiple parameters. This can be achieved by simulating the perfusion process using small-scale screening systems, such as non-instrumented orbitally shaken shake flasks (SF), spin tubes (ST) or microwell plates (MWP) or instrumented stirred ambr15® mini-bioreactor systems operated in semi-perfusion mode (synonymously: pseudo-perfusion) (Bielser et al., 2019; Chotteau, 2015; Chotteau et al., 2023; Gomez et al., 2017; Sewell et al., 2019; Wolf et al., 2018). In semi-perfusion, a medium exchange is performed at a set frequency such as once per day. The typical workflow involves retaining cells through either sedimentation or centrifugation, followed by a partial or total discard of the supernatant. The cells are then resuspended in an equal volume of fresh medium. Both cell retention strategies have been characterised in recent years (Gomez et al., 2017; Sewell et al., 2019; Wolf et al., 2020; Wolf, 2018; Wolf et al., 2019). Centrifugation is

commonly used for manually operated screenings with total medium exchanges, while sedimentation is more often used in automated screenings that utilise a liquid handling arm. To achieve effective cell retention using the sedimentation approach, the settling period may need to be extended, typically exceeding 30 minutes. This extended settling time, however, presents challenges in controlling environmental factors such as CO_2 levels and pH, and can lead to decreased cell viability (Kreye et al., 2019; Sewell et al., 2019). Additionally, the cell pellet resulting from sedimentation tends to be less tightly packed than those obtained through centrifugation. This difference necessitates higher exchange rates with partial medium exchanges to ensure separation efficiency exceeds 95% and to maintain high cell viability for prolonged cultivation (Sewell et al., 2019). For larger volumes (greater than 20 mL) in manual operations, centrifugation is generally the preferred method for cell retention.

As described in **Section 1.2.2.2.1**, the perfusion rate strategy can be based on a stated reactor volume exchange per day (RV d^{-1})-regime (also known as vessel volume exchange per day, VVD) or on CSPR-based regime, which facilitates a thorough comparison at HCD. Previous studies have demonstrated that these exchange regimes can enhance maximum titres and ensure consistency throughout the perfusion bioreactor process (Clincke et al., 2011, 2013; Konstantinov et al., 2006; Nikolay et al., 2020; Ozturk, 1996). Moreover, the rates defined by characteristic dimensions, such as CSPR or RV d^{-1}, can be applied across different perfusion systems, enabling comparisons between multiple systems (Chotteau, 2015; Nikolay et al., 2020). Implementing these exchange regimes in small-scale screening systems (i.e. SF, ST) increases the understanding of cellular performance in perfusion processes. Several studies indicate that parameters such as flow rates, cell-specific consumption rates, productivities, and steady-state stability can be replicated in scaled-up perfusion bioreactors (Bielser et al., 2018; Bissinger et al., 2019; Wolf et al., 2018, 2019). Utilising small-scale screening systems allows for the investigation of multiple conditions in parallel, thus generating a substantial amount of experimental data while minimising total medium usage. HCD cultivation similar to that in bioreactor perfusion systems can be achieved. Therefore, the semi-perfusion process in small-scale models serves as a suitable alternative to bioreactor perfusion, enabling the investigation and pre-determination of specific parameters (Chotteau, 2015; Gomez et al., 2017; Wolf et al., 2018, 2019).

The ambr15® mini bioreactor system is a popular screening tool for developing fed-batch processes. This automated system allows for a reasonable throughput with 24 to 48 vessels running in parallel, which facilitates Design of Experiment studies with minimal manual intervention (Kreye et al., 2019). Unlike SF or ST culture systems, the ambr15® is equipped with online sensors that monitor DO and pH levels, and it uses a de-centred stirrer rather than orbital shaking. Due to its success in fed-batch process development, the ambr15® is also being explored

for developing perfusion processes (Jin et al., 2021; Kreye et al., 2019). However, the system does have limitations. The small working volume and the lack of appropriately sized CRDs restrict their use, typically leading to cell retention through sedimentation methods. Frequent shutdowns of agitation, DO, and pH control, necessary for effective cell retention, can create heterogeneities that may affect cellular performance. While the stirred agitation and submerged gassing are similar to those used in large-scale bioreactors, the de-centred positioning and rectangular shape of the vessels create different mixing patterns compared to conventional large-scale stirred tank reactors (STRs). These differences need to be taken into account when scaling up processes. Furthermore, the costs associated with the ambr15® system are relatively high compared to other cultivation systems.

Small orbital shaken cultivation systems, such as ST and SF, have a working volume comparable to the ambr15 system (V_W = 10 - 25 mL). They have been investigated as an alternative screening tool using semi-perfusion with centrifugation for cell retention. While these systems are more cost-effective and provide reasonable throughput, their operation is manual, which increases labour requirements due to the lack of automation capabilities. Specifically, SF cultures are labour- and resource-intensive because they require transferring cell suspensions from the SFs to a centrifuge tube. In contrast, ST cultures can be centrifuged within the cultivation system itself. Moreover, these cultivation systems often lack consistent online monitoring, and the limited working volume impacts the perfusion rate (i.e. medium exchange). Consequently, perfusion rate is typically based on predetermined growth and uptake rates, resulting in either increased medium exchange volume fractions or shorter time intervals between medium exchanges. In many instances, a fixed perfusion rate (RV d^{-1}) is implemented to ensure a sufficient supply of metabolites. For ease of manual operation, the perfusion rate is typically set at 1 RV d^{-1} equalling a total medium exchange once per day. However, this batch-wise medium exchange and the separation of dead cells during centrifugation can create gradients in metabolites and pH levels that negatively impact culture performance. As a result, the quality attributes of the product—such as the glycosylation profile for protein production or the infectivity for virus production—can be compromised.

Of particular interest are small-scale screening models at MWP scale (<2 mL). Unlike ST and SF, this platform format enables HT experimentation and can be integrated with automation. This allows for the simultaneous screening of several hundred conditions with minimal labour requirements. This is particularly advantageous during the development of cell lines and the screening of cell clones, where MWPs are already frequently employed in fed-batch screenings. They provide a straightforward and user-friendly approach for practical handling and fabrication (Lindström and Andersson-Svahn, 2012). While concerns about lacking online monitoring and

limited working volume still exist, the compact design of MWPs increases experimental throughput, ultimately helping to reduce costs in the early stages of development. Furthermore, previous studies have indicated that MWPs used in semi-perfusion can accurately mimic and predict the performance of a 5 L perfusion bioreactor in terms of growth and productivity (Tregidgo et al., 2023). Nonetheless, there are certain parameters that present challenged for investigation. The small working volumes limit the parameter that can be measured, thereby reducing the amount of information that can be obtained. Similar to SF and ST, the batch-wise exchange of media create metabolite, DO and pH gradients that impact the cellular performance and product quality attributes might differ from large scale.

When using small-scale screening systems, it is important to consider the various geometries available. These include pyramidal-shaped SFs, cylindrical STs with conical bottoms, MWPs with either square or cylindrical cross-sections and various bottom designs (e.g., flat or U-shaped), as well as rectangular vessel of the ambr15®. The differences in geometry, coupled with varying agitation modes—such as orbital shaking versus stirring—create distinct mixing patterns during the cultivation process (Li et al., 2020; Micheletti et al., 2006). Additionally, non-instrumented systems like SFs, STs, and MWPs typically employ head-surface aeration as a passive aeration strategy. In contrast, the ambr15 and STRs implement on-demand aeration through spargers for HCD cultures. These variations in geometry and agitation, alongside the difference in aeration methods, and the design of the CRD, make it challenging to directly compare different perfusion systems (Chotteau, 2015; Wolf et al., 2018). Thus, further investigations at later stages, such as lab-scale bioreactors, are essential to increase process understanding and fine-tune specific parameters including product quality

1.2.3.2 Small-scale bioreactor systems in perfusion mode

The main challenge of small-scale screening systems are the alternative routes for cell retention through centrifugation or sedimentation. While these systems are useful for screening a broad range of conditions and narrowing down the design space, fine-tuning the process still requires the use of bench-top bioreactors with working volumes between 1 and 3 L (Chotteau et al., 2023). These bioreactors strike a good balance between simulating large-scale bioreactor cultures and providing valuable information on critical process parameters (e.g., ATF, TFF, or acoustic settling), albeit at smaller scales. However, at 1–3 L, the demand for medium and labour remains high, making mini-bioreactor systems at sub-litre scale (e.g., >200 mL) more desirable for optimisation (Betts & Baganz, 2006; Chotteau et al., 2023).

Recent advancements in small-sized CRDs have allowed for retrofitting CRDs onto existing bioreactor systems initially designed for fed-batch (Gagliardi et al., 2019; Janoschek et al., 2019; Sewell et al., 2019). The DASBox® system (Eppendorf) fitted with ATF or TFF systems for

effective cell retention, was shown to achieve and maintain stable cell concentrations of up to 100 x 10^6 cells mL^{-1} (Schwarz et al., 2020). Recently, the ambr250® platform (Sartorius) was redesigned to meet the needs of perfusion processes. This updated version includes a recirculation system integrated at the top of the bioreactor and features a dual pitched-blade impeller system (Sartorius Stedim Biotech, 2020). Another study focused on designing a bioreactor at 250 mL scale specifically tailored for perfusion aiming to optimise the hydrodynamic conditions for HCD cultures, while also providing detailed characterisation of flow dynamics and mixing performance (Charalambidou et al., 2024; Tregidgo, Dorn, et al., 2023). Most recently, the Erbi Breez® microbioreactor system was introduced. This automated microfluidic bioreactor, though similar at scale as many HT screening systems with a 2 mL working volume, has an integrated membrane-based cell retention system and is fully equipped with online monitoring of cell density, as well as feedback controls of pH, DO and temperature. This system represents a promising tool to support process development and accelerate timelines. It could potentially replace or complement traditional lab-scale perfusion STR experiments (Chotteau et al., 2023; Schwarz et al., 2023).

1.2.4 Cell line development, screening and selection

Cell line development (CLD) is a crucial step in the bioprocessing of therapeutic proteins. This process involves creating stable cell lines that can produce the desired product at high yields and with high quality. CLD is complex and consists of multiple stages, including transfection, cloning, screening, and selection (Tihanyi & Nyitray, 2020). Each stage is essential for developing a cell line with important characteristics such as high productivity, stability, and product quality. However, these stages can pose various challenges, especially as the process transitions from small-scale laboratory settings to larger industrial production.

The CLD process begins by designing a plasmid that contains the gene of interest, which encodes the desired protein. This plasmid is then introduced into a mammalian host cell, typically CHO cells or other suitable cell types. This introduction can be accomplished using various transfection techniques, such as electroporation, lipofection, or viral transduction. The choice of transfection method depends on factors like efficiency, the specific type of protein being produced, and the desired characteristics of the final cell line (Chong et al., 2021; Li et al., 2010; Munro et al., 2017).

After transfection, successfully transfected cells are identified and selected. The cells are then cultured in 96-well plates using a basal growth medium, often supplemented with selective agents such as MTX for DHFR transformed cells or MSX for GS-mediated cells (Li et al., 2010; Lin et al., 2019). A primary screen is performed using analytical assays like ELISA to eliminate non-producing or low-producing cells. Following this, individual cells are isolated and clonally expanded, ensuring that each clone originates from a single cell and expresses the gene of interest

consistently. The clonal nature of the cell line is crucial for maintaining homogeneity and avoiding the phenotypic variation that can occur in mixed populations. Regulatory agencies require verification of monoclonality, which can be facilitated by systems such as ClonePix or fluorescence-activated cell sorting to ensure colony integrity (Chen et al., 2020; Kim et al., 2012).

After cloning, the next step is to identify the highest-yielding and most stable cell lines. This is done through a combination of screening methods, molecular characterisation, and functional assays. The challenge lies in rapidly identifying the best candidates while managing the large number of clones generated during the cloning process. Screening technologies play a crucial role in evaluating numerous clones in a short time. Automated systems, such as those used for high-throughput screening, reduce variability and increase throughput compared to manual methods (Chong et al., 2013). Hundreds of clones are screened for high titre, which is more efficient in automated systems.

Typically for fed-batch culture, the cells are grown for approximately two weeks in 96-well deepwell plates (DWP) and screened for robust growth and high productivity. Although the cells are grown in DWP, they are continuously fed to mimic conditions expected at a large scale (Jarasch et al., 2015; Li et al., 2010). From this screening, the top 24 to 48 clones are selected for further growth in automated reactor systems, such as ambr15® (Li et al., 2010; Moses et al., 2012). Success in this stage heavily depends on the expertise and experience of the scientists involved, as they must carefully choose the cell lines most likely to succeed in subsequent stages (Li et al., 2010; Munro et al., 2017). The selected top 24 to 48 clones undergo further screening, taking into account critical attributes such as product quality, titre, and stability. This process narrows the selection down to the top 5 to 20 clones. These chosen clones are then screened in systems like ambr250® to optimise process conditions, which accelerates screening and process development (Hong et al., 2018; F. Li et al., 2010). The clones undergo several product quality assessments and stability studies, with materials produced for research and toxicology (Li et al., 2010; Munro et al., 2017). Once the top clones are selected, their performance is evaluated in bioreactors for process optimisation, ultimately leading to the selection of a final clone for large-scale production (Li et al., 2010). This is followed by a series of analytical tests to ensure that the final product meets the desired quality and yield (Frye et al., 2016; Hong et al., 2018).

To accurately predict the performance of clones in large-scale bioreactors, it is essential to implement and test an enriched medium, similar to the final production formulation, alongside an appropriate feeding regime as early as possible in DWP, SF or small-scale bioreactors. At this stage, key attributes of the clones, including product quality, manufacturability, and volumetric productivity, should be thoroughly evaluated. Alongside CLD, development studies are conducted to identify any potential challenges that could impact the stability and potency of the therapeutic

protein. These studies assess biochemical and biophysical properties—such as deamidation, unfolding, solubility, and viscosity—through both computational (in silico) methods and experimental approaches. This helps predict degradation pathways and stability issues (Jain et al., 2017; Yang et al., 2013). Early identification of these risks enables the implementation of corrective measures, such as re-engineering the cells or selecting alternative clones, ensuring that the product remains stable and effective throughout development (Jarasch et al., 2015).

Recent research aimed at advancing the CLD process has focused on gene editing, big data analysis, and high-throughput screening. The current state-of-the-art transfection method leads to random integration of the gene of interest, necessitating lengthy screenings to identify the optimal clone for manufacturing. Techniques like CRISPR/Cas9 have been explored because they enable precise genome editing, allowing for the targeted integration of the gene of interest into specific loci within the host genome. This approach has the potential to enhance expression levels and stability. The other two areas of focus—big data analysis and high-throughput screening—aim to increase consistency and reduce labour and development costs by decreasing processing time. Currently, the process of clone selection is highly dependent on the operator, and a significant amount of data collected during CLD is often not fully utilised. Machine learning and, more recently, artificial intelligence are being explored to analyse large datasets. These technologies can predict the best clone candidates for scale-up, optimise culture conditions, and improve the overall efficiency of the development process. This becomes particularly important with advancements in automated high-throughput screening, which increase data acquisition. The primary challenge in CLD is the selection of high-producing, stable cell lines within a limited timeframe. To expedite this process, various HT methods have been developed, such as well plate formats, ambr15, and ambr250. These formats are commonly employed as HT platforms for selecting clones suitable for batch or fed-batch operations. Previous studies have indicated that implementing the target operation mode (e.g., fed-batch) earlier can be advantageous for cell clone screening. Specifically, it has been shown that implementing an early-stage fed-batch mode in well plates enhances the predictability of performance at a larger scale (Wang, Albanetti, Miro-Quesada, et al., 2018) and can influence the ranking of clones (Markert et al., 2019).

In the CLD process for cell lines aimed at a perfusion mode of operation on a manufacturing scale, true perfusion mode is only used during the bench-scale bioreactor stage (i.e. > 200 mL) after the number of clones has been reduced to approximately 20. Prior to this stage, screenings are performed in fed-batch mode using automatable or automated systems such as well-plates and ambr15®. Recently, the ambr250 has enabled the implementation of perfusion mode at the mini-bioreactor scale (~250 mL). However, only a limited number of studies have investigated cell clone screening in perfusion mode, with most relying on the ambr15® bioreactor system to

combine media and cell clone screening for process optimisation and scale-up (Bielser et al., 2019; Gagliardi et al., 2019; Gomez et al., 2017). One study evaluated cell clone screening using DWPs and STs in a semi-perfusion mode (Bielser et al., 2019). The findings revealed that both small-scale models exhibited comparable growth and productivity, making them potential tools for predicting optimal process conditions in a perfusion bioreactor (Bielser et al., 2019). The effectiveness of clone screening in semi-perfusion mode has been demonstrated, and some studies have looked at the transition between different operation modes. This research could be expanded to further explore cell clone screening, as well as the transition from fed-batch to semi-perfusion modes particularly at small-scale employing semi-perfusion methodologies.

1.3 Concluding remark from the literature survey

The push for ICB is gaining momentum, driven by the need to streamline production processes, reduce costs, and improve product quality (Croughan et al., 2015). This continuous operation integrates both upstream and downstream processes, offering advantages over traditional batch-based processes, including faster production timelines and cost savings. A central feature of ICB is the use of bioreactors in perfusion mode during the upstream stage. In this mode, fresh media is continuously supplied while spent media is removed, allowing cells to remain in an optimal growth phase for extended periods.

A key area of research within this paradigm is the development and optimisation of small-scale models that accurately mimic perfusion processes. These models are essential for process development, enabling HCD cultures and facilitating cost-effective, time-efficient optimisation strategies that can be scaled up for industrial applications (Sandner et al., 2019). Small-scale systems have long been utilised at various stages of developing and optimising manufacturing processes. They allow for rapid data acquisition through high-throughput experimentation, which accelerates process development timelines and reduces costs. For batch and fed-batch processes, a wide range of small-scale systems exists, including high-throughput screening systems and commercially available mini-bioreactors. However, this is not the case for perfusion processes.

Over the past decade, several studies have explored various tools as small-scale systems for perfusion culture. Among these tools are MWP and spin tubes in a semi-continuous semi-perfusion mode as well as small-scale bioreactors retrofitted with cell retention devices to facilitate perfusion (Bielser et al., 2019; Gomez et al., 2017; Tregidgo et al., 2023; Wolf et al., 2018). Nevertheless, the development of small-scale systems specifically for perfusion remains limited compared to fed-batch systems. This area requires ongoing design and engineering characterisation to create a diverse and robust range of small-scale tools for perfusion process development, from automated high-throughput designs for early-phase screening of a broad

range of process variables to mini-bioreactor systems for the investigation of a narrower set of parameters.

Despite the increasing research into small-scale models for optimising bioreactors and significant efforts to improve perfusion processes, there has been little focus on selecting production cell lines that are specifically suited for perfusion systems. Cell clone screening typically begins at the micro- or millilitre scale in MWP. This is followed by screenings in small- to bench-scale bioreactors (ranging from 250 mL to 3 L), with process optimisation continuing through to pilot-scale bioreactors. As the process scales, the number of clones is gradually reduced to identify the optimal clone for large-scale manufacturing. However, traditional cell line development processes generally rely on fed-batch methods for selecting and optimising clones (Li et al., 2010). These methods involve intermittent media feeds rather than continuous feeding. In contrast, perfusion mode is typically only implemented in laboratory-scales above 1 L. As a result, there is a shift in operation mode from fed-batch to perfusion as the process scales up. At well-plate scale, clones are selected under fed-batch conditions before being exposed to the continuous, steady-state conditions of perfusion bioreactors at bench-scale. This transition means that cells selected in fed-batch conditions may not exhibit the same growth characteristics, metabolic profiles, or productivity levels when moved to a perfusion environment. The differences between fed-batch and perfusion operations raise important questions about how these variations affect the ranking of clones during early-stage screenings. Could fed-batch conditions inadvertently exclude clones that might perform well in a perfusion process?

Research on clone screening from a process development perspective is limited, especially for screenings designed specifically for perfusion conditions. Some studies investigating fed-batch cell clone screenings have demonstrated that early implementation of the target operation mode during the cell clone screening and selection process significantly impacts which clones advance to later stages of screening and optimisation (Markert et al., 2019; Wang, Albanetti, Miro-Quesada, et al., 2018). By adapting cell clone screening to better mimic the conditions of perfusion processes, performance could be greatly enhanced. This adaptation would ensure that selected clones are optimised for sustained growth and high productivity needed for a perfusion mode of operation.

1.4 The present contribution

Building on insights from the current literature, this work aims to develop a high-throughput, small-scale methodology specifically tailored to intensified cell culture processes, with a particular focus on early-stage clone screening under perfusion-like conditions. This approach addresses a key gap in existing screening strategies, where conventional fed-batch methods often fail to identify clones best suited for continuous processing. To bridge this gap, the study focuses

on establishing a semi-perfusion platform using MWPs that enables HCD cultures in a scalable and parallelisable format, better aligning early clone selection with the operational mode used in intensified manufacturing.

Building upon an existing semi-perfusion strategy in 24-well MWPs, the platform is further characterised in terms of limitations and capabilities, simulating essential features of a perfusion bioreactor, such as cell bleeds and variations in perfusion rates. A second platform of 6-well deepwell plates will be explored as a tool for scaling up to shake flask scale, while still maintaining the automation advantages provided by well-plate-based systems.

Based on these characterisations, the MWP platform is used in a cell clone screening scenario involving multiple clones from two cell lines in both fed-batch and semi-perfusion modes. The effects of operation mode, medium composition, and perfusion rates are assessed to evaluate the performance and ranking of the clones. Furthermore, the clone ranking strategy is analysed, and potential improvements are explored to develop a robust ranking approach. Finally, the semi-perfusion method is scaled down to a 96-well deepwell plate, where the impact of working volume and agitation speed are investigated. This will include an initial cell clone screening as a precursor towards the establishment of an automated workflow for this method.

1.5 Outline and objectives of the thesis

The remainder of this thesis is organised into 8 chapters. **Chapter 2** outlines the experimental setup for the semi-perfusion methodologies used in well plates, as well as the bioreactor setup for both perfusion and fed-batch modes. The chapter provides details on the corresponding analytical techniques employed for CHO cell culture. Additionally, it outlines the data analysis strategies employed for cell clone screening.

The first three results chapters, **Chapter 3**, **Chapter 4** and **Chapter 5**, focus on the development of the MWP platform and the characterisation of the 24-well MWP in terms of its biological and process capabilities. In these chapters, various strategies were explored to maintain stable conditions typical of perfusion bioreactors, and these were adapted to the semi-perfusion method at the MWP scale.

Chapter 3 builds on the previously established semi-perfusion MWP method and the literature review. It aims to evaluate feasibility and performance of implementing cell bleeds at the plate scale to mimic a stable culture environment. Specifically, this chapter addresses the following:

I. Transfer of cell bleed method: Adapting the cell bleed method from ST to a small-scale model with 10x smaller working volume—the 24-well MWP with a total medium exchange once per day.

II. Technical and Biological Assessment: Evaluating the technical limitations, metabolic performance, and productivity of a model CHO cell line, with comparisons to published literature.
III. 6-well DWP as an Automatable Alternative: Investigating the 6-well DWP format as a scalable and automatable alternative to shake flasks in semi-perfusion and evaluating its suitability as an intermediate model toward bioreactor processes.

In contrast to **Chapter 3**, where a stable culture an environment is mimicked through implementing cell bleeds, **Chapter 4** explores alternative strategies focusing on the variation of perfusion rate. It aims to investigate the feasibility and effectiveness of perfusion rate modulation, using CSPR-based medium exchange strategies, to maintain stable cultures in MWP and DWP formats. The key objectives include:

I. Perfusion Rate Variation: Implementing CSPR-based medium exchanges in 24-well MWP and comparing the resulting perfusion rates and culture performance to the established semi-perfusion method with fixed daily medium exchanges.
II. Scale-Up Evaluation: Exploring the 6-well DWP format as a scale-up option, with working volumes closer to shake flasks, to assess performance and scalability under CSPR-based operation.
III. Bioreactor Validation with CSPR Strategy: Validating the small-scale CSPR-based strategy by transferring the best-performing condition to a 250 mL perfusion bioreactor and comparing growth, metabolism, and productivity to the well-plate models.

Chapter 5 builds on the strategies developed in **Chapters 3** and **4** by combining cell bleed and CSPR-based medium exchange approaches to further stabilise culture environments in small-scale semi-perfusion systems. It aims to evaluate the feasibility and performance of an integrated strategy in both MWP and DWP formats. Specifically, this chapter addresses the following:

I. Combined Cell Bleed and CSPR-based Method: Implementing and assessing a combined cell bleed and CSPR-based medium exchange strategy in 24-well MWPs, focusing on culture stability, metabolic activity, and productivity.
II. Impact Assessment: Evaluating the extent to which culture manipulation via the combined strategy affects cell growth, productivity, and metabolic stability.
III. Scale-Up Evaluation: Exploring the application of the combined strategy in 6-well DWPs to assess operational scalability and suitability as an intermediate model toward bioreactor processes.

Chapter 6 builds on the development of the MWP platform and previous process characterization by applying the system to a key use case: early-stage cell clone screening. It aims to evaluate more

representative approaches for cell line screening in the context of perfusion bioprocesses, where fed-batch methodology remains the industry standard. Specifically, the chapter addresses the following objectives:

I. Comparison of Screening Methods: Evaluating cell clone screening performance using both MWP fed-batch and semi-perfusion methods, with a focus on growth, metabolic activity, and productivity.
II. Clone Ranking Strategy: Assessing and optimizing the clone ranking approach to improve the accuracy and reliability of clone selection outcomes.
III. Reproducibility Assessment: Investigating the consistency and robustness of the screening process across different experimental runs.

Chapter 7 builds on the semi-perfusion platform developed in earlier chapters by evaluating its translation to a miniaturised 96-well DWP format. It aims to assess the feasibility and performance of this further scale-down as a foundation for future development and tech transfer. The main objectives of this chapter are:

I. 96-well DWP Characterisation: Assessing key operational considerations for implementing the semi-perfusion method at the 96-well scale, including working volume limitations, oxygen transfer capacity, and practical handling requirements. This objective also aims to identify critical factors—such as well geometry, mixing dynamics, and mass transfer limitations—that warrant further investigation to support future optimisation of miniaturised culture performance.
II. Benchmarking Against 24-well MWP: Comparing cellular performance metrics to the established 24-well MWP system to evaluate scalability and process consistency.
III. Pilot Clone Screening Study: Conducting a screening of mAb1-producing clones using two established ranking strategies, with evaluation of growth, productivity, and ranking outcomes.
IV. Cross-Platform Comparability: Assessing the consistency of clone rankings across the 96-well and 24-well formats to determine reproducibility and reliability of the screening approach.

The subsequent chapters, **Chapter 8** and **Chapter 9**, conclude the thesis by reflecting on the outcomes and broader relevance of the work. **Chapter 8** provides a consolidated summary of the key experimental findings, emphasising methodological development, performance outcomes across scales, and implications for clone screening and semi-perfusion strategies. It also offers recommendations for future work to support further optimisation and application. **Chapter 9** focuses on the research impact and implementation, discussing the scientific and academic contributions, the industrial relevance through opportunities for automation, scalability, and

integration into early-stage bioprocess development pipelines, as well as the potential impact on broader society.

Chapter 2: Materials and Methods

2.1 Introduction

The following chapter describes all materials and methods used for the experiments. An introduction to the cell lines used in this work is given, as well as an explanation of the cultivation conditions, protocols and analytical methods. All experiments were performed under sterile conditions using a Biological Safety Cabinet (BSCs). The BSC was cleaned with 70 % ethanol before and after use. All equipment used was either pre-packaged sterile equipment or autoclaved before use.

2.2 Cell culture

2.2.1 Cell lines, culture medium and supplements

Three Chinese Hamster Ovary (CHO) cell lines producing a protein product were used for the studies presented in this thesis.

Experiments focused on the microwell platform development were conducted using a CHO cell line named CHO cobra (Cobra Biologics AB, UK), producing trastuzumab. This mAb is used to treat breast and stomach cancer, more specific, cancers that are HER2 receptor positive (EMA, 2008). CHO cobra cells were initially cultivated in chemically defined fed-batch specific CD CHO medium (Gibco®, Thermo Fisher Scientific) and were adapted to grow in perfusion specific High Intensity Perfusion (HIP) medium (Gibco®, Thermo Fisher Scientific). Both media were supplemented with 3.2 mM GlutaMax™ (100X) (Gibco®, Thermo Fisher Scientific), and 2% HT supplement (50X) (Gibco®, Thermo Fisher Scientific). During experimentation with CHO cobra cells, the supplemented base medium was blended with 30% CHO CD EfficientFeed™ B Liquid Nutrient Supplement (v/v) (Gibco®, Thermo Fisher Scientific), if not otherwise indicated.

Cell clone screening experiments were performed with two panels of proprietary clonally-derived CHO cell lines provided by AstraZeneca. The first CHO cell line panel expressed a proprietary monoclonal antibody (mAb1) and comprised eight clones (mAb1_C1 – C8), whilst the second CHO cell line panel expressed a proprietary bispecific antibody (bspAb1) and comprised six clones (bspAb1_C1 – C6). Cells were cultivated in two commercially available media: (1) fed-batch specific CD CHO medium (Gibco®, Thermo Fisher Scientific) and (2) perfusion-specific High Intensity Perfusion (HIP) medium (Gibco®, Thermo Fisher Scientific), both supplemented with

1% HT supplement (100X) (Gibco®, Thermo Fisher Scientific) and 25 µM methyl sulphoximine (MSX, Sigma-Aldrich). During experimentation with mAb1 and bspAb1 cells, medium supplemented with 1% HT supplement (100X) (Gibco®, Thermo Fisher Scientific) was used, if not otherwise indicated.

Non-supplemented CD CHO and HIP media are referred to as base media. CHO CD EfficientFeed™ B Liquid Nutrient Supplement is referred to as Feed B.

2.2.2 Medium adaptation

All CHO cells were initially cultured in CD CHO medium (Gibco®, Thermo Fisher Scientific) and sequentially adapted to grow in HIP medium (Gibco®, Thermo Fisher Scientific). The medium adaptation process involved gradually increasing the proportion of HIP medium over several passages. The procedure was as follows: Passage 1 with 75% CD CHO medium + 25% HIP medium (v/v), Passage 2 with 50% CD CHO medium + 50% HIP medium (v/v), Passage 3 with 25% CD CHO medium + 75% HIP medium (v/v), Passage 4 with 100% HIP medium.

During each passage, viable cell concentration (VCC) and viability were closely monitored. If the cell viability remained above 90%, the medium ratio was adjusted according to the next step in the adaption process. If the viability dropped below 90% the same ratio was maintained multiple times until the viability recovered to above 90%, at which point the next ratio adjustment was introduced.

2.2.3 Preparation of a master and working cell bank

For each medium adaptation of CHO cobra cells, a cell bank 50 vials were created. The passage number for CD CHO-adapted CHO cobra cells was Px+9, for HIP-adapted cells the passage number was Px+13 for both cell banks, respectively. The 'x' represents an unknown passage number at which the cells arrived at the Department of Biochemical Engineering, UCL. For each medium adaptation of mAb1 and bspAb1 CHO cells, a cell bank of 40 vials was created. The passage number for CD CHO-adapted cells was P3, for HIP-adapted cells the passage number was P6 for both cell banks, respectively. Of each cell bank, 20 vials were designated as Master cell bank (MCB) to be used to derive new working cell banks when needed, the remaining vials were designated as working cell bank (WCB) to be used for cell revival for experimentation.

For the preparation of the cell banks, cells were expanded to a VCC up to 10 x 10^6 cells mL^{-1} in 2 L shake flasks. Subsequently, the cells were transferred in 50 mL sterile conical polypropylene centrifuge tubes (Easy Reader™, Fisherbrand™) and centrifuged at 200 g for 5 min (Centrifuge 5910R, Eppendorf). The supernatant was removed, and the cells were gently resuspended in a volume of fresh base medium supplemented with 7.5 % (v/v) Dimethyl sulfoxide (DMSO; Sigma Aldrich) to achieve a VCC of 20 x 10^6 cells mL^{-1}. A volume of 1 mL of cell suspension was then

transferred in sterile cryovials (T301-2 Cryovial®, Simport Scientific), placed in a freezing container (CoolCell® Containers, Corning®) and stored in a freezer for 24 h at -80 °C. After 24 h, the cells were transferred into a storage container placed in liquid nitrogen (LN_2) for long-term storage.

2.2.4 Cell revival

For cell revival, a vial of the WCB stored in LN_2 was thawed in a water bath (SWB15D, Stuart) at 37 °C for 3 min. Subsequently the cells were transferred in 50 mL sterile conical polypropylene centrifuge tubes (Easy Reader™, Fisherbrand™) filled with 10 mL fresh base medium before being centrifuged at 200 g for 5 min (Centrifuge 5910R, Eppendorf). The supernatant was discarded, and the cell pellet gently resuspended in a total volume of 25 mL of fresh supplemented medium. Subsequently the cell suspension was transferred in a non-baffled 125 mL shake flask (Polycarbonate Erlenmeyer culture flask Corning®, USA) to achieve a seeding VCC of 0.3 - 0.8 x 10^6 cells mL^{-1}. For CHO cobra cells, base medium was supplemented with 3.2 mM GlutaMax (Gibco®, Thermo Fisher Scientific) and 2% HT supplement (100X) (Gibco®, Thermo Fisher Scientific), while the base medium for mAb1 and bspAb1 cell lines was supplemented with 2% HT supplement (100X) and 25 µM methyl sulphoximine (MSX, Sigma-Aldrich).

The CHO cells were maintained in non-baffled shake flasks (Polycarbonate Erlenmeyer culture flask Corning®, USA) placed in a CO_2 incubator (MCO-19AIC, Sanyo) at 37 °C with 5 % CO_2, and were agitated at a shaking speed of 180 revolutions per minute (rpm), using an orbital shaker with an orbital diameter (OD) of 25 mm (CO_2 resistant shaker, Thermo Fisher Scientific). Cells were passaged twice a week with a seed cell concentration of 0.3 - 0.8 x 10^6 cells mL^{-1}. For the determination of VCC, viability and diameter the Vi-CELL™ XR Cell Viability Analyzer (Beckman Coulter, USA) was used (cf. section 2.6.1) and the seed volume of cell suspension for passaging was calculated (eq. (1)). For cell expansion, the cells were transferred into SF with increased working volumes (V_W) according to **Table A.1** in the Appendix.

$$V_{seed} = \frac{V_{flask} \cdot X_{seed}}{X} \tag{1}$$

Where V_{Seed} is the seed volume in [mL], V_W the working volume in [mL], X_{Seed} the seeding cell concentration in [cells ml^{-1}] and X the determined VCC in [cells mL^{-1}].

2.3 Cultivations in well plates and shake flasks

2.3.1 Cultivation in 24-well microwell plates

MWP cultures were performed using standard round well ultra-low attachment 24-well MWP (CLS3473, Corning®). The plates were sealed with a Duetz sandwich lid (CR1524, EnzyScreen, Heemstede, Netherlands) to reduce evaporation while maintaining headspace gas exchange. All

cultures were cultivated in a CO_2 incubator at 37 °C, 5 % CO_2, an agitation speed of 250 rpm, and an OD of 19 mm (CO_2 Resistant Shakers, ThermoFisher), if not otherwise indicated. The plates were held in place by a Duetz MWP clamp system (CR1801h, EnzyScreen, Heemstede, Netherlands).

Fed-batch culture in MWP

For fed-batch (FB) cultures, MWPs were inoculated at 1 x 10^6 cells mL^{-1} at a working volume of 1.2 mL in CD CHO medium (day 0). Following a 3-day batch phase, feeding commenced on day 3 for a period of 5 consecutive days. Feeding was conducted as previously described by Silk et al., 2010 and involved a 6% v/v bolus addition of nutrient supplement (EfficientFeed™ B), followed with a 2.5% v/v bolus of 10x diluted bicarbonate solution (0.75 M Na_2CO_3, 0.5 M $NaHCO_3$) to control pH. Due to the limited working volume, sampling was achieved using a sacrificial well method, where samples were taken in triplicate every 24 h from day 3 for quantification of cell growth, metabolites and titre. A centrifugation step was included following sampling for VCC from the 'sampling wells', after centrifugation (50-200 rpm, 5 min) samples for metabolite and titre quantification were collected. This aimed to reduce differences in sampling protocols potentially influencing cell culture performance due to exposure to different stress levels. A schematic overview of the protocol is shown in **Figure 2.2A.**

Semi-perfusion culture in MWP

For semi-perfusion (SP) cultures, MWPs were inoculated at 1 – 40 x 10^6 cells mL^{-1} at a working volume of 1.2 mL in CD CHO or HIP medium. A sacrificial well methodology was used, where samples were taken every 24 h over the duration of 8 days starting either from day 1 or day 3 after an initial 3-day batch phase (with day 0 being the day of inoculation). Samples were taken in triplicates from the 'sampling wells', where 100 µL were taken to determine VCC, viability and diameter prior to centrifugation (50-200 rpm, 5 min). Following centrifugation, 600 µL supernatant were collected to quantify metabolites and 300 µL supernatant was collected to measure product titre from the 'sampling wells'. Subsequently, a partial or total medium exchange was performed in the 'culture wells' to mimic perfusion with cell retention. To compensate for 3% daily evaporation, the volume of medium removed was calculated based on the total working volume (for complete medium exchange) or the adjusted volume for partial exchanges, minus 36 µL. The medium used for medium exchanges was CD CHO, HIP, or a blend of HIP with 20 or 30% Feed B (v/v). A schematic overview of the protocol is shown in **Figure 2.2B - E**.

2.3.2 Cultivation in 6-well deepwell plates

The 6-well DWP cultures were performed using square round-edged 6-well DWP (CR1406, EnzyScreen, Heemstede, NL). The plates were sealed with a Duetz sandwich lid (CR1206a,

EnzyScreen, Heemstede, NL) to reduce evaporation while maintaining headspace gas exchange. All cultures were cultivated in a CO_2 incubator at 37 °C, 5 % CO_2, an agitation speed of 250 rpm, and an OD of 19 mm (CO_2 Resistant Shakers, ThermoFisher), if not otherwise indicated. The plates were held in place by a Duetz MWP clamp system (CR1801h, EnzyScreen, Heemstede, NL).

The 6-well DWPs were inoculated at 1 – 30 x 10^6 cells mL^{-1} at a working volume of 30 mL in HIP medium and cultured over a duration of 8 – 10 days, where the day of inoculation marks day 0, if not otherwise indicated. Samples were taken in triplicates, where 100 µL were taken to determine VCC, viability and diameter prior to centrifugation (50-200 rpm, 5 min). Following centrifugation, 1-2 mL supernatant were collected to quantify metabolites and 1 mL supernatant was collected to quantify product titre. Subsequently, a partial or total medium exchange was performed to mimic perfusion with cell retention. Due to the larger volume of the 6-well DWP, the sample amount taken and evaporation were considered negligible, thus for the entire cultivation period the same three wells per condition were used.

2.3.3 Cultivation in 96-well deepwell plates

The 96-well DWP cultures were performed using square 96-well DWP (CLS3960, Corning®). The plates were sealed with a Duetz sandwich lid (CR1296, EnzyScreen, Heemstede, NL) to reduce evaporation while maintaining headspace gas exchange. All cultures were cultivated in a CO_2 incubator at 37 °C, 5 % CO_2, an agitation speed of 300 rpm, and an OD of 19 mm (CO_2 Resistant Shakers, ThermoFisher), if not otherwise indicated. The plates were held in place by a Duetz MWP clamp system (CR1801h, EnzyScreen, Heemstede, NL).

For semi-perfusion (SP) cultures, 96-well DWPs were inoculated at 0.5 -1 x 10^6 cells mL^{-1} at a range of working volumes between 200 and 400 µL in HIP medium. A sacrificial well methodology was used, where samples were taken every 24 h over the duration of 8 - 10 days starting either from day 1 or day 3 after an initial 3-day batch phase (with day 0 being the day of inoculation). Samples were taken in triplicates from 'sampling wells', where 50 µL were taken to determine VCC, viability and diameter prior to centrifugation (50-200 rpm, 5 min). Following centrifugation, 100 µL supernatant was collected from 'sampling wells' to measure product titre. Subsequently, a partial medium exchange of 0.75 RV d^{-1} was performed in the 'culture wells' to mimic perfusion with cell retention. To compensate of daily evaporation, the volume of medium removed was calculated based on the adjusted volume for partial exchanges, minus 13 µL. The medium used for medium exchanges was HIP, or a blend of HIP with 30% Feed B (v/v).

2.3.4 Cultivation in shake flasks

SF cultures were performed in triplicate using three non-baffled 125 mL SF (polycarbonate Erlenmeyer culture flask Corning®, USA), operated in parallel per condition. All cultures were

cultivated in a CO_2 incubator at 37 °C, 5 % CO_2, an agitation speed of 180 rpm, and an OD of 25 mm. The SFs were inoculated at 1 – 30 x 10^6 cells mL^{-1} at a working volume of 30 mL in HIP medium and cultured over a duration of 8 – 10 days, with day 0 defined as the day of inoculation. Samples were taken in triplicates, where 100 µL were taken to determine VCC, viability and diameter. Prior to centrifugation (50-200 rpm, 5 min), the cell suspension was transferred into 50 mL sterile conical polypropylene centrifuge tubes (Easy Reader™, Fisherbrand™). Following centrifugation, 1-2 mL supernatant were collected to quantify metabolites and 1 mL supernatant was to quantify product titre. Subsequently, a partial or total medium exchange was performed to mimic perfusion with cell retention and the cell suspension was transferred back into the SF. Due to the larger volume of SF, the sample amount and daily evaporation was considered negligible, thus for the entire cultivation period the same three SFs per condition were used.

2.4 Cultivation in 250 mL perfusion bioreactor

The perfusion process was performed with CHO cobra cells in a 250 mL stirred-tank bioreactor fabricated by the Design and Fabrication Facility at UCL. The design and characterisation of the bioreactor were described in detail in Tregidgo, Dorn, et al., 2023, where a first design fabricated with stainless-steal was presented. In this thesis the vessel was made of glass, though the vessel dimension were the same as previously published. In a brief description, the bioreactor consists of a flat bottom vessel and three baffles evenly spaced along the circumvent. The headplate was designed to provide fittings for three probes (i.e. DO, pH and temperature) and ports for liquid addition and gas outlet. Additional ports were placed at the bottom and side of the vessel to connect the cell retention device.

For the cultivation operation, the bioreactor was connected to a BioFlo120 controller (Eppendorf, Germany). Cultivation parameters such as temperature, pH, and oxygen saturation were recorded online by using temperature, pH and Dissolved Oxygen (DO) probes. The bioreactor was equipped with a dual impeller system with a 3-blade pitched-blade impeller with a 30° pitch at the top and a 6-blade flat blade turbine impeller below (Eppendorf, Hamburg, Germany), a drilled-hole L-sparger, a PT100 thermometer, as well as a DO (DasGip, USA), and pH probe (Mettler-Toledo, Germany). Additional installations were a short silicon tube connection with a one-way sampling valve (Eppendorf), a feed tube and small ports for inoculation. Air filters were attached to the air exhaust outlet, and the L-sparger tube (both 0.2 µm 50 mm Sartorius, Germany).

Cell retention was achieved via tangential flow filtration using a Spektrum® MidiKros mPES hollow fibre with a pore size of 0.2 µm, a surface area of 88 cm^2, length of 20 cm and internal diameter of 1 mm (Repligen, Massachusetts, USA) connected to the reactor vessel via the base and side connections. The recirculation flow rate was maintained at 80 mL min^{-1} using a low shear PuraLev® i30SU pump with sterilisable multi-use pump head (PuraLev® i30SU; Levitronix, CH).

For the perfusion, either a fixed RV d^{-1}-based (i.e. 1 RV d^{-1} or 0.75 RV d^{-1}) or a CSPR-based perfusion rate was used. Both strategies were controlled manually, where the media inlet and harvest outlet flow rates were controlled using identical peristaltic pumps (120U Variable-Speed Single-Channel Pump System, Watson-Marlow). For the CSPR-controlled protocol, a CSPR value was chosen based on previous experimental data. The perfusion rate was adjusted based on the VCC after each sampling (c.f. section 2.5.1, eq. (3)). This was done by re-adjusting the peristaltic pump rates if required to maintain the CSPR. A simplified schematic overview of the perfusion bioreactor operation is shown in **Figure 2.1**.

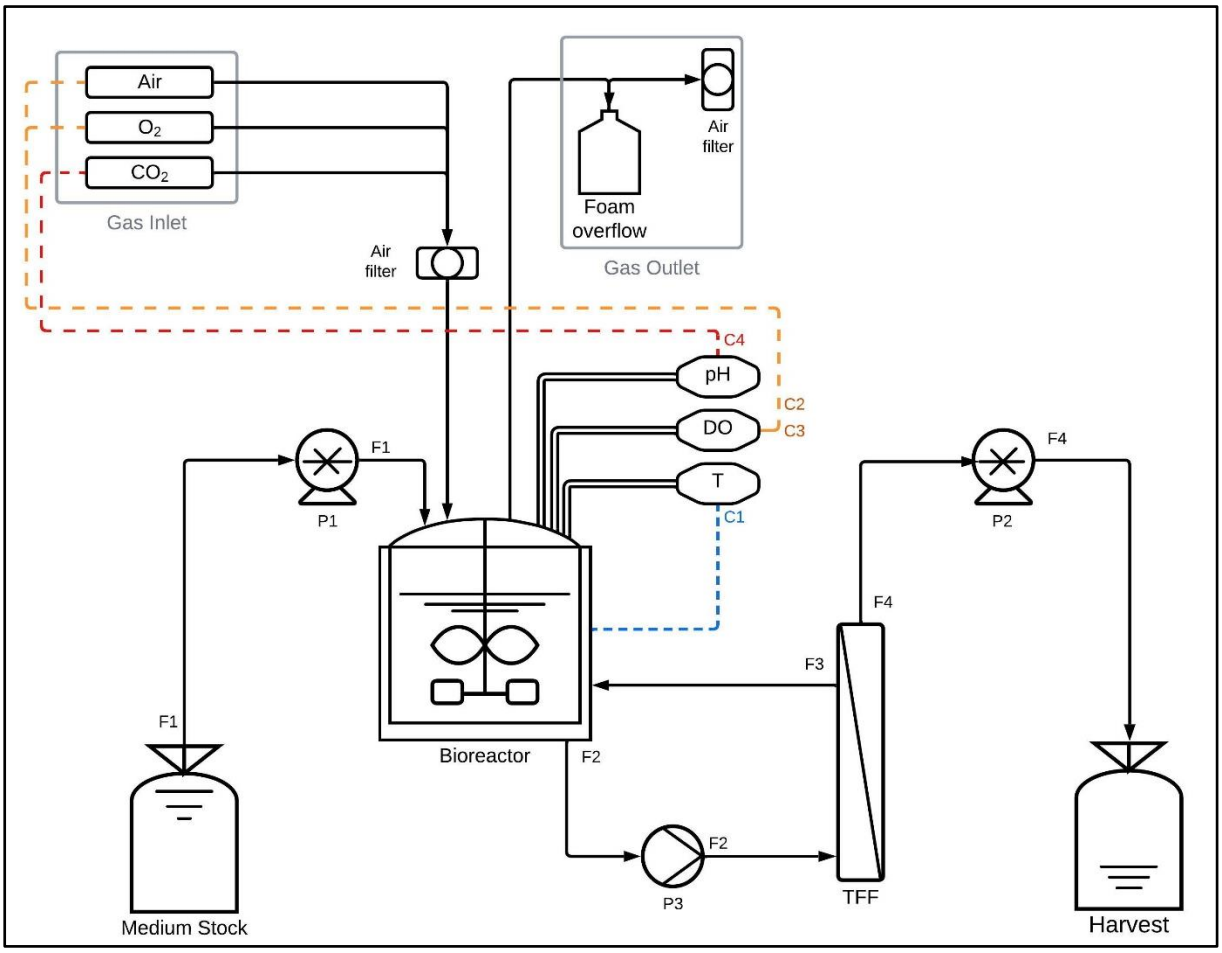

Figure 2.1: Schematic overview of a perfusion bioreactor operation. F1: Medium inlet flow towards bioreactor vessel; F2: cell suspension outlet recirculating towards a cell retention device - here membrane based tangential flow filtration; F3: cell recirculation loop; F4: supernatant outlet flow for harvest collection; P1 and P2: peristaltic pumps; P3: low shear magnetic levitation pump; C1: Temperature feedback; C2 and C3: DO feedback to control gas flow composition by adjusting oxygen and air fractions ; C4 pH feedback to control through CO2.

Before sterilisation, the pH probe was calibrated at pH 7 and pH 4. Post sterilisation additional flasks (2 L) for feed and harvest were connected via peristaltic pump tubing. The bioreactor was placed on a balance. The vessel was filled with prewarmed, sterile HIP medium blended with 30% Feed B and stirred at 250 rpm overnight. The pO_2 probe was calibrated at 100 % air and 0 % air (electronic zero), respectively.

The seed cell culture was maintained in a non-baffled shake flask (V_W = 200 mL) and used to inoculate the bioreactor at a VCC of 1 - 2x10^6 cells mL^{-1} (V_W = 250 mL). A total medium exchange was performed for the seed culture before inoculation. Agitation was set to 250 rpm initially. The temperature was set to 37 °C and the pO_2 setpoint was controlled at 50 %. The perfusion was started when the VCC was between 6 - 10 x10^6 cells mL^{-1}. To enable maintenance of the DO setpoint, the agitation speed was increased, as required, to maximum of 350rpm.

2.5 Perfusion and semi-perfusion cultures

2.5.1 Implementation of different medium exchange regimes

Several strategies for medium exchange can be implemented to achieve perfusion in bioreactors and in small scale systems. The perfusion rate is described as the combined outflow of harvest and bleed from the bioreactor.

$$P = H + B \tag{2}$$

Where P is the perfusion rate in [RV d^{-1}], H the harvest rate in [RV d^{-1}], and B the bleed rate in [RV d^{-1}].

Fixed RV d^{-1}-based exchange regime

The exchange regime based on the reactor volume per day (RV d^{-1}) describes a perfusion flow rate in terms of the total working volume. Thus, the perfusion rate is fixed (e.g. 1 RV d^{-1}) or can be increased stepwise (e.g. 0.75 to 1 to 1.5 to 2.0 RV d^{-1}).

CSPR-based exchange regime

For the operation of a perfusion bioreactor with a manually controlled CSPR-based perfusion rate, the perfusion rate is adjusted after each sampling based on the VCC. In addition, the specific growth rate is taken into account to maintain the CSPR while the cell concentration increases (eq. (3), (Nikolay et al., 2020; Vazquez-Ramirez et al., 2019))

$$Q_{Perf} = \frac{dV_E}{dt} = X_i \cdot V_W \cdot CSPR \cdot e^{\mu \Delta t} \tag{3}$$

For the operation of CSPR-based semi-perfusion, it is assumed that the volume of exchange medium equals the amount of medium exchanged in a continuous perfusion process in the same time interval (eq. (3)). Thus, the exchange volume (V_E) is calculated based on V_W, a constant CSPR and the imminent VCC for a previously fixed schedule (eq. (4)). However, the schedule (Δt) is adapted when > 60 % of the V_W needs to be exchanged (eq. (5), (Nikolay et al., 2020; Vazquez-Ramirez et al., 2019)).

$$V_E = \frac{X_i}{\mu} \cdot \left(e^{\mu \Delta t} - 1\right) \cdot V_W \cdot CSPR \quad (4)$$

$$\Delta t = \frac{ln\left(\frac{0.6\mu}{X \cdot CSPR} + 1\right)}{\mu} \quad (5)$$

Where Q_{Perf} is the perfusion flow rate in [mL d^{-1}], V_W the working volume, X_i the determined VCC, CSPR the cell specific perfusion rate in [mL $cell^{-1}$ d^{-1}], μ the specific growth rate [d^{-1}] and Δt the time between medium exchanges in [d].

2.5.2 Implementation of cell bleeds

The previously established semi-perfusion MWP methodology (Tregidgo et al., 2023) was adapted by implementing a cell bleed step into the workflow (cf. **Figure 2.2C**).

In a first step, the VCC of three wells, so called 'sampling wells', was measured. Based on the measured VCC a cell bleed volume was calculated (eq (6)). The respective bleed rate can be calculated with equation (7). The bleed volume was removed from the 'culture wells' to reset the VCC in the culture. It is noteworthy that the VCC set point value for calculation was lower than the targeted VCC value required to maintain a stable average VCC. After cell bleeding, the MWPs were centrifuged at 50 g for 5 min, followed by supernatant collection of the designated 'sampling wells' for quantification of metabolites and titres. Subsequently, a partial or total medium exchange is performed in the 'culture wells'.

$$V_B = \frac{(X_i - X_{SP}) \cdot V_W}{X_i} \quad (6)$$

$$B = \frac{V_B}{V_W} \frac{1}{\Delta t} \quad (7)$$

Where V_B is the bleed volume, X_i the measured viable cell concentration, X_{SP} the targeted setpoint viable cell concentration, V_W the working volume, B the bleed rate and Δt the time interval between two sampling time points.

The harvest rate can be calculated with equation (8), where for cultures without cell bleed $V_H = V_E$, and for cultures with cell bleed $V_H = V_E - V_B$.

$$H = \frac{V_H}{V_W} \frac{1}{\Delta t} \quad (8)$$

Where V_B is the bleed volume, X_i the measured viable cell concentration, V_W the working volume, H the harvest rate and Δt the time interval between two sampling time points.

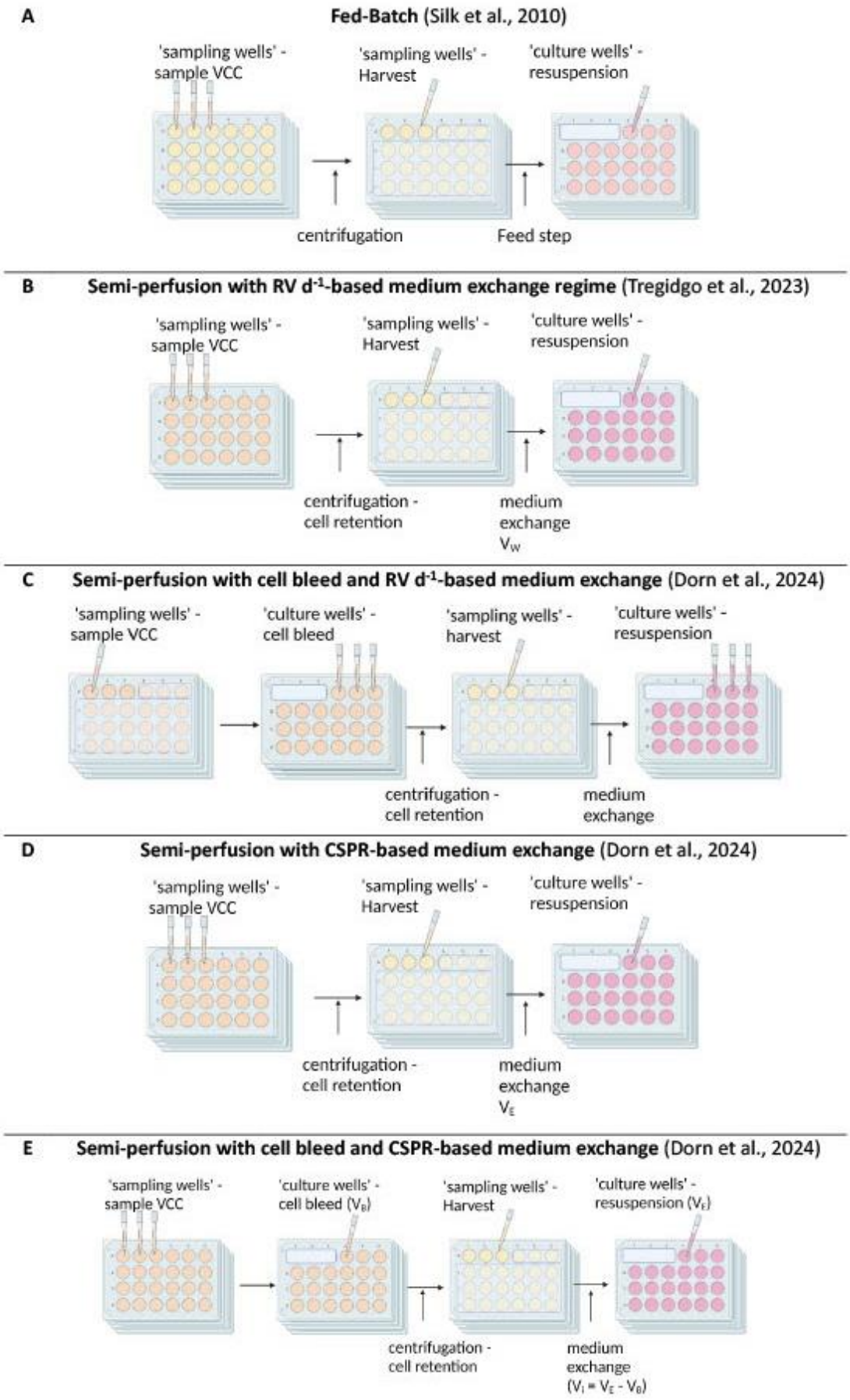

Figure 2.2: Schematic overview of the sacrificial well methods of MWP cultures in fed-batch and semi-perfusion.

Figure 2.2 continued: (A) *Fed-batch method based on (Silk et al., 2010)*: VCC is measured from samples taken from 'sampling wells'. After centrifugation, the supernatant from these wells is collected for titre and metabolite analysis, while for the remaining 'culture wells' a feed step is performed. (B) *Semi-perfusion method with 1 RV d^{-1} perfusion rate (Tregidgo et al., 2023)*: VCC is measured from samples taken from 'sampling wells'. After centrifugation, the cell-free supernatant from these wells is collected for titre and metabolite analysis. A complete medium exchange is then performed in the remaining 'culture wells'. (C) *Semi-perfusion with cell bleed and 1 RV d^{-1} perfusion rate (Dorn et al., 2024a)*: VCC is measured from samples taken from 'sampling wells', and based on this, a cell bleed is performed to reach a target VCC setpoint in the remaining 'culture wells' (V_B). After centrifugation, the cell-free supernatant from the 'sampling wells' is collected for titre and metabolite quantification. In the 'culture wells', the medium is completely removed, and cells are resuspended in fresh medium. (D) *Semi-perfusion with CSPR-based perfusion rate (Dorn et al., 2024b)*: VCC is measured from samples taken from 'sampling wells'. After centrifugation, the supernatant from the 'sampling wells' is collected for titre and metabolite quantification. In the remaining 'culture wells', an amount of medium equivalent to the previously calculated exchange volume (V_E) is replaced. (E) *Semi-perfusion method with cell bleed and CSPR-based perfusion rate (Dorn et al., 2024b):* VCC is measured from samples taken from 'sampling wells', and based on this, a cell bleed is performed to reach a target VCC setpoint in the remaining 'culture wells' (V_B). After centrifugation, the cell-free supernatant from 'sampling wells' is collected for titre and metabolite analysis. In the remaining 'culture wells', the medium is removed, taking into account the previously removed bleed volume ($V_H = V_E - V_B$). The wells are then resuspended with fresh medium equal to the calculated exchange volume (V_E). The workflow is repeated every 24 h over the course of 8 days, where the 'sampling wells' and 'culture wells shift to the next three wells. Created with biorender.com.

2.6 Analytical techniques

2.6.1 Determination of cell concentration and characterisation of cell growth

The VCC and total cell concentration (TCC), viability and diameter were determined using the Vi-CELL™ XR Cell Viability Analyzer (Beckman Coulter, USA). For these measurements a sample of 0.5 - 1 mL cell broth was taken and measured in 50 images per sample. For samples at HCD, the sample was diluted with PBS before the measurement as required to an end volume of 0.5 - 1 mL for measurement. For the distinction of viable and dead cells, the measurement was performed using the trypan blue exclusion method. Dead cells and cells with damaged membrane were stained with trypan blue due to the higher permeability of the membrane. The measurement setting for the CHO cell lines used is presented in **Table A2** in the **Appendix Section A.1**.

Integrated Viable cell concentration

The integrated viable cell concentration (IVCC) was calculated based on the following equation (9) utilising the VCC.

$$IVCC_i = \int_{t=0}^{t} VCC(t)dt \approx \sum_{i=1}^{n} \frac{X_i + X_{i-1}}{2} \times (\Delta t) \tag{9}$$

Where IVCC is the integrated VCC in [cells h^{-1} mL^{-1}], X_i the VCC at time point i in [cells mL^{-1}], the VCC at time point i-1 in [cells mL^{-1}] and Δt the time interval between two sampling time points.

Specific growth rate μ

The specific growth rate is the proportionality factor correlating the growth rate with the VCC in the exponential phase of the cell growth (eq. (10)). Through integration over time the exponential

growth kinetics can be described based on the initial cell concentration (eq. (11)). For cultures with a cell bleed the cell bleed rate has to be taken into account.

$$r_X = \frac{dX}{dt} = \mu \cdot X \tag{10}$$

$$X = X_0 \cdot e^{\mu \cdot \Delta t} \tag{11}$$

Where r_X is the growth rate in [cells h^{-1} mL^{-1}], μ the specific growth rate in [h^{-1}], X_0 the initial VCC in [cells mL^{-1}], and X the VCC in [cells mL^{-1}]. For cultures with a cell bleed the cell bleed rate has to be taken into account.

2.6.2 Determination of extracellular metabolites

The Optocell CuBiAn VC biochemistry analyzer (4BioCell; Bielefeld, Germany) was used for the quantification of the extracellular metabolites (glucose, lactate, and ammonium) of MWP cultures (c.f. Appendix **Table A.3** for validated range of metabolite measurement). For the quantification 600 µl cell-free supernatant was collected in 1.5 mL Eppendorf tubes.

Extracellular metabolites of DWP and SF cultures were determined with BioProfile FLEX analyzer (Nova biomedical, UK), if not otherwise indicated. Both machines were previously validated using the same batch of medium and give comparable results (e.g. glucose: 76.93 mmol L^{-1} and 73.16 mmol L^{-1}). The samples were measured immediately after collection or stored at - 20 °C for later quantification as required.

Specific consumption and production rate $q_{s,i}$

The cell-specific consumption and production rates of key metabolites can be calculated from the substrate concentration. For nutrients (e.g. glucose, glutamine) the specific consumption rate ($q_{S,n}$) is calculated based on equation (12), while for by-products (e.g. lactate, ammonium) the specific production rate ($q_{S,bp}$) is calculated based on equation (13).

$$q_{S,n} = \left(\frac{\Delta c_{Sn}}{\Delta t} + (H_i + B_i) \cdot (c_{S,0} - c_{S,i})\right) \cdot \frac{1}{\overline{X}} \tag{12}$$

$$q_{S,bp} = \left(\frac{\Delta c_{Sbp}}{\Delta t} + (H_i + B_i) \cdot (c_{S,i} - c_{S,0})\right) \cdot \frac{1}{\overline{X}} \tag{13}$$

Where $q_{S,i}$ is the specific uptake rate in [mmol 10^{-9} $cells^{-1}$ h^{-1}], c_S the substrate concentration in [mmol L^{-1}], $c_{S,0}$ the substrate concentration of the medium provided, Δt the time interval between two sampling time points, H_i the harvest rate at time point I in [RV d^{-1}], B_i the bleed rate at time point I [RV d^{-1}] and $\overline{X}$ the daily average of VCC in [cells mL^{-1}].

2.6.3 Determination of osmolality

Osmolality was determined using a freeze point osmometer (Gonotec® Osmomat 3000).

2.6.4 Protein product quantification

For the quantification of the antibody titre, a sample of 300 µl cell-free supernatant were collected. The samples were stored in 1.5 mL Eppendorf tubes at - 20 °C.

To determine the IgG titre, a HPLC (HPLC Agilent 1100 series; Agilent, USA) with 1mL Protein G column (HiTrap™ Protein G HP, Cytiva) was used. Therefore, the samples were placed in a 96-well HPLC plate and sealed with a HPLC lid. A running buffer (Buffer A) containing 20 mM sodium phosphate ($NaH_2PO_4 \cdot H_2O$, Na_2HPO_4, Sigma-Aldrich) at pH 7.0 was used for loading the samples onto the column. Samples were eluted using an elution buffer (Buffer B) containing 20 mM glycine (Sigma-Aldrich) at pH 2.8.

To quantify the IgG concentration a calibration curve was generated. Therefore, an IgG standard of known concentration was diluted in running buffer and run through the column. A linear correlation of diluted standard concentrations and the corresponding peak areas results in a linear regression (eq. (14)). This equation was re-arranged and used to calculate the sample titre concentrations from the respective measured peak areas (eq. (15)).

$$Peak\ area = m \cdot c_{Titre} + n \tag{14}$$

$$c_{titre} = \frac{Peak\ area - n}{m} \tag{15}$$

Where c_{titre} is the titre concentration in [g L^{-1}].

2.6.5 Derived productivity parameters

For comparative analysis between different operation modes and perfusion rate strategies, the following equations were used to determine cell specific rates, and yields (Bausch *et al.*, 2019). The space-time-yield (STY) can be used for the comparison of the overall productivity and is calculated using equation (16).

$$STY = \frac{Y_i}{V_{W,BR} \cdot (t_i - t_0)} \tag{16}$$

$$Y_i = \int_0^i c_{titre,i} \cdot H_i \cdot V_{W,BR}\ dt \tag{17}$$

For fed-batch operations these equations can be simplified to:

$$STY = \frac{c_{titre,i}}{(t_i - t_0)} \tag{18}$$

$$Y_i = c_{titre,i} \cdot V_{W,BR} \tag{19}$$

Where STY is the space-time-yield in [g L^{-1} d^{-1}], Y_i the yield equal to the accumulated mass produced since start of the cultivation in [g], c_{titre} the antibody concentration in [g L^{-1}], $V_{W,BR}$ the

bioreactor working volume in [mL], t the cultivation time in [d], H the harvest rate in [RV d^{-1}]. In addition to the overall productivity described by the STY, the volumetric productivity (VP) describes the current productivity at a given time for perfusion operation with equation (20) and fed-batch operation with equation (21).

$$VP = c_{titre,i} \cdot H_i = X_i \cdot q_P \tag{20}$$

$$VP = \frac{c_{titre,i} - c_{titre,i-1}}{t_i - t_0} \tag{21}$$

Where VP is the volumetric productivity in [g L^{-1} d^{-1}], c_{titre} the product concentration, H the harvest rate in [RV d^{-1}], X the VCC in [x 10^6 cells mL^{-1}], and q_P the cell specific productivity in [pg cell d^{-1}]. The cell specific productivity can be calculated using equation (22) for perfusion operations and equation (23) for fed-batch operations.

$$q_P = \left(\frac{c_{titre,i} - c_{titre,i-1}}{t_i - t_{i-1}} + (H_i + B_i) \cdot c_{titre,i}\right) \cdot \frac{1}{\bar{X}} \tag{22}$$

$$q_P = \frac{c_{titre,i} - c_{titre,i-1}}{t_i - t_{i-1} \cdot \bar{X}} \tag{23}$$

Where q_P is the cell-specific productivity in [pg $cell^{-1}$ d^{-1}], c_{titre} the product concentration, t_i the sampling time point, t_{i-1} the previous sampling time point, H the harvest rate, B the bleed rate and $\bar{X}$ the daily average of VCC between two sampling time points in [x 10^6 cells mL^{-1}].

2.7 Cell ranking strategies

2.7.1 Single-parameter clone ranking

Cell clone rankings based on a single parameter were performed by sorting the parameter values from best to worst. Some parameters are considered "best" for the maximum value and "worst" for the minimum value such as VCC or q_P, while others, such as lactate concentrations, have a reverse rating where the minimum value is considered "best" and the highest value considered "worst". The single-parameter ranking was based on a productivity parameter, where the cell specific productivity q_P was selected for a fair comparison between different operation modes, if not otherwise indicated.

2.7.2 Multi-parameter clone ranking

In order to consider multiple parameters for the cell clone rankings a metric called manufacturability index (MI_{CL}), previously introduced by Goldrick et al., 2023, was used. The MI_{CL} treats the selection of cell clones as a multi-criteria decision-making problem, where data on growth characteristics, metabolites, and productivities are integrated into a single metric. This metric allows for the evaluation of m cell lines according to *n* criteria and assessing the performance of each individual clone (Goldrick et al., 2023).

The MI_{CL} was adapted to 24-well MWP operation and for the comparison of fed-batch and semi-perfusion operations. To achieve a fair comparison with an equal number of parameters and to account for the differences in feeding and medium exchange protocols, the following parameters and criteria were selected: maximum values of VCC, growth rate, STY and product-over-glucose yield ($Y_{P/Gluc}$), minimum values of viability, and lactate concentration, as well as average values of cell specific production and consumption rates of the product and metabolites (q_P, q_{Gluc}, q_{Lac}, q_{Amm}). While these parameters and criteria were fixed for the purposes of this work, they can be adjusted according to specific user requirements. The MI_{CL}, previously adapted for 24-well plates, was applied to rank clones in 96-well DWPs. To enable fair comparison under semi-perfusion conditions, accounting for partial medium exchanges, the following parameters and criteria were selected: maximum values of VCC, growth rate, and STY, minimum values of viability as well as average values of q_P.

The calculation and data visualisation were performed in MATLAB 2021b based on the following equations previously described by Goldrick et al., 2023, where the MI_{CL} was calculated using equation (24).

$$MI_{CL,i} = \sum_{j=1}^{j=n} w_j \times r_{ij} \qquad for\ i = 1, 2, 3, \dots m \tag{24}$$

Where w_i is the normalised weight of each criteria j, r_{ij} a dimensionless rating per clone i and selection criteria j:

$$r_{ij} = \left| \frac{x_{ij} - x_{j,worst}}{x_{j,best} - x_{j,worst}} \right| \tag{25}$$

In equation. (25) x_{ij} is the individual ranking of cell clone i for criteria j, $x_{j,best}$ the best overall ranking, $x_{j,worst}$ the worst overall ranking for criteria j. $x_{j,best}$ and $x_{j,\ worst}$ were defined as maximum or minimum values based on expertise from industry, where some parameters are considered "best" for the maximum value and "worst" for the minimum value of the parameter j (e.g. VCC or q_P) while others have a reverse rating where the minimum value is considered "best" and the highest value considered "worst" (e.g. lactate concentrations). The normalised weights were set to 1 for this study but could be adjusted in the future or depending on individual process requirements.

2.8 Concluding remarks

This chapter has outlined the experimental methods and cell lines employed throughout this work. The analytical techniques and equations used to derive key parameters have also been described. The resulting data, along with their interpretation, are presented and discussed in **Chapters 3** to **7**.

Chapter 3: Platform development for high-throughput perfusion optimisation – Implementation of cell bleeds in well plates and shake flasks*

3.1 Introduction

Perfusion processes are designed to sustain a physiologically stable environment for cell cultures by continuously supplying fresh medium and removing spent medium and waste products. This dynamic approach allows for the maintenance of constant cell concentrations at HCD, typically by adjusting perfusion rates and/or implementing a cell bleed. Achieving true steady-state conditions in perfusion operations requires not only a cell retention device for cell-free harvesting, but also a controlled bleed stream to remove excess biomass (Chotteau, 2015).

Maintaining a stable VCC while keeping cells in an active growth phase is essential for ensuring consistent productivity and metabolic performance. This is generally accomplished by balancing the cell bleed rate with the cell growth rate, thereby establishing a "quasi steady-state" environment (Chotteau, 2015; Chotteau et al., 2023).

Developing and optimising perfusion bioreactor processes often requires screening numerous conditions, which can be resource-intensive at laboratory scale. Scale down models (SDMs) with millilitre-scale working volumes offer a practical solution, enabling early-stage process optimisation at reduced cost and time. To be effective, SDMs must replicate key perfusion features, such as medium exchange, and the ability to maintain HCD through cell retention and controlled cell bleed. Ideally, they would also support high-throughput operation to facilitate efficient parallel experimentation during process development.

---

* Some of the results presented in this chapter are included in:

Dorn, M., Klottrup-Rees, K., Lee, K., & Micheletti, M. (2024). Platform development for high-throughput optimization of perfusion processes—Part I: Implementation of cell bleeds in microwell plates. Biotechnology and Bioengineering, 121(6), 1759–1773. https://doi.org/10.1002/bit.28682

Previous studies have shown that HCD cultivation is feasible in 24-well MWPs operated in semi-perfusion mode (Tregidgo et al., 2023). Building on this work, the current chapter investigates whether this platform can also support the maintenance of HCD at defined VCC targets, thereby enabling "quasi steady-state" operation. To this end, a cell bleed strategy was integrated into the existing MWP-based semi-perfusion method, allowing cultures to be operated at controlled, approximately constant VCCs.

To assess scalability and robustness, the system was further evaluated in six-well DWPs and SFs, both operated at 30 mL working volume. Scaling up from MWP to SF introduces changes in geometry and hydrodynamics, which can impact mixing, gas transfer, and consequently, cellular performance. DWPs were included as a potential intermediate scale-up model, offering similar working volumes to SFs while retaining handling characteristics closer to MWPs and better compatibility with automation. However, differences in geometry across formats may influence process outcomes. For comparative purposes, the geometries of MWPs, DWPs, and spin tubes—an established SDM—are illustrated in **Figure 3.1**.

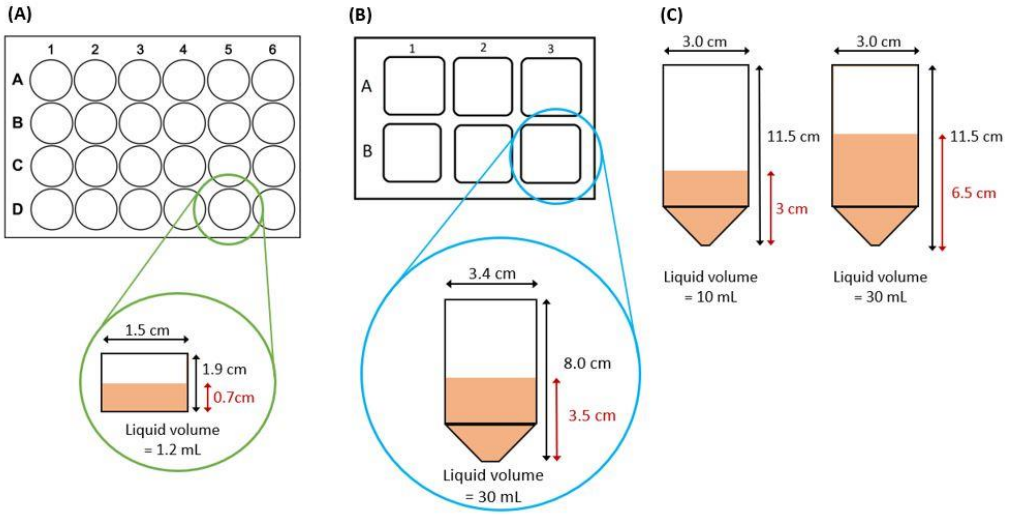

Figure 3.1: Schematic representation of 3 scale-down models. (A) 24-standard round well microwell plate and single well dimensions; (B): squared 6-well deepwell plate and singe well dimension; (C): spin tubes with two different working volumes.

The aim of this chapter is to implement and evaluate a cell bleed strategy within small-scale semi-perfusion platforms to maintain stable, "quasi steady-state" culture conditions at defined VCC targets (conditions labelled as stable growth (SG)). To achieve this, the first objective is to adapt the cell bleed method to the 24-well MWP, operating at a fixed perfusion rate of 1 RV d^{-1}. The second objective is to assess the technical feasibility and biological performance of this strategy in the 24-well MWP by monitoring growth, metabolism, and productivity of a model CHO cell line. Third, the 6-well DWP format is explored as a scale-up option, offering working volumes comparable to conventional shake flasks. Parallel cultivations in DWPs and SFs are performed to compare growth, metabolism, and productivity, thereby assessing the scalability and robustness

of the semi-perfusion workflow. This approach provides insights into the suitability of DWPs as an intermediate SDM and supports the development of a scalable and automatable semi-perfusion workflow.

3.2 Results

This section of the chapter is divided into three main sections presenting the results obtained and is followed by a discussion section to contextualise the findings. **Section 3.2.1** details the integration of the cell bleed strategy within the MWP system, while **Section 3.2.2** extends this approach to DWP and SF, followed by a comparative analysis across platforms in **Section 3.2.3**. All experiments presented in this chapter were conducted using the CHO Cobra cell line.

3.2.1 Implementation of cell bleed strategy in 24-well microwell plate

Previous studies using the CHO cobra cell line have demonstrated that HCD of up to 70 × 10^6 cells mL^{-1} and high productivities can be achieved using the perfusion-specific medium HIP blended with 30% of Feed B (data not shown). However, for the purpose of evaluating a cell bleed strategy under controlled HCD conditions, four target viable cell concentrations (VCCs) were selected below this maximum. These targets were chosen to align with previously published data using spin tube cultures so to enable direct comparison. Each of the selected stable VCC targets - 10, 20, 30 and 40 × 10^6 cells mL^{-1} – represent a progressively increasing HCD condition under which stable growth was investigated. The cell bleed strategy was assessed using these four average VCC targets, as illustrated in **Figure 3.2**. The MWP were inoculated close to the respective VCC target levels, specifically at 8, 16, 26, and 36 × 10^6 cells mL^{-1}. These conditions are henceforth referred to as MWP-SG10, MWP-SG20, MWP-SG30, and MWP-SG40, corresponding to the average VCC targets of 10, 20, 30 and 40 × 10^6 cells mL^{-1}, respectively.

Figure 3.2 presents the corresponding growth profiles, key process parameters, and production rates for the MWP cultivations. As shown in **Figure 3.2A,** a characteristic 'saw-wave' growth pattern was maintained across all setpoints throughout the experimental period. The resulting average VCCs were 13.1±1.2, 23.8±1.5, 29.8±2.0, and 38.4±2.5 × 10^6 cells mL^{-1} for MWP-SG10, MWP-SG20, MWP-SG30 and MWP-SG40, respectively. Overall, the average VCCs closely aligned with the intended targets across all four conditions. However, at the higher density conditions (MWP-SG30 and MWP-SG40), a reduction in growth was observed toward the end of the cultivation period (day 8). In these cases, the VCC peaks typically achieved in the previous days for each cell bleed were not reached, likely contributing to average values falling slightly below the set targets. In contrast, for MWP-SG10 and MWP-SG20, the average VCCs slightly exceeded the targets, although they remained within the range of experimental error. A similar trend was observed for the cell viability measurements. Cultures maintained at lower VCCs (MWP-SG10 and MWP-SG20) exhibited viabilities consistently above 95% throughout the cultivation period. In

comparison, MWP-SG30 and MWP-SG40 experienced a gradual decline in viability beginning on day 6, dropping from initially above 95% to approximately 70% by day 8.

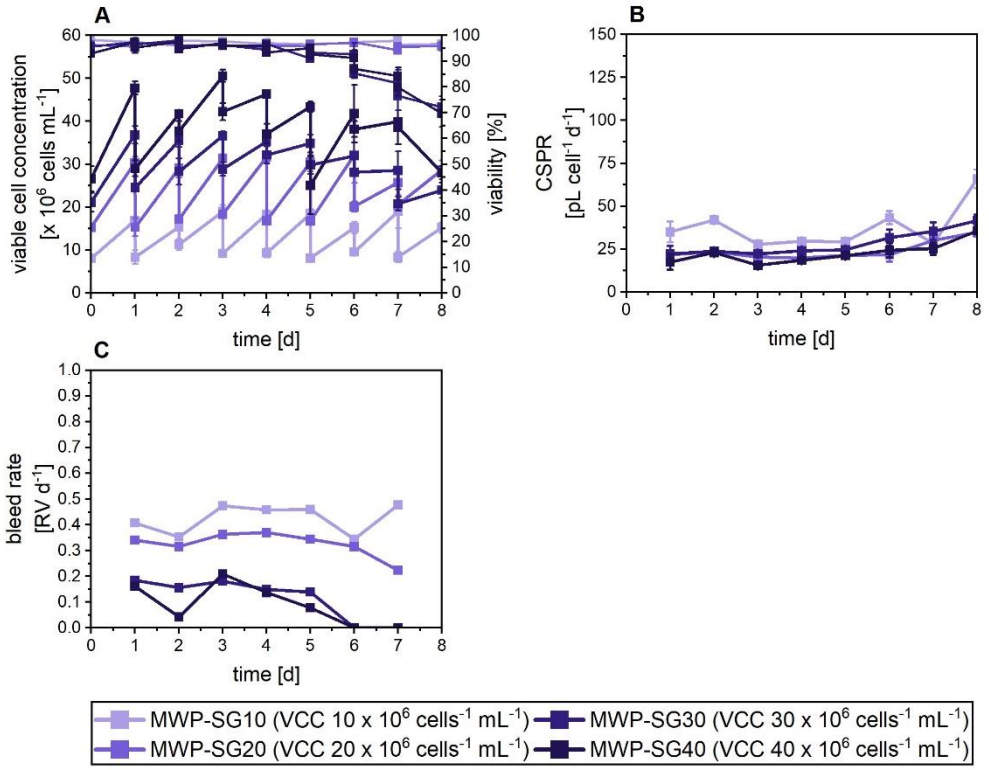

Figure 3.2: Growth, cell-specific perfusion rates, and bleed rates for CHO cobra cells in 24-well MWP cultivations in semi-perfusion with implemented cell bleeds. Cells were inoculated at 10, 20, 30, and 40 × 10^6 cells mL^{-1} and cultivated in HIP medium supplemented with 30% Feed B (v/v). (a) VCC (filled) and viability (open); (b) CSPR; (c) bleed rate. Targeted average VCCs (×10^6 cells mL^{-1}): 10 (■, light), 20 (■, medium-light), 30 (■, medium-dark), 40 (■, dark). Mean of N = 3 wells. Error bars indicate standard deviation for growth and CSPR. The bleed rate was calculated on average values of VCC each day and does not contain error bars. CHO, Chinese hamster ovary; CSPR: cell specific perfusion rate; HIP, high intensity perfusion medium; MWP, microwell plate; SG: stable growth; VCC, viable cell concentrations.

Nonetheless, cultures exhibited stable growth over time, as reflected in the relatively constant CSPRs and bleed rates across conditions (**Figure 3.2B** and **C**). CSPR trends stabilised after day 2 in all conditions, though the levels varied depending on the targeted VCC. As expected, lower average CSPRs were observed at higher VCC targets, with values of 27.7±3.2, 24.3±1.7, 28.3±2.8, and 22.7±2.0 pL $cell^{-1}$ d^{-1} for MWP-SG10, MWP-SG20, MWP-SG30, and MWP-SG40, respectively. Toward the end of the cultivation period, CSPRs gradually increased across all conditions. This rise was most pronounced for MWP-SG10, which reached a final CSPR exceeding 60 pL $cell^{-1}$ d^{-1}. In contrast, for the other conditions maximum CSPRs were in the range of 35 to 40 pL $cell^{-1}$ d^{-1} (**Figure 3.2B**). Similarly, bleed rates stabilised at distinct levels across conditions, ranging from 0.1 to 0.5 RV d^{-1}. MWP-SG10 required the highest bleed rate approaching 50% of the working volume whereas cultures targeting higher VCCs exhibited lower bleed requirements of approximately 10–20% of the working volume. Notably, for MWP-SG30 and MWP-SG40, the bleed

rates dropped to zero by the end of the cultivation period, a result which is consistent with the reduced growth observed under these conditions.

Similar to the trends observed for bleed rate and CSPR, the analysis of external metabolites – glucose, lactate and ammonium – showed condition-dependent stabilisation patterns (**Figure 3.3A, B** and **C**). While glucose concentrations exhibited some fluctuations, relatively stable levels were observed between day 1 and day 7 for all conditions except MWP-SG10, which stabilised slightly later, between day 3 and day 7 (**Figure 3.3A**). A clear trend emerged, wherein higher VCC targets corresponded to lower average glucose concentrations, reaching a maximum of 42.7 mmol L^{-1} at a VCC of 10×10^6 cells mL^{-1} (MWP-SG10) and minimum of 14.2 mmol L^{-1} at a VCC of 40×10^6 cells mL^{-1} (MWP-SG40). On day 8, glucose concentrations increased across all cultures (**Figure 3.3A**).

In contrast to glucose, lactate levels remained relatively stable throughout the cultivation period, with average concentrations ranging from 9.2 to 15.5 mmol L^{-1} (**Figure 3.3B**) Interestingly, MWP-SG10 exhibited the highest lactate concentrations (15.5 mmol L^{-1}), despite also having the highest glucose levels (42.8 mmol L^{-1}). Typically, glucose is converted to lactate in a 1:2 molar ratio, meaning lower glucose concentrations would be expected to result in higher lactate concentration. However, the observed data suggest a potential metabolic shift from lactate production to consumption at the higher VCC conditions (MWP-SG30 and MWP-SG40), even though glucose was not depleted.

To explore this possibility, the lactate-to-glucose yield ($Y_{Lac/Gluc}$) was calculated (**Figure 3.3D**). A metabolic shift toward lactate consumption would be expected to result in a decrease in this yield. However, the $Y_{Lac/Gluc}$ remained largely stable, with a slight increase from day 4 onwards, indicating continued and consistent glucose-to-lactate conversion. Notably, $Y_{Lac/Gluc}$ values at MWP-SG10 were twice as high as those observed at higher VCC targets (**Figure 3.3D**).

Ammonium concentrations remained within a relatively narrow and stable range of 5.5–8.5 mmol L^{-1} throughout the cultivation (**Figure 3.3C**). Interestingly unlike glucose and lactate, ammonium concentrations stabilised at two distinct concentrations rather than displaying a clear VCC dependent trend across all four conditions. Specifically, MWP-SG10 and MWP-SG20 stabilised at approximately 6 mmol L^{-1} while MWP-SG30 and MWP-SG40 maintained higher levels around 7.5 mmol L^{-1} (**Figure 3.3C**). The deviation from the anticipated pattern of distinct, VCC-specific stabilization indicates that ammonium accumulation may not exhibit a linear correlation with viable cell concentration under the given conditions. This observation may also be attributed to amino acid degradation, which can release ammonium as a byproduct.

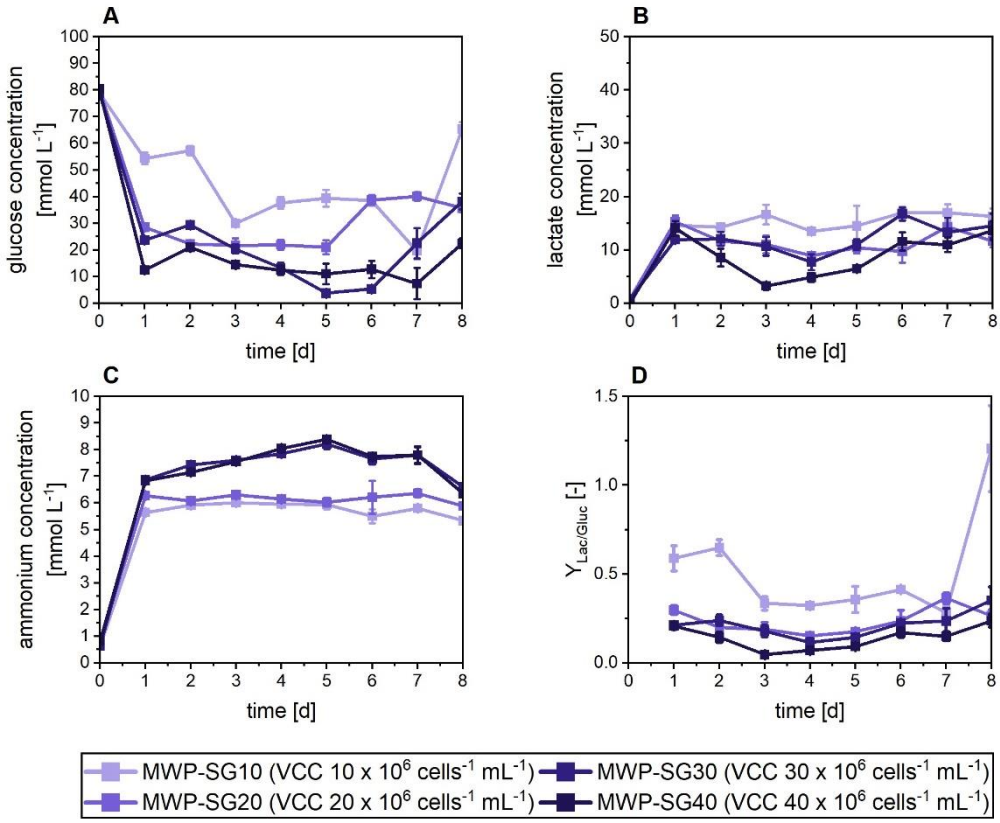

Figure 3.3: Metabolite concentrations for CHO cobra cells in 24-well MWP cultivations in semi-perfusion with implemented cell bleeds. Cells were inoculated at 10, 20, 30, and 40 × 10^6 cells mL^{-1} and cultivated in HIP medium supplemented with 30% Feed B (v/v). (a) glucose; (b) lactate; (c) ammonium; (d) $Y_{Lac/Gluc}$. Targeted average VCCs (×10^6 cells mL^{-1}): 10 (■, light), 20 (■, medium-light), 30 (■, medium-dark), 40 (■, dark). Mean of N = 3 wells. CHO, Chinese hamster ovary; CSPR: cell specific perfusion rate; HIP, high intensity perfusion medium; MWP, microwell plate; SG: stable growth; VCC, viable cell concentrations.

In addition to metabolic profiling, cell-specific productivity (q_P) and space-time-yields (STY) were assessed across the VCC conditions (**Figure 3.4**). Interestingly, q_P increased with rising VCC targets, reaching a maximum of 39.6 ± 2.8 pg $cell^{-1}$ d^{-1} at a VCC of 40 × 10^6 cells mL^{-1} (MWP-SG40), compared to a minimum of 18.3 ± 1.7 pg $cell^{-1}$ d^{-1} (MWP-SG10, **Figure 3.4A**). Statistical analysis confirmed that q_P values for MWP-SG10 differed significantly from all other conditions ($p < 0.001$), while MWP-SG20 was significantly different to MWP-SG30 and MWP-SG40 ($p < 0.05$). No statistically significant difference was observed between MWP-SG30 and MWP-SG40, indicating a plateau in q_P at the higher VCC range (**Figure 3.4A**).

STY profiles exhibited an initial rise before reaching a steady state, with the duration of increase varying between conditions (**Figure 3.4B**). Cultures with higher VCC targets (MWP-SG30 and MWP-SG40) showed prolonged STY increases until day 4, while MWP-SG20 stabilised by day 2, and MWP-SG10 plateaued after day 1. Once stabilised, STY levels were distinct and positively correlated with VCC targets. Specifically, the average STY between days 4 and 8 was 0.07, 0.20, 0.48 and 0.71 g L^{-1} d^{-1} for MWP-SG10, MWP-SG20, MWP-SG30 and MWP-SG40, respectively (**Figure 3.4B**).

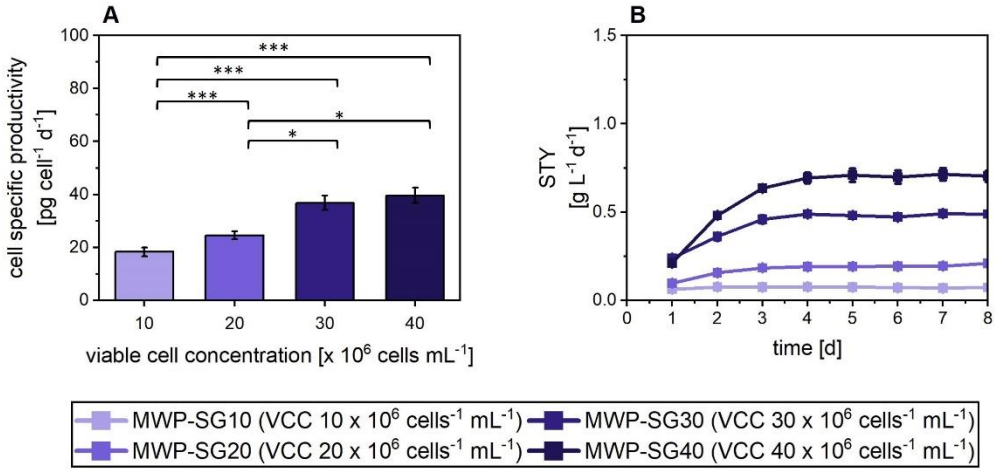

Figure 3.4: Productivity for CHO cobra cells in 24-well MWP cultivations in semi-perfusion with implemented cell bleeds. Cells were inoculated at 10, 20, 30, and 40 × 10^6 cells mL^{-1} and cultivated in HIP medium supplemented with 30% Feed B (v/v). (a) cell specific productivity; (b) STY. Targeted average VCCs (×10^6 cells mL^{-1}): 10 (■, light), 20 (■, medium-light), 30 (■, medium-dark), 40 (■, dark). Mean of *N = 3* wells. Error bars indicate standard deviation. Significant difference was evaluated with a two-sample t-test assuming equal variance with * $p < 0.05$ and ** $p < 0.001$. CHO, Chinese hamster ovary; HIP, high intensity perfusion medium; MWP, microwell plate; SG: stable growth; STY: space time yield; VCC, viable cell concentrations.

3.2.2 Implementation of cell bleeds in 6-well deep plates and shake flasks

Based on the evaluation of the MWP system, the two most promising conditions were selected for scale-up into a larger working volume (V_W = 30 mL), representative of a 125 mL shake flask (SF) as scale-down model. The chosen VCC targets – 20 × 10^6 and 30 × 10^6 cells mL^{-1} – were selected as optimal trade-offs between stable cell growth, favourable metabolic profiles, and high productivity. To further investigate scalability and operational feasibility, a novel deep-well plate (DWP) configuration was investigated in parallel with conventional SF cultures assessing cellular performance and manual handling requirements across platforms at the same scale (DWP vs. SF). As in previous experiments, cultures were inoculated near their respective VCC targets—specifically at 16, and 26 × 10^6 cells mL^{-1}. The conditions are hereafter referred to as DWP-SG20 and DWP-SG30 for the 6-well DWP format, and SF-SG20 and SF-SG30 for the 125 mL SF format, corresponding to target average VCCs of 20, and 30 × 10^6 cells mL^{-1}, respectively.

The agitation speed of DWP cultures was set to 250 rpm, consistent with conditions used for MWP studies. This speed lies within the supplier-recommended range for CHO cell cultures (typically 225 rpm at an orbital diameter of 25 mm), and was selected to ensure sufficient oxygen transfer, particularly under HCD conditions, as well as to allow direct comparison with the MWP results. In contrast, SF cultures were agitated at 180 rpm for safety concerns. Unlike plate-based systems, which were supported by a clamp system within the incubator, SFs rest only on adhesive pads on the shaker platform without additional clamp systems, making higher agitation speeds potentially unstable. Concerns regarding potential oxygen limitations due to the reduced agitation rate in SF cultures were evaluated. However, the larger gas–liquid interface in SFs, combined with the

absence of viability loss in prior internal studies at HCD (data not shown), led to the conclusion that the chosen agitation conditions were sufficient to support the targeted VCCs.

All cultivations exhibited the characteristic "saw-wave" VCC profile throughout the 10-day process (**Figure 3.5A**). The resulting average VCCs were 21.8±2.5, and 28.3±3.1 × 10^6 cells mL^{-1} for DWP-SG20 and DWP-SG30, respectively as well as 24.0±1.5, and 32.7±2.3 × 10^6 cells mL^{-1} for SF-SG20 and SF-SG30, respectively. Overall, the average VCCs closely aligned with the intended targets across both systems and VCC targets. However, SF cultures achieved consistently higher VCCs compared to their DWP counterparts at both VCC targets. Notably, for DWP-SG30, a decline in cell growth was observed during the final two days of cultivation (day 9 and 10) during which the pre-bleed VCC peak was not reached. This decline coincided with a drop in viability, which decreased from 80–90% on day 5 to below 70% by day 10. This trend may be indicative of insufficient mass transfer or underlying metabolic shifts, which are explored in the subsequent discussion. In contrast, all SF cultures, as well as the DWP-SG20 condition, maintained viabilities above 90% throughout the entire cultivation period (**Figure 3.5A**).

Despite some variability, all cultures exhibited stable growth trends over time, as evidenced by relatively consistent CSPRs and bleed rates across conditions (**Figure 3.5B** and **C**). CSPR dynamics stabilised after day 2, maintaining constant levels for the majority of the cultivation period. Specifically, average CSPRs were 27.7±2.9, 27.8±2.2, 25.8±1.3, and 24.3±1.5 pL $cell^{-1}$ d^{-1} for DWP-SG20, DWP-SG30, SF-SG20, and SF-SG30, respectively. Toward the end of cultivation, CSPRs gradually increased across all conditions, with the most pronounced rise observed in the DWP cultures. Final CSPR exceeding 41.7 and 45.6 pL $cell^{-1}$ d^{-1}, DWP-SG20 and DWP-SG30, respectively, whereas SF cultures reached lower maxima of 31 - 34 pL $cell^{-1}$ d^{-1} by day 10 (**Figure 3.5B**). Bleed rates exhibited greater fluctuations but overall stabilised around two distinct levels based on the respective VCC targets and remained largely consistent between the DWP and SF systems (**Figure 3.5C**). For the 20 × 10^6 cells mL^{-1} condition, the bleed rate stabilised around 0.3 RV d^{-1}, whereas for the 30 × 10^6 cells mL^{-1} conditions, it decreased to 0.1 RV d^{-1}. Notably, DWP-SG30 exhibited increased fluctuations in bleed rate from day 5 onward, including several instances where the rate dropped to zero (**Figure 3.5C**). This pattern corresponded with the observed decline in viability and cell growth for this condition (**Figure 3.5A** and **C**).

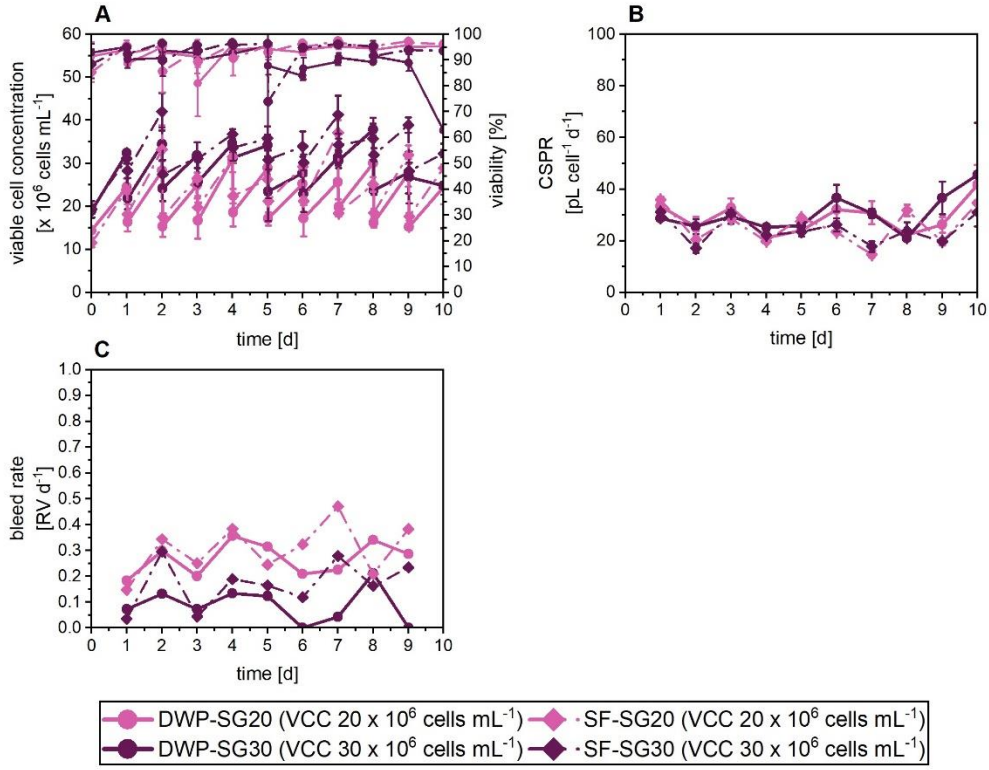

Figure 3.5: Growth, cell-specific perfusion rates, and bleed rates for CHO cobra cells in six-well deepwell plate and shake flask (SF) cultivations in semi-perfusion with implemented cell bleed strategy. Cells were inoculated at 20 and 30 × 10^6 cells mL^{-1} and cultivated in HIP medium supplemented with 30% Feed B (v/v). (a) VCC (filled) and viability (open); (b) CSPR; (c) bleed rate. SDM model: DWP (●, straight), SF (◆, dashed), targeted average VCCs (× 10^6 cells mL^{-1}): 20 (pink), 30 (purple). Mean of N = 3 wells. Error bars indicate standard deviation. CHO, Chinese hamster ovary; DWP, deepwell plate; SDM: scale-down model; SF: shake flask; SG: stable growth; VCC, viable cell concentrations.

The evaluation of extracellular metabolites across both VCC setpoints and cultivation systems revealed comparable overall trends, with metabolite concentrations stabilising shortly after the initiation of semi-perfusion (**Figure 3.6**). Glucose and ammonium levels demonstrated VCC target-dependent stabilisation. For cultures targeting 20 × 10^6 cells mL^{-1}, glucose concentration stabilised around 33 - 34 mmol L^{-1}, whereas lower concentrations were observed for the 30 × 10^6 cells mL^{-1} target – approximately 20 mmol L^{-1} for DWP-SG30 and 27 mmol L^{-1} for SF-SG30 (**Figure 3.6A**). Ammonium levels remained below 10 mmol L^{-1} throughout most of the cultivation period, with average values of approximately 5.5 for the 20 × 10^6 cells mL^{-1} target and 8.0 mmol L^{-1} for the 30 × 10^6 cells mL^{-1} target (**Figure 3.6C**). A slight increase in ammonium concentration was noted toward the end of the process, exceeding 10 mmol L^{-1} only in DWP-SG30. In contrast, lactate concentrations did not show a VCC target-dependent stabilisation pattern (**Figure 3.6B**). Instead, lactate levels plateaued at similar concentrations across all conditions and cultivation systems, averaging between 10 and 11 mmol L^{-1} in both DWP and SF cultures. Despite these differences in absolute metabolite levels, the lactate-to-glucose yield ($Y_{Lac/Gluc}$) remained consistent across most conditions, with values stabilising around 0.22. The only exception was observed in DWP-SG20, which exhibited a slightly elevated yield of 0.29 (**Figure 3.6D**).

Owing to the larger sample volumes available in the DWP and SF cultures, it was possible to quantify an additional extracellular metabolite – glutamate (**Figure 3.6E, F**). Glutamate concentrations remained stable around 5.5 mmol L^{-1} across all conditions, except DWP-SG30, which exhibited a marked increase beginning on day 4, reaching up to 7.7 mmol L^{-1}. This increase coincided with a decline in cell viability observed from day 5 onward in the same culture. Notably, the specific glutamate production rate in DWP-SG30 was significantly higher ($p < 0.001$) compared to DWP-SG20 and SF-SG30 (**Figure 3.6E, F**), suggesting a possible link between increased glutamate accumulation and reduced culture performance. (**Figure 3.6E, F**). Furthermore, glutamate production was significantly higher in SF-SG20 compared to the corresponding DWP condition ($p < 0.05$) but remained significantly lower than that observed in SF-SG30 ($p < 0.05$).

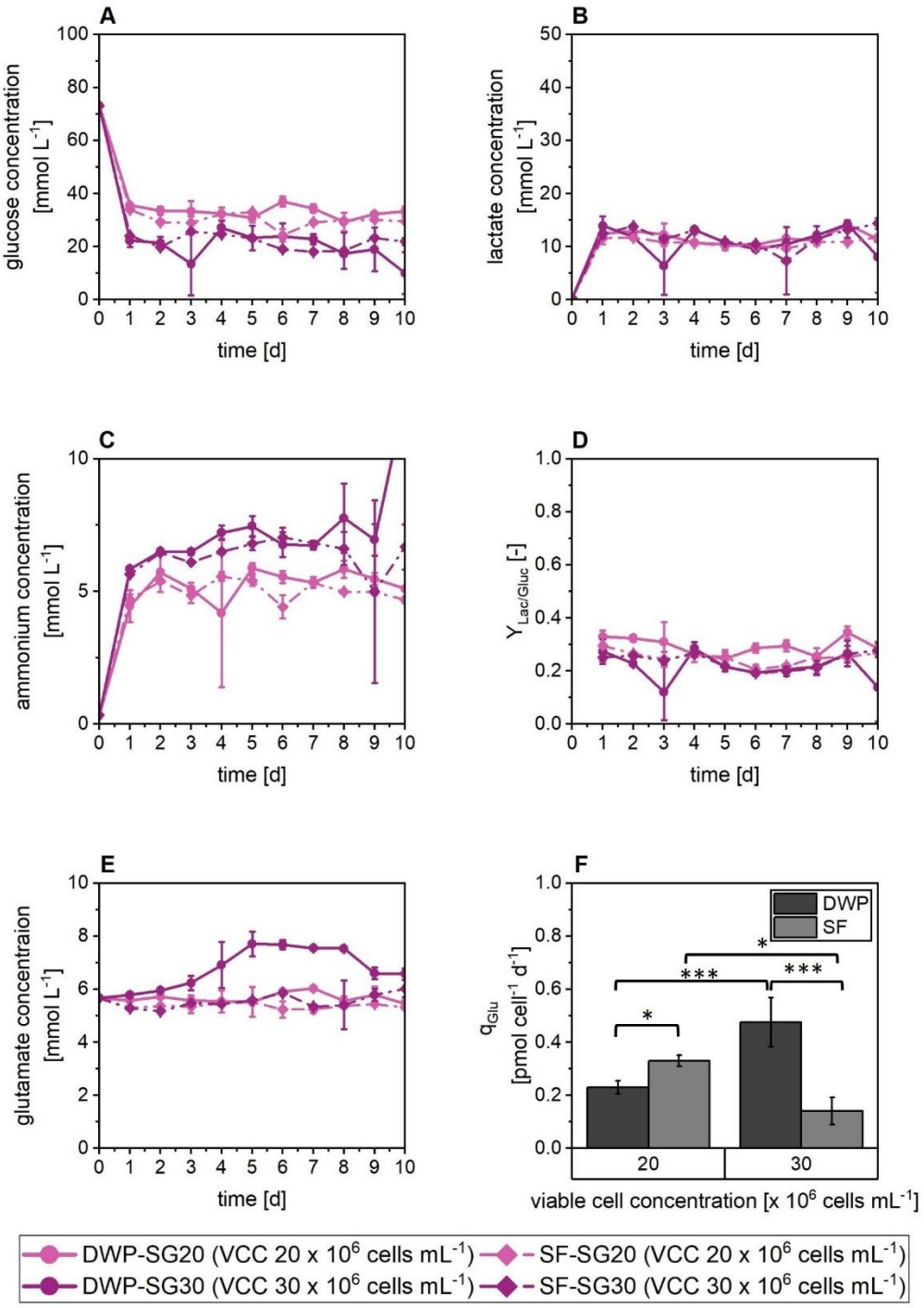

Figure 3.6: Metabolite concentrations for CHO cobra cells in 6-well DWP and SF cultivations in semi-perfusion with implemented cell bleed strategy. Cells were inoculated at 20 and 30 × 10^6 cells mL^{-1} and cultivated in HIP medium supplemented with 30% Feed B (v/v). (a) glucose; (b) lactate; (c) ammonium; (d) glutamate (e) $Y_{Lac/Gluc}$. SDM model: DWP (●, straight), SF (◆, dashed), targeted average VCCs (× 10^6 cells mL^{-1}): 20 (pink), 30 (purple). Mean of *N = 3* wells. Error bars indicate standard deviation. Significant difference was evaluated with a two-sample t-test assuming equal variance with * $p < 0.05$ and ***$p < 0.001$. CHO, Chinese hamster ovary; DWP, deepwell plate; SDM: scale-down model; SF: shake flask; SG: stable growth; VCC, viable cell concentrations.

In addition to metabolic profiling, cell-specific productivity (q_P) and space-time-yields (STY) were assessed across the VCC conditions (**Figure 3.7**). In DWP cultures, q_P values were comparable between the two VCC targets, averaging approximately 30 pg $cell^{-1}$ d^{-1} (**Figure 3.7A**). In contrast, SF cultures displayed a significant difference in q_P between VCC targets ($p < 0.01$), with SF-SG20

yielding lower values of 22 pg cell^{-1} d^{-1}, while SF-SG30 achieved q_P levels similar to those observed in DWP cultures (~30 pg cell^{-1} d^{-1}). A cross-system comparison revealed a significant difference ($p < 0.001$) between DWP and SF cultures at the 20 × 10^6 cells mL^{-1} target, whereas no significant difference was observed at the higher target (**Figure 3.7A**).

The STY profiles exhibited an initial increase before reaching a plateau (**Figure 3.7B**). Most cultures displayed a rise in STY until day 3, after which values stabilised. However, SF-SG30 showed a continuous increase until day 7, followed by a slight decline towards day 10. Though STY levels were distinct and positively correlated with VCC targets. Overall, STY levels were distinct and positively correlated with the VCC target. Specifically, the average STY between days 3 and 10 were 0.25, 0.37, 0.20 and 0.38 g L^{-1} d^{-1} for DWP-SG20, DWP-SG30, SF-SG20 and SF-SG30, respectively (**Figure 3.7B**).

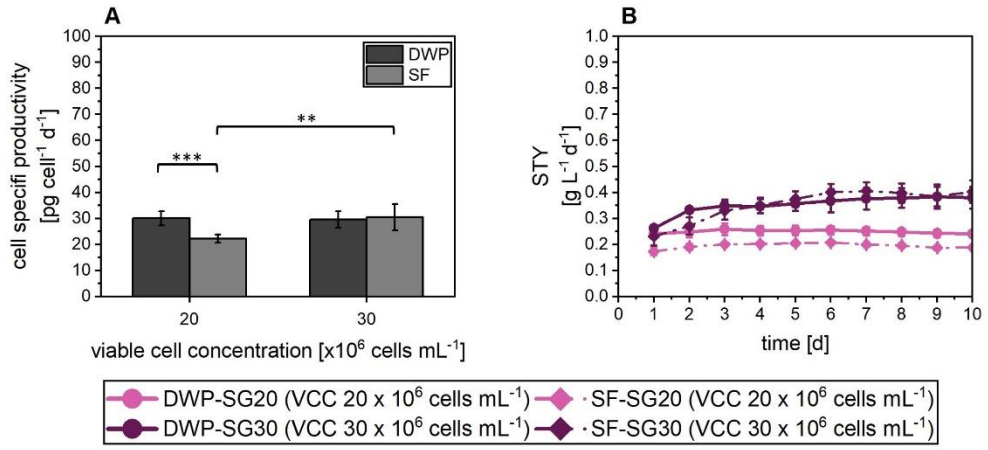

Figure 3.7: Productivity for CHO cobra cells in 6-well DWP and SF cultivations in semi-perfusion with implemented cell bleed strategy. Cells were inoculated at 20 and 30 × 10^6 cells mL^{-1} and cultivated in HIP medium supplemented with 30% Feed B (v/v). (a) cell specific productivity; (b) STY. SDM model: DWP (●, straight), SF (◆, dashed), targeted average VCCs (× 10^6 cells mL^{-1}): 20 (pink), 30 (purple). Mean of *N = 3* wells. Error bars indicate standard deviation. Significant difference was evaluated with a two-sample t-test assuming equal variance with ** $p < 0.01$ and ***$p < 0.001$. CHO, Chinese hamster ovary; DWP, deepwell plate; SDM: scale-down model; SF: shake flask; SG: stable growth; STY: space time yield; VCC, viable cell concentrations.

3.2.3 Comparison across scales – MWP vs DWP and SF

In the following section, a comparative evaluation of the three cultivation systems is presented. To enable a realistic assessment across scales, key performance indicators—including viable cell growth, specific growth rate, bleed rate, and cell-specific productivity—are shown in **Figure 3.8**, while specific glucose consumption rates, lactate and ammonium production rates, and the lactate-to-glucose yield are presented in **Figure 3.9** for both VCC targets of 20 and 30 × 10^6 cells mL^{-1}.

Viable cell concentration and viability for the two VCC targets are shown in **Figure 3.8A** and **B**, respectively. Across all three cultivation systems, comparable growth profiles and viabilities were observed, particularly at the lower VCC target of 20 × 10^6 cells mL^{-1}. However, some divergence

was evident at the higher VCC target of 30 × 10^6 cells mL^{-1}. In these conditions, both plate-based systems exhibited reduced growth, characterised by their inability to reach the intended VCC prior to cell bleeding, as well as a more pronounced decline in cell viability over time. This may be attributed to cell exhaustion over time, whereby the cellular reserves were depleted. In contrast, the SF cultures maintained robust cell growth throughout the cultivation period and consistently high viability levels (**Figure 3.8A** and **B**).

Across all cultivation systems, the average specific growth rates (over the entire cultivation period) exhibited similar trends at both VCC targets, showing a consistent decline in their value with increasing VCC. Specifically, the growth rates decreased from 0.02 to 0.01 h^{-1}, accompanied by a corresponding reduction in bleed rates from 0.3 to 0.1 RV d^{-1}, reflecting their direct dependence on cellular proliferation (**Figure 3.8C** and **D**). While the daily cell bleed and medium exchange procedures were designed to achieve a consistent perfusion rate of 1 RV d^{-1} across all systems, the operational workflows differed slightly between well plate formats (MWP and DWP) and shake flasks (SF). In the case of SF cultures, the cell bleed required transferring the culture into centrifuge tubes, followed by centrifugation, removal of the supernatant, and resuspension of the cell pellet in fresh medium prior to returning the culture to the flask. By contrast, in the MWP and DWP systems, centrifugation and medium exchange could be performed directly within the cultivation vessel, streamlining the workflow and reducing manual handling.

Although the cell specific productivity was largely comparable between the MWP, DWP and SF cultures (**Figure 3.8E**), significant difference was observed at the lower VCC target of 20 × 10^6 cells mL^{-1} between the DWP and MWP systems at the 5% significance level ($p < 0.05$). However, this difference was not statistically significant at the more stringent 1% level ($p < 0.01$) (**Figure 3.8E**), as previously observed between SF and DWP cultures (**Figure 3.7A**). The comparison of STY profiles demonstrated similar overall dynamics across the three systems (**Figure 3.8F**). Notably, MWP-SG30 achieved higher STY values compared to the corresponding DWP and SF conditions, whereas MWP-SG20 exhibited STY dynamics that were closely aligned with both DWP and SF cultures.

A summary of the resulting titres and cell-specific productivities for the MWP, DWP, and SF systems is presented in **Table 3.1**, alongside a comparison with published data using spin tubes as a scale-down model (SDM).

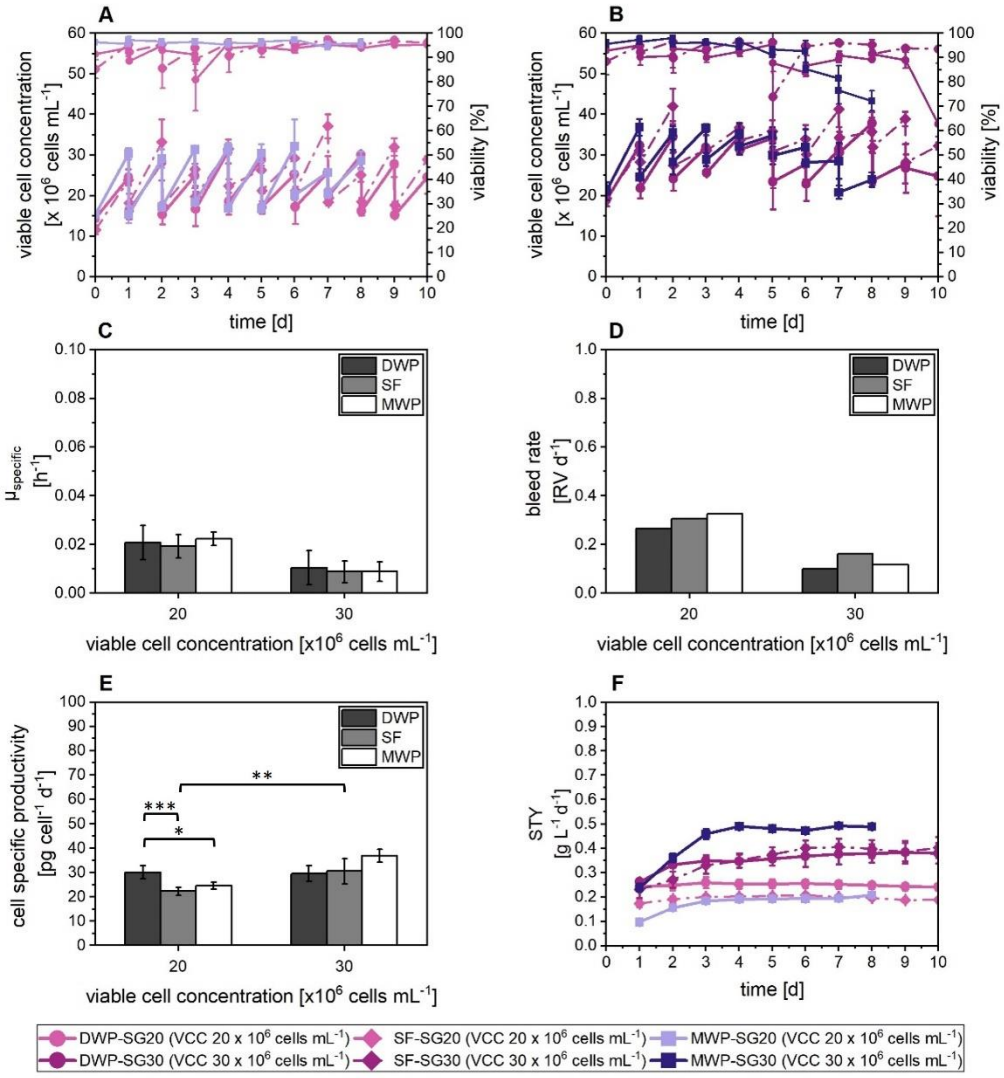

Figure 3.8: Growth, process flow rates and productivities for CHO cobra cells in 24-well MWP cultivation, 6-well DWP cultivations and SFs. Cells were inoculated at 20 and 30 × 10^6 cells mL^{-1} and cultivated in HIP medium supplemented with 30% Feed B (v/v). (a) VCC (filled) and viability (open); (b) CSPR; (c) growth rate; (d) bleed rate; (e) cell specific productivity; (f) STY. SDM model: MWP (■, straight), SDM model: DWP (●, straight), SF (◆, dashed), targeted average VCCs (× 10^6 cells mL^{-1}): 20 (light shaded), 30 (dark shaded), mean of N = 3 wells. Error bars indicate standard deviation. Significant difference was evaluated with a two-sample t-test assuming equal variance with * $p < 0.05$, ** $p < 0.01$ and ***$p < 0.001$. CHO, Chinese hamster ovary; DWP, deepwell plate; MWP: microwell plate; μ: specific growth rate; SDM: scale-down model; SF: shake flask; SG: stable growth; STY: space time yield; VCC, viable cell concentrations.

A comparative analysis of cell-specific metabolism across the three cultivation systems revealed consistent trends in nutrient consumption and by-product formation. Specifically, the q_{Gluc} were comparable across all cultivation systems and VCC targets, with no statistically significant differences observed (**Figure 3.9A**). This consistency extended to q_{Lac} and q_{Amm} values (**Figure 3.9B** and **C**). At the lower VCC target of 20 × 10^6 cells mL^{-1}, q_{Lac} values were marginally higher than those observed at 30 × 10^6 cells mL^{-1} across all systems. The lowest q_{Lac} was observed in SF cultures at the higher VCC target; however, this difference was within the margin of error and not statistically significant. A similar pattern was noted for q_{Amm}, with slightly reduced production at higher VCC but no significant variation between cultivation formats. Importantly, q_{Lac} and q_{Amm}

values remained below 1.0 pmol cell^{-1} d^{-1} in all systems and across both VCC targets, indicating consistent metabolic by-product generation and accumulation under semi-perfusion conditions (**Figure 3.9B** and **C**).

In addition to the specific consumption and production rates, the lactate-to-glucose yield ($Y_{Lac/Gluc}$) was evaluated to assess the efficiency of glucose utilisation (**Figure 3.9D**). In MWP cultures, $Y_{Lac/Gluc}$ decreased during the early cultivation phase, reaching minimum values between 0.11 and 0.15 $mmol_{Lac}$ $mmol_{Glc}^{-1}$ on day 4, followed by a gradual increase until the end of cultivation on day 8. In contrast, DWP and SF cultures exhibited more stable $Y_{Lac/Gluc}$ profiles throughout the cultivation period. Nevertheless, all systems maintained similar overall yield values across both VCC targets, indicating consistent metabolic efficiency.

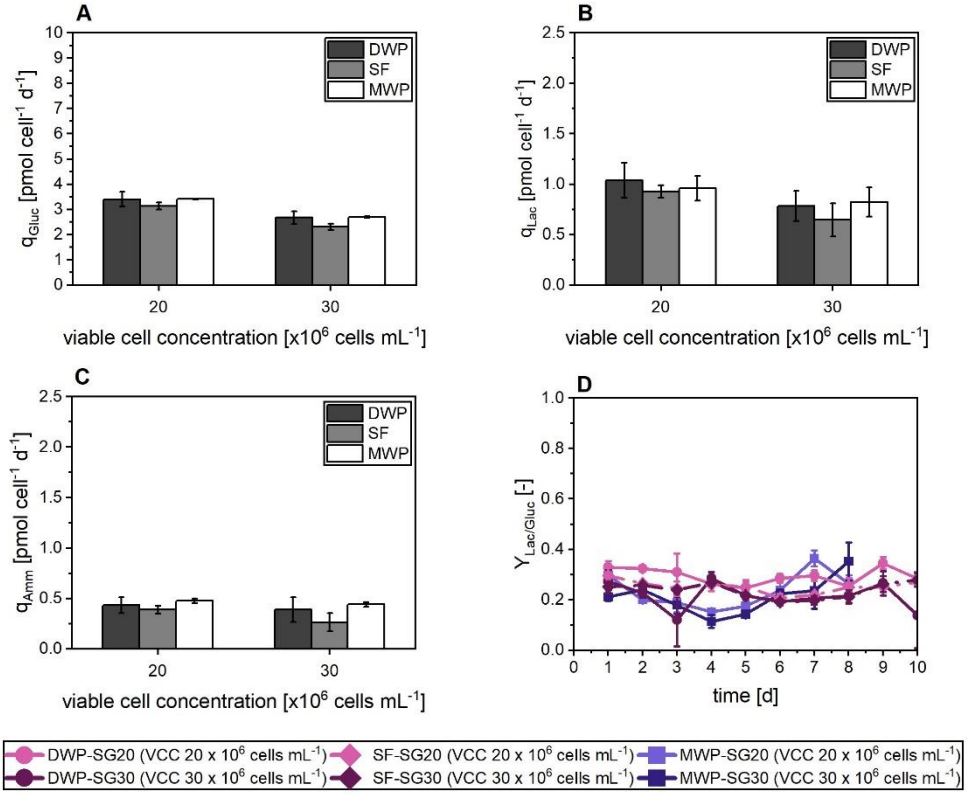

Figure 3.9: Cell specific metabolic rates for CHO cobra cells in 24-well MWP cultivation, 6-well DWP cultivations and SFs. Cells were inoculated at 20 and 30 × 10^6 cells mL^{-1} and cultivated in HIP medium supplemented with 30% Feed B (v/v). (a) cell specific glucose consumption rate; (b) cell specific lactate production rate; (c) cell specific ammonium production rate; (d) $Y_{Lac/Gluc}$. SDM model: MWP (■, straight), SDM model: DWP (●, straight), SF (◆, dashed), targeted average VCCs (× 10^6 cells mL^{-1}): 20 (light shaded), 30 (dark shaded), mean of N = 3 wells. Error bars indicate standard deviation. CHO, Chinese hamster ovary; DWP, deepwell plate; MWP: microwell plate; SDM: scale-down model; SF: shake flask; SG: stable growth; VCC, viable cell concentrations.

It is also noteworthy that the medium consumption associated with screening both VCC conditions in MWPs was substantially lower compared to DWP and SF systems. The MWP format consumed approximately 260 mL of medium over an 8-day period using a sacrificial well approach, whereas each DWP and SF system required approximately 1800 mL over 10 days to assess the same two conditions within a single unit. This represents nearly a 7-fold increase in

medium usage for the larger-scale systems, underscoring the resource efficiency of MWPs for early-stage process development.

Table 3.1: Comparison of scale-down models in semi-perfusion with implemented cell bleed. Literature values are compared to experimental MWP, DWP and SF results obtained for cultivations with perfusion medium in regards of productivities and perfusion parameters.

Reference/ Experiment	**SDM**	**V_W [mL]**	**VCC target [x10^6 cells mL^{-1}]**	**titre [g L^{-1}]**	**q_P [pg cell^{-1} d^{-1}]**
Wolf et al. (2018)*^{o}	ST	10	10	0.1 ± 0.01	N/A
			20	0.21 ± 0.01	10.12 ± 0.65
			30	0.32 ± 0.03	N/A
			40	N/A	10.00 ± 1.77
		30	20	N/A	N/A
Mayrhofer et al. (2021)**	ST	10	46	0.7	18
			45	0.6	16
Microwell culture in "quasi steady-state" condition***	MWP	1.2	10	0.11 ± 0.01	18.3 ± 1.6
			20	0.26 ± 0.01	24.5 ± 0.1
			30	0.49 ± 0.03	36.8 ± 2.6
			40	0.68 ± 0.03	39.6 ± 2.8
Scale-up of "quasi steady-state" condition#	DWP	30	20	0.33 ± 0.03	30.1 ± 2.7
			30	0.41 ± 0.05	29.57 ± 3.2
	SF		20	0.26 ± 0.01	22.2 ± 1.5
			30	0.49 ± 0.03	30.5 ± 5.1

*values are given for the last 5 days of culture; proprietary CHO cell line in chemically defined medium (both Merck)
**values are given for days 6 – 14 of culture; CHO-K1 cell line in ActiPro + CB1/3 or NS0 + CB1/3
***values are given for 8 days of culture
values are given for 10 days of culture
^{o} productivity and titre values were not measured due to reduced cellular performance caused by oxygen limitation
SDM: scale down model; ST: spin tube; MWP: microwell plate; V_W: working volume; VCC: viable cell concentration; P: perfusion rate; RV: reactor volume; q_P: cell specific productivity, N/A: data not available.

3.3 Discussion

In this chapter, the feasibility of MWPs as a small-scale model to operate at a "quasi steady-state" with cell bleeds was evaluated. Additionally, a 6-well deepwell plate (DWP) was evaluated as a potential scale-up model, transitioning from the small-scale MWP system to a larger working volume of 30 mL. The results were then compared across different scales and cultivation systems with the aim to assess their suitability for a robust screening platform.

The implementation of a cell bleed step aimed at establishing a "quasi steady-state" environment to the cell culture. Thus, maintaining an on average stable VCC throughout the cultivation process was critical for ensuring stable metabolic activity and consistent productivity. The results show

that the implementation of the cell bleed step allowed for the stabilisation of the culture conditions, as evidenced by the stabilisation of CSPRs, bleed rates and metabolite concentrations after day 2 of cultivation.

Previous studies had explored the use of spin tubes (V_W = 10 mL) as SDMs for the development and optimisation of steady-state perfusion bioreactor operations using suspension CHO cell cultures in chemically defined media (Mayrhofer et al., 2021; Wolf et al., 2018). These investigations demonstrated that spin tubes are capable of reliably mimicking key aspects of perfusion bioreactors, including productivity, flow rates, and steady-state stability. However, it has also been noted that greater comparability to bioreactor systems may be achieved through the use of more automated platforms (Wolf et al., 2018). Despite their utility, spin tubes are limited by their lack of automation capabilities, resulting in labour-intensive workflows and restricted experimental throughput.

In contrast well plate systems have already been integrated into automated platforms for fed-batch operations (Wang, Albanetti, Miro-Quesada, et al., 2018), offering the potential for high-throughput and more controlled experimentation. Nevertheless, methodologies to extend their application to perfusion-like conditions remain underexplored.

The results obtained from MWP experiments in this chapter indicated improved performance in key process parameters—such as flow rates, cell growth, and productivity—when compared to previous studies using spin tubes (**Table 3.1**, Mayrhofer et al., 2021; Wolf et al., 2018). Metabolite trends observed in this work were consistent with those reported in spin tube cultivations, particularly with respect to lactate accumulation at lower VCC targets (Wolf et al., 2018). This similarity supports the potential of MWP-based systems, operated in semi-perfusion with cell bleeds, as a suitable and alternative platform for predicting key parameters relevant to steady-state perfusion bioreactors.

Although the small working volume of MWPs poses some limitations in terms of metabolite analysis, essential metabolites such as glucose, lactate, and ammonium—commonly monitored in industrial settings—were successfully measured, providing valuable insight into cellular performance. Importantly, the inherent compatibility of MWPs with automation enables high-throughput screening under controlled conditions, offering a distinct advantage over spin tubes for early-stage process development and optimisation.

In addition to the MWP-based experiments, this study investigated the application of a novel DWP format as a potential scale-up platform with a working volume of 30 mL. The geometry of the DWP—specifically its liquid height, inner diameter, and bottom shape (**Figure 3.1**)—more closely resembles that of a spin tube than a SF, making it an appealing intermediate SDM. Previous work

by Wolf et al., 2018 assessed STs at working volumes of 10 mL and 30 mL and found that growth performance was comparable at a VCC target of 20 × 10^6 cells mL^{-1}. However, at a higher VCC target of 40 × 10^6 cells mL^{-1}, growth could not be sustained, which was hypothesised to result from oxygen limitations.

The DWP system supported growth at both VCC targets of 20 and 30 × 10^6 cells mL^{-1} though a decline in viability was observed at the higher VCC toward the end of cultivation. One explanation for this decline could be insufficient oxygen supply, as was previously hypothesised in the ST system. However, in contrast to ST results, the viability decrease in DWP cultures was observed earlier in the process, while growth was only affected later in the cultivation. Notably, the maximum VCC tested in the DWP system was 30 × 10^6 cells mL^{-1}, compared to 40 × 10^6 cells mL^{-1} in STs, which may explain the better performance in terms of growth maintenance. It is plausible that oxygen limitations could become more critical in the DWP format at even higher cell densities.

Another hypothesis for the observed viability decline—particularly from day 5 onward—is related to changes in metabolite profiles. Although lactate concentrations remained stable and comparable across conditions, elevated extracellular glutamate levels on top of the lactate concentrations may have contributed to a reduction in pH. This hypothesis emerged following metabolite analyses; however, pH measurements were not recorded during sampling, preventing its confirmation. Future work should include pH monitoring to verify this effect.

Furthermore, the focus for metabolite analysis was set on toxic by-products, given the increasing industrial use of glutamine synthetase (GS) cell lines, which can grow in glutamine-free media. Nonetheless, future studies may benefit from the inclusion of glutamine quantification to better characterise metabolic dynamics in CHO cell lines that require external glutamine supplementation.

The comparison of DWP and SF cultivations revealed similar trends in cell growth and productivity, with only minor differences in average VCC. Notably, SF cultures consistently reached slightly higher VCCs, which is likely attributable to differences in the centrifugation step. While MWP centrifugation produces tightly packed pellets that allow efficient medium removal without disturbing the cells, the larger volume in DWPs and SFs requires longer or more forceful centrifugation. SF cultures were transferred to 50 mL centrifuge tubes and spun at higher speeds, consistent with literature protocols (Bielser, 2019; Mayrhofer et al., 2021; Wolf et al., 2018). In contrast, DWPs were centrifuged as intact units using the same speed as MWPs, but for an extended duration (50 g, 10 min). This resulted in less compact cell pellets in DWPs and likely caused greater unintended cell loss during supernatant removal.

Despite these operational challenges, DWP handling was relatively straightforward and did not require additional consumables, such as centrifuge tubes, thereby reducing labour and contamination risks. In contrast, SF processing was more labour-intensive and generated more waste due to the need for additional handling steps and materials. From a sustainability perspective, the DWP system also offered benefits in terms of reduced incubator space and consumable usage. For example, two conditions in triplicate could be accommodated in a single DWP, whereas six individual SFs would be required for the same experimental design.

Both DWP and SF systems yielded comparable results to those observed in the MWP format, suggesting consistency across scales. However, based on two key observations, the DWP system appeared to offer a closer representation of the MWP model. First, at the higher VCC target of 30×10^6 cells mL^{-1}, both MWP and DWP cultures exhibited a similar reduction in growth toward the end of the cultivation period, whereas SF cultures did not. Second, at the lower VCC target of 20×10^6 cells mL^{-1}, the cell specific productivity (q_P) increased upon scaling from MWP to DWP, but declined when scaling from MWP to SF. These findings highlight the potential of the DWP as an intermediate, automatable SDM that effectively bridges high-throughput small-scale systems (e.g., MWP) and larger-scale bioreactor processes at bench-scale (1 – 5 L).

3.4 Concluding remarks

The objective of the work presented in this chapter was to implement and evaluate a cell bleed strategy in the 24-well MWP platform. The results demonstrated that high cell concentrations could be maintained at defined setpoints, leading to a stable culture environment indicative of "quasi steady-state" conditions. Importantly, this strategy proved to be scalable to DWP and SF, with performance metrics showing good agreement with alternative SDMs and perfusion bioreactor data reported in the literature.

These findings confirm that MWPs operated in semi-perfusion with an integrated cell bleed step can effectively mimic perfusion bioreactor conditions, similarly to previously established spin tube models. Key process parameters—including cell growth, metabolite concentrations, and productivity—were consistent across scales, supporting the predictive value of this approach. Furthermore, MWPs enable high-throughput parallel testing of multiple cell bleed strategies, significantly accelerating early-stage process development while reducing material use and hands-on time.

The DWP format also showed promising results at two different viable cell concentration (VCC) targets, with trends in metabolic activity and productivity comparable to those observed in MWPs. Unlike spin tubes or shake flasks, DWPs offer improved potential for automation and ease of handling. However, operational limitations were identified, particularly in relation to

centrifugation efficiency and potential cell loss during medium exchange. Despite these challenges, the DWP format provides notable advantages in terms of reduced labour intensity, lower consumable use, and better utilisation of incubator space, contributing to more sustainable process development.

In summary, this study supports the combined use of MWP and DWP platforms as a robust, scalable, and automatable SDM strategy. This approach enables efficient and cost-effective screening of “quasi steady-state” perfusion conditions, providing a strong foundation for the development and scale-up of perfusion bioreactor processes.

Chapter 4: Platform development for high-throughput perfusion optimisation – Variation of perfusion rate strategies across platforms and scales*

4.1 Introduction

The continuous medium exchange is one of the main characteristics of a perfusion bioreactor as it generates stable process conditions avoiding the accumulation of unwanted and often toxic by-products while providing constant nutrient levels. This results in low product residence times, leading to consistent and improved product quality (Chotteau, 2015).

The amount of exchanged medium is dependent on the perfusion rate and must be optimised for each cell line individually. A widely used strategy involves adjusting the perfusion rate based on the CSPR (Chotteau, 2015), which varies the flow rate in proportion to the VCC and results in a constant CSPR. This leads to a stable metabolic environment throughout the cultivation period (Ozturk, 1996). Additionally, this strategy supports HCD and sustained productivity, provided that the cellular activity remains consistent over time and VCC.

Several approaches have been proposed in the literature to determine the CSPR corresponding to the highest productivity (Chotteau, 2015; Gagnon et al., 2018; Konstantinov et al., 2006). Typically, the perfusion rate is optimised at the bioreactor scale. Rather than operating multiple perfusion bioreactors in parallel with a single condition each, the cell culture is exposed to a different CSPR setpoint by either increasing or decreasing the VCC or perfusion rate. Each exposure lasts several days to allow the system to establish a new steady state before transitioning to another setpoint. During this time, growth, metabolism, and productivity are monitored to identify any limitations.

* Some of the results presented in this chapter are included in:

Dorn, M., Lucas, C., Klottrup-Rees, K., Lee, K., & Micheletti, M. (2024). Platform development for high-throughput optimization of perfusion processes—Part II: Variation of perfusion rate strategies in microwell plates. Biotechnology and Bioengineering, 121(6), 1774–1788. https://doi.org/10.1002/bit.28685

However, operating a perfusion bioreactor is labour- and resource-intensive, and only a limited number of CSPRs can be examined. Alternatively, SDMs such as MWPs could serve as an initial screening tool, as they have been shown to accurately predict primary perfusion parameters such as CSPR, growth, and productivity. In addition, the smaller footprint and working volume allow to investigate a larger range of conditions in high-throughput studies while reducing medium consumption. However, current literature primarily discusses their operation with a fixed perfusion rate strategy based on RV d^{-1} (Mayrhofer et al., 2021; Tregidgo et al., 2023; Villiger-Oberbek et al., 2015; Wolf et al., 2018).

Perfusion processes are designed to create and maintain a physiologically constant environment for the cells. In the previous chapter (**Chapter 3**), cell bleeds were implemented to regulate cell concentration and establish a quasi-steady state under the assumption of constant metabolic consumption. This was achieved through total medium exchanges at a perfusion rate of 1 RV d^{-1}. This chapter is focused on the variation of the perfusion rate to establish a stable environment by adopting a CSPR-based approach, which better reflects a true perfusion bioreactor operation Unlike fixed-rate perfusion, this method adjusts medium exchange dynamically, resulting in partial exchanges occurring once or multiple times per day to ensure adequate nutrient supply for cell growth and production.

The aim of this chapter is to investigate the feasibility and effectiveness of perfusion rate modulation using CSPR-based medium exchange strategies to maintain stable cultures in both MWP and DWP formats. To achieve this aim, the first objective is to implement CSPR-based medium exchange in the 24-well MWP platform and compare the resulting perfusion rates and culture performance to those obtained with a conventional semi-perfusion method using fixed daily medium exchanges. The second objective focuses on exploring the 6-well DWP format as a scale-up option, leveraging its larger working volume to assess the scalability and robustness of the CSPR-based approach. The third objective is to validate the small-scale strategy by transferring the best-performing CSPR condition to a 250 mL perfusion bioreactor, where growth, metabolism, and productivity are evaluated in comparison to the well-plate models. This comparison provides insights into the extent to which small-scale systems can mimic larger bioreactors and supports the development of more scalable and efficient perfusion processes.

4.2 Results

This section of the chapter is divided into two main sections presenting the results and is followed by a discussion section to contextualise the findings. **Section 4.2.1** details the implementation of the CSPR-based perfusion rate strategy across different well-plate scales, while **Section 4.2.2** explores its application in a 250 mL perfusion bioreactor and compares performance with the well-plate systems. All experiments in this chapter were conducted using the CHO cobra cell line.

4.2.1 Implementation of a CSPR-based perfusion rate in well plates

4.2.1.1 24-well microwell plate with CSPR-based perfusion rate

Evaluation of Growth and metabolism of CHO cobra cells with CSPR-based perfusion rate

CSPR values close to the $CSPR_{min}$ were previously associated with optimal productivities while also resulting in a reduction of cost of goods manufactured by allowing a greater number of cells to be sustained per given volume of medium. For the CHO cobra cell line previous studies have indicated a minimum CSPR in the range of 13 – 15 pL cell^{-1} d^{-1} (data not shown). For the CSPR-based perfusion rate strategy, CSPR targets must be selected prior to cultivation with daily medium exchange volumes calculated accordingly. To maintain conditions as close as possible to the $CSPR_{min}$, three CSPR targets – 10, 15 and 20 pL cell^{-1} d^{-1} – were selected and investigated in a maximum growth (MG) condition aiming to achieve HCD. The CSPR-based medium exchange strategy was evaluated with two inoculation concentrations, as shown in **Figure 4.1**. The MWPs were inoculated at CCD between 0.5 – 2.0 x 10^6 cells mL^{-1} and at HCD between 10 – 20 x 10^6 cells mL^{-1}. Additionally, control cultures using a perfusion rate of 1 RV d^{-1} and inoculated at CCD (one) and HCD (two) serve as comparison for growth and productivity outcomes. The MWP cultures with CSPR-based perfusion rate strategy are referred to as CSPR-cultures in general or MWP-MG_10, MWP-MG_15, and MWP-MG_20, for the CSPR targets of 10, 15 and 20 pL cell^{-1} d^{-1}, respectively. Further, cultures with a perfusion rate of 1 RV d^{-1} are referred to as MWP-MG_R1 and MWP-MG_R2 for 1st and 2nd run, respectively.

As shown in **Figure 4.1A**, **B** for cultures inoculated at CCD, all cultures exhibited similar growth patterns with viabilities consistently above 95% throughout the cultivation period. After a brief lag-phase, the cells grew exponentially reaching maximum values between 20.0 and 30.0 × 10^6 cells mL^{-1}. Notably, MWP-MG_R1 (total medium exchange) and MWP-MG_20 (partial medium exchange) achieved nearly identical maximum VCCs of 32.4 ± 1.5 ×10^6 cells mL^{-1} on day 8 and 31.1 ± 0.9 × 10^6 cells mL^{-1} on day 7, respectively. In contrast, MWP-MG_10 and MWP-MG_15 cultures plateaued at 23.0 × 10^6 cells mL^{-1} closely around their maximum VCC values. This suggests that the growth phase of MWP-MG_10 and MWP-MG_15 cultures shifted from an exponential to stationary, whereas MWP-MG_20 continued to grow and reached its maximum VCC at the end of the 8-day period. This observation prompted further investigation in cultures inoculated at HCD, evaluating growth, metabolic, and production performance.

The culture inoculated at HCD exhibited exponential growth from the beginning, as illustrated in **Figure 4.1B**. However, distinct differences emerged between the control cultures MWP-MG_R1 and MWP-MG_R2 starting from day 2. MWP-MG_R1 showed similar performance to the CSPR-cultures, both of which plateaued around 40.0 × 10^6 cells mL^{-1} by day 3. Specifically, MWP-MG_10, MWP-MG_15 and MWP-MG_20 reached maximum VCCs of 46.6 ± 4.4, 44.4 ± 1.2, and

44.7 ± 1.8 × 10^6 cells mL^{-1}, respectively, while MWP-MG_R1 reached 43.5 ± 7.0 × 10^6 cells mL^{-1}. CSPR-cultures maintained VCCs around 40.0 × 10^6 cells mL^{-1} throughout the cultivation period. In contrast, the VCC of MWP-MG_R1 declined from day 6, falling below 30.0 × 10^6 cells mL^{-1} by day 8. Meanwhile, MWP-MG_R2 continued to grow reaching peak values of approximately 70.0 × 10^6 cells mL^{-1} on days 3 and 4. After this peak, the VCC rapidly declined to around 50.0 × 10^6 cells mL^{-1} and continued to decline. Viability remained above 95% for all cultures until day 4, after which it began to decrease. By day 8, viability dropped below 70% for MWP-MG_R1 and MWP-MG_15, and below 80% for the MWP-MG_10. However, MWP-MG_R2 and MWP-MG_20 maintained viabilities above 90% throughout the cultivation period. Overall, the cultures inoculated at HCD reached higher maximum VCCs and plateaued at elevated values, suggesting that the inoculation concentration influences the maximum VCCs achievable in the culture.

The analysis of external metabolites (glucose, lactate, and ammonium) revealed similar dynamics across culture runs with different perfusion rate strategies (**Figure 4.1C-H**). These similar dynamics were unexpected, given the differences in nutrient supply between the perfusion strategies.

For glucose consumption, a more pronounced decline was anticipated in cultures using the CSPR strategy, as the medium exchange was only partial, unlike the total medium exchange in the control culture. However, for CCD inoculation (**Figure 4.1C**), glucose concentrations consistently decreased until day 8. MWP-MG_20 initially had lower glucose concentrations compared to other cultures, however concentrations were similar across all conditions by day 5. Although MWP-MG_R1 had the highest glucose concentration at the end of the experiment, the values were within the error margin when compared to MWP-MG_15 and MWP-MG_20, all of which maintained glucose levels above 20 mmol L^{-1}. In contrast, glucose concentrations of MWP-MG_10 dropped to 12 mmol L^{-1} (**Figure 4.1C**). For the HCD inoculation (**Figure 4.1D**), glucose concentrations reached a minimum of 3 – 5 mmol L^{-1} on day 5, with no complete depletion observed in any culture, regardless of perfusion rate strategy. An increase in glucose concentration was observed on day 8 in all cultures, except MWP-MG_20, coinciding with a reduction in VCC (**Figure 4.1D**). The cell-specific glucose consumption rates (q_{Gluc}, average over days 2 – 8) ranged from 3.6 to 7.6 pmol $cell^{-1}$ d^{-1} and 1.7 to 2.0 pmol $cell^{-1}$ d^{-1} for CSPR cultures at CCD and HCD, respectively. Control cultures utilising a total medium exchange exhibited q_{Gluc} values of 7.0 pmol $cell^{-1}$ d^{-1} (MWP-MG_R1 at CCD) and 1.3 pmol $cell^{-1}$ d^{-1} (MWP-MG_R2 at HCD).

Similarly, for lactate (**Figure 4.1E, F**) and ammonium concentrations (**Figure 4.1G, H**), higher values were expected in cultures using the CSPR-based perfusion rate strategy, as well as in cultures with HCD inoculation. As shown in **Figure 4.1E**, lactate concentrations in cultures with CCD inoculation remained within a similar range throughout the cultivation period, with slightly

higher concentrations observed for MWP-MG_10 and MWP-MG_15. However, lactate levels stayed around or below 15 mmol L^{-1}. In cultures with HCD inoculation, lactate concentrations were, as anticipated, slightly higher compared to those with CCD inoculation, but remained predominantly below 20 mmol L^{-1} across all conditions. MWP-MG_20 exhibited higher lactate concentrations than the other CSPR cultures, and an increase in lactate levels was observed on day 8 for both MWP-MG_R2 and MWP-MG_15. For cultures using the CSPR-based perfusion rate strategy, cell-specific lactate consumption rates (q_{Lac}) ranged from 1.3 to 2.3 pmol $cell^{-1}$ d^{-1} for CCD inoculations and 0.4 to 0.6 pmol $cell^{-1}$ d^{-1} for HCD inoculations. For control cultures, q_{Lac} was 1.8 pmol $cell^{-1}$ d^{-1} for MWP-MG_R1 at CCD and 0.3 pmol $cell^{-1}$ d^{-1} for MWP-R2_R2 at HCD.

Regarding ammonium concentrations, for the CCD inoculation, ammonium levels gradually increased but remained within the same range across all conditions (**Figure 4.1G**). In cultures with HCD inoculation, ammonium concentrations were lower in CSPR cultures compared to control cultures, which was surprising given the expectation of ammonium accumulation in CSPR cultures (**Figure 4.1H***).* Nevertheless, ammonium concentrations remained well below 10 mmol L^{-1} for both CCD and HCD inoculations and both perfusion rate strategies, with all CSPR cultures at HCD inoculation staying below 8 mmol L^{-1} (**Figure 4.1G**, **H**). For CSPR cultures, cell-specific ammonium production rates (q_{Amm}) ranged from 0.6 to 1.0 pmol $cell^{-1}$ d^{-1} for CCD inoculation and 0.2 to 0.3 pmol $cell^{-1}$ d^{-1} for HCD inoculation. Control cultures exhibited q_{Amm} values of 1.0 pmol $cell^{-1}$ d^{-1} at CCD and 0.2 pmol $cell^{-1}$ d^{-1} for R2 at HCD.

A hypothesis can be postulated for the similar metabolic behaviour observed between cultures run using different perfusion rate strategies. Cultures using a CSPR-based perfusion rate are adapting to the partial medium exchanges by altering and potentially slowing down their metabolism, while cultures with RV d^{-1}-based perfusion rate experience more drastic changes of nutrient supply and toxic by-product removal which potentially enhance cell metabolism.

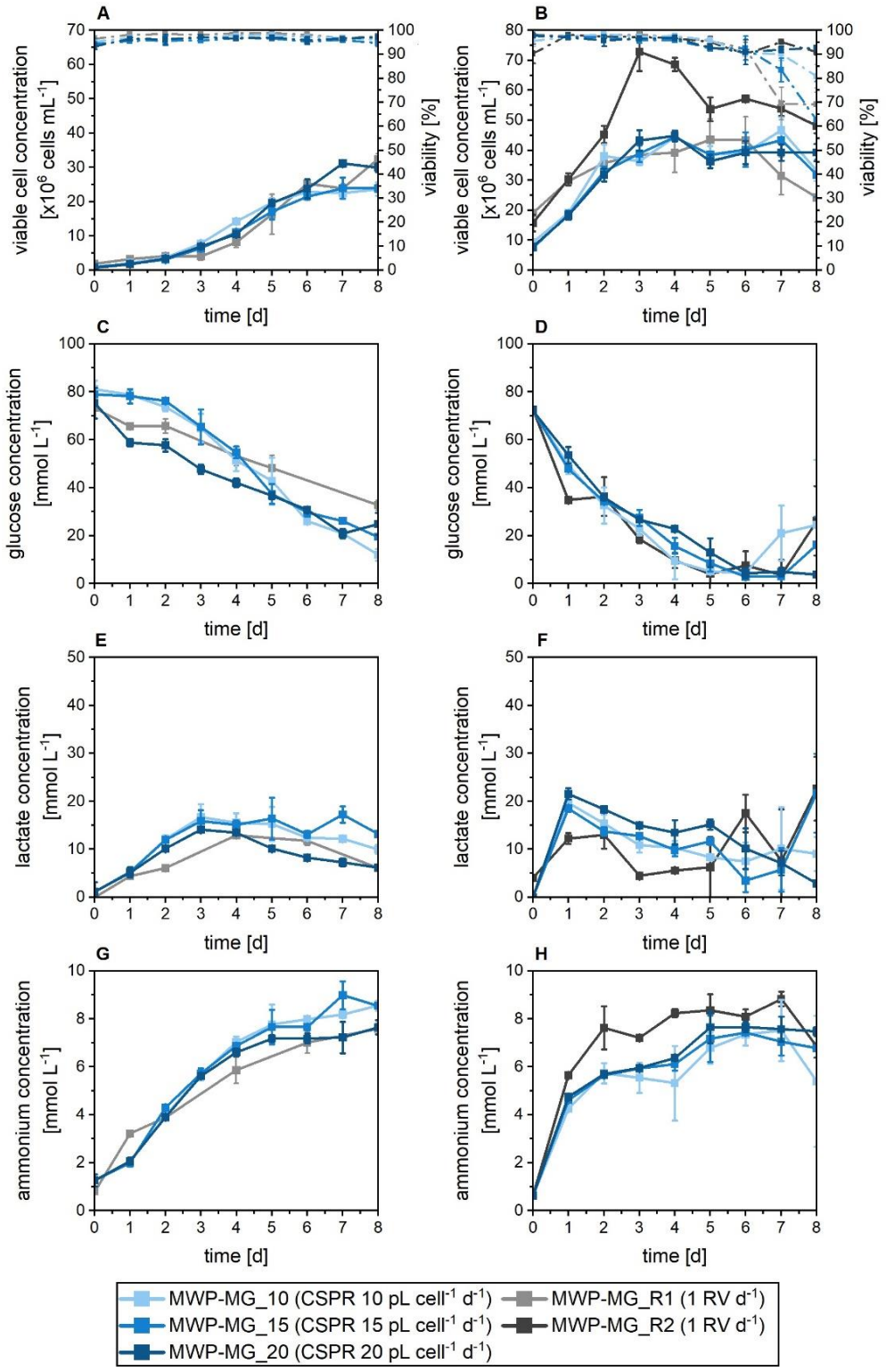

Figure 4.1: Cell growth and metabolite concentrations for CHO cobra cells in 24-well MWP cultivations in semi-perfusion with different perfusion rate strategies. Cells were inoculated at 0.5 - 1 × 10^6 cells mL^{-1} A, C, E and G and at 10 – 20 × 10^6 cells mL^{-1} B, D, F and H, and cultivated in HIP medium supplemented with 30% Feed B (v/v). A: Inoculation at 0.5 – 1 x 10^6 cells mL^{-1}; B: Inoculation at 10-20 x 10^6 cells mL^{-1}; Growth (filled) and viability (open). C and D: glucose; E and F: lactate; G and H: ammonium. Semi-perfusion was performed with a perfusion rate strategy based on CSPR targeting 10 (■), 15 (■), and 20 pL $cell^{-1}$ d^{-1} (■) and with a perfusion rate equal to 1 RV d^{-1}: R1 (■), R2 (■), where the R2 run was only performed at HCD inoculation. Mean of *N = 3* wells. Error bars indicate standard deviation. CHO: Chinese hamster ovary; CSPR: cell-specific perfusion rate; HCD: high cell density; HIP: high-intensity perfusion medium; MWP: microwell plate.

The evaluation of the productivity across cultures under different conditions focused on normalised parameters such as cell-specific production (q_p) and space-time yield (STY) to allow comparison between different perfusion rate strategies (Bausch et al., 2019). The different perfusion rate strategies employed led to partial rather than total medium exchanges. Consequently, for cultures with partial medium exchanges, it is essential to account for the remaining product concentration in the culture. **Figure 4.2A** and **B** illustrate the q_P values for cultures inoculated with CCD and HCD, respectively.

For cultures inoculated at CCD, MWP-MG_R1 exhibited lower q_p values compared to CSPR-based cultures, with a significant difference ($p < 0.05$) observed between the different perfusion strategies (**Figure 4.2A**). At HCD, q_p values for CSPR-based cultures were lower than those for CCD-inoculated cultures, aligning more closely with the values obtained in control cultures. The q_p values for control cultures were consistent across inoculation concentrations. However, no significant differences in q_p values were found between the perfusion rate strategies (**Figure 4.2B**). The STY values shown in **Figure 4.2C** and **D** for CCD and HCD inoculations, respectively, take into account the different medium exchange volumes of the perfusion rate strategies. For CCD-inoculated cultures (**Figure 4.2C**), CSPR-cultures achieved higher STY on day 8, ranging from 0.1 to 0.15 g L^{-1} d^{-1}, while the STY of MWP-MG_R1 cultures was 3-fold lower than the STY of MWP-MG_20 below 0.05 g L^{-1} d^{-1}. In contrast, for HCD-inoculated cultures, MWP-MG_R1 and MWP-MG_R2 cultures achieved higher STY than CSPR cultures, with MWP-MG_R2 reaching up to 0.7 g L^{-1} d^{-1} on day 8. The STYs for MWP-MG_R1 and MWP-MG_20 were 0.6 ± 0.1 g L^{-1} d^{-1} and 0.5 ± 0.03 g L^{-1} d^{-1}, respectively, which were within the error range (**Table 4.1**). Although higher STYs were observed for the control cultures at HCD inoculation, their reported reduction in VCC, in contrast to the stable growth observed in MWP-MG_20, suggests that the beneficial effects of partial medium exchange on productivity may become more evident over extended cultivation periods. Evaluating the conditions in terms of growth, metabolism, and productivity reveals that MWP-MG_20 exhibited the highest productivities and maintained robust growth.

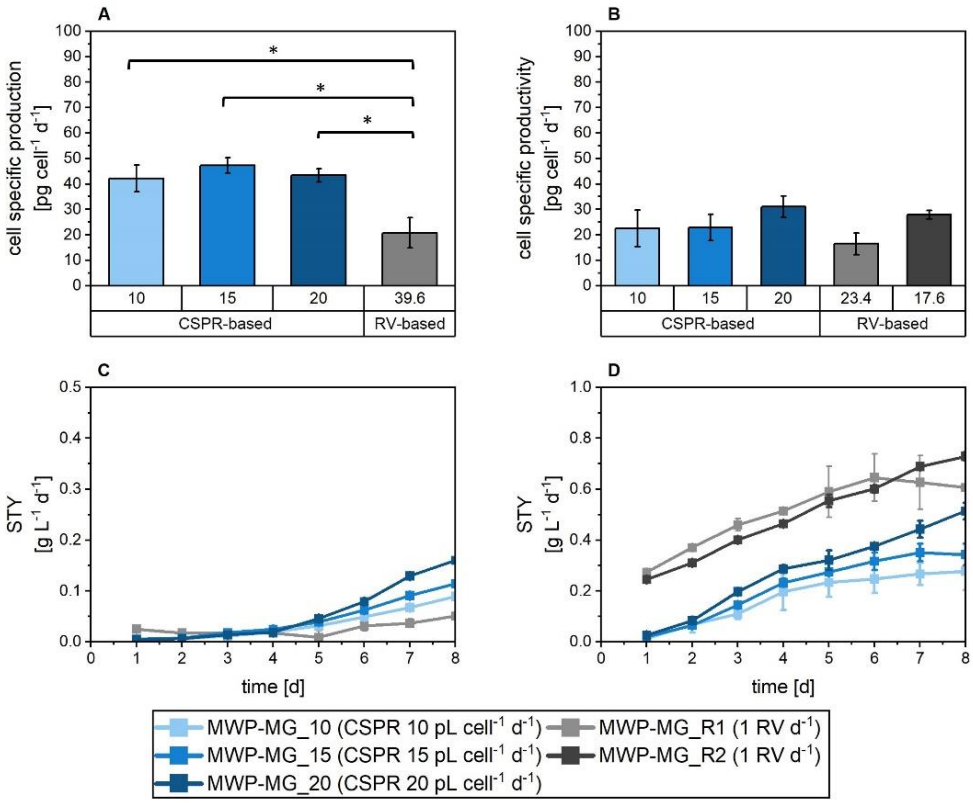

Figure 4.2: Cell-specific productivity and Space-Time-Yield for CHO cobra cells in 24-well MWP cultivations in semi-perfusion with different perfusion rate strategies. Cells were inoculated at 0.5 - 1 × 10^6 cells mL^{-1} (A, C) and at 10 – 20 × 10^6 cells mL^{-1} (B, D) and cultivated in HIP medium supplemented with 30% Feed B (v/v). A and B: cell specific productivity. C and D: STY. Semi-perfusion was performed with a perfusion rate strategy based on CSPR targeting 10 (■), 15 (■), and 20 pL $cell^{-1}$ d^{-1} (■) and with a perfusion rate equal to 1 RV d^{-1}: R1 (■), R2 (■), where the R2 run was only performed at HCD inoculation. Mean of *N = 3* wells. Error bars indicate standard deviation. Significant difference was evaluated with a two-sample t-test assuming equal variance with * $p < 0.05$. CHO: Chinese hamster ovary; CSPR: cell-specific perfusion rate; HCD: high cell density; HIP: high-intensity perfusion medium; MWP: microwell plate; STY: Space-Time-Yield.

Evaluation of process flow rates

In addition to quantitatively evaluating cell performance through growth, metabolism, and mAb production, it is essential to analyse the perfusion rate and actual CSPR, as shown in **Figure 4.3**. For cultures MWP-MG_R1 and MWP-MG_R2, the perfusion rate was constant at 1 RV d^{-1}, whereas in the CSPR-targeted cultures, the perfusion rate is dependent on cell growth. As expected, an increase in perfusion rate was observed as VCC increased for both CCD and HCD inoculation cultures (**Figure 4.3A,** and **B**). Additionally, higher perfusion rates were associated with higher target CSPR values. In cultures inoculated at HCD, the perfusion rate stabilised at different levels once the VCC plateaued (**Figure 4.3A** and **B**). The stabilisation levels were dependent on the targeted CSPR, where perfusion rates of approximately 0.5, 0.7, and 0.8 RV d^{-1} were obtained for cultures with respective stable CSPR targets of 10, 15, and 20 pL $cell^{-1}$ d^{-1}.

The objective of this study was to maintain stable CSPRs during the growth phase and the culture duration, through applying a different perfusion rate. Thus, the actual CSPRs were analysed for all

CSPR-cultures and compared with control cultures using the RV d^{-1}-based perfusion rate strategy (**Figure 4.3C, D** and **E**).

For CCD inoculated cultures, a significant difference in CSPRs was observed between the two perfusion strategies. The total medium exchange in MWP-MG_R1 cultures led to a decrease in CSPR from above 500 pL $cell^{-1}$ d^{-1} to as low as 40 pL $cell^{-1}$ d^{-1} by day 7 (**Figure 4.3C**), which was well above the target CSPRs for CSPR-cultures (**Figure 4.3C, E**). In contrast, using the CSPR-based perfusion rate strategy, CSPRs were effectively maintained near the target values. During the early phase of cultivation, actual CSPRs were initially lower and fluctuated around the target. However, from day 4 onwards, the target CSPR was consistently achieved, resulting in average CSPRs of 10.3 ± 0.6, 15.9 ± 1.4, and 21.1 ± 1.3 pL $cell^{-1}$ d^{-1} over the final 4 days of culture for targets of 10, 15, and 20 pL $cell^{-1}$ d^{-1}, respectively (**Figure 4.3E**, **Table 4.1**).

For HCD inoculated cultures, smaller variations in CSPRs were observed (**Figure 4.3D**). Similar to earlier observations, CSPRs in control cultures initially declined before stabilising around day 3 at values around 25 and 20 pL $cell^{-1}$ d^{-1} for MWP-MG_R1 and MWP-MG_R2, respectively. A slight increase in CSPRs was observed for both MWP-MG_R1 and MWP-MG_R2 on day 8. Both the stabilisation of CSPRs and the slight increases observed at the end of culture corresponded with the VCC trends observed in **Figure 4.3B**. In contrast, the actual CSPRs for cultures using the CSPR-based perfusion rate strategy were maintained throughout cultivation, with average values of 11.3 ± 0.8, 16.8 ± 1.5, and 21.1 ± 1.5 pL $cell^{-1}$ d^{-1} for target CSPRs of 10, 15, and 20 pL $cell^{-1}$ d^{-1}, respectively (**Figure 4.3D**, **Table 4.1**).

Overall, cultures with a perfusion rate of 1 RV d^{-1} used a total medium volume of 129 mL per plate when employing a sacrificial well method. In comparison, cultures utilising the CSPR-based perfusion rate strategy consumed 40, 43, and 45 mL for CCD inoculation at target CSPRs of 10, 15, and 20 pL $cell^{-1}$ d^{-1}, respectively, and 67, 83, and 100 mL for HCD inoculation under the same conditions. This represents a reduction in medium consumption of up to 70% for low seeding densities and up to 50% for high seeding densities. Specifically, comparing the conditions targeting a CSPR of 20 pL $cell^{-1}$ d^{-1} with control cultures MWP-MG_R1 and MWP-MG_R2, similar maximum VCC and productivities were achieved, while overall medium consumption was reduced by 65% for CCD inoculation and by 23% for HCD inoculation.

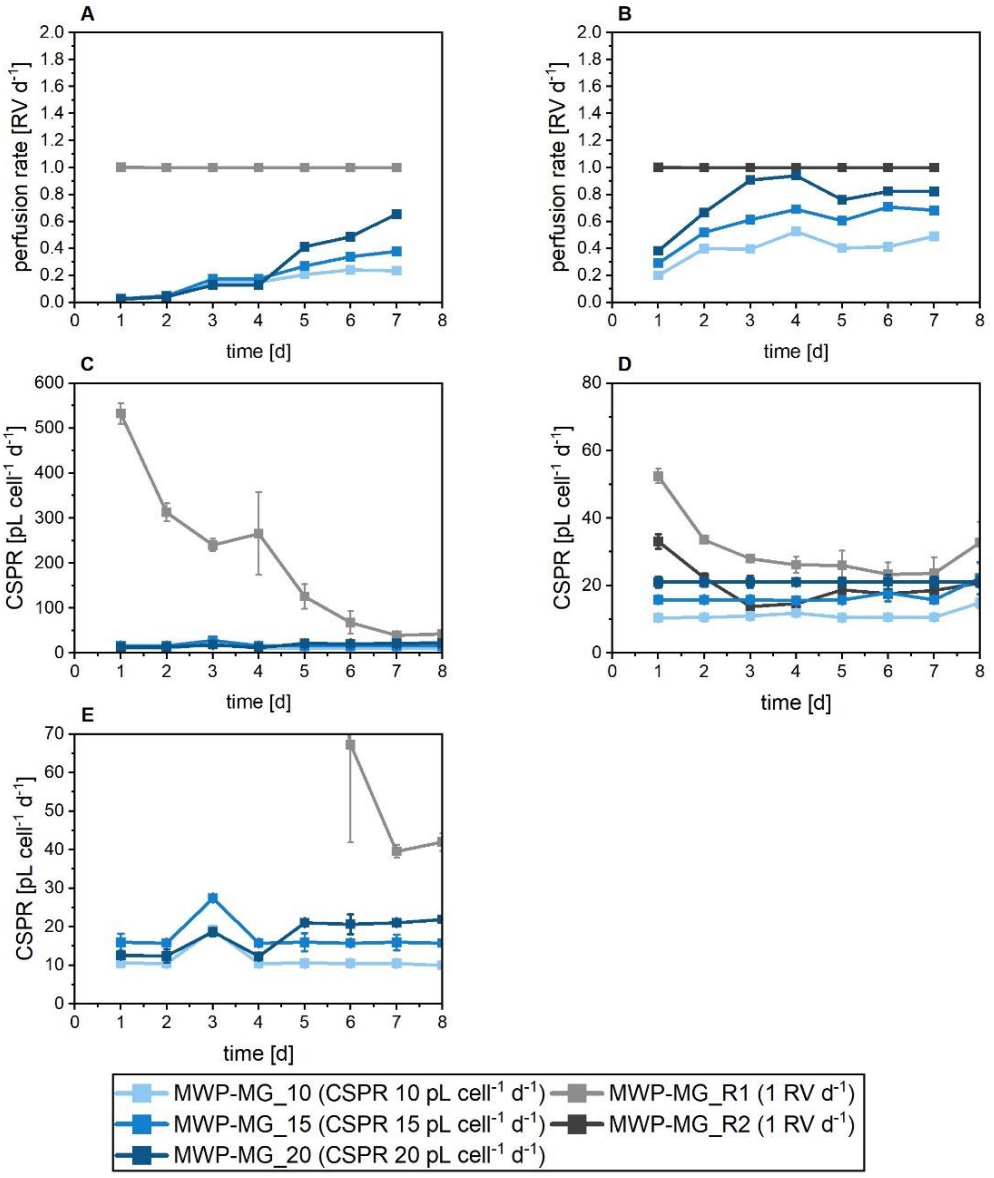

Figure 4.3: Process rates for CHO cobra cells in 24-well MWP cultivations in semi-perfusion with different perfusion rate strategies. Cells were inoculated at 0.5 - 1 × 10^6 cells mL^{-1} (A, C, E) and at 10 – 20 × 10^6 cells mL^{-1} (B, D) and cultivated in HIP medium supplemented with 30% Feed B (v/v). A and B: perfusion rate. C and D: CSPR; E: Zoom of C. Semi-perfusion was performed with a perfusion rate strategy based on CSPR targeting 10 (■), 15 (■), and 20 pL $cell^{-1}$ d^{-1} (■) and with a perfusion rate equal to 1 RV d^{-1}: R1 (■), R2 (■), where the R2 run was only performed at HCD inoculation. Mean of *N = 3* wells. Error bars indicate standard deviation. CHO: Chinese hamster ovary; CSPR: cell-specific perfusion rate; HCD: high cell density; HIP: high-intensity perfusion medium; MWP: microwell plate.

Table 4.1: Process and cellular performance values for CHO cobra cells in 24-well MWP culture comparing RV d^{-1} and CSPR-based perfusion rate strategies.

Inoculation	**CCD**				**HCD**				
Perfusion rate strategy	**RV d^{-1}**	**CSPR**			**RV d^{-1}**		**CSPR**		
CSPR target [pL $cell^{-1}$ d^{-1}]	**R1**	**10**	**15**	**20**	**R1**	**R2**	**10**	**15**	**20**
average CSPR [pL $cell^{-1}$ d^{-1}]	39.6 ± 1.6[+]	10.4 ± 0.6	15.9 ± 1.4	21.1 ± 1.3	23.4 ± 3.5[+]	13.8 ± 1.2[+]	11.3 ± 0.8	16.8 ± 1.5	21.1 ± 1.5
max. VCC [x 10^6 cells mL^{-1}]	32.4 ± 1.5	23.7 ± 1.9	23.9 ± 3.0	31.1 ± 0.9	43.5 ± 6.9	72.9 ± 6.4	46.6 ± 4.4	44.4 ± 1.2	44.8 ± 1.8
STY [g L^{-1} d^{-1}][#]	0.03 ± 0.01	0.09 ± 0.00	0.09 ± 0.00	0.13 ± 0.00	0.61 ± 0.11	0.73 ± 0.02	0.28 ± 0.07	0.34 ± 0.04	0.51 ± 0.03
q_P [pg $cell^{-1}$ d^{-1}]	20.8 ± 5.9	42.1 ± 5.3	47.3 ± 3.0	43.4 ± 2.5	16.5 ± 4.2	27.9 ± 1.6	22.5 ± 7.1	22.8 ± 5.1	31.0 ± 4.1
V_M [mL]	129.6	39.8	42.9	44.7	129.6	129	66.2	82.4	99.8

Cells were cultivated in HIP medium supplemented with 30 % Feed B (v/v).
[+]minimum value
[#]endpoint value on day 8
Yield and productivity values are given as average and standard deviation of N = 3 wells over the entire culture duration of 8 days.
CCD: conventional cell density; HCD: high cell density; RV: reactor volume; VCC: viable cell concentration; CSPR: cell specific perfusion rate; STY: space-time-yield; q_p: cell specific productivity; V_M: volume of consumed medium

4.2.1.2 6-well deepwell plate with CSPR-based perfusion rate

Following the exploration of the CSPR-based perfusion rate the two better performing CSPR targets – 15 and 20 pL cell^{-1} d^{-1} – were scaled up to the DWP system and investigated in a maximum growth (MG) condition to assess the reproducibility of the MWP experiments. This section is divided into two parts: first, a discussion of the DWP results, followed by a comparison of the outcomes from both the MWP and DWP systems.

Growth and productivity of DWP cultures with CSPR-based perfusion rate strategy

Similarly to the MWP, the CSPR-based perfusion rate strategy was evaluated with two inoculation concentrations, as shown in **Figure 4.4**. The DWPs were inoculated at CCD between 0.5 – 2.0 x 10^6 cells mL^{-1} and at HCD between 10 – 20 x 10^6 cells mL^{-1}. Additionally, a control culture for each inoculation concentration was established using a perfusion rate of 1 RV d^{-1} to serve as comparison for growth and productivity outcomes. The DWP cultures with CSPR-based perfusion rate strategy are referred to collectively as CSPR-cultures or DWP-MG_15, and DWP-MG_20, for the CSPR targets of 15 and 20 pL cell^{-1} d^{-1}, respectively. The control culture is referred to as DWP-MG_R1.

Figure 4.4 shows the growth and process flow rate dynamics for both inoculation concentration. For cultures inoculated at CCD (**Figure 4.4A**), similar growth patterns were observed between the CSPR-cultures and control cultures. However, from day 4 onward, a divergence in growth trajectories became apparent. The CSPR-cultures showed a more gradual growth pattern, reaching a stable plateau between 20 – 25 × 10^6 cells mL^{-1} from day 7 to 10. DWP-MG_15 and DWP-MG_20 achieved maximum VCCs of 25.0±0.9 and 26.4±3.0× 10^6 cells mL^{-1} on day 8 and 10, respectively. In contrast, the DWP-MG_R1 exhibited exponential growth till about day 6, after which growth began to plateau reaching a peak VCC of 34.4±2.9 × 10^6 cells mL^{-1} on day 8 before slightly declining to 28.4±0.1× 10^6 cells mL^{-1} on day 10 (**Figure 4.4A**). Throughout the cultivation period, cell viabilities remained above 95% for all conditions. The control culture (DWP-MG_R1) was the only one to show a decline in viability, dropping to 85% by day 10, which coincided with the decrease in cell concentration following the attainment of maximum VCCs (**Figure 4.4A**).

Cultures inoculated at HCD displayed a growth pattern similar to that observed in the CCD inoculated cultures. In both cases, the control culture exhibited faster growth and reached higher cell concentrations, while CSPR cultures showed slower growth, as illustrated in **Figure 4.4B**. CSPR cultures continued to grow until day 3, at which point they entered a "steady-state" phase with stable VCCs around 30 × 10^6 cells mL^{-1}. From day 8 onwards, their VCCs slightly declined to around 25 × 10^6 cells mL^{-1}. Thereby DWP-MG_15 and DWP-MG_20 reached nearly identical maximum VCCs of 33.4±1.5 and 33.2±2.8× 10^6 cells mL^{-1}, respectively (**Figure 4.4B**). In contrast, the control culture, DWP-MG_R1, grew until day 4, peaking at a VCC of 49.9±5.3 × 10^6 cells mL^{-1},

before plateauing 45 × 10^6 cells mL^{-1} – about 1.3-fold higher than CSPR-cultures. After the plateau, a slight continuing decrease in VCCs was observed towards the end of the culture period. Viabilities remained above 90% till day 6, after which it gradually decreased to approximately 80% by day 10 (**Figure 4.4B**).

As the VCCs stabilised and plateaued, the perfusion rate also stabilised for CSPR-based cultures (**Figure 4.4C, D**). While the perfusion rate for DWP-MG_R1 remained constant at 1 RV d^{-1}, the perfusion rate for CSPR-targeted cultures varied with cell growth. As expected, an increase in perfusion rate was observed as VCCs rose for both CCD and HCD inoculated cultures (**Figure 4.4A, C and Figure 4.4B, D**). Additionally, higher target CSPR values were linked to higher medium exchange volumes, resulting in higher perfusion rates. This trend was evident in the divergence of perfusion rates from day 3 in CCD inoculated cultures, where DWP-MG_15 had a lower perfusion rate than DWP-MG_20. In both cases, the perfusion rate continued to rise until around day 8, after which it stabilised. A similar pattern was observed in HCD inoculated cultures, where perfusion rates increased until day 3 before levelling off. The culture with the higher CSPR target of 20 pL $cell^{-1}$ d^{-1} exhibited a higher perfusion rate compared to DWP-MG_15. Perfusion rates of approximately 0.6, and 0.8 RV d^{-1} were achieved for DWP-MG_15 and DWP-MG_20, respectively. Interestingly, the perfusion rate of DWP-MG_20 dropped suddenly from day 8, coinciding with the reduction of VCC in this culture (**Figure 4.4B, D**).

The analysis of the actual CSPR is presented in **Figure 4.4E, F** and **G.** In cultures inoculated with CCD, a significant difference in CSPRs was observed between the two perfusion strategies**. Figure 4.4E,** and **G** illustrate the CSPR dynamics, with **Figure 4.4G** providing a zoomed-in view of **Figure 4.4E** to highlight the details at lower CSPRs. In the DWP-MG_R1 cultures, the total medium exchange resulted in a CSPR decrease from > 500 pL $cell^{-1}$ d^{-1} to as low as 29.2±2.5 pL $cell^{-1}$ d^{-1} by day 8 (**Figure 4.4E**). This value remained well above the target CSPRs for CSPR-cultures (**Figure 4.4E, G**). In contrast, with the CSPR-based perfusion rate strategy, CSPRs were effectively maintained at stable levels, though slightly above the target values. The average CSPRs were 18.5 ± 0.9 pL $cell^{-1}$ d^{-1} for DWP-MG_15 and 25.0 ± 2.4 pL $cell^{-1}$ d^{-1} from days 2 to 10 (**Figure 4.4E, G**). A minor fluctuation, less than 8% of the stable value, was observed on day 1, which can be attributed to the manual handling of the DWP.

For cultures inoculated at HCD, the actual CSPRs for CSPR-cultures were maintained stable throughout the cultivation period (**Figure 4.4F**). As observed with the CCD inoculation, these values remained slightly above the target CSPRs of 15 and 20 pL $cell^{-1}$ d^{-1}. The average CSPRs were 18.6 ± 1.5 pL $cell^{-1}$ d^{-1} for DWP-MG_15 and 24.9 ± 1.6 pL $cell^{-1}$ d^{-1} for DWP-MG_20 In contrast, the control culture experienced a reduction in CSPR, dropping from approximately 50 pL $cell^{-1}$ d^{-1} to as low as 20.2 pL $cell^{-1}$ d^{-1} on day 5 (**Figure 4.4F**).

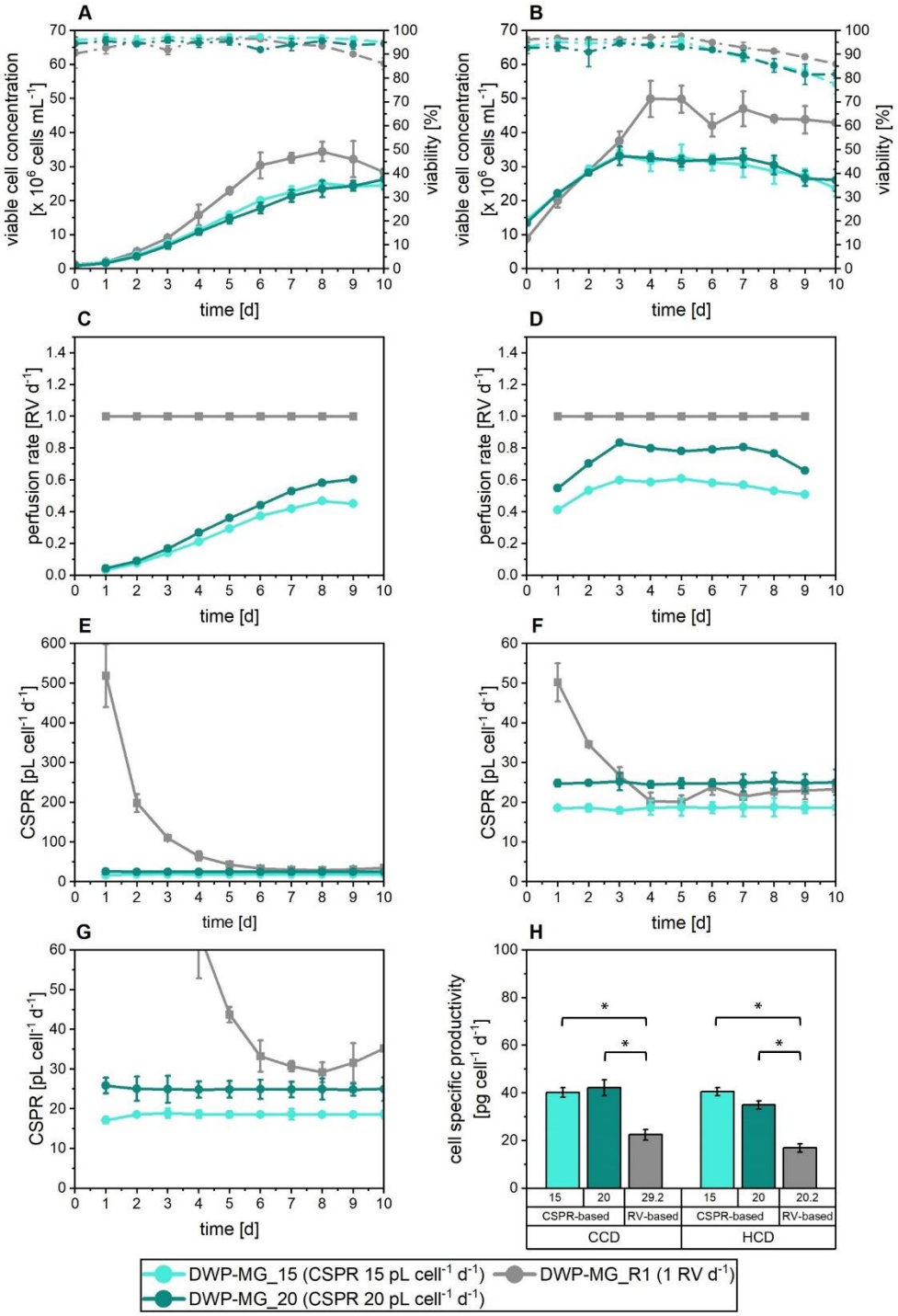

Figure 4.4: Growth and process rates for CHO cobra cells in 6-well DWP cultivations in semi-perfusion with different perfusion rate strategies. Cells were inoculated at 0.5 - 1 × 10^6 cells mL^{-1} (A, C, E, G) and at 10 – 20 × 10^6 cells mL^{-1} (B, D) and cultivated in HIP medium supplemented with 30% Feed B (v/v). A and B: viable cell concentration (filled-straight) and viability (open-dashed); C and D: perfusion rate; E and F: CSPR; G: Zoom of C; H: cell specific productivity. Semi-perfusion was performed with a perfusion rate strategy based on CSPR targeting 15 (●), and 20 pL $cell^{-1}$ d^{-1} (●) and with a perfusion rate equal to 1 RV d^{-1}: R1 (●). Mean of *N = 3* wells. Error bars indicate standard deviation for growth and CSPR. The perfusion rate was calculated on average values each day and does not contain error bars. Significant difference was evaluated with a two-sample t-test assuming equal variance with * $p < 0.05$. CHO: Chinese hamster ovary; CSPR: cell-specific perfusion rate; DWP: deepwell plate; HCD: high cell density; HIP: high-intensity perfusion medium.

Regarding medium consumption, employing the DWP with a perfusion rate strategy of 1 RV d^{-1} resulted in a total medium volume of 900 mL per 3 wells. In comparison, the CSPR-based perfusion rate strategy consumed 353 and 426 mL for CCD inoculation at target CSPRs of 15, and 20 pL $cell^{-1}$ d^{-1}, respectively, and 573 and 750 mL for HCD inoculation under the same condition. For both perfusion rate strategies, the same 3 wells were used throughout the cultivation duration. The reduction in medium consumption of up to 54% for low seeding densities and 38% for high seeding densities. For example, comparing DWP-MG_20 with DWP-MG_R1 the overall medium consumption was reduced by 54% for CCD inoculation and by 19% for HCD inoculation.

Figure 4.4H shows the cell-specific productivities (q_P) for cultures inoculated with CCD and HCD. For both inoculation densities, DWP-MG_R1 exhibited lower q_P values compared to CSPR-cultures, and a significant difference ($p < 0.05$) was observed between the two perfusion strategies for both inoculation concentrations (**Figure 4.4H**). Specifically for CCD inoculation, CSPR-cultures achieved q_P values of 40.2±2.0 pg $cell^{-1}$ d^{-1} for DWP-MG_15 and 42.2±3.4 pg $cell^{-1}$ d^{-1} for DWP-MG_20, while DWP-MG_R1 achieved 22.4±2.3 pg $cell^{-1}$ d^{-1}. For HCD-inoculated cultures, q_P values were slightly lower than for CCD-inoculated cultures, with DWP-MG_15, DWP-MG_20 and DWP-MG_R1 reaching 40.6±1.7, 35.0±1.8 and 16.9±1.7 pg $cell^{-1}$ d^{-1}, respectively.

Building on an earlier hypothesis it could be that the differences in productivities between the two perfusion rates is caused by a differing metabolic activity caused by the different supply of nutrient and accumulation of by-products for the CSPR-based perfusion rate. To explore this further, an analysis of external metabolites such as glucose, lactate, and ammonium could provide valuable insights.

The glucose concentrations in CCD-inoculated CSPR cultures showed a steady decline until day 7, reaching a minimum of 20.0 mmol L^{-1} (**Figure 4.5A**). Toward the end of the culture, a slight increase in glucose concentrations was observed. This trend aligns with the growth dynamics, where VCCs began to decline in the final 2 days, suggesting reduced glucose consumption and consequently an increase in residual glucose. In the control culture DWP-MG_R1, glucose concentrations also declined, but remained higher than those in CSPR-cultures, with a minimum concentration of 32.0 mmol L^{-1}. Although DWP-MG_R1 had the highest glucose levels throughout the culture, by the end of the cultivation, glucose concentrations were comparable across all conditions and within the range of error (**Figure 4.5A**).

In contrast, for HCD-inoculated cultures, glucose concentrations declined exponentially across all conditions (**Figure 4.5B**). CSPR-cultures showed a drop until day 2, from above 75 mmol L^{-1} to approximately 21 mmol L^{-1}. While DWP-MG_15 maintained a stable glucose concentration, with only a minor increase to 28.7 mmol L^{-1} on day 10, DWP-MG_20 exhibited greater fluctuations, peaking at 38.6 mmol L^{-1} on days 8 and 9. The stabilisation of glucose levels and the subsequent

increase toward the end of the culture coincided with the reduction in VCC for both CSPR-cultures (**Figure 4.5B, Figure 4.4B**). However, the larger fluctuations observed in DWP-MG_20 could not be explained by changes in VCC, as these remained stable throughout the cultivation period. The control culture experienced a reduction in glucose until day 5, after which glucose levels stabilised (**Figure 4.5B**). These concentrations fluctuated around 15 mmol L^{-1}, with minimum values of 11 mmol L^{-1} and maximum values of 17 mmol L^{-1} until the end of the culture. Similar to the CSPR-cultures, the stabilisation of glucose was in line with the VCC trend, which also stabilised around the same time. Further, the lower glucose concentrations for control cultures were expected as higher VCCs were achieved in those cultures (**Figure 4.5B, Figure 4.4B**).

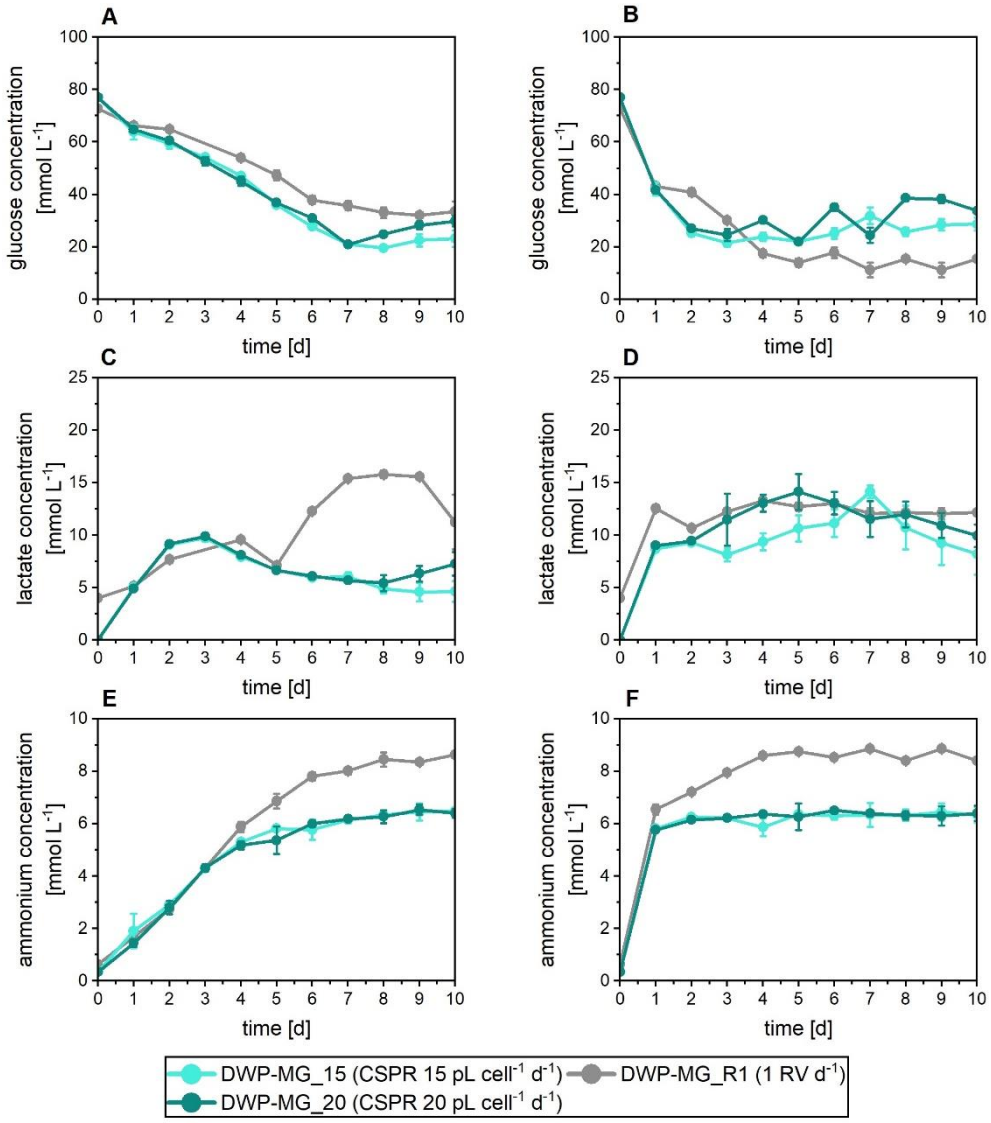

Figure 4.5: Metabolite concentrations for CHO cobra cells in 6-well DWP cultivations in semi-perfusion with different perfusion rate strategies. Cells were inoculated at 0.5 - 1 × 10^6 cells mL^{-1} (A, C, E) and at 10 – 20 × 10^6 cells mL^{-1} (B, D, F) and cultivated in HIP medium supplemented with 30% Feed B (v/v). A and B: glucose; C and D: lactate; E and F: ammonium. Semi-perfusion was performed with a perfusion rate strategy based on CSPR targeting 15 (●), and 20 pL $cell^{-1}$ d^{-1} (●) and with a perfusion rate equal to 1 RV d^{-1}: R1 (●). Mean of *N = 3* wells. Error bars indicate standard deviation. CHO: Chinese hamster ovary; CSPR: cell-specific perfusion rate; DWP: deepwell plate; HCD: high cell density; HIP: high-intensity perfusion medium.

For lactate (**Figure 4.5C, D**) and ammonium (**Figure 4.5E, F**), higher concentrations were expected in CSPR-based cultures due to accumulation from the partial medium exchanges. In CCD-inoculated cultures, lactate concentrations initially increased in all cultures (**Figure 4.5C**). However, CSPR-cultures experienced a peak in lactate on day 3, reaching a maximum of around 10 mmol L^{-1}, followed by a steady decline towards stabilisation around 5 mmol L^{-1} In contrast, DWP-MG_R1 cultures showed a continuous rise in lactate, reaching 15.6±0.4 mmol L^{-1} by day 8 before decreasing to 11 mmol L^{-1} on day 10. The drop on day 5 is likely due to a measurement inconsistency, as no changes in VCC or glucose data from day 5 provide an explanation for this sudden fluctuation. Cultures inoculated at HCD exhibited immediate stabilisation of lactate concentrations by day 1, maintaining levels between 8 to 14 mmol L^{-1} (**Figure 4.5D**). Notably, DWP-MG_R1 cultures, although slightly elevated, showed less fluctuation, with an average concentration of 11.2±0.3 mmol L^{-1} In comparison, DWP-MG_15 and DWP-MG_20 had average lactate concentrations of 9.05±1.0 and 10.41±1.1 mmol L^{-1}, respectively, when calculated over days 1 to 10. A similar trend was observed for ammonium concentrations, with control cultures consistently showing higher levels than CSPR-cultures. In CCD-inoculated cultures, ammonium concentrations increased initially at the same rate across all conditions (**Figure 4.5E**). However, a divergence between the two perfusion strategies became evident on day 4, where CSPR-cultures showed a dampened increase, stabilising around 6 mmol L^{-1}. In contrast, DWP-MG_R1 cultures continued to rise until plateauing at approximately 9 mmol L^{-1} between days 8 and 10. For HCD-inoculated cultures, CSPR-cultures exhibited an immediate stabilisation at 6 mmol L^{-1} starting from day 1, while ammonium concentrations in the control cultures continued to rise until day 4, levelling off at around 9 mmol L^{-1} (**Figure 4.5F**).

Comparison of growth and productivity between MWP and DWP cultures with CSPR-based perfusion rate strategy

The comparison of MWP and DWP cultures is shown in **Figure 4.6**. For both cultivation systems, the growth of CSPR targets followed a similar pattern at CCD inoculation, with maximum VCCs reaching approximately 25 × 10^6 cells mL^{-1}, while viabilities remained above 90%. However, the MWP-MG_20 culture achieved slightly higher maximum VCCs, around 30 × 10^6 cells mL^{-1}. In the case of HCD inoculation, the MWP system reached 1.3-fold higher maximum VCCs (approximately 40 × 10^6 cells mL^{-1}) and maintained these levels for several days. In contrast, the DWP system, while achieving lower maximum VCCs, demonstrated less fluctuation in VCCs compared to the MWP. For both cultivation systems, cultures inoculated at HCD consistently reached higher maximum VCCs, plateauing at elevated levels. This suggests that inoculation concentration plays an important role in determining the maximum achievable VCCs, independent of the cultivation system. However, the effect was more pronounced in the MWP system, which saw a notable increase in maximum VCCs from 30 to 40 × 10^6 cells mL^{-1}. In contrast, the DWP system showed

only a marginal increase, from 25 to 30 × 10^6 cells mL^{-1}. Additionally, the DWP system experienced a reduction in growth, stabilising at the same maximum value observed for the CCD-inoculated cultures. On the other hand, the VCC in the MWP system at HCD remained above those of CCD-inoculated cultures, even with a slight reduction observed in the MWP-MG_15 culture on day 8. Both cultivation systems showed a similar decline in viability. For MWP-MG_20 cultures, viability decreased from over 90% to 85% by day 8, while for DWP cultures, viability decreased to 80% by day 10.

The comparison of STY showed similar dynamics for the CCD inoculated cultures in both systems (**Figure 4.6C, D**), with an initial lag before showing continuously increasing STY achieving similar values on day 8 (0.09 g L^{-1} d^{-1} for MWP-MG_15 and 0.13 g L^{-1} d^{-1} for MWP-MG_20; 0.13 g L^{-1} d^{-1} for DWP-MG_15 and 0.15 g L^{-1} d^{-1} for DWP-MG_20). For HCD inoculated cultures some differences are observable. Although the STY increased initially in both systems, values stabilised from day 5 in DWP while only MWP-MG_15 showed a similar stabilisation from day 7. STYs of MWP-MG_20 continued to increase until end of culture.

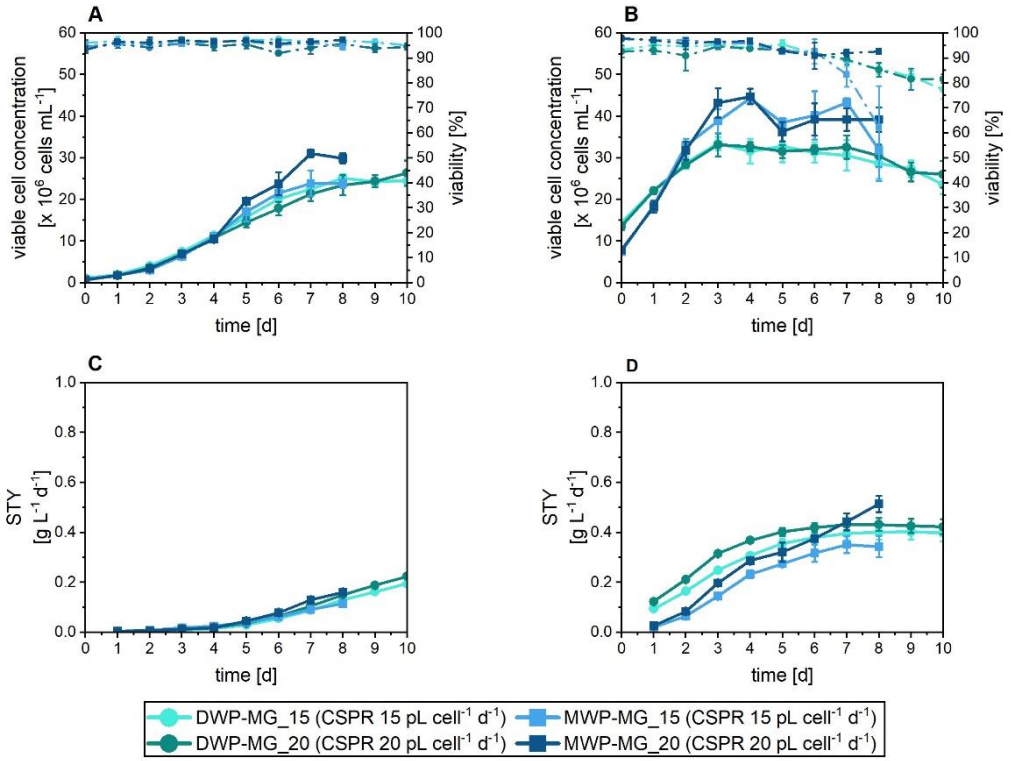

Figure 4.6: Growth and Productivity comparison for CHO cobra cells in 24-well MWP cultivation and 6-well DWP cultivations in semi-perfusion with different perfusion rate strategies. Cells were inoculated at 0.5 - 1 × 10^6 cells mL^{-1} (A, C) and at 10 – 20 × 10^6 cells mL^{-1} (B, D) and cultivated in HIP medium supplemented with 30% Feed B (v/v). A and B: viable cell concentration (filled-straight) and viability (open-dashed); C and D: STY. Semi-perfusion was performed with a perfusion rate strategy based on CSPR targeting 15 pL cell d^{-1} in MWP (■) and DWP (●), and 20 pL $cell^{-1}$ d^{-1} in MWP (■) and DWP (●). Mean of *N = 3* wells. Error bars indicate standard deviation. CHO: Chinese hamster ovary; CSPR: cell-specific perfusion rate; DWP: deepwell plate; HCD: high cell density; HIP: high-intensity perfusion medium; MWP: microwell plate; STY: space-time-yield.

4.2.2 Validation of CSPR-based perfusion rate strategy in 250 mL perfusion bioreactor

In a final step, the CSPR-based perfusion rate strategy was investigated in the 250 mL stirred-tank bioreactor fabricated by the Design and Fabrication Facility at UCL. This bioreactor was equipped with tangential flow filtration (TFF) for cell retention. The objective of this evaluation was to assess the validity of the MWP and DWP as screening tools and to examine the scalability of parameters from these non-instrumented screening tools to the controlled bioreactor system. This section is divided into two parts: first, the presentation of the perfusion bioreactor results, followed by a comparison of the outcomes across three scales—from MWP and DWP to the bioreactor (BR) system.

Growth and productivity of 250 mL perfusion bioreactor cultures with CSPR-based perfusion rate strategy

Two independent bioreactor runs were conducted aiming to maintain a CSPR of 20 pL cell^{-1} d^{-1} throughout the cultivation period after the start of perfusion. Each culture was inoculated at 0.5-2 × 10^{6} cells mL^{-1}. The runs are referred to as BR#1-MG_20, and BR#2-MG_20. It should be noted that BR#1-MG_20 was terminated after 7 days due to an issue with the gas supply.

Figure 4.7 shows the growth, key metabolites, productivity and process operation for both bioreactor runs. Both cultures exhibited similar growth patterns (**Figure 4.7A**). A rapid growth phase was observed from days 1 to 3, followed by a slowdown. While BR#1-MG_20 continued to increase slowly until day 7, reaching 18.4±2.0 × 10^{6} cells mL^{-1}, BR#2-MG_20 reached 20.4±0.9 × 10^{6} cells mL^{-1} by day 5 and stabilised at this value with a minor increase to approximately 26 x 10^{6} cells mL^{-1} by day 9. Viabilities in both bioreactors were largely above 90% with a minor drop to 87% observed for BR#2-MG_20 on day 7, which recovered by day 10 to 92% (**Figure 4.7A**). Despite the later start of perfusion in BR#2-MG_20 on day 3, compared to day 2 for BR#1-MG_20, the growth performance of BR#2-MG_20 was improved.

The actual CSPR and perfusion rates are displayed in **Figure 4.7B**. As expected, the perfusion rate increased with the rise in VCCs in both bioreactors, where BR#1-MG_20 exhibited a slower increase in perfusion rate compared to BR#2-MG_20. Notably, the perfusion rate for BR#2-MG_20 did not stabilise as the VCC did but instead showed a gradual increase from days 5 to 7 before continuing to rise, reaching 0.75 RV d^{-1} by day 10. The actual CSPR also showed less stable dynamics: for BR#1-MG_20, the CSPR remained below the target of 20 pL cell^{-1} d^{-1}, though it reached 18.5 pL cell^{-1} d^{-1} on days 5 and 6. On average, the actual CSPR of BR#1-MG_20 was 15.7±0.7 pL cell^{-1} d^{-1} from day 3 to day 7. For BR#2-MG_20, the CSPR was 22.0±1.0 pL cell^{-1} d^{-1} on average (from day 4 to 10). On day 4, the CSPR was well below target, increasing to near-target

levels for days 5 to 7. However, from days 8 to 10, the CSPR exhibited larger fluctuations, exceeding the target, reaching up to 30 pL cell^{-1} d^{-1}.

The STY was determined using the measured titre of the harvest. Titre measurements were therefore only available starting from day 2 for BR#1-MG_20 and day 3 for BR#2-MG_20, following the initiation of perfusion (**Figure 4.7C**). Notably, the STY dynamics were very similar between both bioreactor runs until day 5, after which the STY continued to increase moderately for BR#1-MG_20 reaching 0.04±0.00 g L^{-1} d^{-1} on day 7. In contrast, the STY for BR#2-MG_20 exhibited an exponential increase until the end of the culture, with a brief stabilisation on days 7 and 8, reaching 0.34±0.3 g L^{-1} d^{-1} on day 10 (**Figure 4.7C**).

The analysis of external metabolites—glucose, lactate, and ammonium—displayed in **Figure 4.7D**, **E** and **F**, respectively, show similar dynamics between both bioreactor runs. Glucose concentrations which started at 26.4 and 28.0 mmol L^{-1} for BR#1-MG_20 and BR#2-MG_20, respectively, decreased until the initiation of perfusion on days 2 and 3 (**Figure 4.7D**). For BR#1-MG_20, glucose concentrations dropped to as low as 15 mmol L^{-1} but after perfusion started, they remained stable for days 3 and 4 before gradually increasing to 21 mmol L^{-1} by day 7. BR#2-MG_20 stabilised at an average glucose concentration of 16 mmol L^{-1}. from days 4 to 8. Only in the final two days of the culture did glucose concentrations fall 10 mmol L^{-1} (**Figure 4.7D**).

Lactate concentrations increased as expected during the initial batch phase (**Figure 4.7E**). However, contrary to expectations, lactate concentrations in BR#1-MG_20 continued to rise until day 3, following the initiation of perfusion on day 2. Lactate concentrations peaked on days 3 and 4 at 27 mmol L^{-1} before declining until day 7. In contrast, BR#2-MG_20 peaked at 19.1±0.1 mmol L^{-1} on day 3 and showed decreasing trends following that day with started perfusion followed by a decrease after perfusion began. Lactate concentrations then stabilised at around 4 mmol L^{-1} from days 6 to 9, before increasing again to 11±0.1 mmol L^{-1} on day 10 (**Figure 4.7E**). Ammonium concentrations exhibited similar trends in both bioreactor runs (**Figure 4.7F**). After an initial increase, ammonium levels stabilised at approximately 5.3 mmol L^{-1} for BR#1-MG_20 and 5.5 mmol L^{-1} for BR#2-MG_20 following the initiation of perfusion. Notably, BR#2-MG_20 showed an increase in ammonium levels on day 10, rising to 9.1±0.0 mmol L^{-1}.

Figure 4.7G, **H** and **I** present the online-measured process parameters—DO, pH, and gas flow rate—for BR#2-MG_20. While measurements were recorded every 5 seconds, only one value per minute was selected for visual representation.

The DO was largely maintained at a constant level throughout the cultivation, though a few notable fluctuations were observed. As expected, DO initially decreased towards the set point in the early days of culture; however, it dropped to approximately 15%, significantly below the set

point of 50%, before recovering and stabilising at the target level (**Figure 4.7G**). Additional declines were observed on days 6 and 8, with DO reaching 15% and 20%, respectively. In response, the agitation speed was increased from 250 rpm to 300 rpm on day 7, and the gas flow rate range was expanded from 0.1–0.5 to 0.1–0.8 sL min^{-1} on day 6 (**Figure 4.7G, I**). The pH remained stable throughout the cultivation, with minor fluctuations observed on days 0 and 1, coinciding with initial DO instability (**Figure 4.7H**). Once DO stabilised on day 2 and perfusion was initiated on day 3, pH remained consistently at the set point of 7.2 (**Figure 4.7H**).

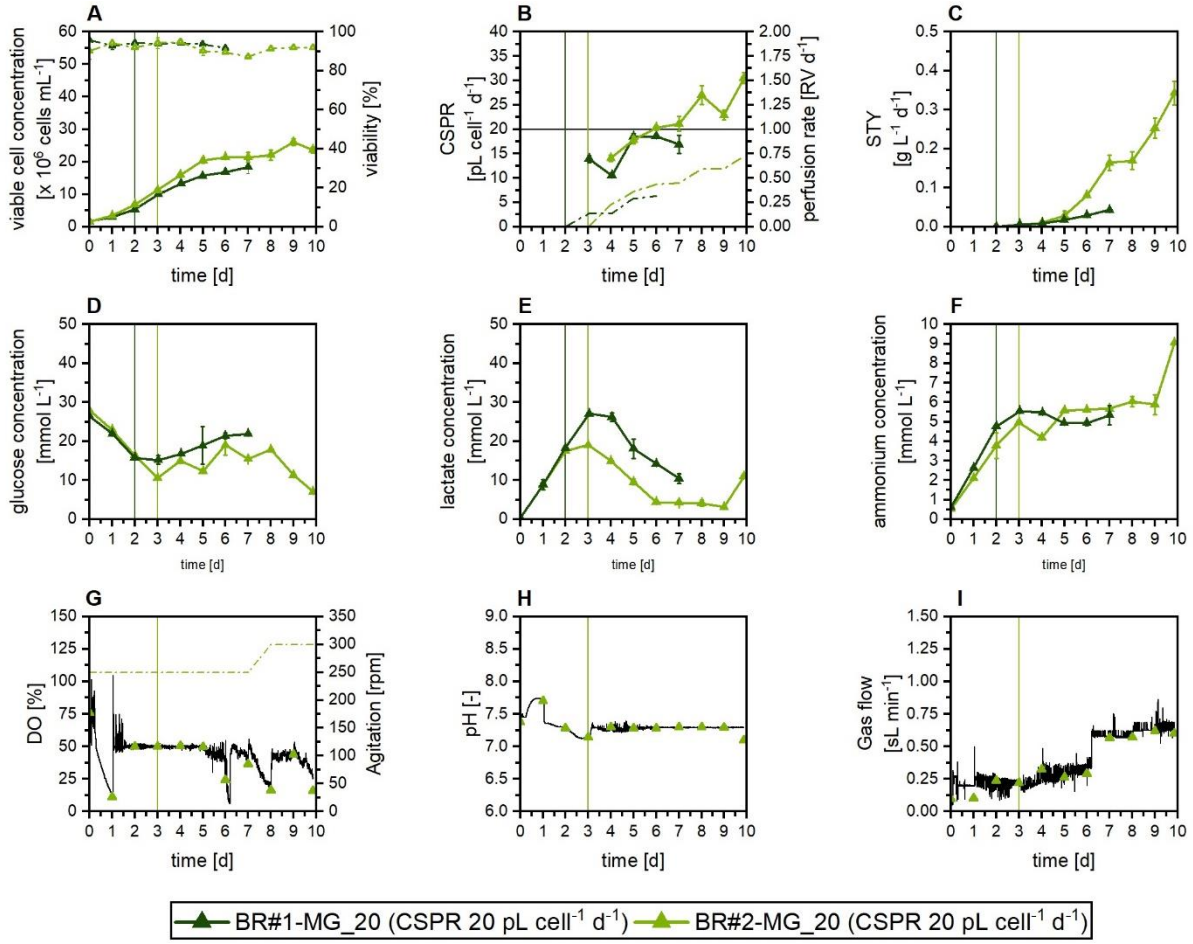

Figure 4.7: Growth, productivity and process operation for CHO cobra cells in 250 mL perfusion bioreactor. Cells were inoculated at 0.5 - 2 × 10^6 cells mL^{-1} and cultivated in HIP medium supplemented with 30% Feed B (v/v). Perfusion was performed with a perfusion rate strategy based on CSPR targeting 20 pL cell^{-1} d^{-1} in BR#1 (▲) and BR#2 (▲). Vertical lines indicate start of perfusion. A: viable cell concentration (filled-straight) and viability (open-dashed); B: CSPR (straight) and perfusion rate (dashed); C: STY; D: glucose E: lactate; F: ammonium; Process data are shown exemplary for BR#2 (▲). G: DO (black, straight) and agitation (dashed); H: pH; I: Gas flow. Mean of *N = 3* samples. Error bars indicate standard deviation. BR: bioreactor; CHO: Chinese hamster ovary; CSPR: cell-specific perfusion rate; HIP: high-intensity perfusion medium; STY: space-time-yield

Comparison of growth, metabolism and productivity between MWP, DWP and 250 mL perfusion bioreactor

The comparison of the MWP, DWP, and the second perfusion bioreactor culture at the target CSPR of 20 pL cell^{-1} d^{-1} is shown in **Figure 4.8**. The peak VCC across all culture systems were comparable, reaching approximately 25 × 10^6 cells mL^{-1} with high viabilities maintained

throughout the culture period (**Figure 4.8A**, **Table 4.2**). The MWP culture achieved slightly higher VCCs, peaking at 31.1 ± 0.9 × 10^6 cells mL^{-1}, while the growth data for DWP-MG_20 and BR#2-MG_20 were closely aligned, reaching 26.4 ± 3.0× 10^6 cells mL^{-1} and 26.0 ± 1.0× 10^6 cells mL^{-1}, respectively.

Figure 4.8B presents the actual CSPRs and perfusion rates. Notably, distinct trends were observed in the actual CSPR across the systems (**Figure 4.8B, Table 4.2**). While DWP-MG_20 maintained a stable CSPR throughout the culture, the MWP and both perfusion bioreactor runs initially exhibited values below the target (< 20 pL $cell^{-1}$ d^{-1}) before increasing to match the desired CSPR. In the MWP cultures, the CSPR remained at the target until the end of the shorter culture period (8 days). In contrast, BR#2-MG_20 showed a continued increase in CSPR after a brief stabilisation. The similarities in CSPR fluctuations between the MWP and bioreactors are particularly interesting given the earlier hypothesis that small volume variations during manual medium exchanges in the MWP contributed to these fluctuations. Although perfusion bioreactors operate with larger daily medium volumes, their continuous nature relies on pumps capable of delivering extremely low flow rates, which may also contribute to variations in CSPR. The perfusion rates showed increasing dynamics following the trend of the VCCs (**Figure 4.8B**), though while the VCCs of both DWP and perfusion bioreactor cultures were stabilising on the last days of culture, only the perfusion rate of the bioreactor showed a continued increase.

The productivity data for all three culture systems is shown in **Figure 4.8C**, and **D** (c.f. also **Table 4.2**)**.** The q_P values were comparable across systems, ranging from 42 to 46 pg $cell^{-1}$ d^{-1}. Similarly, STY trends were well aligned across systems, with an increase observed on days 9 and 10 in both the DWP and BR#2-MG_20 cultures. Notably, BR#2-MG_20 achieved a higher STY, reaching 0.34 ± 0.03 g L^{-1} d^{-1} on day 10, compared to 0.22 ± 0.00 g L^{-1} d^{-1} for DWP-MG_20 on the same day.

Metabolic comparisons across the systems were assessed based on cell specific glucose consumption, and lactate and ammonium production rates (**Figure 4.8E, F** and **G**). Interestingly the q_{Gluc} was significantly higher in the well plate systems, with values of 3.6±0.4 and 5.1±0.4 pmol $cell^{-1}$ d^{-1}, compared to the perfusion bioreactor, which had a value of 1.3±0.1 pmol $cell^{-1}$ d^{-1}. In contrast, q_{Lac} and q_{Amm} were similar across systems averaging around 1.3 and 0.5 pmol $cell^{-1}$ d^{-1} respectively, with slightly lower values observed for the bioreactor cultures. These differences may be attributed to variations in perfusion rates and the differences between the controlled environment of the perfusion bioreactor and the semi-perfusion approach in the well plates, where medium exchanges were performed in a batch-wise manner. The differences in perfusion mode and control parameters may have influenced the metabolic activity of the cultures, leading to the observed differences in glucose consumption rates.

Finally, it is important to consider medium consumption across the systems. Despite achieving similar growth and productivity, a single perfusion bioreactor culture required 1183.6 mL of medium over the 10-day period, whereas the DWP, with three wells operated in parallel, required only 426.7 mL over the same duration.

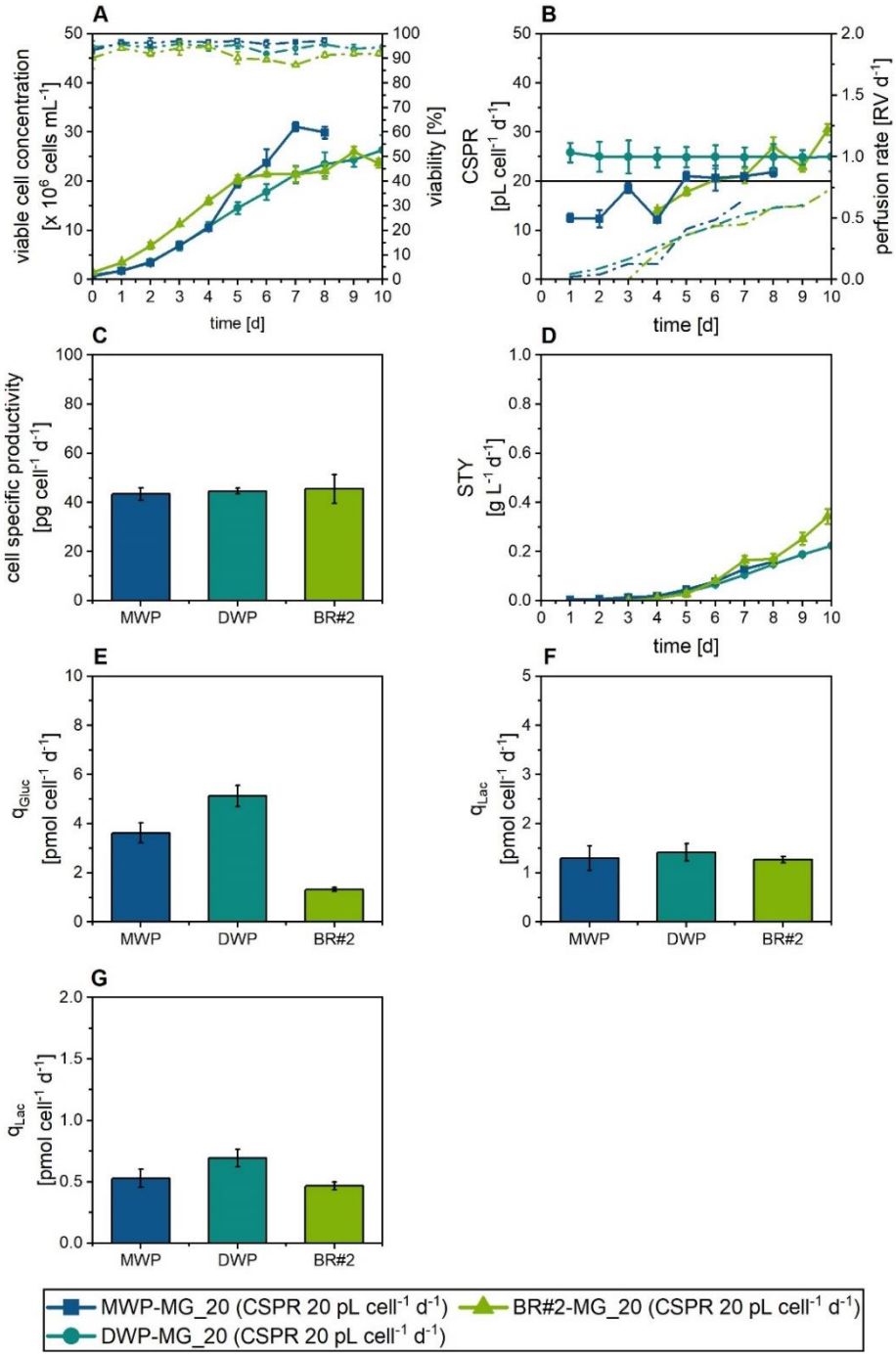

Figure 4.8: Growth, productivity and metabolic comparison for CHO cobra cells in semi-perfusion MWP and DWP, and 250 mL perfusion bioreactor with a CSPR-based perfusion rate. Cells were inoculated at 0.5 - 2 × 10^6 cells mL^{-1} and cultivated in HIP medium supplemented with 30% Feed B (v/v). A: viable cell concentration (filled-straight) and viability (open-dashed); B: CSPR (straight) and perfusion rate (dashed); C: cell specific productivity; D: STY; E: q_{Gluc}; F: q_{Lac}; G: q_{Amm}. Semi-perfusion and perfusion were performed with a perfusion rate strategy based on CSPR targeting 20 pL $cell^{-1}$ d^{-1} in MWP (■), DWP (●), and BR#2 (▲). Mean of *N = 3* wells/samples. Error bars indicate standard deviation. BR: bioreactor; CHO: Chinese hamster ovary; CSPR: cell-specific perfusion rate; DWP: deepwell plate; HIP: high-intensity perfusion medium; MWP: microwell plate; q_{Gluc}; cell specific glucose consumption; q_{Lac}; cell specific lactate production; q_{Amm}: cell specific ammonium production; STY: space-time-yield.

Table 4.2: Process and cellular performance values for CHO cobra cells in 24-well MWP, 6-well DWP and 250 mL perfusion bioreactor culture comparing the CSPR-based perfusion rate across scales.

Inoculation	**CCD**						**HCD**			
Culture system	**MWP**		**DWP**		**BR#1**	**BR#2**	**MWP**		**DWP**	
CSPR target [pL cell^{-1} d^{-1}]	**15**	**20**	**15**	**20**	**20**	**20**	**15**	**20**	**15**	**20**
average CSPR [pL cell^{-1} d^{-1}]	15.9 ± 1.4	21.1 ± 1.3	18.5 ± 0.9	25.0 ± 2.4	15.7 ± 0.7	22.0 ± 1.0	16.8 ± 1.5	21.1 ± 1.5	18.6 ± 1.5	24.9 ± 1.6
max. VCC [× 10^6 cells mL^{-1}]	23.9 ± 3.0	31.1 ± 0.9	25.2 ± 0.9	26.4 ± 3.0	18.4 ± 2.0	26.0 ± 1.0	44.4 ± 1.2	44.8 ± 1.8	33.4 ± 2.3	33.2 ± 2.8
STY [g L^{-1} d^{-1}]$^{\#}$	0.09 ± 0.00	0.13 ± 0.00	0.19 ± 0.00	0.22 ± 0.00	0.04 ± 0.00	0.34 ± 0.03	0.34 ± 0.04	0.51 ± 0.03	0.40 ± 0.30	0.42 ± 0.03
q_P [pg cell^{-1} d^{-1}]	47.3 ± 3.0	43.4 ± 2.5	40.2 ± 2.0	42.2 ± 3.4	21.8 ± 2.3	45.6 ± 5.9	22.8 ± 5.1	31.0 ± 4.1	40.6 ± 1.7	34.9 ± 1.8
V_M [mL]	42.9	44.7	353.1	426.7	548.0	1183.6	82.4	99.8	573.5	750.5

Cells were cultivated in HIP medium supplemented with 30 % Feed B (v/v).
$^{+}$minimum value
$^{\#}$endpoint value on day 8
Yield and productivity values are given as average and standard deviation of N = 3 wells over the entire culture duration of 8 days.
CCD: conventional cell density; HCD: high cell density; RV: reactor volume; VCC: viable cell concentration; CSPR: cell specific perfusion rate; STY: space-time-yield; q_p: cell specific productivity; V_M: volume of consumed medium

4.3 Discussion

In this chapter, two perfusion rate strategies—RV d^{-1}-based and CSPR-based—were implemented and compared in a small-volume platform to evaluate their effects on cell growth, productivity, and metabolic performance, with the goal of assessing their suitability for robust screening platform. Previously published studies on non-instrumented small-scale semi-perfusion models have exclusively used a fixed RV d^{-1}-based perfusion rate strategy, typically involving manual medium exchanges once or twice daily (Mayrhofer et al., 2021; Tregidgo et al., 2023; Villiger-Oberbek et al., 2015; Wolf et al., 2018). However, this approach does not account for the actual state of the cell culture, potentially leading to under- or over-supply of metabolites and the accumulation of inhibitory by-products, which can significantly impact cell growth and productivity (Karst, Steinebach, et al., 2017; Nikolay et al., 2020). In contrast, the CSPR-based strategy adjusts the perfusion rate based on the VCC at the time of sampling, enabling partial medium exchange. Assuming cellular activity remains stable, this method helps maintain a constant CSPR and medium composition, supporting consistent production (Chotteau, 2015; Ozturk, 1996). To investigate the impact of these strategies both RV d^{-1}-based and CSPR-based perfusion rates were applied to achieve maximum VCCs. The experiments were conducted in 24-well MWP and selected conditions subsequently transferred to a 6-well DWP format for extended studies. Finally, the best-performing condition was scaled up to a 250 mL perfusion bioreactor for validation of the well-plate results.

MWP cultures

Experiments in 24-well MWPs were inoculated at CCD and HCD concentrations. In both cases, growth and metabolic outcomes were comparable across all CSPR targets for both strategies. However, an exception was observed in the MWP-MG_R2 culture which used the RV d^{-1}-based strategy at HCD inoculation and achieved maximum VCCs 1.6-fold higher than MWP-MG_R1 and all CSPR-based cultures.

In contrast to the CSPR cultures, the control cultures (MWP-MG_R1 and MWP-MG_R2) exhibited a rapid decline in VCCs after reaching their peak, while all CSPR cultures sustained stable VCCs throughout the cultivation period. Notably, MWP-MG_20, which aimed to maintain a stable CSPR of 20 pL $cell^{-1}$ d^{-1}, kept the VCCs steady at approximately 40 × 10^6 cells mL^{-1}, with less than 10% variation and high viability (>90%) from day 2 onwards, continuing through the remainder of the cultivation. This observation suggests that a "steady-state" may have been achieved, even without intentional cell bleed, where the medium, combined with a perfusion rate strategy targeting a CSPR of 20 pL $cell^{-1}$ d^{-1}, supported growth to cell densities of approximately 40 × 10^6 cells mL^{-1}. The stabilisation of glucose and ammonium concentrations by days 5 and 6 further supports this hypothesis. In contrast, lactate levels continued to decline until day 8, which may indicate a

metabolic shift toward lactate consumption, despite the continued availability of glucose, as previously reported (Altamirano et al., 2000, 2001, 2004; Dorai et al., 2009). This could reflect the culture's adaptation to metabolic conditions or a shift in cellular priorities, potentially linked to nutrient limitation or other factors like pH.

A concern during the cultivation was the accumulation of toxic by-products. The accumulation of toxic by-products, especially lactate and ammonium, may negatively impact pH and membrane transport (Hassell et al., 1991; Martinelle & Häggström, 1993). Although neither lactate nor ammonium reached concentrations known to be toxic for CHO cells (Fu et al., 2016; Hansen & Emborg, 1994; Lao & Toth, 1997), further studies are needed to investigate the pH dynamics in MWPs. Additionally, strategies that incorporate pH monitoring and control, such as buffer supplementation, should be explored to mitigate any possible effects.

In CSPR cultures, partial medium exchanges may induce an adaptive response, slowing cellular metabolism and leading to lower maximum VCCs. In contrast, RV d^{-1}-based cultures experience larger fluctuations in nutrient supply (providing high concentrations of nutrients) and by-product removal, which may stimulate cellular metabolism and lead to higher maximum VCCs. The comparable values of cell-specific consumption and production rates across the different perfusion rate strategies suggest that nutrient supply and toxic by-product removal were sufficient to support cell growth. Specifically, the similar q_{Gluc} values indicate that glucose was not a limiting factor in CSPR-based cultures, while the similar q_{Lac} and q_{Amm} values suggest that the accumulation of toxic by-products was not significantly higher than in control cultures, making it unlikely to be a limiting factor for growth. Thus, the decline in VCC and viability observed in MWP-MG_R1, MWP-MG_10 and MWP-MG_15, cannot be fully explained with results obtained from metabolite measurements and might have been caused by the depletion or accumulation of unmeasured factors such as amino acids and their catabolised products. However, since the MWP is a small-scale system with limited working volume, a trade-off must be made between the lack of data due to unmeasured factors and the benefit of measuring key metabolic factors.

Although growth and metabolism were comparable across different perfusion rate strategies and showed similar dynamics between inoculation concentrations, slight differences were noted in the productivity outcomes. At CCD inoculation, STY in MWP-MG_R1 was three times lower than in MWP-MG_20. Conversely, at HCD inoculation, MWP-MG_R1 and MWP-MG_R2 cultures exhibited higher STYs. Despite these variations, the final STYs for MWP-MG_R1 and MWP-MG_20 were comparable (within 5%). Additionally, since MWP-MG_R1 and MWP-MG_R2 cultures showed decreasing VCCs while MWP-MG_20 maintained stable growth, prolonged cultivation could reveal potential productivity benefits of partial medium exchanges.

Unexpectedly, q_P for CCD-inoculated CSPR cultures was nearly twice as high as that of control and HCD-inoculated cultures. The elevated q_P values in CCD-inoculated cultures compared to corresponding control cultures may indicate a metabolic shift from exponential growth to a more stable growth phase. In this phase, CSPR cultures may transition from biosynthesis to mAb production as VCCs stabilise at the end of culture, while control cultures remain in the exponential growth phase. However, the VCCs of HCD-inoculated CSPR cultures, which suggest a prolonged stable growth phase, would generally be associated with higher mAb production, which contradicts the observed results. One possible explanation is that despite the stable VCCs, a decline in cell viability—especially in MWP-MG_10 and MWP-MG_15—could have led to a sharp reduction in q_P values. This may also explain why MWP-MG_20 exhibited the highest q_P values of all CSPR cultures at HCD, even though these values were still about 30% lower than those observed in CCD cultures, as MWP-MG_20 maintained high viability throughout the cultivation. In contrast, control cultures largely remain in exponential growth, with MWP-MG_R1 showing only a brief stabilisation of VCCs before a drastic decline, likely driven by reduced viability, which could explain the lower productivities. However, it remains unclear why the q_P of the control culture MWP-MG_R2 was as high as that of MWP-MG_20, considering MWP-MG_R2 exhibited the highest VCCs, showing drastic exponential growth in the first half of the culture and only stabilising later. It is possible that the later stabilisation of VCCs at higher levels than seen for CSPR cultures contributed to the similarly high q_P observed.

Overall, for HCD inoculated cultures, the q_P and STY of MWP-MG_20 closely aligned with MWP-MG_R1 and MWP-MG_R2 results. These findings suggest that while all CSPR targets supported cell growth, lower CSPRs negatively impacted productivity, aligning with previous reports (Lin et al., 2017). Instead, a trade-off must be made between low medium consumption and optimising for high productivity as the highest productivity may occur at CSPRs higher than the minimum CSPR.

To ensure stable CSPRs throughout the growth phase, the dynamics of perfusion rates and actual CSPRs were further analysed. As expected, perfusion rate variations followed VCC trends for both CCD and HCD inoculations. The lower perfusion rate in CSPR cultures indicates reduced medium consumption. Notably, at CCD inoculation, the actual CSPR showed an up to 50-fold increase for MWP-MG_R1 cultures, compared to CSPR-cultures, clearly indicating that the culture is being overfed when using the perfusion rate strategy based on a fixed RV d^{-1}. Overfeeding may lead to nutrient imbalances and metabolic stress, potentially impacting the cell culture performance that could impact scalability of results. Even though the actual CSPR of CSPR-cultures exhibited fluctuations at the beginning of the culture —particularly for CCD-inoculated cultures—these were likely caused by the small, manually handled medium exchange volumes. To investigate this and other observations, two of the three CSPR setpoints were transferred into the larger 6-well

DWP with a working volume of 30 mL for further investigation and comparison to the 24-well MWP.

DWP cultures

The 6-well DWP cultures exhibited a similar response to different perfusion rate strategies, as observed in the 24-well MWP. As in previous experiments, cultures were inoculated at both CCD and HCD. Cultures inoculated at HCD achieved higher maximum VCCs and plateaued at elevated levels, indicating that inoculation concentration influences the maximum achievable VCC. Both control and CSPR cultures plateaued near their peak VCCs and maintained these levels throughout the cultivation period. Notably, CSPR cultures exhibited less variation in VCCs (fluctuating by less than 10% between day 4 and 8), whereas the DWP-MG_R1 control culture showed greater variability (14% variation from day 4 to day 8).

The perfusion rate followed a similar dynamic as VCC, increasing and stabilising in response to cell growth as expected. This adaptive behaviour ensured that the CSPR targets remained stable as intended. However, the DWP-MG_R1 culture exhibited an up to 27-fold increase in actual CSPRs, compared to CCD-inoculated CSPR-cultures, and a more than 2-fold increase compared to HCD inoculated CSPR cultures. This suggests that a fixed RV d^{-1} based perfusion rate strategy leads to overfeeding.

An interesting observation was made regarding productivity. While q_P values decreased from CCD to HCD inoculation, this difference was minor and not statistically significant, falling within the experimental error when comparing individual conditions. However, as observed in MWP cultures, the q_P values in the control cultures were lower at both CCD and HCD inoculation, whereas CSPR cultures consistently achieved nearly 2-fold higher q_P values. Since control cultures exhibited higher VCCs, this suggests a metabolic shift favouring cell growth over mAb production. Previous studies have shown that the growth phase is characterised by high nutrient consumption, particularly of glucose and glutamine (Coulet et al., 2022), with up to 75% of glucose converted into lactate. However, this distribution is dependent on the operation mode. Goudar et al. demonstrated that perfusion cultures exhibited a more balanced metabolism, with only ~55% of glucose redirected to lactate production (Goudar et al., 2010). During later stages of the exponential phase glucose consumption decreases and lactate is increasingly metabolised. In contrast, the stationary phase is characterised by reduced carbon and nitrogen source consumption, as cellular energy shifts toward biosynthesis. The hypothesis is supported by the VCC dynamics observed in this study: control cultures exhibited prolonged exponential growth compared to CSPR cultures, likely due to higher nutrient availability, which extended the growth phase and delayed the transition to the stationary phase.

While most metabolite concentration dynamics were comparable across different perfusion rate strategies, several noteworthy observations emerged. Control cultures achieved higher VCCs at both inoculation densities, which would typically suggest greater glucose consumption and, consequently, lower or similarly low residual glucose concentrations compared to CSPR cultures. However, this trend was only observed in HCD-inoculated cultures, where glucose concentrations in control cultures were lower than in CSPR cultures. In contrast, CCD-inoculated CSPR cultures exhibited lower glucose levels than their control counterparts. This discrepancy suggests that, in CCD-inoculated cultures, partial medium exchange in CSPR cultures was the primary factor contributing to reduced glucose concentrations, whereas the total medium exchange in control cultures provided sufficient nutrients to sustain high VCCs without depleting glucose to lower levels. Notably, all CSPR cultures maintained glucose levels above 20 mmol L^{-1} regardless of the perfusion rate strategy, indicating adequate nutrient availability for both growth and productivity. In contrast, control cultures exhibited glucose concentrations above 30 mmol L^{-1} for CCD-inoculated cultures and above 10 mmol L^{-1} for HCD-inoculated cultures. Additionally, at both CCD and HCD inoculations, control cultures exhibited 1.5-fold higher ammonium concentrations than CSPR-cultures. Neither lactate nor ammonium concentrations reached or exceeded levels reported toxic to CHO cell culture either individually or in combination (Fu et al., 2016; Hansen & Emborg, 1994; Lao & Toth, 1997). Interestingly, CSPR-cultures stabilised at similar low glucose and similar high ammonium concentrations across both inoculation conditions. In contrast, lactate concentrations stabilised at varying levels, despite CCD cultures reaching peak lactate concentration similar to those of HCD cultures.

The analysis of external metabolites supports the hypothesis that the reduced productivity observed in control cultures is due to a metabolism primarily focused on growth. As previously described, CCD cultures initially enter growth phase, and are transitioning to the stationary phase around day 8, while control cultures exhibit prolonged exponential growth. In contrast, HCD cultures primarily exhibit the stationary phase for both perfusion rate strategies. This is further supported by the average cell-specific glucose consumption (q_{Gluc}) and lactate production (q_{Lac}) rates observed in both CCD and HCD cultures. In CSPR cultures, the average q_{Gluc} over the 10-day cultivation period ranges from 4.5 to 5.1 pmol $cell^{-1}$ d^{-1} for CCD-inoculated cultures and from 2.3 to 2.4 pmol $cell^{-1}$ d^{-1} for HCD-inoculated cultures. In comparison, control cultures exhibited a more pronounced difference, with q_{Gluc} values of 9.9 pmol $cell^{-1}$ d^{-1} for CCD and 2.2 pmol $cell^{-1}$ d^{-1} for HCD inoculated cultures. A similar trend was observed for q_{Lac} values, with higher values in CCD-inoculated cultures compared to HCD cultures. Specifically, q_{Lac} ranged from 1.2 to 1.4 pmol $cell^{-1}$ d^{-1} in CSPR cultures (2.0 pmol $cell^{-1}$ d^{-1} for control cultures) for CCD inoculation, while in HCD cultures, ranging from 0.6 to 0.7 in CSPR cultures (0.7 pmol $cell^{-1}$ d^{-1} for control cultures).

The much higher average q_{Gluc} values for control cultures, particularly for CCD inoculated cultures, further indicate a metabolism directed to cell growth rather than mAb production. While average q_{Gluc} values for HCD-inoculated cultures were similar across both perfusion rate strategies, their daily q_{Gluc} trends differed notably. In control cultures, q_{Gluc} started at 5.0 pmol cell^{-1} d^{-1} and gradually declined to a steady value of 1.6 pmol cell^{-1} d^{-1} by day 5. In contrast, CSPR cultures exhibited an initial q_{Gluc} of 2.9 and 3.3 pmol cell^{-1} d^{-1} (for DWP-MG_15 and DWP-MG_20, respectively), stabilising more rapidly at 2.3 and 2.4 pmol cell^{-1} d^{-1} from day 2 onwards. A similar pattern was observed for daily q_{Lac} values, where HCD-inoculated control cultures experienced a gradual decrease over multiple days, while CSPR cultures stabilised after day 1. This suggests that the metabolism of control cultures remains in flux for a longer period, potentially delaying the transition from a growth phase to a stationary phase, where metabolism shifts from biomass synthesis to mAb production, compared to CSPR cultures. These findings further support the conclusion that lower productivities in control cultures resulted from metabolic differences between the two perfusion strategies.

Comparing both systems showed that similar growth and productivity were achieved for both CSPR targets. In addition, the previously observed fluctuation of the actual CSPR for CCD-inoculated MWP cultures did not appear in the CCD-inoculated DWP cultures. This suggests that these fluctuations were likely caused by the manual handling of small volumes. Automated systems, such as robotic platforms, are less susceptible to day-to-day handling errors and could provide more consistent liquid handling. However, it is important to evaluate whether the reduction in fluctuation is purely due to automation or whether other factors, such as the larger working volume in DWP cultures, also contribute.

It was previously hypothesised that the partial medium exchange led to a slowdown in growth and consequently the stabilisation of VCCs, indicating the reaching of a “steady-state” without intentional cell bleed (**Section 3.2.1**). However, while these results suggest a steady-state-like environment, further investigation is required to confirm whether this is a true steady-state, as defined by sustained metabolic balance and consistent growth over extended periods, or if it represents a pseudo-steady-state. Specifically, MWP-MG_20 achieved comparable VCCs with high viabilities and improved productivities relative to control cultures. These observations were speculated to be due to the establishment of a stable environment. However, the sacrificial well methodology and the resulting short process duration meant that longer culture times were required to fully assess system stability, including the consistency of cell growth and metabolic dynamics over time. Future studies will be critical to determine if the trends observed in these shorter cultures persist over longer durations and to further validate the system’s stability.

When comparing the MWP and the DWP systems, both of which were operated under conditions targeting 15 and 20 pL cell^{-1} d^{-1}, growth and viability dynamics were similar across both scales. The extended culture times and the stable dynamics observed, particularly in the HCD-inoculated DWP cultures, suggest that a more stable environment may have been achieved. Additionally, the dynamics of the STY for HCD-inoculated cultures further support the hypothesis that the culture reached a stable production phase, often associated with a "steady-state" environment. However, the observed decline in viability towards the end of the culture in HCD-inoculated cultures, both in MWP and DWP systems, warrants further investigation. This is especially important if these systems are to be used beyond their current role as screening platforms in process development, where long-term process stability is fine-tuned and evaluated at the bioreactor scale.

Perfusion bioreactor

The perfusion bioreactors in this study were operated for 10 days, which is shorter than typical bench-top bioreactors. However, the primary objective of these experiments was to compare well-plate systems to the bioreactor, rather than conduct long-term process development studies. The 10-day duration was chosen to align with the maximum culture time of the DWP format, ensuring a direct comparison. Since well-plate systems are intended as screening tools, the key objective was to assess the reliability of early-stage results in comparison to the perfusion bioreactor. Nevertheless, it is recognised that additional studies at larger bioreactor scales are required for comprehensive process development.

The CSPR target of 20 pL cell^{-1} d^{-1} demonstrated the best growth and productivity performance. Consequently, this condition was selected for further validation in 250 mL perfusion bioreactor cultures. Due to an issue with the gas supply, the first bioreactor run (BR#1-MG_20) had to be terminated prematurely at day 7, making it the shortest experiment across all scales. Despite this, both perfusion runs showed comparable growth and similar CSPR trends until day 7.

Notably, the earlier start of perfusion in BR#1-MG_20 did not confer an advantage in growth or productivity. Instead, the later initiation of perfusion in BR#2-MG_20 appeared to result in similar or slightly faster growth (growth rate average between day 0 and day 5 of 0.019 h^{-1} and 0.22 h^{-1} for BR#1-MG_20 and BR#2-MG_20, respectively) and increased productivity. By day 7, the STY in BR#2-MG_20 was 3.7-fold higher than in BR#1-MG_20. One possible explanation is that the delayed start of perfusion in BR#2-MG_20 led to a more favourable balance for STY calculation (with respect to the medium volume consumption), given that growth, metabolic performance (glucose and ammonium levels), and CSPR were comparable between both runs until day 7. Another factor to consider is the higher lactate concentrations observed in BR#1-MG_20. While still below toxic levels for CHO cells (Fu et al., 2016; Hansen & Emborg, 1994; Lao & Toth, 1997), elevated lactate levels could have negatively impacted productivity.

Additionally, the later onset of perfusion in BR#2-MG_20 may have facilitated an earlier stabilisation of cell growth, which could have contributed to variations in cell culture performance, particularly in terms of productivity. As previously mentioned, productivity tends to be higher during the stable growth phase and lower during the exponential growth phase. It is possible that BR#2-MG_20 transitioned into a stable growth phase sooner, leading to higher productivity by day 7 and over the longer process duration compared to BR#1-MG_20.

Despite the stabilisation of VCC from day 5 or 6 onwards, as well as stable metabolite concentrations between days 6 and 9, the actual CSPRs showed major fluctuations though similar in both bioreactor runs, fluctuating above and below the target value of 20 pL cell^{-1} d^{-1}. These fluctuations could have contributed to variations in cell culture performance. The most likely cause of the fluctuating CSPR was the manual control of perfusion rates, which were adjusted daily based on VCC measurements and controlled via external Watson Marlow pumps. Due to the low working volumes of the perfusion bioreactor system, the required perfusion flow rates—including both feed and harvest rates—were as low as 56 mL d^{-1} (2.3 mL h^{-1}), necessitating very low pump speeds, even with small-diameter tubing (1.6 mm). The Watson Marlow pumps used in this experiment operate at speeds between 0.1 and 32.0 rpm (with an accuracy of one decimal point), allowing for flow rates between 39 mL d^{-1} and 12 L d^{-1} with the tubing used. Before each run, a pump calibration was performed to establish the correlation between pump rate and flow rate. During perfusion operation, achieving the target CSPR of 20 pL cell^{-1} d^{-1} required pump speeds between 0.1 and 0.5 rpm, often necessitating an accuracy of two decimal points to maintain the desired perfusion rate. Since the pumps only allowed adjustments to one decimal point, calculated perfusion rates were rounded up (≥0.05) or down (<0.05). This resulted in deviations from the intended flow rates, affecting CSPR dynamics, nutrient supply, and overall cell culture performance. Additionally, tubing wear over extended process durations may further contribute to inaccuracies in fluid flow rate. While the effects may be minor at lower flow rates, this factor should be considered in longer process development runs to maintain precise perfusion control.

Lastly, the online process parameters—DO, pH, and gas flow rate—were monitored for BR#2-MG_20. While these parameters remained largely stable as intended, notable fluctuations in DO and pH were observed. The DO drop on day 1 was traced to a loose connection in the sparger tubing on the control tower. Once the tubing was reconnected, DO rapidly recovered and remained stable at the set point of 50%. The pH fluctuations observed on days 0 and 1 coincided with these DO disturbances, likely due to interactions between the pH and DO control loops particularly in relation to CO_2 sparging settings. Since CO_2 sparging is used to regulate pH, its override during low DO conditions may have contributed to the transient pH instability. Once DO stabilised on

day 2 and perfusion was initiated on day 3, pH remained stable at its set point of 7.2. Other fluctuations in DO were managed by manually adjusting the agitation speed and modifying the gas flow rate range to allow for higher sparge rates. However, the latter adjustment led to an increase in foaming—an important consideration for longer process development runs. Excessive foaming has previously been associated with reduced cell performance and lower productivity due to bubble-induced cell damage (Trinh et al., 1994; Walls et al., 2017).

The comparison across both well plate systems and the 250 mL perfusion bioreactor showed similar growth and largely similar productivities for the CSPR target of 20 pL cell^{-1} d^{-1}. While the CSPR in the DWP remained stable, similar fluctuations in the MWP and bioreactor systems were observed. It was previously hypothesised that the manual pipetting of small volumes in the MWP contributed to CSPR variability. Although the bioreactor cultures had a higher working volume, parallels can be drawn between the MWP and perfusion bioreactor in terms of the origin of these fluctuations. In the MWP, medium is exchanged once per day in a batch-wise manner, with small volumes manually pipetted each day. In contrast, the perfusion bioreactor relies on continuous medium exchange, with the exchange rate controlled by external pumps (not connected to the control tower). Although the bioreactor exchanges a larger total volume, the low flow rates required for continuous exchange, combined with the accuracy of the pumps, could have led to similar fluctuations. The need for manual adjustments to maintain fixed flow rates in the bioreactor may have had effects comparable to the manual pipetting in the MWP.

These fluctuations, along with the differences in medium exchange modes (batch-wise vs. continuous), may account for the minor variations observed between the systems regarding productivity and glucose consumption. While q_P values were comparable across all conditions and STY remained similar until day 8, the endpoint STY in the bioreactor was nearly 1.5-fold higher than in DWP cultures. This increase in productivity is likely due to the more tightly controlled environment in the bioreactor, particularly with respect to pH and DO, as well as the more stable nutrient supply provided by continuous medium exchange, in contrast to the more abrupt changes associated with batch-wise exchanges in the semi-perfusion system.

The glucose consumption rate in the bioreactor culture was 2.5- to 4-fold lower than in the well plate cultures, likely due to differences in the initial medium composition. Unlike the MWP and DWP cultures, which were seeded with HIP + 30% Feed B, the bioreactor was initially seeded with HIP without Feed B. However, the perfused medium used throughout the experiment contained the targeted HIP + 30% Feed B composition.

This adjustment to the initial medium was made in response to pH control issues observed in earlier runs. The HIP + 30% Feed B medium has a higher pH (~7.4) compared to HIP without

Feed B (~7.2). The control system attempted to regulate pH to the set point of 7.2 (with a deadband of 0.1) using CO_2 sparging. However, the relatively high CO_2 concentration required to achieve this control negatively impacted cell growth, leading to stagnation and eventual cell death shortly after seeding.

To prevent excessive CO_2 sparging and overshooting of the control loop, the initial seed medium for the 3-day batch phase was switched to HIP without Feed B. This modification resulted in more moderate CO_2 sparging and improved cell culture performance. It can be speculated that at higher seed cell concentrations, using the targeted HIP + 30% Feed B medium from the start may not pose the same issue. In such a scenario, lactate production from the cells would naturally reduce pH, thereby decreasing the need for CO_2 sparging and allowing for more stable pH control.

Overall, cell performance in terms of growth, productivity, and metabolic activity was highly comparable across the three culture systems (MWP, DWP, and perfusion bioreactor). Notably, the medium consumption for a single MWP condition (using the sacrificial well method) was 27-fold lower than that of a single perfusion bioreactor run and 10-fold lower than that of one condition in a DWP (comprising three wells). This substantial reduction in medium usage represents a significant cost-saving advantage, making MWPs a more resource-efficient option for early-stage process development and screening.

4.4 Concluding remarks

The objective of the work presented in this chapter was to implement and evaluate the CSPR-based perfusion rate strategy in the 24-well MWP platform. The results demonstrated that HCD cultivation could be achieved with this approach, while maintaining a stable culture environment. Furthermore, dynamic CSPR adjustments were scalable to both deep-well plates (DWP) and a 250 mL perfusion bioreactor, reinforcing the applicability of MWPs as predictive scale-down models.

These findings highlight that CSPR-based semi-perfusion in 24-well MWPs can effectively mimic perfusion bioreactor conditions, making them a valuable tool for early-stage optimisation. Key process parameters—including cell growth, metabolic activity, and productivity—showed good agreement between 24-well MWPs and the 250 mL perfusion bioreactor. Additionally, MWPs offer a high-throughput screening platform, enabling rapid evaluation of multiple CSPR conditions in parallel, which is not feasible in larger, resource-intensive bioreactors. This accelerates process development while reducing material costs and experimental time.

However, some challenges remain. Small medium exchange volumes in MWPs and low flow rates in the perfusion bioreactor led to difficulties in maintaining a stable CSPR. Automating the MWP workflow—such as through an automated liquid handling system—could reduce manual

pipetting variability, while improved pump control and more frequent perfusion rate adjustments may enhance stability in bioreactor setups.

A key outcome of this study was the successful implementation of partial medium exchanges in the MWP without major impacts on cell culture performance, demonstrating feasibility for automated operation. Unlike total medium exchanges, partial exchanges allow for integration with a liquid handling arm, avoiding disturbances to cell pellets (centrifugation) or cell clouds (sedimentation). This makes the platform more suitable for process development applications, including medium development, cell clone screening, and early-stage process optimisation.

To further explore the capabilities and limitations of the MWP platform, the next chapter will build on the findings of **Chapter 3** and **Chapter 4**, combining cell bleed with CSPR-based perfusion to assess their combined impact on culture performance.

Chapter 5: Platform development for high-throughput perfusion optimisation – Integrating cell bleed and CSPR-based perfusion rate strategies in well plates *

5.1 Introduction

A key strategy in perfusion processes is to maintain stable cell density while keeping cells in a growth phase, which can be achieved by bleeding cells at a rate approximately equal to the cell growth rate to establish a "quasi steady-state" (Chotteau, 2015). However, the bleed stream is often considered waste and is associated with product loss. To minimise this, it is crucial to reduce the growth rate during the "steady-state" phase while maintaining high cell viability. Several approaches have been proposed to reduce growth, such as chemical addition (e.g., butyrate) or hypothermia (Chotteau et al., 2023). Alternatively, growth can be reduced by limiting nutrient availability, for example, by employing a CSPR-based perfusion strategy and lowering the CSPR target. However, risks such as depletion of amino acids and vitamins, or potential product degradation due to reduced growth, must be managed (Chotteau et al., 2023). This can be mitigated through additional online or offline control strategies that monitor product quality and media composition.

In **Chapter 3**, a cell bleed strategy was implemented to maintain a stable cell concentration (stable growth (SG)), establishing a “quasi-steady state” with medium exchanges corresponding to a perfusion rate of 1 RV d^{-1}. **Chapter 4** explored variable perfusion rates to create a stable environment while targeting maximum cell densities (maximum growth (MG)). This chapter builds on the successful implementation of the cell bleed strategy in **Chapter 3** and the implementation of a CSPR-based-perfusion rate strategy in **Chapter 4**. Here, both strategies – the cell bleed and the CSPR-based perfusion rate - are integrated, mimicking the combination of bleed and varying harvest rates typically seen in perfusion processes.

---

* Some of the results presented in this chapter are included in:

Dorn, M., Lucas, C., Klottrup-Rees, K., Lee, K., & Micheletti, M. (2024). Platform development for high-throughput optimization of perfusion processes—Part II: Variation of perfusion rate strategies in microwell plates. Biotechnology and Bioengineering, 121(6), 1774–1788. https://doi.org/10.1002/bit.28685

This integration more closely mimics the stable growth and production phase at HCD, reflecting the practices of many bioreactor operations that use CSPR-based perfusion rates to minimise medium usage while maximising productivity. The combined approach allows for the investigation of individual sections of a perfusion process at small scale, facilitating screenings and fine-tuning before scaling up to bench-scale bioreactors.

This chapter aims to evaluate the feasibility and performance of an integrated strategy that combines cell bleed and CSPR-based perfusion rate control, applied across both 24-well MWP and 6-well DWPs. The focus is on understanding how much manipulation of the cell culture environment can be performed without significantly impacting cell performance in small-scale systems. In the MWP format, the combined strategy is assessed in terms of culture stability, metabolic activity, and productivity. The DWP format, meanwhile, serves as an intermediate scale, offering insight into the scalability of the approach and its potential as a stepping stone toward full perfusion bioreactor operations. Through this integrated approach, the chapter explores whether distinct phases of a perfusion bioreactor process can be effectively replicated and studied in scale-down systems.

5.2 Results

This section of the chapter is divided into two main sections presenting the results of the study and is followed by a discussion section to set the results in context. **Section 5.2.1** details the integration of cell bleed and CSPR-based perfusion rate in 24-well MWP plates, while **Section 5.2.2** discusses the scale up to the 6-well DWP. In all experiments in this chapter the CHO cobra cell line was used.

5.2.1 24-well microwell plate with combined cell bleed and CSPR-based perfusion rate

Evaluation of growth and metabolism

The experiments in this section were based on results presented in the previous two chapters, **Chapter 3** and **Chapter 4**. Similar to previous experiments, the goal was to maintain a stable VCC of approximately 20 ×10^6 cells mL^{-1} in all cultures and with all perfusion rate strategies. The chosen CSPR targets were informed by results from the previous chapters, with a total of three target CSPRs investigated. **Chapter 4** concluded that cultures targeting a CSPR of 15 and 20 pL $cell^{-1}$ d^{-1} provided good support for cell growth and achieved high productivity (**Section 4.2.1**), making these two conditions the primary focus of further analysis in this chapter. Additionally, a third CSPR target of 30 pL $cell^{-1}$ d^{-1} was included, selected based on the average CSPRs observed in cultures maintaining a stable VCC of 20 x 10^6 cells mL^{-1} at a perfusion rate of 1 RV d^{-1}, as detailed in **Chapter 3**. MWP cultures employing a combined cell bleed and CSPR-based

perfusion rate strategy to maintain stable growth conditions are referred to as MWP-SG20_15, MWP-SG20_20, and MWP-SG20_30, corresponding to CSPR targets of 15, 20 and 30 pL cell^{-1} d^{-1}, respectively. To facilitate comparison, the MWP-SG20 (1 RV d^{-1}) condition from **Chapter 3** was included as control condition.

Figure 5.1 presents the cell growth, actual CSPR dynamics and process flow rates over the culture duration for CSPR-cultures and the control culture. Across all conditions, a characteristic "saw-tooth" oscillation around the target average VCC was observed (**Figure 5.1A**). This oscillatory pattern was maintained throughout the cultivation in the control culture, which achieved an average VCC of 23.8 ± 1.5 × 10^{6} cells mL^{-1}. In contrast, cultures with CSPR-based perfusion rate strategy exhibited greater fluctuations around the targeted average value starting on day 3 (**Figure 5.1A**), with the oscillation amplitude between consecutive days gradually decreasing over time. Despite these fluctuations, the average VCC values for the MWP-SG20_15, MWP-SG20_20, and MWP-SG20_30 cultures were 20.7 ± 1.7, 21.4 ± 1.9, and 21.6 ± 2.4 × 10^{6} cells mL^{-1}, respectively (**Table 5.1**). Overall, cell viabilities remained above 90%, with only a slight decline observed toward the end of the cultivation (**Figure 5.1A**).

The analysis of actual CSPRs revealed fluctuations, with target CSPRs not always being reached or maintained in CSPR-cultures. Initially, the actual CSPRs for all CSPR-cultures were lower than their respective targets. MWP-SG20_15 and MWP-SG20_20 reached their target CSPRs of 15 and 20 pL cell^{-1} d^{-1} on days 4 and 3, respectively. While MWP-SG20_15 was able to maintain its target CSPR from that point onward, MWP-SG20_20 remained slightly below its target throughout the cultivation. In contrast, MWP-SG20_30 never fully reached its target CSPR of 30 pL cell^{-1} d^{-1}, though a gradual increase was observed over time. The overall average CSPRs were 14.5 ± 0.9, 17.6 ± 1.4, and 24.3 ± 2.1 pL cell^{-1} d^{-1} for MWP-SG20_15, MWP-SG20_20 and MWP-SG20_30, respectively (**Table 5.1**). The control culture, by comparison, exhibited an initial decline in CSPR, stabilising around 23 pL cell^{-1} d^{-1} between days 2 and 6 before increasing toward the end of the cultivation (**Figure 5.1B**, **Table 5.1**).

Despite the variation in CSPR performance, process flow rates remained generally stable over the course of the experiment (**Figure 5.1C** and **D**). Perfusion rates showed minor fluctuations stabilising at distinct levels across the CSPR-based cultures, with average values of 0.6, 0.7, and 0.9 RV d^{-1} for MWP-SG20_15, MWP-SG20_20 and MWP-SG20_30, respectively. Hence, perfusion rates for all CSPR-based cultures were, on average, lower than that of the control cultures (**Figure 5.1C**, **Table 5.1**). Bleed rates, shown in **Figure 5.1D**, fluctuated more noticeably in CSPR-cultures, but remained on average within the range of 0.2 to 0.3 RV d^{-1}, slightly lower than the average bleed rate of around 0.4 RV d^{-1} observed in control cultures. These larger variations in bleed rates reflect

differences in growth behaviour between the perfusion rate strategies, particularly the reduced growth in the CSPR-based cultures compared to the control.

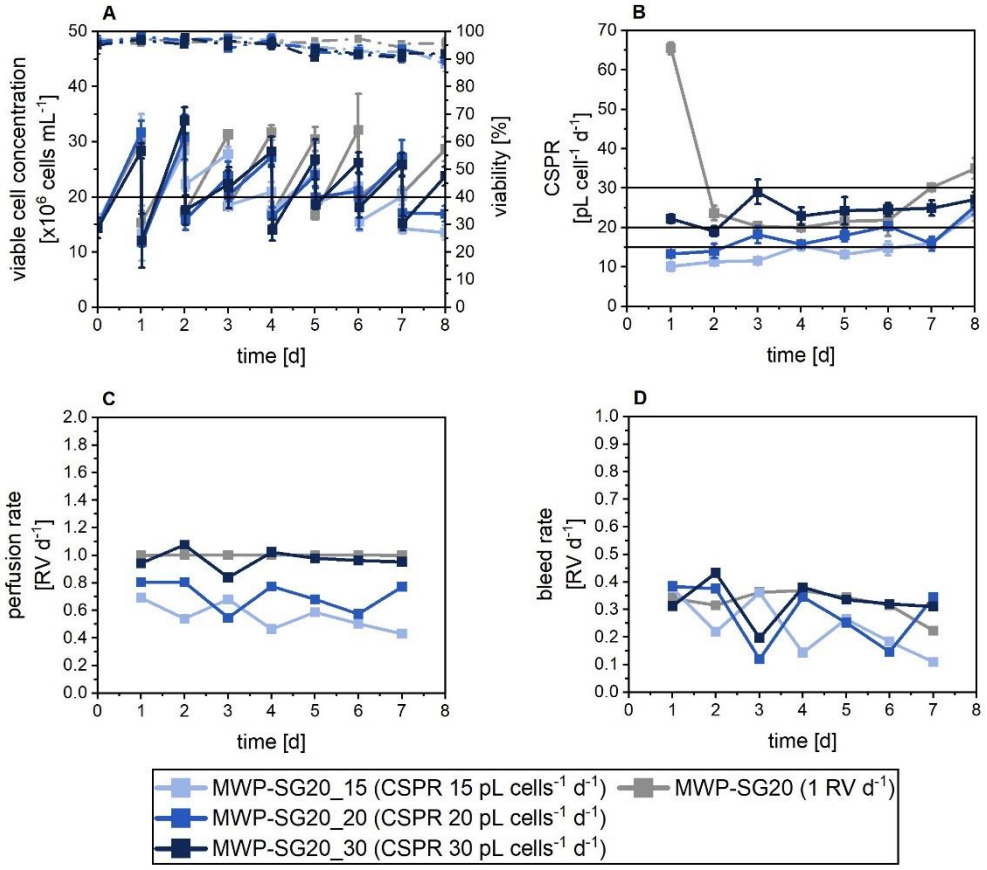

Figure 5.1: Growth and perfusion process flow rates for CHO cobra cells in 24-well MWP cultivations in semi-perfusion with different perfusion rate strategies and implemented cell bleeds. Cells were inoculated at 20 x 10^6 cells mL^{-1} and cultivated in HIP medium supplemented with 30% Feed B (v/v). A: viable cell concentration (filled) and viability (open); B: CSPR; C: perfusion rate; D: bleed rate. Targeted CSPRs (pL $cell^{-1}$ d^{-1}): 15 (■), 20 (■), 30 (■). Perfusion rate equal to 1 RV d^{-1} (■). Mean of *N = 3* wells. Error bars indicate standard deviation. CHO: Chinese Hamster ovary; CSPR: cell-specific perfusion rate; MWP: microwell plate.

The analysis of external metabolites—glucose, lactate, and ammonium—presented in **Figure 5.2**, further highlights the metabolic dynamics across the conditions. Stable glucose and lactate concentrations were observed after day 1 across all cultures (**Figure 5.2**). As expected, cultures targeting lower CSPRs exhibited the lowest glucose concentrations, with MWP-SG20_15 and MWP-SG20_20 yielding average glucose levels of 23.1 ± 1.5 and 25.2 ± 0.9 mmol L^{-1}, respectively (**Figure 5.2A**, **Table 5.1**). In contrast, targeting a stable CSPR of 30 pL $cell^{-1}$ d^{-1}, as well as those with a perfusion rate of 1 RV d^{-1}, showed comparable glucose concentrations of 32.6 ± 2.0 and 28.7 ± 1.5 mmol L^{-1}, respectively. Additionally, both conditions exhibited an increase in glucose concentration from day 6. These trends align with the dynamics observed in the actual CSPR values for both conditions, suggesting similar metabolic behaviour across the different medium exchange strategies.

Building on the trends observed in glucose concentrations, it was anticipated that cultures targeting lower CSPRs would exhibit higher lactate levels due to the smaller exchange volumes typically leading to lactate accumulation. However, the lowest lactate concentrations were observed in the MWP-SG20_15 and MWP-SG20_20 cultures, with average values of 9.0 ± 0.5, 10.6 ± 0.4, and 12.2 ± 0.6 mmol L^{-1} for cultures targeting CSPRs of 15, 20, and 30 pL $cell^{-1}$ d^{-1}, respectively (**Figure 5.2B**). In comparison the control culture, which utilised total medium exchange, maintained stable lactate concentrations of 11.6 ± 1.0 mmol L^{-1}.

Ammonium concentrations stabilised after day 1, where CSPR conditions obtained slightly higher concentrations than control cultures (**Figure 5.2C**). However, the concentration remained below 10 mmol L^{-1} across all conditions (q_{Amm} < 0.6 pmol $cell^{-1}$ d^{-1}) (**Table 5.1**).

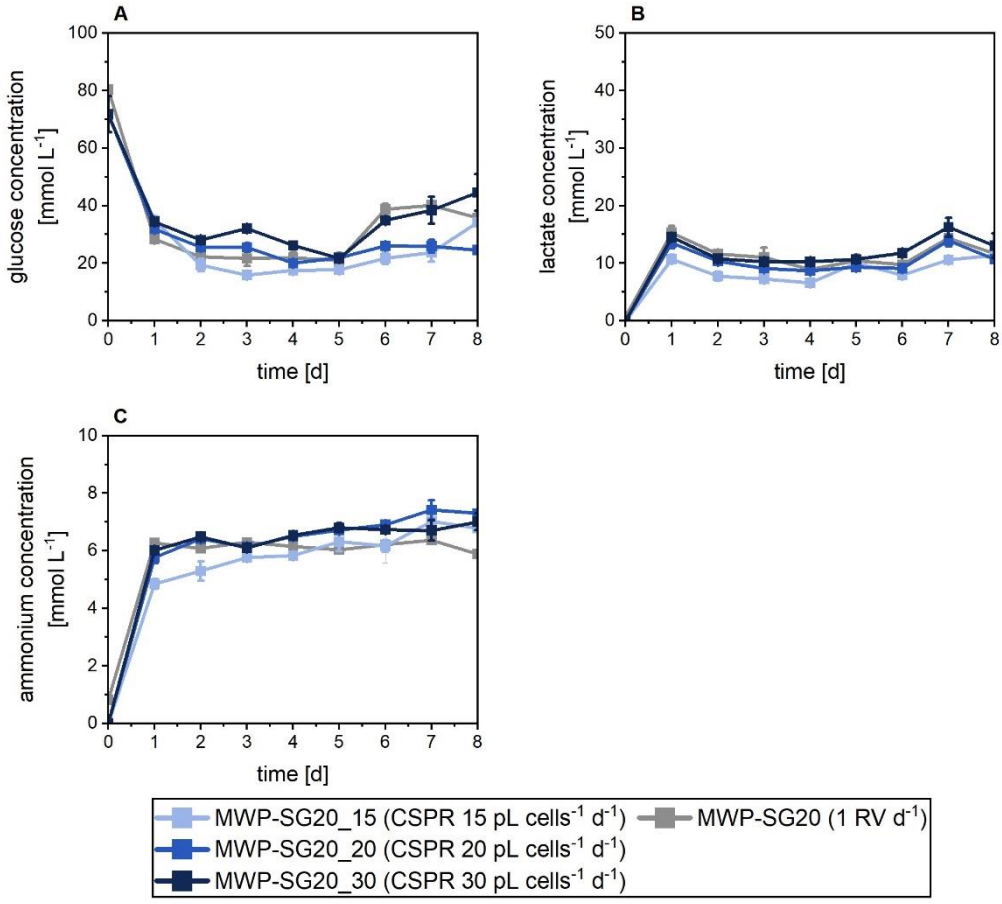

Figure 5.2: Metabolite concentrations for CHO cobra cells in 24-well MWP cultivations in semi-perfusion with different perfusion rate strategies and implemented cell bleeds. Cells were inoculated at 10, 20, 30 and 40 x 10^6 cells mL^{-1} and cultivated in HIP medium supplemented with 30% Feed B (v/v). A: glucose; B: lactate; C: ammonium. Targeted CSPRs (pL $cell^{-1}$ d^{-1}): 15 (■), 20 (■), 30 (■). Perfusion rate equal to 1 RV d^{-1} (■). Mean of N = 3 wells. Error bars indicate standard deviation. CHO: Chinese Hamster ovary; CSPR: cell-specific perfusion rate; MWP: microwell plate; STY: Space-Time-Yield.

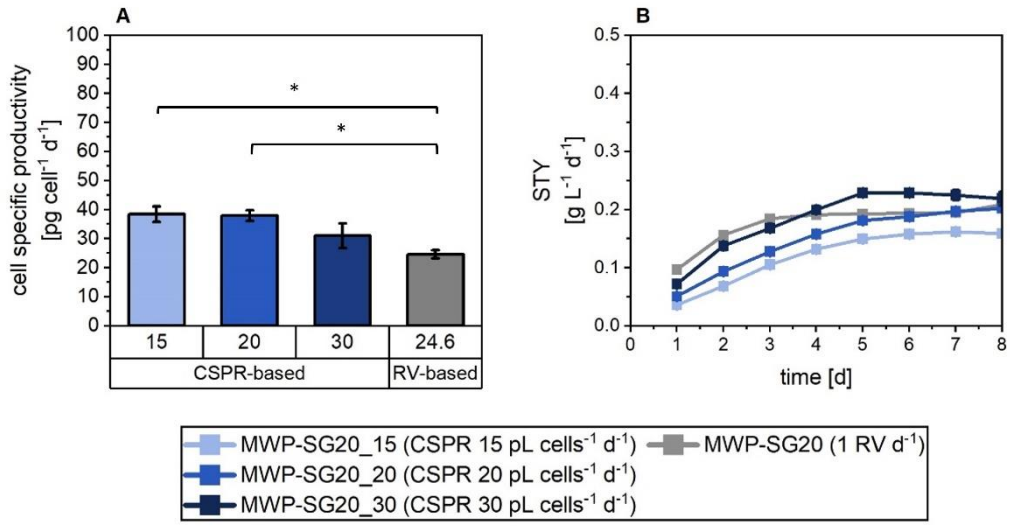

Figure 5.3: Productivities for CHO cobra cells in 24-well MWP cultivations in semi-perfusion with different perfusion rate strategies and implemented cell bleeds. Cells were inoculated at 20 x 10^6 cells mL^{-1} and cultivated in HIP medium supplemented with 30% Feed B (v/v). A: cell-specific production rate; B: STY. Targeted CSPRs (pL $cell^{-1}$ d^{-1}): 15 (■), 20 (■), 30 (■). Perfusion rate equal to 1 RV d^{-1} (■). Mean of *N = 3* wells. Error bars indicate standard deviation. Significant difference was evaluated with a two-sample t-test assuming equal variance with * $p < 0.05$. CHO: Chinese Hamster ovary; CSPR: cell-specific perfusion rate; MWP: microwell plate; STY: Space-Time-Yield.

The cell specific productivity (q_P) and STY were calculated and used as parameters to account for differences in perfusion rates and enable comparison of productivity across conditions. The resulting values are presented in **Figure 5.3**. Regardless of the perfusion rate strategy, similar trends were observed for both q_P (**Figure 5.3A**) and STY (**Figure 5.3B**). CSPR-cultures consistently exhibited higher q_P values compared to the control cultures, with a significant difference ($p < 0.05$) observed between the two perfusion rate strategies. CSPR-cultures achieved an average q_P of 36.0 pg $cell^{-1}$ d^{-1}, while control cultures reached 24.5 ± 1.4 pg $cell^{-1}$ d^{-1} (**Figure 5.3A**). Initially, STY increased for all cultures before stabilising around 0.2 g L^{-1} d^{-1}. MWP-SG20_30 achieved an STY of 0.22 g L^{-1} d^{-1} on day 8, nearly identical to the value observed in cultures using total medium exchange 0.21 g L^{-1} d^{-1} (**Figure 5.3B**). The good agreement of both q_P and STY suggests that despite slower cell growth, productivity was not adversely affected. Given that cell viabilities remained above 90% throughout the cultivation period, exploring these conditions with extended cultivation times would be valuable. Such an investigation could provide further insights into how slower growth impacts productivity, as previous studies have indicated that reduced cell growth and induced cell arrest can lead to increased productivities (Ducommun et al., 2002; Gagnon et al., 2018; Wang et al., 2018).

In terms of medium consumption, the total volume of 129 mL per plate used for cultures with a perfusion rate of 1 RV d^{-1} was reduced to 61, 72, and 92 mL for MWP-SG20_15, MWP-SG20_20, and MWP-SG20_30, respectively. This represents a reduction in medium consumption of up to 53%.

Table 5.1: Steady-state values for CHO cobra cells in 24-well MWP culture with implemented cell bleed and with different perfusion rate strategies targeting an average VCC of 20 x 10^6 cells mL^{-1}.

Perfusion rate strategy	**RV d^{-1}**	**CSPR**		
CSPR target [pL $cell^{-1}$ d^{-1}]	**R1**	**15**	**20**	**30**
average VCC [x 10^6 cells mL^{-1}]	23.8 ± 1.5	20.7 ± 1.7	21.4 ± 1.9	21.6 ± 2.4
Metabolites⁺				
Gluc [mmol L^{-1}]	28.7 ± 1.5	23.1 ± 1.5	25.2 ± 0.2	32.6 ± 1.9
Lac [mmol L^{-1}]	11.6 ± 1.0	9.0 ± 0.5	10.6 ± 0.4	12.2 ± 0.6
Amm [mmol L^{-1}]	6.2 ± 0.2	6.0 ± 0.2	6.6 ± 0.1	6.6 ± 0.2
q_{Gluc} [mmol L^{-1}]	3.4 ± 0.2	2.9 ± 0.2	2.9 ± 0.1	3.0 ± 0.3
q_{Lac} [mmol L^{-1}]	1.0 ± 0.1	0.7 ± 0.1	0.9 ± 0.1	1.1 ± 0.1
q_{Amm} [mmol L^{-1}]	0.5 ± 0.0	0.5 ± 0.0	0.5 ± 0.0	0.6 ± 0.1
Productivity				
STY [g L^{-1} d^{-1}]#	0.16 ± 0.00	0.20 ± 0.00	0.22 ± 0.00	0.21 ± 0.01
q_P [pg $cell^{-1}$ d^{-1}]	24.6 ± 1.4	38.4 ± 2.6	37.9 ± 1.8	31.0 ± 4.2
Flow rates⁺				
Perfusion [RV d^{-1}]	1.00	0.56	0.71	0.97
Harvest [RV d^{-1}]	0.75	0.32	0.43	0.64
Bleed [RV d^{-1}]	0.35	0.24	0.28	0.33
CSPR [pL $cell^{-1}$ d^{-1}]	24.7 ± 1.7	14.5 ± 1.0	17.6 ± 1.4	24.3 ± 2.1
V_M [mL]	129.6	60.5	71.1	92.2

Cells were cultivated in HIP medium supplemented with 30 % Feed B (v/v).
#endpoint value on day 8
⁺average value over days 1 to 8
Yield and productivity values are given as average and standard deviation of *N = 3* wells over the entire culture duration of 8 days.
RV: reactor volume; VCC: viable cell concentration; CSPR: cell specific perfusion rate; Gluc: glucose; Lac: lactate; Amm: Ammonium; STY: space-time-yield; q_p: cell specific productivity; V_M: volume of consumed medium

5.2.2 6-well deepwell plate with combined cell bleed and CSPR-based perfusion rate

Following the exploration of the combined approach of cell bleed strategy and CSPR-based perfusion rate in the MWP, the two better performing CSPR targets – 15 and 20 pL $cell^{-1}$ d^{-1} – were scaled up to the DWP system to assess the reproducibility of the MWP experiments. In the MWP, these CSPR targets showed promising results, with MWP-SG20_15 and MWP-SG20_20 cultures achieving stable growth and productivity, despite fluctuations in perfusion rates and bleed strategies. The MWP cultures targeting these CSPR values exhibited q_P values higher than those of the control culture, and both showed good agreement in STY. Building on these findings, this section is divided into two parts: first, the results from the DWP system are presented, followed

by a comparison of outcomes from both the MWP and DWP systems to evaluate their reproducibility and performance across scales.

Growth and productivity of DWP cultures

The DWP cultures targeting stable growth (SG) conditions through a combination of cell bleed and CSPR-based perfusion rate strategies are referred to as DWP-SG20_15, and DWP-SG20_20 for the CSPR targets of 15, and 20 pL cell^{-1} d^{-1}, respectively. For comparison, the condition DWP-SG20 (1 RV d^{-1}), discussed in **Chapter 3**, was included as control condition.

The analysis of cell growth, actual CSPR dynamics, and process flow rates throughout the cultivation period is presented in **Figure 5.4**. All conditions exhibited a "saw-wave" oscillation pattern around the target average VCC (**Figure 5.4A**). While the control culture maintained stable, high cell concentrations (approximately 30.0 × 10^6 cells mL^{-1}) before each cell bleed, CSPR-cultures experienced a daily decline in maximum VCC, with DWP-SG20_20 achieving approximately 22.0 × 10^6 cells mL^{-1}. This decline was more pronounced at the lower CSPR target, leading to progressively smaller oscillations, reflecting a gradual slowdown in growth. By day 7, the target VCCs were no longer achieved (**Figure 5.4A**). The average VCC values, for DWP-SG20_15 and DWP-SG20_20, were 17.8 ± 1.4 and 18.4 ± 1.8 × 10^6 cells mL^{-1}, respectively. Despite this, cell viability remained above 90% until day 6, after which it gradually decreased, reaching approximately 83% by day 10 (**Figure 5.4A**).

The analysis of the actual CSPRs revealed that while the target values were generally achieved, some fluctuations were observed across all conditions (**Figure 5.4B**). For DWP-SG20_15, the CSPR fluctuations were minimal, maintaining an average value of 14.5 ± 1.2 pL cell^{-1} d^{-1}. In contrast, DWP-SG20_20 exhibited more pronounced fluctuations, with an average CSPR of 21.4 ± 1.2 pL cell^{-1} d^{-1} oscillating between low values of 15.6 and high values of 25.0 pL cell^{-1} d^{-1}. The control culture displayed the largest fluctuations, with the CSPR oscillating around 30.0 pL cell^{-1} d^{-1} and a noticeable increase toward the end of the cultivation period (**Figure 5.4B**).

The previously mentioned smaller oscillations of VCCs, and gradual slowdown in growth is reflected in the process flow rates. Process flow rates stabilised after day 3, following a gradual decline throughout the cultivation (**Figure 5.4C** and **D**). On day 2, the perfusion rates of DWP-SG20_15 and DWP-SG20_20 showed a sharp increase, with DWP-SG20_20 reaching a perfusion rate of 1 RV d^{-1}. From day 3 to day 6, the perfusion rates remained stable at approximately 0.4 RV d^{-1} for DWP-SG20_15 and 0.7 RV d^{-1} for DWP-SG20_20, before decreasing to around 0.3 and 0.5 RV d^{-1}, respectively, on day 9. On average, the perfusion rates of CSPR-cultures were lower than those of the control cultures (**Figure 5.4C**). The bleed rates exhibited a similar dynamic with a notable increase on day 2 due to a high VCC measurement on that day. From day 3 onwards, the bleed rate remained mostly below 0.1 RV d^{-1} for DWP-SG20_15 and below 0.2 RV d^{-1} for DWP-

SG20_20, showing a declining trend towards 0 RV d^{-1} on day 9. In contrast, the bleed rate of the control culture remained consistent, fluctuating around 0.3 RV d^{-1} throughout the culture period.

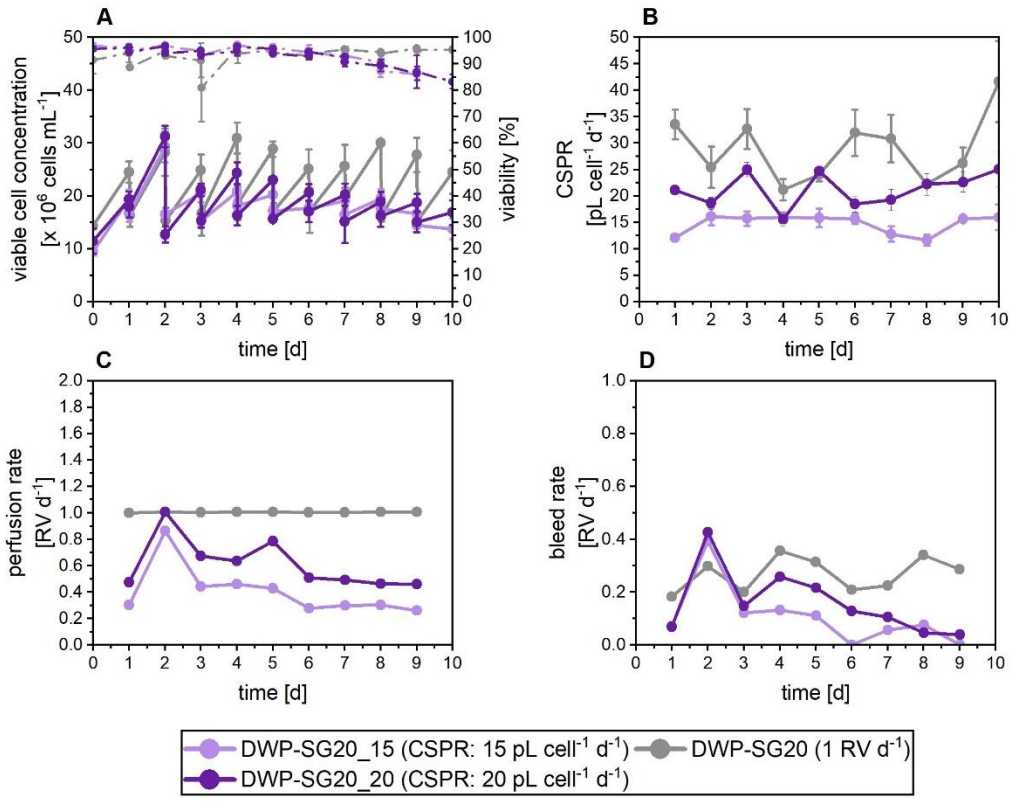

Figure 5.4: Growth and perfusion process flow rates for CHO cobra cells in 6-well DWP cultivations in semi-perfusion with different perfusion rate strategies and implemented cell bleeds. Cells were inoculated at 20 x 10^6 cells mL^{-1} and cultivated in HIP medium supplemented with 30% Feed B (v/v). A: viable cell concentration (filled) and viability (open); B: CSPR; C: perfusion rate; D: bleed rate. Targeted CSPRs (pL $cell^{-1}$ d^{-1}): 15 (●), 20 (●). Perfusion rate equal to 1 RV d^{-1} (●). Mean of *N = 3* wells. Error bars indicate standard deviation. CHO: Chinese Hamster ovary; CSPR: cell-specific perfusion rate; DWP: deepwell plate.

The analysis of external metabolites glucose, lactate and ammonium are presented in **Figure 5.5**. As anticipated, glucose concentrations were consistently higher in the control cultures compared to the CSPR-cultures (**Figure 5.5A**). Both culture types experienced a sharp decline in glucose concentrations, occurring by day 1 for control cultures and by day 2 for CSPR-cultures. Following this initial decrease, glucose levels of control cultures stabilised at 33.2 ± 2.2 mmol L^{-1}, while CSPR-cultures displayed a more gradual reduction in glucose concentration over time (**Figure 5.5A**). Among the CSPR-cultures, DWP-SG20_15 exhibited the lowest glucose levels, which decreased from 27.4 ± 4.6 mmol L^{-1} on day 3 to 14.5 ± 0.3 mmol L^{-1} on day 9, followed by a sudden increase on day 10. Conversely, DWP-SG20_20, also displayed a gradual decrease in glucose concentrations beginning from day 5 (**Figure 5.5A**). However, this culture experienced an unexpected spike in glucose concentration on day 4, the cause of which remains unclear. The q_{Gluc} values were 3.0 ± 0.2 and 2.8 ± 0.3 pmol $cell^{-1}$ d^{-1} for DWP-SG20_15 and DWP-SG20_20, respectively, with the control culture showing a slightly higher value of 3.4 ± 0.3 pmol $cell^{-1}$ d^{-1}.

Lactate concentrations exhibited an unexpected dynamic, as it was initially anticipated that CSPR-cultures would display higher lactate concentrations. However, the control culture had the highest lactate concentration, as shown in **Figure 5.5B**. After an initial increase in lactate concentrations on day 1, control cultures stabilised around 11.7 ± 0.8 mmol L^{-1}. In contrast, CSPR-cultures showed a gradual decrease in lactate concentrations starting from day 3, with values stabilising at lower levels. Specifically, DWP-SG20_15 reached a stable value of 5.0 ± 0.4 mmol L^{-1} while DWP-SG20_20 stabilised at 8.1 ± 0.3 $mmol^{-1}$ (**Figure 5.5B**). The q_{Lac} values of control cultures were 2 to 3-fold higher compared to CSPR-cultures. Specifically, CSPR-cultures obtained q_{Lac} values of 0.3 ± 0.03 pmol $cell^{-1}$ d^{-1} for DWP-SG20_15 and 0.5 ± 0.06 pmol $cell^{-1}$ d^{-1} for DWP-SG20_20 as opposed to 1.0 ± 0.2 pmol $cell^{-1}$ d^{-1} for the control culture.

Ammonium concentrations stabilised after day 1, with CSPR conditions resulting in slightly higher concentrations compared to control cultures (**Figure 5.5C**). Despite this difference, ammonium concentrations remained consistently below 10 mmol L^{-1} across all conditions. The q_{Amm} values was around 0.4 pmol $cell^{-1}$ d^{-1} for all cultures, regardless of the perfusion rate regime.

The cell specific productivity (q_P) data, presented in **Figure 5.5D**, showed some notable observations. The q_P value for DWP-SG20_15 was significantly higher ($p < 0.05$) than those for both DWP-SG20_20 and the control culture, reaching 42.9 ± 4.7 pg $cell^{-1}$ d^{-1}. In comparison, DWP-SG20_20 and the control culture achieved 24.1 ± 3.3 and 30.0 ± 2.8 pg $cell^{-1}$ d^{-1}, respectively.

Regarding medium consumption, the control condition, which involved a total medium exchange, consumed 990 mL. In contrast, the CSPR-cultures used 260.2 mL for DWP-SG20_15 and 403.7 mL for DWP-SG20_20, resulting in reductions of 74.0 % and 59.3 % in medium consumption, respectively.

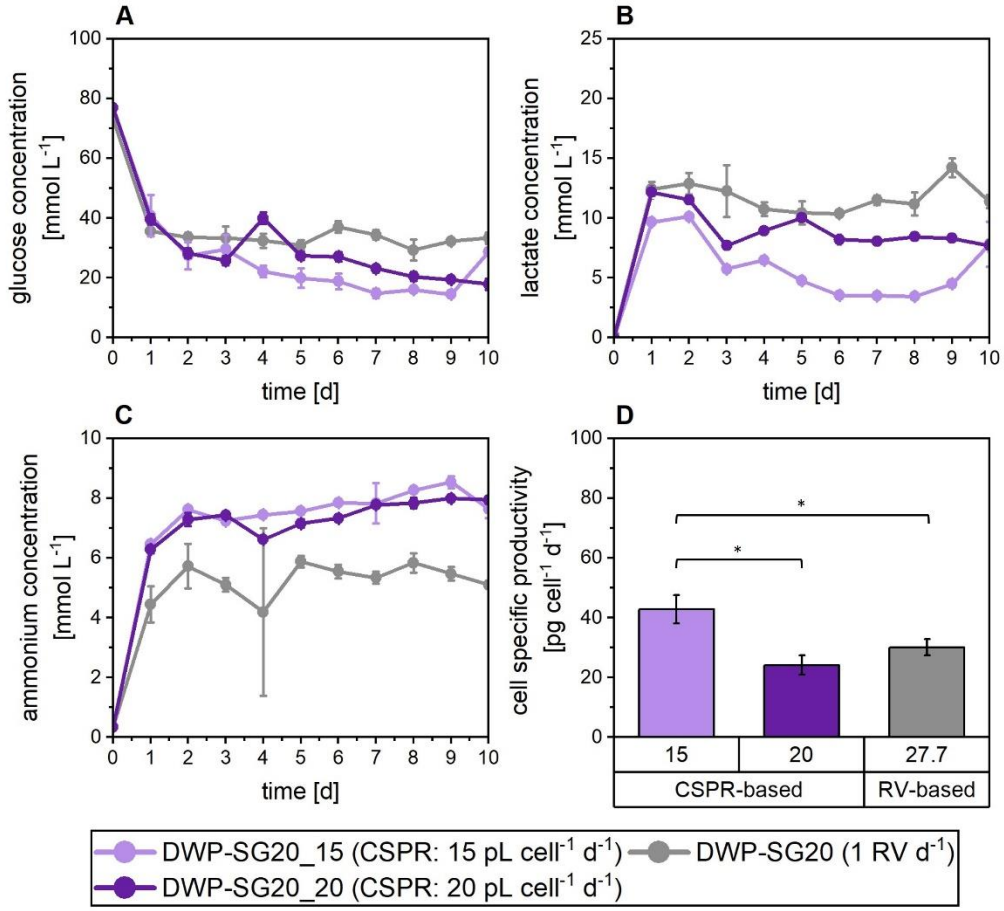

Figure 5.5: Metabolite concentrations and productivity for CHO cobra cells in 6-well DWP cultivations in semi-perfusion with different perfusion rate strategies and implemented cell bleeds and. Cells were inoculated at 20 x 10^6 cells mL^{-1} and cultivated in HIP medium supplemented with 30% Feed B (v/v). A: glucose; B: lactate; C: ammonium; D: cell-specific production rate. Targeted CSPRs (pL $cell^{-1}$ d^{-1}): 15 (●), 20 (●). Perfusion rate equal to 1 RV d^{-1} (●). Mean of *N = 3* wells. Error bars indicate standard deviation. Significant difference was evaluated with a two-sample t-test assuming equal variance with * $p < 0.05$. CHO: Chinese Hamster ovary; CSPR: cell-specific perfusion rate; DWP: deepwell plate.

Comparison of growth and productivity between MWP and DWP cultures

The comparison of growth and productivity between the MWP and DWP systems, both utilising a cell bleed strategy and a CSPR-based perfusion rate, is presented in **Figure 5.6**. The growth dynamics for both systems followed a similar pattern, with both exhibiting a "saw-wave" oscillation in the VCCs. This oscillation was characterised by a decreasing amplitude, where the "high" VCCs (measured before cell bleed) declined throughout the cultivation period, and this trend was more pronounced in the DWP system. This is supported by the average VCCs achieved for the two CSPR targets, which were between 17 and 18 × 10^6 cells mL^{-1} for the DWP and 20 and 21 × 10^6 cells mL^{-1} for the MWP culture (**Figure 5.6A**, **Table 5.2**). Viability in both culture systems decreased from day 6 onwards, with a continued decrease in the DWP system as the cultivation time was extended. The stability of cell viability in the MWP system until day 6 reflects a better growth environment in terms of the perfusion strategy and process management. However, the DWP cultures, while showing a decline in cell viability over time, still maintained viability above

80% at the end of the cultivation period, which is consistent with the overall productivity trends observed.

The comparison of STY revealed similar trends in both systems, with a slight increase observed from days 1 to 3, followed by a stable progression at approximately 0.15 g L^{-1} d^{-1} in both MWP and DWP systems. This suggests that, despite the slowed down growth and reduced viability over time, the overall medium exchange strategy did not have a detrimental effect on the productivity of the cultures. Interestingly, the DWP cultures exhibited slightly more stable STY values compared to the MWP, indicating that the larger system may provide more consistent conditions for the culture environment. In terms of specific productivity (q_P), values comparable across all MWP cultures, with DWP-SG20_15 reaching between 37.9 and 42.7 pg $cell^{-1}$ d^{-1}. The only exception was DWP-SG20_20, which achieved a lower q_P value of 24.1 pg $cell^{-1}$ d^{-1}.

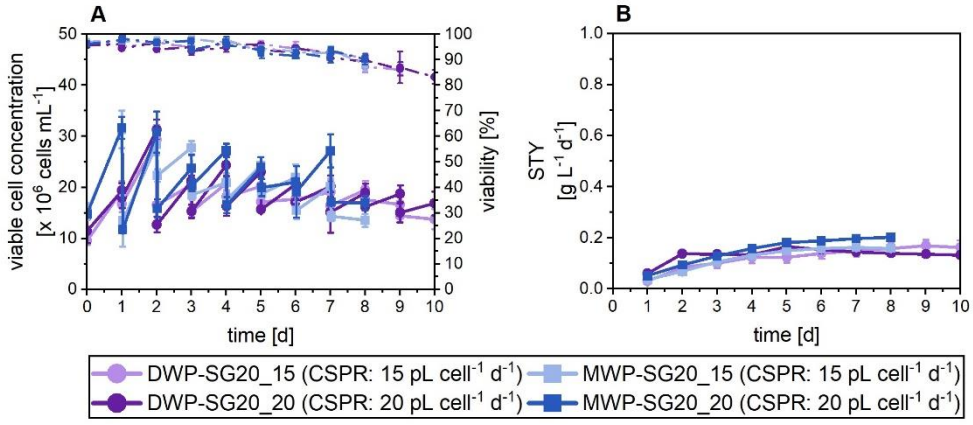

Figure 5.6: Growth and Productivity comparison for CHO cobra cells in 24-well MWP cultivation and 6-well DWP cultivations in semi-perfusion with different perfusion rate strategies and implemented cell bleeds. Cells were inoculated at 20 x 10^6 cells mL^{-1} and cultivated in HIP medium supplemented with 30% Feed B (v/v). A: glucose; B: lactate; C: ammonium. Semi-perfusion was performed with a perfusion rate strategy based on CSPR targeting 15 pL cell d^{-1} in MWP (■) and DWP (●), and 20 pL $cell^{-1}$ d^{-1} in MWP (■) and DWP (●). The target average VCC was 20 x 10^6 cells mL^{-1}. Mean of *N = 3* wells. Error bars indicate standard deviation. CHO: Chinese Hamster ovary; CSPR: cell-specific perfusion rate; DWP: deepwell plate; HIP: high-intensity perfusion medium; MWP: microwell plate; STY: space-time-yield.

A comparative analysis of the metabolic rates across the MWP and DWP systems showed strong similarities in glucose consumption and ammonium production, as indicated by the q_{Gluc} and q_{Amm} values. Across all CSPR-cultures, q_{Gluc} ranged narrowly between 2.8 to 3.0 pmol $cell^{-1}$ d^{-1}, and q_{Amm} values remained consistent at 0.4 to 0.5 pmol $cell^{-1}$ d^{-1}, suggesting similar metabolic demands and by-product formation in both systems in terms of glucose and ammonium. For lactate production, however, a deviation was observed. Specifically, DWP cultures exhibited markedly lower lactate production, particularly under the lower CSPR target of 15 pL $cell^{-1}$ d^{-1}, where q_{Lac} dropped to 0.3 ± 0.0 pmol $cell^{-1}$ d^{-1} compared to 0.7 ± 0.1 pmol $cell^{-1}$ d^{-1} in the equivalent MWP condition.

A comparison of the flow rates between the two systems further highlights differences in key operational parameter. Perfusion rates were consistently higher in MWP cultures than in DWP cultures for equivalent CSPR targets. For instance, the MWP-SG20_20 culture maintained a

perfusion rate of 0.71 RV d^{-1}, while the corresponding DWP-SG20_20 culture operated at 0.63 RV d^{-1}. Bleed rates were generally similar across systems but remained slightly elevated in MWP cultures (0.24 – 0.28 RV d^{-1}) compared to DWP (0.12 – 0.17 RV d^{-1}),

In terms of CSPR stability, cultures targeting a lower CSPR of 15 pL $cell^{-1}$ d^{-1} were more successful at achieving and maintaining their intended setpoints across both systems. In contrast and against intuition, maintaining a stable higher CSPR of 20 pL $cell^{-1}$ d^{-1} proved more challenging. Among all conditions, only DWP-SG20_20 successfully met the target, achieving an actual CSPR of 20.6 ± 1.2 pL $cell^{-1}$ d^{-1}, while the corresponding MWP culture remained below the CSPR target throughout.

Table 5.2: Steady-state values for CHO cobra cells in 24-well MWP and 6-well DWP culture with implemented cell bleed and with CSPR-based perfusion rate strategies targeting an average VCC of 20 x 10^6 cells mL^{-1}.

Cultivation system	**MWP**		**DWP**	
CSPR target [pL $cell^{-1}$ d^{-1}]	**15**	**20**	**15**	**20**
average VCC [x 10^6 cells mL^{-1}]	20.7 ± 1.7	21.4 ± 1.9	17.8 ± 1.4	18.4 ± 1.8
Metabolites⁺				
q_{Gluc} [pmol $cell^{-1}$ L^{-1}]	2.9 ± 0.2	2.9 ± 0.2	3.0 ± 0.2	2.8 ± 0.3
q_{Lac} [pmol $cell^{-1}$ L^{-1}]	0.7 ± 0.1	0.9 ± 0.1	0.3 ± 0.0	0.5 ± 0.1
q_{Amm} [pmol $cell^{-1}$ L^{-1}]	0.5 ± 0.0	0.5 ± 0.0	0.4 ± 0.0	0.4 ± 0.0
Productivity				
STY [g L^{-1} d^{-1}]#	0.16 ± 0.00	0.20 ± 0.00	0.16 ± 0.03	0.13 ± 0.01
q_P [pg $cell^{-1}$ d^{-1}]⁺	38.4 ± 2.6	37.9 ± 1.8	42.9 ± 4.7	24.1 ± 3.3
Flow rates⁺				
Perfusion [RV d^{-1}]	0.56	0.71	0.42	0.63
Harvest [RV d^{-1}]	0.32	0.43	0.29	0.45
Bleed [RV d^{-1}]	0.24	0.28	0.12	0.17
CSPR [pL $cell^{-1}$ d^{-1}]	14.5 ± 1.0	17.6 ± 1.4	14.5 ± 1.2	20.6 ± 1.2
V_M [mL]	60.5	71.1	260.2	403.7

Cells were cultivated in HIP medium supplemented with 30 % Feed B (v/v).
#endpoint value on day 8
⁺average values over days 1 to 8
Yield and productivity values are given as average and standard deviation of *N = 3* wells per day over the entire culture duration of 8 days for MWP and 10 days for DWP
RV: reactor volume; VCC: viable cell concentration; CSPR: cell specific perfusion rate; Gluc: glucose; Lac: lactate; Amm: Ammonium; STY: space-time-yield; q_P: cell specific productivity; V_M: volume of consumed medium

In terms of medium usage, estimates based on single-condition normalisation for a total medium exchange, the MWP system (1 condition per plate, using a sacrificial well approach) consumed approximately 129 mL over 8 days. In contrast, the DWP system (1 condition per 3 wells, over 10 days) required 900 mL per condition. Both systems demonstrated significant medium savings

compared to a full medium exchange strategy, with reductions of approximately 45% in MWP and 55% in DWP CSPR cultures. The slightly lower saving in the MWP system is attributable to the sacrificial well method, which increases the effective volume used per measurement. Nevertheless, the overall medium volume required in the MWP remains considerably lower, underscoring its utility for high-throughput applications with minimal resource input.

Taken together, these results demonstrate the successful integration of a cell bleed strategy with CSPR-based perfusion at both the MWP and DWP scales. Moreover, the consistency observed in growth dynamics, productivity outcomes, and key operational parameters between the two platforms supports the scalability and robustness of this approach.

5.3 Discussion

In this chapter, the cell bleed strategy and CSPR-based perfusion rate previously investigated for MWP cultures in **Chapter 3** and **Chapter 4,** respectively, were integrated, and their effects on cell growth, productivity, and metabolic performance were evaluated. Previously published studies on non-instrumented small-scale semi-perfusion models have exclusively used a fixed RV d^{-1}-based perfusion rate strategy in combination with a cell bleed (Mayrhofer et al., 2021; Villiger-Oberbek et al., 2015; Wolf et al., 2018).

MWP cultures

During the 24-well MWP experiments, three different CSPR setpoints were tested—two previously examined in the MG cultivations and a third, higher CSPR. Overall, all cultures (CSPR-cultures and control cultures) exhibited very similar dynamics in terms of growth and metabolism, regardless of the perfusion rate strategy employed. Key metabolite concentrations —glucose, lactate, and ammonium—remained stable throughout the cultivation, fluctuating by no more than 5% from the mean while both lactate and ammonium remained well below toxicity thresholds. Notably, the metabolic consumption and production rates were stable and in similar ranges across different perfusion rate strategies. This indicated a similar metabolic activity in terms of the measured key metabolites, glucose, lactate and ammonium.

While the metabolite profiles between CSPR-cultures were consistent, cell growth appeared to slow down in CSPR-cultures, with increased variability in growth from day to day. This slower growth affected the bleed rate, which showed greater fluctuations compared to the culture using the RV d^{-1}-based perfusion rate strategy. The reduced growth could have been due to the accumulation or near depletion of other metabolites that were not measured, such as essential ammino acids or vitamins, which have been shown to cause apoptosis when depleted (Chotteau et al., 2023).

Additionally, the analysis of the actual CSPR revealed fluctuations across CSPR-based cultures, with some cases showing lower-than-intended values. This resulted in a reduced nutrient supply, which may have further influenced growth dynamics. It was hypothesised that manual handling of both the cell bleed (removal of cell suspension) and partial medium exchange (removal of supernatant and addition of fresh medium) after centrifugation introduced errors that contributed to the reduced CSPR and disrupted the cell culture. Careful attention will be required when transferring this method to a prospective automated platform to minimise disturbances and ensure that additions and removals from the bulk volume have minimal impact on the culture.

Nevertheless, productivity analysis revealed that, despite the slower growth observed in CSPR cultures, productivity was not negatively impacted. On the contrary, productivity appeared to be enhanced in CSPR cultures compared to the control condition. This improvement may reflect a transition from exponential to stable growth phase, which is often associated with increased productivity. Although cell-specific metabolic consumption and production rates remained within a similar range as those observed in the control culture—indicating comparable metabolic activity across perfusion rate strategies—the observed increase in productivity suggests a potential shift in cellular priorities toward recombinant protein synthesis over proliferation.

Given that cell viabilities remained above 90% throughout the cultivation period, extended cultivation in larger systems could offer additional insights into the relationship between slower growth and productivity. This is particularly relevant in light of previous studies demonstrating that reduced growth rates and induced cell cycle arrest can enhance recombinant protein production (Ducommun et al., 2002; Gagnon et al., 2018; Wang et al., 2018). To further investigate this phenomenon and assess the scalability of the combined CSPR strategy, two of the three CSPR setpoints were transferred to a larger-scale system using 6-well DWP.

DWP cultures

The cultures in 6-well DWP exhibited greater differences between perfusion rate strategies compared to those observed in the MWP. While key metabolite concentrations (glucose, lactate, and ammonium) remained stable throughout the cultivation per culture condition their levels varied across perfusion strategies, albeit with minimal fluctuations. Importantly, all measured toxic by-products remained well below known toxicity thresholds (Altamirano et al., 2001, 2013; Dorai et al., 2009).

The glucose and lactate concentrations were highest under the control condition, whereas ammonium concentrations were lowest in the same condition. These observations are consistent with expectations for the CSPR-based perfusion strategy, where the partial medium exchange reduces the availability of fresh nutrients (e.g., glucose) while promoting the accumulation of metabolic by-products (e.g., ammonium and lactate). In line with this, elevated ammonium

concentrations were observed in the CSPR cultures relative to the control. However, contrary to expectations, lactate concentrations were lower under CSPR conditions, despite the limited medium exchange, which would typically be expected to favour lactate accumulation due to reduced clearance.

The mechanism underlying the reduced lactate concentration in CSPR-cultures remains unclear. One possible explanation is that the combination of limited glucose availability and gradual lactate accumulation may have led to a shift toward a more metabolically balanced state. This may have involved cellular adaptations that reduced glucose uptake and glycolytic activity, thereby decreasing lactate production. Such a shift would be consistent with enhanced metabolic efficiency under nutrient-limited conditions.

This interpretation is further supported by cell-specific metabolite production and consumption rates, which exhibited clear differences across the evaluated perfusion strategies. Specifically, q_{Gluc} and q_{Lac} values were highest in the RV d^{-1}-based control condition, indicating elevated glucose uptake and lactate production rates, and suggesting a higher overall metabolic activity. In contrast, CSPR-cultures displayed lower q_{Gluc} and q_{Lac} values, consistent with a more balanced, and potentially more energy-efficient metabolism. Interestingly, an increasing trend in q_{Gluc} and q_{Lac} was observed with higher CSPR targets—corresponding to larger medium exchange volumes—highlighting the influence of perfusion intensity on cellular metabolic activity and overall culture behaviour.

In CSPR-based cultures, cell growth rates were reduced relative to the control condition. As no evidence of nutrient depletion or accumulation of toxic by-products was observed, it is likely that the reduced proliferation in these cultures was driven by the accumulation or near-depletion of unmeasured metabolites, which may have influenced cellular metabolism and growth. The decreased growth rates also contributed to increased variability in both bleed and perfusion rates. Nevertheless, despite this variability, the actual CSPRs achieved remained close to the intended target values, indicating that the perfusion strategy was implemented with reasonable accuracy across conditions.

Interestingly, the q_P of DWP-SG20_15 was nearly 2-fold and 1.5-fold higher than that of DWP-SG20_20 and control cultures, respectively. Based on growth and metabolite data, the lower q_P values in the control condition and DWP-SG20_20 may be attributed to differences in metabolic activity. These differences suggest a shift in cellular activities—either favouring biomass synthesis (as observed in DWP-SG20_20 and DWP-SG20) or biosynthesis (i.e., mAb production, as seen in DWP-SG20_15). Specifically, DWP-SG20_15 may have entered the stable growth phase, characterised by reduced growth rates, lower lactate concentrations, lower q_{Lac}, and increased productivity. In contrast, the productivity results suggest that DWP-SG20_20 and the control

culture (DWP-SG20) remained in the exponential growth phase, evidenced by high glucose consumption, elevated q_{Lac} values, rapid cell proliferation, and comparatively lower productivity. However, while this interpretation is consistent with the control culture, DWP-SG20_20 exhibited a slowdown in growth similar to DWP-SG20_15. Furthermore, the lower q_{Lac} observed in DWP-SG20_20 relative to the control condition suggest that this culture may have been transitioning from exponential to stable growth.

Lastly, the comparison of CSPR-cultures across scales (MWP vs DWP) showed that all cell specific metabolic rates as well as the actual CSPRs, bleed and perfusion rates for CSPR targets 15 and 20 pg cell^{-1} d^{-1}, were comparable between the two systems and scales. Although actual CSPR values in MWP cultures were lower than the set targets, DWP cultures were able to achieve their target rates with minimal fluctuations. This supports the earlier hypothesis mentioned in **Chapter 4** that manual handling of medium exchanges in the small-volume MWP system contributed to fluctuations and reduced CSPR accuracy. In contrast, the larger working volume and improved handling in the DWP format enabled more consistent implementation of the perfusion strategy, facilitating more stable culture conditions.

Productivity values were also comparable across MWP and DWP, with similar end-point STY and comparable q_P observed in all MWP cultures and DWP-SG20_15. However, DWP-SG20_20 exhibited a nearly two-fold reduction in q_P compared to the other conditions This finding is particularly noteworthy given the earlier hypothesis that DWP-SG20_20 was transitioning from exponential to stable growth, while DWP-SG20_15 may have entered stable growth phase. Additionally, it is plausible that the MWP CSPR cultures also entered a stable growth phase, as previously suggested. The observation of reduced q_P in DWP-SG20_20 despite consistent metabolic parameters—including cell-specific metabolic rates, actual CSPRs, bleed rates, and perfusion rates—suggests that an unidentified factor may be contributing to the observed productivity loss. This emphasises the complexity of metabolic regulation during culture transitions and highlights the need for further investigation.

While the data supports the hypothesis that both DWP-SG20_15 and MWP CSPR cultures may have entered a stable growth phase, further studies utilising additional markers, such as cell cycle analysis or productivity-related gene expression, would help confirm these growth phase transitions. Additionally, extending these experiments in (automated) perfusion bioreactor systems would be essential for assessing the scalability and robustness of the combined cell bleed and CSPR strategy.

5.4 Concluding remarks

The objective of this chapter was to integrate and evaluate the combined strategy of cell bleed and CSPR-based perfusion rate in the 24-well MWP platform. The results demonstrate that HCD cultivations can be maintained stably at a given setpoint when combining the cell bleed with CSPR-based medium exchange. Although a reduction in growth over time was observed in the CSPR cultures, productivity was not negatively impacted, suggesting that the combined strategy did not hinder cellular performance.

However, variations in productivity during scale-up from MWP to DWP underscore the need for further investigation into the scalability of individual parameters, both across well plate scales and to larger perfusion bioreactors. These findings highlight the importance of refining scale-up strategies to ensure consistent culture performance.

Challenges previously identified in **Chapter 4**, such as the manually handled small medium exchange volumes, were re-iterated. The added complexity of dual manipulation (cell bleed and medium exchange) was a major contributing factor to increased variability. These outcomes reinforced the need for an automated workflow to enhance the robustness of the results and minimise variability.

Nonetheless, the successful implementation of the cell bleed strategy from **Chapter 3** and the CSPR-based perfusion rate strategy from **Chapter 4** highlight the versatility of the platform and further emphasising its potential for process development applications, including medium development, cell clone screening, and early-stage process optimisation.

Chapter 6: Application of the microwell plate platform to cell clone selection – Impact of Operation Modes and Medium Exchange Strategies on Clone Ranking *

6.1 Introduction

Following the development and characterisation of the MWP semi-perfusion platform described and discussed in **Chapters 3** to **5**, the system was applied to a specific use case in process development, namely cell clone selection. As the biopharmaceutical industry increasingly shifts from traditional batch and fed-batch processes toward perfusion to enable more flexible, cost-effective, and time-efficient manufacturing, most development efforts have focused on optimising perfusion processes for established production cell lines (Bielser et al., 2019; Clincke, Molleryd, Samani, et al., 2013; Clincke, Molleryd, Zhang, et al., 2013; Romann et al., 2023; Wolf et al., 2019). In contrast, limited attention has been given to applying perfusion strategies during the early stages of cell line development, particularly during cell clone screening.

Clone screening aims to reduce thousands of candidates to a single lead clone that delivers high productivity and desired product quality. This is typically initiated in well plates at micro- to milli-litre scales, followed by screening in progressively larger scales (12 mL to 3 L) and final selection for GMP production. While perfusion is conventionally implemented at >1 L lab scale, recent advances in small-scale retention systems such as TFF and ATF have enabled perfusion studies at volumes as low as 250 mL, increasing throughput and reducing resource requirements (Schwarz et al., 2020; Tregidgo, Dorn, et al., 2023; Tregidgo et al., 2023).

Despite this progress, early clone screening in MWP still predominantly relies on fed-batch operation (Rouiller et al., 2016; B. Wang, Albanetti, Miro-Quesada, et al., 2018). Fed-batch involves initial growth in basal medium, followed by bolus or continuous nutrient feeds to extend culture duration (Xu et al., 2023).

---

* Some of the results presented in this chapter are included in:

Dorn, M., Ferng, C., Klottrup-Rees, K., Lee, K., & Micheletti, M. (2025). Cell clone selection—Impact of operation modes and medium exchange strategies on clone ranking. Frontiers in Bioengineering and Biotechnology, 12. https://doi.org/10.3389/fbioe.2024.1479633

In contrast, perfusion employs continuous medium exchange, resulting in a more stable environment by removing waste and replenishing nutrients (Chen et al., 2018; Chotteau, 2015). This fundamental difference can affect cellular behaviour and performance (Chatterjee, 2012; Walther et al., 2019), raising key questions: Does the choice of operation mode during clone screening affect clone ranking? Could fed-batch-based screening exclude clones better suited for perfusion?

Some studies suggest that aligning the screening mode with the intended production mode improved predictability and may influence clone selection (Markert et al., 2019; Wang et al., 2018). However, only a few have explored clone screening under semi-perfusion conditions, typically using spin tubes or ambr®15 systems, in integrated media and clone screening studies (Bielser et al., 2019; Gagliardi et al., 2019; Gomez et al., 2017). Bielser et al., (2019) also showed that deep-well plates and spin tubes in semi-perfusion led to a comparable performance. Despite this, a systematic comparison of clone screening in fed-batch versus semi-perfusion mode remains lacking.

The aim of this chapter is to apply the developed MWP platform to a key use case in bioprocess development: early-stage cell clone screening. This work seeks to evaluate more representative methodologies for perfusion-based processes, particularly in light of the continued dominance of fed-batch approaches within the industry. To achieve this aim, the first objective is to assess clone screening performance under both fed-batch and semi-perfusion conditions within the MWP format. This includes evaluating the reproducibility of clone performance both within a single protein product—specifically a monoclonal antibody (mAb)—and across different products, including a bispecific antibody (bspAb). The second objective is to refine the clone ranking methodology to improve the accuracy and reliability of selection outcomes. The third objective is to investigate the robustness of the screening process across multiple experimental runs, with a focus on reproducibility and operational consistency.

6.2 Results

This section of the chapter is divided into two main parts, a presentation of the study results followed by a discussion. **Section 6.2.1** details the core of the study, which evaluates a selection of clonally derived CHO cell lines producing monoclonal antibody (mAb1). In this section, growth, metabolism, and productivity are assessed, and two ranking strategies are introduced. **Section 6.2.2** presents the evaluation of a second selection of clonally derived CHO cell lines expressing a bispecific antibody (bspAb1). In total, the cell clone screening experiments were conducted using two antibody-producing cell lines, mAb1 and bspAb1, consisting of a total of 14 clones provided by AstraZeneca. The mAb1 clones served as the base case study, with additional experiments

using bspAb1 clones to highlight the methodology's applicability to different cell lines and protein products.

6.2.1 mAb1 cell line

6.2.1.1 Comparison of Fed-batch and Semi-perfusion – Growth and metabolism

First, the growth performance and metabolism of the mAb1 cell clones were investigated using MWP methodologies in fed-batch and semi-perfusion with a perfusion rate equal to 1 RV d^{-1}, typically used for manual semi-perfusion operation, and two media. Experiments are referred to as FB for fed-batch, SP-CD CHO and SP-HIP for semi-perfusion in CD CHO and HIP (without any additional supplementation) at 1 RV d^{-1}, respectively.

Figure 6.1 presents the growth performance as well as the measurements of external metabolites and osmolality for all eight clones producing mAb1. All eight clones exhibited expected growth patterns across both methodologies, with SP cultures achieving higher VCCs than FB cultures (**Figure 6.1**, **Row 1**). Specifically, while FB cultures reached maximum VCCs ranging from 4 – 21 x 10^6 cells mL^{-1} between days 5 and 7, SP cultures in both CD CHO and HIP media attained peak values of 23 - 54 × 10^6 cells mL^{-1} and 25 - 41 × 10^6 cells mL^{-1}, respectively. The highest maximum VCC across all three experiments was observed for mAb1_C7, reaching 21, 54 and 36 x 10^6 cells mL^{-1} for FB, SP-CD CHO and SP-HIP, respectively. Cell viability remained above 95% for all clones during the growth phase. However, for FB cultures, viability began to decline on day 6, dropping below 50% by day 10, with the exception of mAb1_C4, which maintained a viability of approximately 70% on day 10. In contrast, SP-CD CHO cultures maintained viability above 90% throughout the cultivation period, while HIP-adapted cultures showed a decline starting on day 8, with viabilities ranging from 60 to 80% by day 10 (**Figure 6.1**, **Row 1**). Notably, although mAb1_C7 achieved the highest VCCs, its viability dropped significantly soon after, resulting in endpoint viabilities on day 10 of below 20% for FB cultures and below 80%, and 70% for SP-CD CHO and SP-HIP, respectively.

Metabolite concentrations of glucose, lactate, and ammonium are presented in **Figure 6.1** in, **Row 2**, **3**, and **4**, respectively. Both CD CHO and HIP media initially contained similar glucose concentrations, around 30 mmol L^{-1} at the start of the cultivation. All culture exhibited a decline in glucose concentrations towards depletion between days 6 and 10 (**Figure 6.1**, **Row 2**), with SP cultures depleting glucose slightly earlier than FB cultures. By day 10, glucose concentrations were 0 mmol L^{-1} for all clones, operation modes and media combinations. The only exception was observed for mAb1_C7 in SP-HIP, where glucose concentrations increased on days 9 and 10, in correspondence to a decrease in VCC and viability.

Lactate concentrations exhibited more pronounced differences between operation modes and media compared to glucose (**Figure 6.1**, **Row 3**). Clones cultured in CD CHO medium for both FB and SP modes showed mostly similar dynamics, with nearly identical lactate concentration profiles. These profiles revealed an initial increase to concentrations ranging from 15 to 20 mmol L^{-1}, which remained stable for 4 days, followed by a gradual decrease towards the end of the culture. Some clones, such as mAb1_C4, reached slightly higher lactate concentrations of around 25 mmol L^{-1} in FB cultures but otherwise displayed similar dynamics. For mAb1_C3 and mAb1_C8, greater differences were observed between the operation modes. After the initial increase, lactate concentrations decreased in SP-CD CHO cultures, while they remained stable in FB cultures. In contrast to FB and SP-CD CHO cultures, all clones in SP-HIP cultures exhibited an initial increase in lactate concentrations, ranging from 20 to 30 mmol L^{-1}. These concentrations remained stable for 3 to 4 days, followed by a decrease toward the end of the culture, with complete depletion occurring in the last two days. The decline in lactate levels for all cultures coincided with the depletion of glucose, suggesting a shift from lactate production to lactate consumption (**Figure 6.1**, **Row 3**).

Ammonium concentrations increased over time for all cultures and operation modes (**Figure 6.1**, **Row 4**). However, ammonium concentrations were generally lower in CD CHO cultures compared to HIP cultures and remained stable for several days. In SP-HIP cultures, ammonium concentrations were higher, with a pronounced increase toward the end of the culture, coinciding with a reduction in lactate. Overall, endpoint ammonium concentrations ranged from 3 to 8 mmol L^{-1} for cultures in CD CHO and from 6 to 10 mmol L^{-1} for SP-HIP cultures.

Osmolality remained stable throughout the cultivation period for all experiments, though it was slightly higher for SP-HIP cultures, ranging from 330 to 370 mOsm kg^{-1} (**Figure 6.1**, **Row 5**). In contrast, cultures in CD CHO media exhibited osmolality values ranging from 270 to 320 mOsm kg^{-1} (**Figure 6.1**, **Row 5**).

In summary, a comparative analysis of fed-batch and semi-perfusion cultivation revealed distinct differences in cell growth patterns, with clones cultured under semi-perfusion conditions consistently achieving higher VCCs than those in fed-batch mode. While glucose, ammonium, and osmolality levels exhibited similar trends across both methods and media, lactate concentration dynamics showed more pronounced differences between the two cultivation strategies and media types.

6.2.1.2 Comparison semi-perfusion with total and partial medium exchange

Second, after assessing the impact of operation mode, the clones were further investigated under SP conditions with varying perfusion rates, which involved comparing a total medium exchange (1 RV d^{-1}) to a partial medium exchange (0.75 RV d^{-1}). The aim was to explore potential differences

in clone performance between a typical manual SP operation with 1 RV d^{-1} and a prospective automated workflow using partial medium exchange, which would rely on a liquid handling arm and sedimentation as the cell retention method. It is important to note that the same SP-HIP dataset used in **Section 6.2.1.1** was also used for comparison with the partial medium exchange, which will be referred to as SP-HIP-75%.

The comparison of SP-HIP cultures for all clones under the two different perfusion rates is shown in **Figure 6.2**. Overall, all clones exhibited similar growth patterns at both perfusion rates (**Figure 6.2**, **Row 1**). However, some notable differences were observed in clones mAb1_C1 and mAb1_C3, which achieved slightly higher maximum VCCs with the partial medium exchange (mAb1_C1: 31 × 10^6 cells mL^{-1} and mAb1_C3: 40 × 10^6 cells mL^{-1}) compared to the total medium exchange (mAb1_C1: 25 × 10^6 cells mL^{-1} and mAb1_C3: 33 × 10^6 cells mL^{-1}). In contrast, mAb1_C2 and mAb1_C5 reached marginally higher maximum VCCs with the total medium exchange. These differences were not statistically significant, and the maximum VCCs ranged from 28 to 38 × 10^6 cells mL^{-1} for SP-HIP-75% cultures and from 27 to 40 × 10^6 cells mL^{-1} for SP-HIP cultures (**Figure 6.2**, **Row 1**). The viability remained above 90% for all clones until day 7, after which it decreased to 60–80% by day 10, with minimal to no differences between the two perfusion rates. The only exception was mAb1_C7, where viability in SP-HIP cultures began to decrease as early as day 6, whereas in SP-HIP-75% cultures, viability dropped from day 8. However, by day 10, the viabilities for both experiments were within the range of error and equal to approximately 60% (**Figure 6.2**, **Row 1**).

In line with the growth dynamics, metabolite profiles (**Figure 6.2**, **Row 2–4**) exhibited similar trends between both medium exchange conditions. Interestingly for most clones glucose and lactate concentrations showed very comparable levels and dynamics. It was expected that glucose depletion would occur more rapidly in SP-HIP-75% cultures, but only clones mAb1_C4 and mAb1_C7 showed earlier glucose consumption, with depletion occurring on day 6 and day 5, respectively, compared to one day later in SP-HIP cultures (**Figure 6.2**, **Row 2**).

Regarding lactate concentration, it was anticipated that SP-HIP-75% cultures would exhibit higher concentrations due to accumulation (**Figure 6.2**, **Row 2**). However, this was observed only for mAb1_C2 and mAb1_C4, with lactate concentrations reaching up to 30 mmol L^{-1} in SP-HIP-75% cultures compared to the respective SP-HIP cultures that reached 20–25 mmol L^{-1} for 3–4 days. Clones mAb1_C6 and mAb1_C7 also showed slightly elevated lactate concentrations, though only for 2–3 days, with values ranging from 25 to 28 mmol L^{-1} for SP-HIP-75% compared to 20 - 25 mmol L^{-1} for SP-HIP. Overall, the concentration dynamics were identical between the two perfusion rates, with lactate concentrations initially increasing, plateauing at stable levels, and then decreasing around days 6 and 7, ultimately depleting by day 10 (**Figure 6.2**, **Row 3**).

Ammonium concentrations increased steadily throughout the culture period for all clones, with a sharp rise around day 7 that coincided with glucose depletion and a significant reduction in lactate. By day 10, ammonium concentrations ranged from 6 to 10 mmol L^{-1} for both perfusion rates (**Figure 6.2**, **Row 4**).

In summary, a comparison of growth and metabolic performance between clones cultured under semi-perfusion conditions with total and partial medium exchange revealed substantial similarities. While some clones demonstrated slightly higher VCCs under partial medium exchange, these differences were not statistically significant.

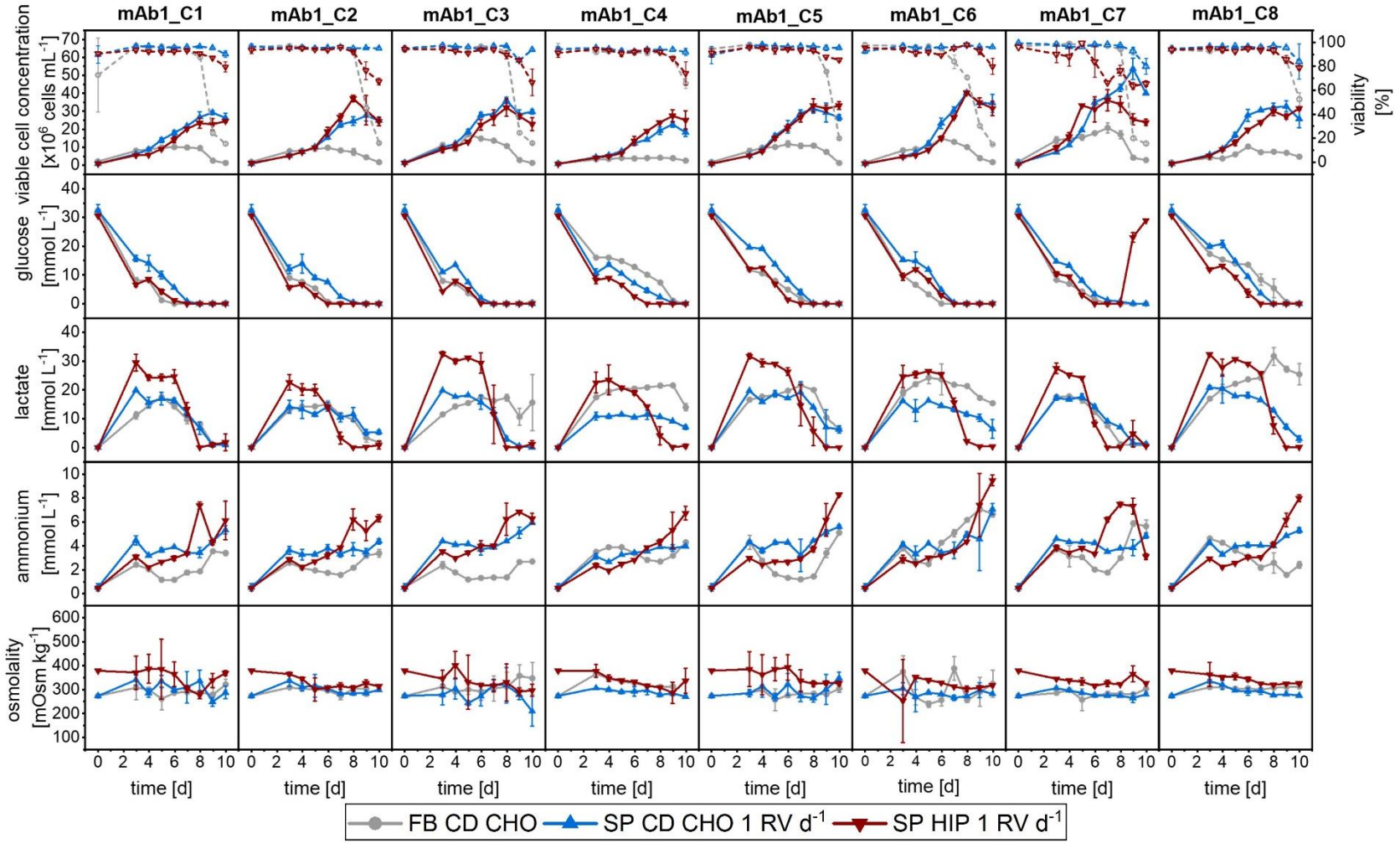

Figure 6.1: Overview of growth and metabolites for mAb1 CHO cell clones in MWPs using fed-batch and semi-perfusion methodologies. Cells were inoculated at 1×10^6 cells mL^{-1} for all methodologies. For fed-batch cultures, cells were cultivated in CD CHO with a feed step from day 3 to day 7 (●). For semi-perfusion cultures, a perfusion rate of 1 RV d^1 was used from day 3 to day 10 and cells were cultivated in CD CHO (▲) and HIP media (▼). Row 1: viable cell concentration (closed, straight) and viability (open, dashed), Row 2: glucose concentration; Row 3: lactate concentration; Row 4: ammonium concentration; Row 5: osmolality. Columns display the eight individual clones. Mean of N = 3 wells. Error bars indicate standard deviation.

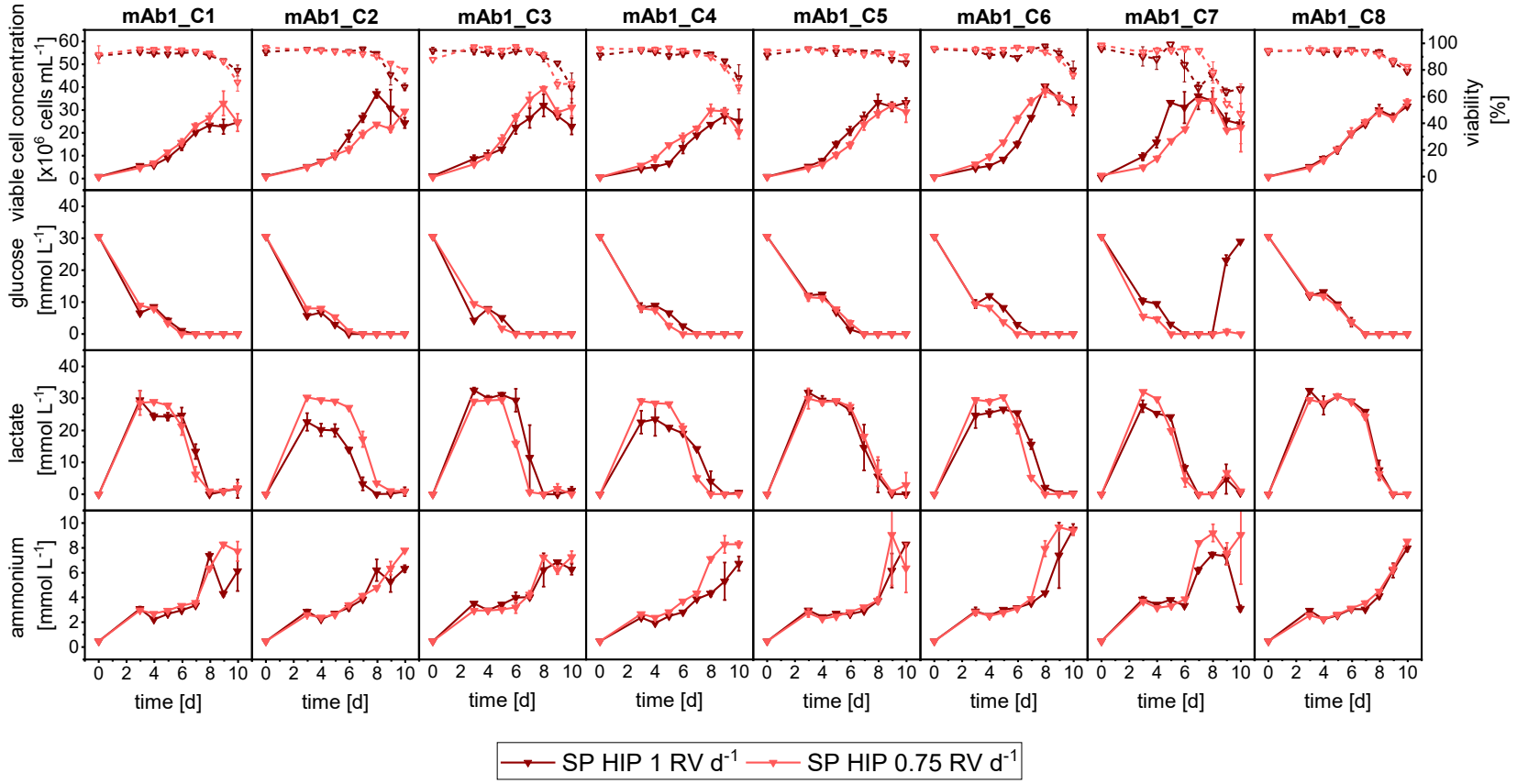

Figure 6.2: Overview of growth and metabolites for mAb1 CHO cell clone screening in MWPs using semi-perfusion methodologies with different fixed perfusion rates. Cells were inoculated at 1 × 10^6 cells mL^{-1} and cultivated in HIP medium with a perfusion rate of 1 RV d^{-1} (▼) and 0.75 RV d^{-1} (▼). Row 1: viable cell concentration (closed, straight) and viability (open, dashed), Row 2: glucose concentration; Row 3: lactate concentration; Row 4: ammonium concentration. Columns display the eight individual clones. Mean of N = 3 wells. Error bars indicate standard deviation.

6.2.1.3 Cell clone ranking

Following the evaluation of clone performance, a clone ranking analysis was conducted using two distinct strategies. The first strategy ranked clones based on a single parameter, cell-specific productivity (q_P), while the second approach considered multiple parameters and used the Manufacturability Index (MI_{CL}) as a metric.

Single-parameter clone ranking – cell specific productivity

The initial clone ranking analysis was based on cell-specific productivity (q_P) for all FB and SP cultures described in **Sections 6.2.1.1** and **6.2.1.2**. **Table 6.1** presents the clone rankings based on q_P, with a colour code used to visually distinguish each clone, ranging from violet (mAb1_C1) to dark red (mAb1_C8). This aims to simplify the visual presentation of the rankings. The raw q_P values, which are reported in **Table 6.3** as a summary over all experiments, range as follows: 1.64 – 25.47 pg cell^{-1} d^{-1} for FB cultures, 17.31 – 41.95 pg cell^{-1} d^{-1} for SP-CD CHO, 16.46 – 39.14 pg cell^{-1} d^{-1} for SP-HIP, and 16.46 – 46.57 pg cell^{-1} d^{-1} for SP-HIP-75%. Notably, the q_P values for all SP cultures fell within a similar range, whereas FB cultures exhibited q_P values 2 – 8-fold lower. It is important to note that the ranking was performed for each experiment individually, with q_P values evaluated relative to the specific range of each respective experiment.

The clone ranking between operation modes (FB vs. SP) showed large differences, while for SP-CD CHO and SP-HIP only minor differences were obtained at low-ranking positions (#6 – #8; **Table 6.1**). For simplicity of comparison the rankings of SP-CD CHO and SP-HIP are treated as equal and referred to as SP rankings. Individual differences are highlighted separately and where needed. While the same clone mAb1_C4 was identified as the top performer in both operation modes, notable differences were observed in the rankings of other clones. For instance, mAb1_C6 and mAb1_C1 ranked 2nd and 3rd, respectively, in SP (q_P values ranged from 16.46 to 41.95 pg cell^{-1} d^{-1}, with mAb1_C6: 30.1–33.1 pg cell^{-1} d^{-1} and mAb1_C1: 28.9–29.7 pg cell^{-1} d^{-1}). In contrast, these clones ranked much lower in FB, at positions #6 and #5, with q_P values ranging from 1.64 to 25.47 pg cell^{-1} d^{-1} (mAb1_C6: 5.40 pg cell^{-1} d^{-1} and mAb1_C1: 6.08 pg cell^{-1} d^{-1}). Clone mAb1_C8 ranked 3rd in FB (q_P: 9.55 pg cell^{-1} d^{-1}) but was placed at the bottom two positions in SP (#7 and #8), with q_P values of 16.58 and 17.31 pg cell^{-1} d^{-1} for SP-HIP and SP-CD CHO, respectively (**Table 6.1**).

Interestingly, some clones exhibited consistent ranking trends across both operation modes. For example, mAb1_C2 ranked in the middle positions (#4 and #5), while mAb1_C3 consistently ranked in the lower positions (#7 or #8) across all conditions (**Table 6.1**).

When comparing clone rankings in SP at different perfusion rates (1 RV d^{-1} vs. 0.75 RV d^{-1}), differences were observed, despite similar q_P ranges: 16.46–39.14 pg cell^{-1} d^{-1} for SP-HIP and

16.46–46.57 pg cell^{-1} d^{-1} for SP-HIP-75%. Clone mAb1_C4 was among the top two performer in both SP-HIP and SP-HIP-75% with q_P values of 39.14 and 32.14 pg cell^{-1} d^{-1}, respectively, however the top performer of SP-HIP-75% was mAb1_C5. The top performer of SP-HIP-75% was ranked 4th in SP-HIP (mAb1_C5, with q_P values of 29.45 pg cell^{-1} d^{-1} for SP-HIP and 46.57 pg cell^{-1} d^{-1} for SP-HIP-75%). Similarly, mAb1_C6, the second-best performer in SP-HIP (q_P: 33.06 pg cell^{-1} d^{-1}), dropped to #6 in SP-HIP-75% (q_P: 22.13 pg cell^{-1} d^{-1}). Despite these shifts, a consistent trend was observed, with clones maintaining similar rankings in the low (e.g., mAb1_C7), middle (e.g., mAb1_C1), or high (e.g., mAb1_C4) positions across both perfusion rates (**Table 6.1**).

In summary, the ranking of clones based on the q_P parameter revealed mAb1_C4 as a shared top clone between FB and SP with total medium exchange (1 RV d^{-1}). However, disparities emerged in the subsequent clone rankings when comparing FB and SP with total medium exchange, as well as when comparing SP cultures with total versus partial medium exchange. These findings suggest that the operation mode employed, and the perfusion rate utilised in SP can substantially influence the clone ranking outcomes. Consequently, these observations prompted the investigation of an alternative ranking strategy incorporating multiple performance parameters to provide a more comprehensive assessment of clone manufacturability.

Table 6.1: Ranking of eight mAb1 CHO cell clones based on average cell specific productivity values for fed-batch and semi-perfusion operation with total and partial medium exchanges in CD CHO and HIP medium. Ranking from top to bottom considered best to worst performing.

Ranking position	FB	SP-CD CHO	SP-HIP	SP-HIP-75%
	-	1 RV d^{-1}	1 RV d^{-1}	0.75 RV d^{-1}
#1	mAb1_C4	mAb1_C4	mAb1_C4	mAb1_C5
#2	mAb1_C5	mAb1_C6	mAb1_C6	mAb1_C4
#3	mAb1_C8	mAb1_C1	mAb1_C1	mAb1_C2
#4	mAb1_C2	mAb1_C5	mAb1_C5	mAb1_C1
#5	mAb1_C1	mAb1_C2	mAb1_C2	mAb1_C8
#6	mAb1_C6	mAb1_C7	mAb1_C3	mAb1_C6
#7	mAb1_C3	mAb1_C3	mAb1_C8	mAb1_C3
#8	mAb1_C7	mAb1_C8	mAb1_C7	mAb1_C7

Colour code to simplify the ranking visually.

Multiple-parameter clone ranking – manufacturability index

While the previous single-parameter analysis based on q_P provided valuable insights, it was inherently limited by its exclusion of other critical performance indicators such as cell growth and metabolic activity. To address this limitation, the clone selection process was reframed as a multi-criteria decision-making problem, building on the strategy proposed by Goldrick et al., (2023). This methodology was adapted for application at the MWP scale and specifically tailored to

facilitate comparisons across different operational modes. It incorporates a broader spectrum of parameters—including cell growth, metabolism, and additional productivity metrics—alongside q_P, to generate a composite score referred to as the Cell Line Manufacturability Index (MI_{CL}).

The raw MI_{CL} values are reported in Table 6.3 with observed ranges of 0.14–1.00 for FB, 0.62–1.00 for SP-CD CHO, 0.38–1.00 for SP-HIP, and 0.43–1.00 for SP-HIP-75%. As detailed in **Chapter 2 Section 2.7.2**, the MI_{CL} is normalised such that the maximum attainable value is 1, allowing for relative evaluation within the specific range of each experiment. Notably, the FB condition exhibited the widest MI_{CL} range, while the SP-CD CHO condition had the narrowest. SP-HIP and SP-HIP-75% showed similar ranges.

Figure 6.3 presents the clone ranking based on the MI_{CL}, using the same colour-coding scheme previously applied for the q_P-based ranking, ranging from violet (mAb1_C1) to dark red (mAb1_C8). When comparing FB and SP cultures operated at a full medium exchange (1 RV d^{-1}), substantial differences in clone ranking were observed across both operation modes and media types. Although some minor variations were present between SP-CD CHO and SP-HIP, overall trends in clone performance were consistent, where the same clones tended to cluster within high-, mid-, or low-ranking positions across both SP media. For instance, mAb1_C8 consistently ranked last in both SP-CD CHO and SP-HIP, with MI_{CL} values of 0.61 and 0.38, respectively (within overall MICL ranges of 0.61 – 1.00 and 0.38 – 1.00). Similarly, clones mAb1_C4 and mAb1_C6 occupied the second and third ranking positions in both media. A notable exception was mAb1_C7, which achieved the highest rank in SP-CD CHO (MI_{CL}: 1.00) but fell to #7 in SP-HIP (MI_{CL}: 0.42).

In contrast, larger differences were observed between FB and SP. Although mAb1_C4 was the top-ranked clone in FB and remained within the top three positions across SP conditions, other clones showed more divergence. For example, mAb1_C8 ranked third in FB (MI_{CL}: 0.54; range: 0.14 – 1.00) but dropped to the lowest position in both SP-CD CHO and SP-HIP. Likewise, mAb1_C2 ranked slightly higher in FB than in SP, while mAb1_C6 performed better under SP conditions (#2 and #3) compared to its FB ranking (#6).

When comparing SP-HIP and SP-HIP-75%, the differences in clone ranking were relatively minor. Both conditions identified mAb1_C5 as the top-performing clone. Positions #2 and #3 were shared by mAb1_C4 (MI_{CL}: 0.89 in SP-HIP-75% and 0.78 in SP-HIP) and mAb1_C6 (MI_{CL}: 0.75 and 0.80, respectively). In both conditions, mAb1_C7 consistently ranked among the lowest positions. The only significant exception was mAb1_C8, which ranked last in SP-HIP (MI_{CL}: 0.38) but rose to #4 in SP-HIP-75% (MI_{CL}: 0.69).

Interestingly, clones mAb1_C1 and mAb1_C3 maintained consistent middle-to-low ranking positions across all conditions, regardless of operation mode, medium composition, or perfusion rate.

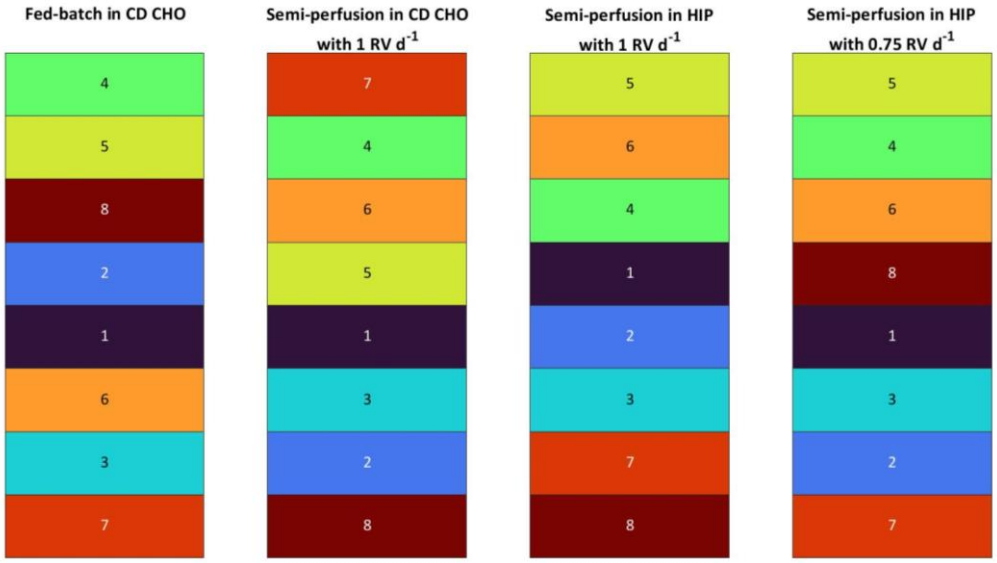

Figure 6.3: Ranking of eight mAb1 CHO cell clones based on manufacturability index for fed-batch and semi-perfusion operation with total and partial medium exchanges in CD CHO and HIP medium. Ranking from top to bottom considered best to worst performing.

A comparative analysis of the clone rankings based on q_P (**Table 6.1**) and the MI_{CL} (**Figure 6.3**) revealed consistent outcomes for the FB mode, where identical clone rankings were observed across both strategies. In contrast, substantial discrepancies were noted for SP conditions, particularly for SP-CD CHO. This condition exhibited the most pronounced shifts in ranking across the two strategies. For example, mAb1_C7, which was ranked #6 based on q_P (19.64 pg cell^{-1} d^{-1}; range: 17.31 – 41.95 pg cell^{-1} d^{-1}), emerged as the top-performing clone under the MI_{CL} strategy (MICL: 1.00; range: 0.61 – 1.00). Similarly, mAb1_C2 dropped from fifth place in the q_P ranking (24.03 pg cell^{-1} d^{-1}) to seventh in the MI_{CL}-based ranking (MI_{CL}: 0.69).

For SP-HIP, the differences between the two ranking strategies were less pronounced, with most clones shifting by only one or two positions. The most notable exception was mAb1_C5, which ranked fourth based on q_P (29.45 pg cell^{-1} d^{-1}; range: 16.46 – 39.14 pg cell^{-1} d^{-1}), but rose to the top position in the MI_{CL} ranking (MI_{CL}: 1.00; range: 0.38 – 1.00). Similarly, in SP-HIP-75%, the top two clones (mAb1_C5 and mAb1_C4) were consistently identified by both ranking strategies, although mAb1_C2 and mAb1_C6 swapped positions, indicating moderate discrepancies in middle rankings.

Overall, the MI_{CL}-based ranking, which integrates multiple parameters beyond productivity, largely corroborated key trends identified using the q_P strategy while providing additional granularity. Although FB yielded identical clone rankings across both approaches, SP — particularly SP-CD CHO — displayed greater sensitivity to the choice of ranking

methodology. These findings reinforce the importance of incorporating multi-parametric assessment strategies such as MI_{CL}, especially under conditions where process variables (e.g. medium type, perfusion rate) influence clone performance. Despite the differences observed, a consistent trend across SP conditions was evident, wherein certain clones repeatedly occupied top or bottom ranking positions.

6.2.1.4 Reproducibility

While the previous investigations, described in **Sections 6.2.1.1**, **6.2.1.2**, and **6.2.1.3,** demonstrated the influence of operation mode on growth, metabolism, and clone ranking, it is essential to establish the reproducibility of these findings to ensure their reliability and robustness. To this end, a reproducibility assessment was undertaken, focusing on growth performance and clone ranking outcomes. A second experimental run of the SP-HIP-75% condition was performed, using a 2^{nd} independently thawed vial for each clone. The results from this second run were then compared to those obtained in the original SP-HIP-75% experiment described in **Section 6.2.1.2** hereafter referred to as Run 1.

The growth performance and external metabolite profiles for both runs are presented in **Figure 6.4**. Overall, similar dynamic trends were observed between Run 1 and Run 2. In particular, metabolite concentrations were highly consistent across runs (**Figure 6.4, Row 2-4**), with only minor deviations. Notably, two clones (mAb1_C2 and mAb1_C6) exhibited differences in lactate dynamics, characterised by a delayed onset of lactate reduction in Run 2. In contrast, greater variability was observed in the growth performance between runs (**Figure 6.4**, **Row 1**). Specifically, maximum VCCs were generally lower in Run 2 compared to Run 1. For example, mAb1_C2 achieved a peak VCC of 29.44×10^6 cells mL^{-1} in Run 1, compared to 17.51×10^6 cells mL^{-1} in Run 2. An exception to this trend was mAb1_C7, which reached approximately 45×10^6 cells mL^{-1} in Run 2, exceeding its maximum VCC of around 35×10^6 cells mL^{-1} in recorded Run 1. Despite these differences in cell growth, the viability dynamics remained largely consistent between runs. In both cases, viabilities stayed above 90% for all clones until day 7, after which they declined to between 60–80% by day 10. The only exception was mAb1_C1, where viability in Run 2 dropped sharply after day 8, reaching below 50% by day 10, whereas in Run 1, viability declined more gradually to approximately 70% by day 10 (**Figure 6.4**, **Row 1**).

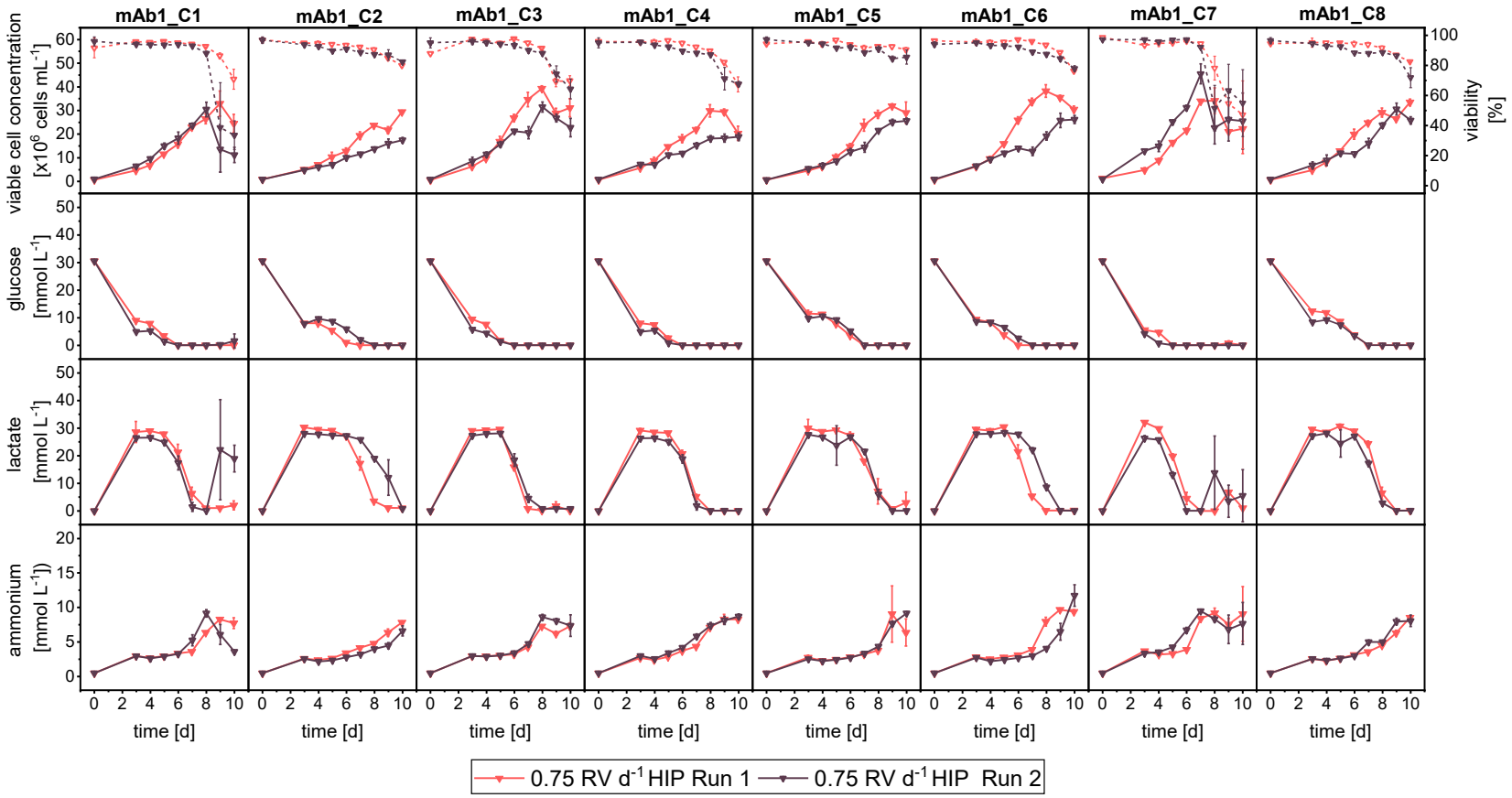

Figure 6.4: Overview of growth and metabolites for mAb1 CHO cell clone screening in MWPs using semi-perfusion methodologies. Cells were inoculated at 1 × 10^6 cells mL^{-1} and cultivated in HIP medium with a perfusion rate of 0.75 RV d^{-1} Run 1(▼) and 0.75 RV d^{-1} Run 2 (▼). Row 1: viable cell concentration (closed, straight) and viability (open, dashed), Row 2: glucose concentration; Row 3: lactate concentration; Row 4: ammonium concentration. Columns display the eight individual clones. Mean of N = 3 wells. Error bars indicate standard deviation.

Following the assessment of growth and metabolite reproducibility, the consistency of clone ranking between runs was evaluated using both the single-parameter (q_P) strategy and the multi-criteria MI_{CL} strategy. The raw q_P values ranged from 16.46 – 46.57 pg cell^{-1} d^{-1} for Run 1 and from 12.21 – 40.98 pg cell^{-1} d^{-1} for Run 2, while MI_{CL} values ranged from 0.43 – 1.00 in both runs, as reported in **Table 6.3**. Overall, the ranges of q_P and MI_{CL} were comparable between the two runs, suggesting a similar performance spread across clones.

The clone rankings based on q_P are presented in **Table 6.2**. Both runs identified the same two top-performing clones — mAb1_C5 ranked #1 (q_P: 46.57 and 40.98 pg cell^{-1} d^{-1} for Run 1 and 2 respectively) and mAb1_C4 ranked #2 (q_P: 32.14 and 35.13 pg cell^{-1} d^{-1} for Run 1 and 2, respectively) — as well as the same lowest-ranking clones (mAb1_C3 at #7, mAb1_C7 at #8). However, variations were observed among the middle-ranked clones, with several clones shifting by multiple positions between runs. For example, mAb1_C6 ranked #6 in Run 1 (q_P: 22.13 pg cell^{-1} d^{-1}), but improved to #4 in Run 2 (q_P: 28.77 pg cell^{-1} d^{-1}), while mAb1_C2 shifted from #3 in Run 1 (q_P: 27.58 pg cell^{-1} d^{-1}) to #5 in Run 2 (q_P:23.66 pg cell^{-1} d^{-1}).

When incorporating multiple parameters using the MI_{CL} approach (**Figure 6.5**), greater consistency between runs was observed. Clone rankings differed by no more than one position, except for mAb1_C8. In both runs, mAb1_C5 consistently emerged as the top-ranked clone (#1). Furthermore, clones at positions #7 and #8 (mAb1_C2 and mAb1_C7, with MI_{CL} values of 0.63/0.43 and 0.43/0.54, respectively) and positions #5 and #6 (mAb1_C1 and mAb1_C3, MICL values of 0.69/0.57 and 0.68/0.65, respectively) remained consistent between runs. The only notable deviation was observed for mAb1_C8, which ranked #4 in Run 1 (MI_{CL}: 0.69) but improved to #2 in Run 2 (MI_{CL}: 0.86).

Table 6.2: Ranking of eight mAb1 CHO cell clones based on average cell specific productivity values for semi-perfusion operation with partial medium exchanges in HIP medium. Ranking from top to bottom considered best to worst performing.

Ranking position	SP-HIP-75%	SP-HIP-75%
	Run 1	Run 2
#1	mAb1_C5	mAb1_C5
#2	mAb1_C4	mAb1_C4
#3	mAb1_C2	mAb1_C8
#4	mAb1_C1	mAb1_C6
#5	mAb1_C8	mAb1_C2
#6	mAb1_C6	mAb1_C1
#7	mAb1_C3	mAb1_C3
#8	mAb1_C7	mAb1_C7

Colour code to simplify the ranking visually. For SP cultures the average was calculated from day 3 to day 10.

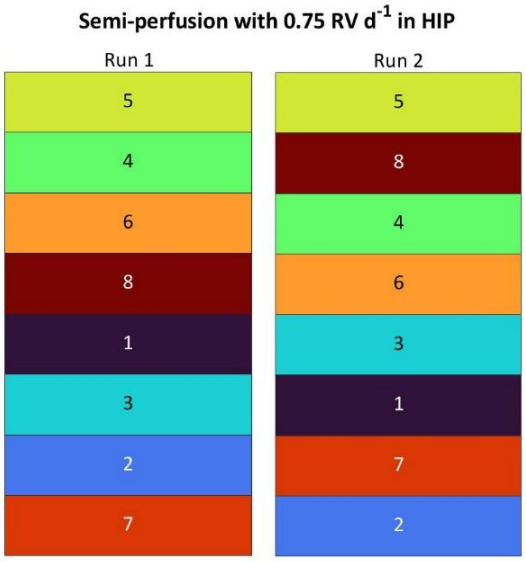

Figure 6.5: Ranking of eight mAb1 CHO cell clones based on manufacturability index for semi-perfusion operation with partial medium exchanges in HIP medium. Ranking from top to bottom considered best to worst performing.

Moreover, when comparing the ranking results from **Table 6.2** (based on q_P) and **Figure 6.5** (based on MI_{CL}), consistent trends were observed for the highest-performing clones across both methods. In particular, mAb1_C5 ranked consistently at #1 (q_P: 46.57 and 40.98 pg cell^{-1} d^{-1}) and mAb1_C4 was among the top 3 candidates (q_P: 32.14 and 35.13 pg cell^{-1} d^{-1}; MI_{CL}: 0.89 and 0.83, for Run 1 and 2, respectively). However, discrepancies emerged for certain clones when comparing the two ranking approaches. For instance, mAb1_C2 ranked considerably worse using the MI_{CL} strategy (#7 and #8) compared to its middle-tier ranking based on q_P (#3 and #5). A similar pattern was observed for mAb1_C3, which ranked #5 and #6 by MI_{CL} (MI_{CL}: 0.68 and 0.65), but consistently ranked at the lower (#7) based on q_P (q_P: 20.18 and 18.81 pg cell^{-1} d^{-1}). Conversely, for mAb1_C6, the MI_{CL} strategy resulted in a better ranking (#3 and #4; MI_{CL}: 0.75 and 0.74) compared to its q_P-based ranking (q_P: 22.13 and 28.77 pg cell^{-1} d^{-1}).

In summary, the reproducibility of clone performance was assessed through two independent SP-HIP-75% experiments, which demonstrated comparable growth and metabolite profiles between runs. The q_P-based ranking approach consistently identified the same top two clones, although greater variability was observed among lower-ranking clones. In contrast, the MI_{CL}-based ranking not only confirmed the same top-performing clone across runs but also showed greater consistency and reproducibility across the full ranking spectrum.

Table 6.3: Summary of cell specific productivities and manufacturability index values of 8 mAb1 clones for fed-batch and semi-perfusion operations with total and partial medium exchanges.

Clones	q_P [pg cell^{-1} d^{-1}]					MI_{CL}				
	FB	SP-CD CHO	SP-HIP	SP HIP-75%		FB	SP-CD CHO	SP-HIP	SP HIP-75%	
				Run 1	Run 2				Run 1	Run 2
mAb1_C1	6.08±0.89	28.86±3.10	29.69±4.46	26.98±4.41	18.99±5.25	0.48	0.94	0.58	0.69	0.57
mAb1_C2	7.38±1.20	24.03±2.86	23.47±4.18	27.58±5.53	23.66±2.09	0.54	0.69	0.57	0.63	0.43
mAb1_C3	5.04±0.83	18.41±2.87	17.55±2.42	20.18±7.62	18.81±1.78	0.47	0.82	0.52	0.68	0.65
mAb1_C4	25.47±4.85	41.95±4.09	39.14±3.48	32.14±7.44	35.13±2.15	1.00	0.97	0.78	0.89	0.82
mAb1_C5	9.58±1.82	24.87±5.59	29.45±9.35	46.57±13.98	40.98±3.73	0.92	0.95	1.00	1.00	1.00
mAb1_C6	5.40±1.71	30.08±3.27	33.06±3.37	22.13±8.04	28.77±1.18	0.47	0.96	0.80	0.75	0.746
mAb1_C7	1.64±0.39	19.64±1.42	16.46±2.27	16.46±2.29	12.21±2.15	0.14	1.00	0.43	0.43	0.54
mAb1_C8	9.55±2.52	17.31±1.11	16.58±2.56	24.94±3.37	24.94±3.37	0.55	0.62	0.38	0.69	0.86

Productivity values are given as average and standard deviation of N = 3 wells over 8 days from day 3 to day 10.
q_p: cell specific productivity; MI_{CL}: cell line manufacturability index

6.2.2 bspAb1 cell line

Following the reproducibility assessment of the first CHO clone selection expressing a monoclonal antibody (mAb1), a second group consisting of six clones expressing a bispecific antibody (bspAb1) was evaluated to further investigate the impact of operation mode and medium. These experiments were conducted under comparable conditions, assessing fed-batch, semi-perfusion in CD CHO, and semi-perfusion in HIP medium with total and partial medium exchanges, labelled as FB, SP-CD CHO, SP-HIP and SP-HIP-75% as for the previous experiments.

Overall, the second group of clones exhibited growth and metabolite dynamics similar to those observed for the mAb1 clones, as illustrated in **Figure 6.6**. The most notable difference observed for the bspAb1 clones compared to the mAb1 clones was the significantly shorter duration of the FB cultures, which lasted only 7 days instead of 10. This was due to an earlier decline in viability, beginning around day 5. In contrast, the SP cultures (SP-CD CHO and SP-HIP) were maintained for 10 days. As with the mAb1 clones, the maximum VCCs achieved were higher in SP-HIP than in SP-CD CHO; however, clones cultured in SP-CD CHO maintained higher viabilities until the end of the cultivation period. The metabolite concentration dynamics were also comparable between the mAb1 and bspAb1 clones. In both cases, glucose depletion occurred earlier in SP-HIP cultures (around day 5) compared to SP-CD CHO cultures (around day 7). Correspondingly, lactate concentrations declined around days 5–6 in SP-HIP cultures, coinciding with glucose depletion, whereas lactate levels remained stable throughout the cultivation period in FB and SP-CD CHO conditions. Across all modes, lactate concentrations remained below 30 mmol L^{-1}, and ammonium concentrations remained below 10 mmol L^{-1}, except for a sharp increase observed between days 5 and 6 in SP-HIP cultures. Furthermore, the comparison between SP-HIP and SP-HIP-75% showed nearly identical growth and metabolite profiles for the bspAb1 clones, consistent with findings for the mAb1 panel. The only exception was bspAb1_C3, which exhibited markedly lower VCCs under SP-HIP-75% compared to SP-HIP conditions.

Clone ranking was subsequently performed as described previously, using first the q_P-based strategy and then the MI_{CL}-based strategy. The q_P-based rankings for the bspAb1 clones are presented **Table 6.4** where a colour-coding scheme was applied to facilitate visualisation: each clone was assigned a colour gradient ranging from dark blue (bspAb1_C1) to dark red (bspAb1_C8). Additionally, the raw q_P values for each operation mode are reported in **Table 6.5**. The q_P values ranged from 1.37–6.82, 11.07–23.90, 6.31–14.93, and 6.90–26.62 pg $cell^{-1}$ d^{-1} for FB, SP-CD CHO, SP-HIP, and SP-HIP-75%, respectively. Similarly, the MI_{CL} values ranged from 0.06–1.00, 0.39–1.00, 0.30–1.00, and 0.27–1.00 for FB, SP-CD CHO, SP-HIP, and SP-HIP-75%, respectively.

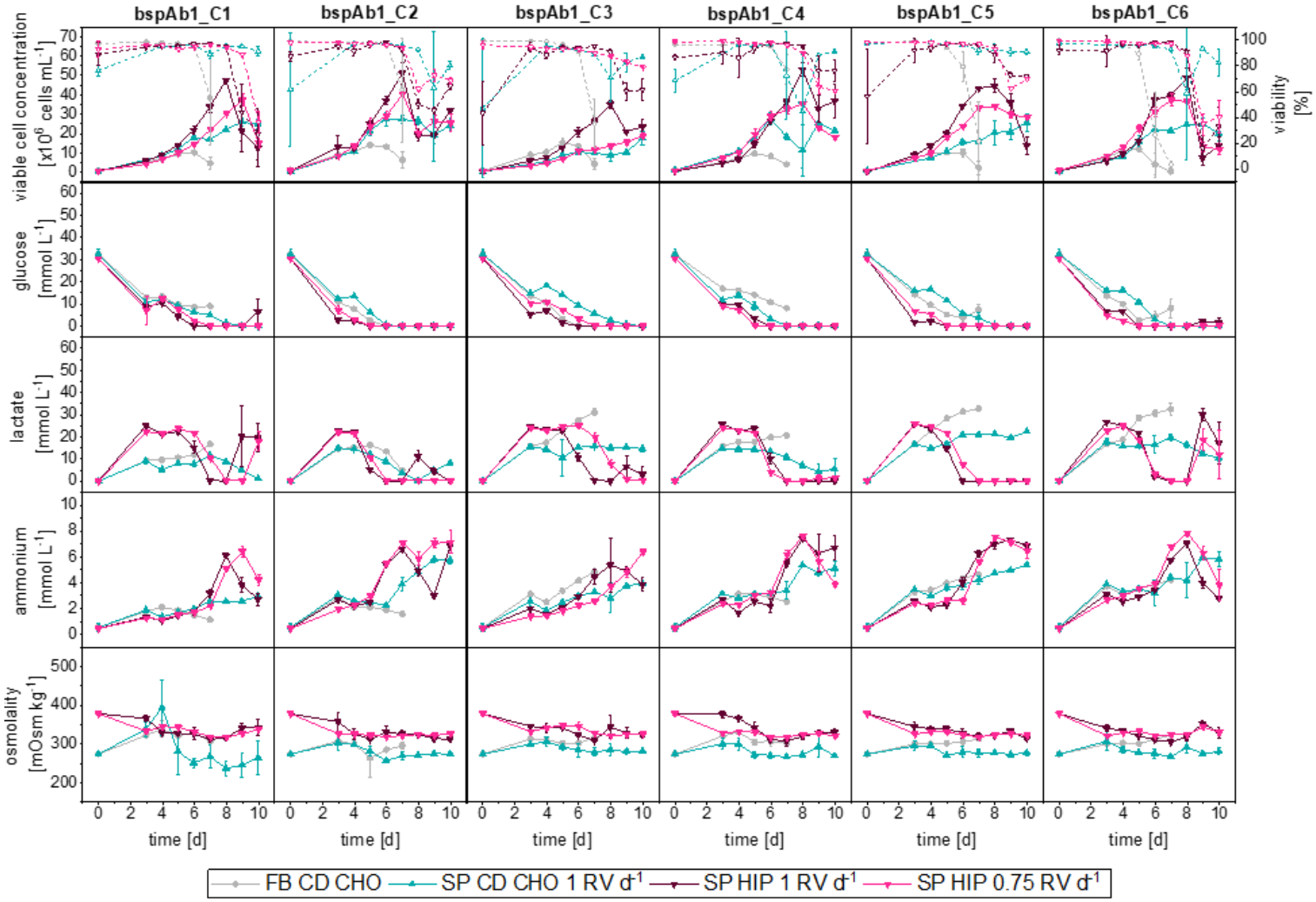

Figure 6.6: Overview of growth and metabolites for bspAb1 CHO cell clone screening in MWPs using fed-batch and semi-perfusion methodologies. Cells were inoculated at 1 × 10^6 cells mL^{-1} for all used methodologies. For fed-batch cultures, cells were cultivated in CD CHO with a feed step from day 3 to day 7 (●). For semi-perfusion cultures, cells were cultivated in CD CHO (▲) and HIP media (▼) with a perfusion rate of 1 RV d^{-1} and in HIP medium with a perfusion rate of 0.75 RV d^{-1} (▼). Row 1: viable cell concentration (closed, straight) and viability (open, dashed), Row 2: glucose concentration; Row 3: lactate concentration; Row 4: ammonium concentration; Row 5: osmolality. Columns display the 6 individual clones. Mean of N = 3 wells. Error bars indicate standard deviation.

While for the mAb1 cell line the same clone consistently ranked highest across all operation modes (FB, SP-CD CHO, and SP-HIP) using the q_P-based strategy, the opposite trend was observed for the bspAb1 clones. Here, it was not the top clone but the lowest-performing clone (bspAb1_C6) that remained consistent across conditions. Furthermore, some differences in clone ranking were observed between SP-CD CHO and SP-HIP. For the bspAb1 panel, although the top-ranked clone differed between these two conditions, subsequent ranking positions were generally preserved. In contrast, for the mAb1 panel, the higher-ranking clones were consistently identified, while variability was more pronounced among the lower-ranked clones.

Despite these differences, general trends across operation modes (FB vs SP) were evident. For instance, bspAb1_C2 consistently ranked lower in SP conditions (#5; q_P: 14.2 pg cell^{-1} d^{-1} (11.07 – 23.90 pg cell^{-1} d^{-1}) for SP-CD CHO and 12.3 pg cell^{-1} d^{-1} (6.31 – 14.93 pg cell^{-1} d^{-1}) for SP-HIP) compared to FB (#2; q_P 5.3 pg cell^{-1} d^{-1} (1.37 – 6.82 pg cell^{-1} d^{-1})). Conversely, bspAb1_C5 demonstrated improved ranking under SP conditions (#3) compared to FB (#5). When comparing partial versus total medium exchanges (SP-HIP vs SP-HIP-75%), further differences in ranking were observed, particularly among the higher-ranked clones. Nevertheless, the two clones bspAb1_C2 and bspAb1_C6 consistently occupied lower ranking positions (#5 and #6) across both conditions. Specifically, for SP-HIP and SP-HIP-75%, bspAb1_C2 achieved q_P values of 12.34 and 11.22 pg cell^{-1} d^{-1}, respectively, while bspAb1_C6 showed q_P values of was 6.31 and 6.90 pg cell^{-1} d^{-1} for SP-HIP and SP-HIP-75%, respectively. It is also noteworthy that the range of q_P values achieved was broader for SP-CD CHO (11.07 – 23.9 pg cell^{-1} d^{-1}) and SP-HIP-75% (6.90 – 26.62 pg cell^{-1} d^{-1}) compared to SP-HIP (6.31 – 14.93 pg cell^{-1} d^{-1}), whereas for the mAb1 clones, q_P ranges across SP modes were more consistent (**Section 6.2.1.3, Table 6.4**).

Table 6.4: Ranking of six bspAb1 CHO cell clones based on average cell specific productivity values for fed-batch and semi-perfusion operation with total and partial medium exchanges in CD CHO and HIP medium. Ranking from top to bottom considered best to worst performing.

Ranking position	**FB**	**SP-CD CHO**	**SP-HIP**	**SP-HIP-75%**
	-	**1 RV d^{-1}**	**1 RV d^{-1}**	**0.75 RV d^{-1}**
#1	bspAb_C1	bspAb_C1	bspAb_C4	bspAb_C3
#2	bspAb_C2	bspAb_C3	bspAb_C3	bspAb_C1
#3	bspAb_C4	bspAb_C5	bspAb_C5	bspAb_C4
#4	bspAb_C3	bspAb_C4	bspAb_C1	bspAb_C5
#5	bspAb_C5	bspAb_C2	bspAb_C2	bspAb_C2
#6	bspAb_C6	bspAb_C6	bspAb_C6	bspAb_C6

Colour code to simplify the ranking visually. Average of q_P for FB cultures was calculated from day 3 to day 7, for SP cultures the average was calculated from day 3 to day 10.

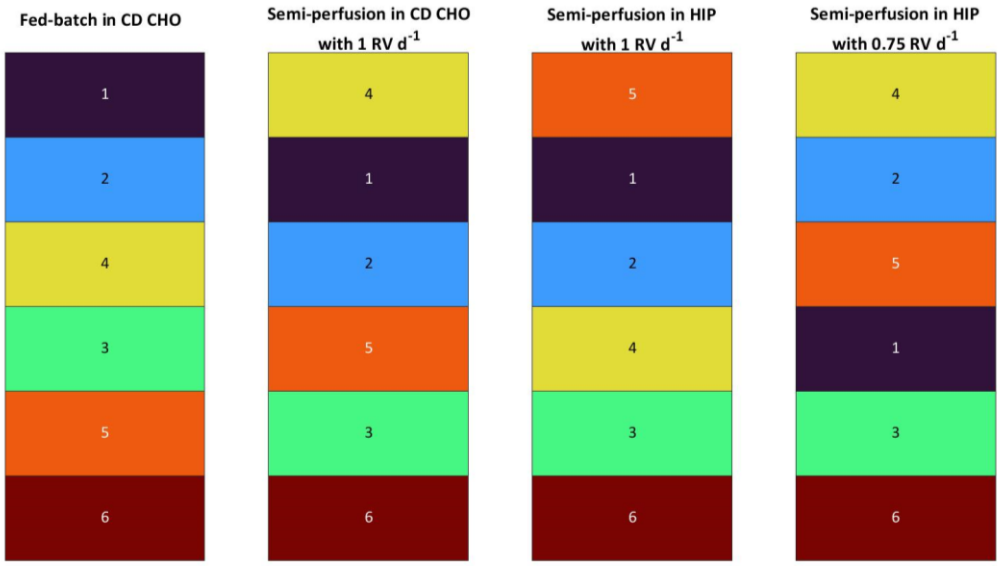

Figure 6.7: Ranking of 6 clones of bspAb1 CHO cell line based on Manufacturability index for fed-batch and semi-perfusion operation with total and partial medium exchanges in CD CHO and HIP medium. Ranking from top to bottom considered best to worst performing.

Table 6.5: Summary of cell specific productivities and manufacturability index values of six bspAb1 CHO cell clones for fed-batch and semi-perfusion operations with total and partial medium exchanges.

Clones	q_P [pg cell^{-1} d^{-1}]				MI_{CL}			
	FB	SP-CD CHO	SP-HIP	SP HIP-75%	FB	SP-CD CHO	SP-HIP	SP HIP-75%
bspAb1_C1	6.82±0.83	23.90±2.91	12.93±2.87	21.03±2.61	1.00	0.94	0.94	0.83
bspAb1_C2	5.28±0.69	14.20±1.93	12.34±1.83	11.22±2.05	0.81	0.83	0.90	0.98
bspAb1_C3	3.64±1.11	22.98±4.81	13.66±0.94	26.62±3.84	0.54	0.55	0.66	0.59
bspAb1_C4	4.80±2.51	14.28±4.19	14.93±2.03	20.26±1.94	0.54	1.00	0.84	1.00
bspAb1_C5	2.25±0.61	17.80±3.76	13.48±2.12	11.60±1.43	0.33	0.69	1.00	0.95
bspAb1_C6	1.37±1.23	11.07±0.35	6.31±1.08	6.90±0.36	0.06	0.39	0.30	0.27

Productivity values are given as average and standard deviation of N = 3 wells over 5 days for FB from day 3 to day 7 and 8 days from day 3 to day 10.
q_P: cell specific productivity; MI_{CL}: cell line manufacturability index

When considering multiple parameters and using the MI_{CL} as a basis for ranking, both FB and SP cultures, as well as those with total and partial medium exchanges, showed similar ranking patterns to those observed with the q_P strategy (**Figure 6.7**). However, some notable differences emerged across the two ranking methods. Interestingly, for both q_P and MI_{CL} strategies, the FB ranking remained identical. Additionally, the worst-performing clone, bspAb1_C6, was consistently identified as the lowest-ranked clone across all operation modes, perfusion rates, and ranking strategies. For SP cultures, however, variability was observed: some clones ranked consistently worse with the q_P strategy compared to the MI_{CL} strategy, and vice versa. For example,

bspAb1_C2 ranked at #5 and #3 for q_P and MI_{CL}, respectively, while bspAb1_C3 ranked at #5 for MI_{CL} but in the top two positions for the q_P strategy.

In summary, to evaluate the broader applicability of the findings from the panel of mAb1-producing CHO cell lines, the study was replicated using a second panel of six CHO cell line producing bspAb1. Similar to the mAb1 cell line, growth dynamics varied between FB and SP cultures. Although glucose, ammonium, and osmolarity concentrations followed comparable trends across the operation modes, lactate levels diverged in SP-HIP and SP-HIP-75% cultures compared to FB and SP-CD CHO. Clone rankings from the bspAb1 cell line revealed shared low-ranking clones, which differed from those observed for the mAb1 clones. Nevertheless, distinct ranking patterns emerged between FB and SP cultures with varying media and perfusion rates, supporting the previous findings regarding the influence of operation mode on clone performance.

6.3 Discussion

In this chapter eight cell clones producing mAb1 were investigated under both fed-batch and semi-perfusion conditions within a small-volume platform. The growth and metabolic performance of these clones were assessed, followed by a ranking based on a single or a combination of performance parameters. The analysis was extended to six cell clones expressing bspAb1, allowing for a comparison across different clones and methodologies. The primary objective of this work was to explore how different operational modes influence early-stage cell clone rankings, providing valuable insights for optimising cell line selection and process design in the context of bioprocess development.

6.3.1 Evaluation of growth and metabolic clone performance

The initial step involved screening cell clones using a MWP methodology in both fed-batch (Silk et al., 2010) and semi-perfusion (1 RV d^{-1}) systems (Tregidgo et al., 2023), employing both fed-batch and perfusion-specific media. The primary objective of these experiments was to evaluate the impact of media composition on cell clone performance, as well as to investigate the effects of the operational mode shift on clone behaviour.

For the mAb1-expressing cell lines, the growth dynamics observed in the SP cultures, with total medium exchanges, were similar across both media, resulting in a 2- to 5-fold increase in maximum VCCs compared to the FB cultures. A comparable trend was observed for the bspAb1-expressing cell clones (**Figure 6.6**). Additionally, the viability of FB cultures declined more rapidly than that of the SP cultures. This was particularly evident in the bspAb1-expressing clones, where FB cultures reached a significantly shorter cultivation time (7 days) compared to the semi-perfusion cultures (10 days).

The initial hypothesis proposed that glucose depletion, observed in all clones across all operation modes, in combination with the accumulation of toxic by-products such as lactate and ammonium, contributed to the observed reduction in viability. Previous studies on CHO cells have indicated a 25% reduction in growth at lactate concentrations of 60 mmol L^{-1} or ammonium concentrations exceeding 10 – 15 mmol L^{-1} (Lao & Toth, 1997). However, the lactate and ammonium concentrations in the FB cultures (for both mAb1 and bspAb1-producing clones) were found to be similar to or lower than those observed in the SP cultures, irrespective of the media type. Additionally, lactate concentrations remained below 30 mmol L^{-1}, and ammonium concentrations were consistently below 10 mmol L^{-1} across all cultivations and cell lines, levels typically considered non-toxic.

Interestingly in the SP cultures a reduction in lactate concentration was observed, which coincided with glucose depletion and suggested a shift in metabolism from lactate production to lactate consumption, as previously described for CHO cells (Altamirano et al., 2000, 2004; Mulukutla et al., 2012). Notably, only the SP cultures in HIP medium (for both cell lines) exhibited a drastic reduction and eventual depletion of lactate by the end of cultivation. The depletion of both glucose and lactate in these cultures is likely the primary cause of the reduced growth and more substantial decrease in viability observed in the semi-perfusion HIP cultures, compared to the semi-perfusion CD CHO cultures, where lactate depletion did not occur.

In addition to the evaluation of operation modes, SP was further explored by applying different perfusion rates to assess potential differences in cell clone performance and subsequent rankings. Specifically, a comparison was made between a typical manual SP operation at 1 RV d^{-1} and a prospective automated workflow utilising a partial medium exchange, often at a fixed rate (e.g., no more than 75 % of the working volume – 0.75 RV d^{-1}). The automated workflow would involve the use of a liquid handling arm and sedimentation as the cell retention method (Bielser et al., 2019; Jin et al., 2021). The growth and metabolic performance of both mAb1 and bspAb1 cell lines were found to be nearly identical for both perfusion rates. While a more rapid reduction and depletion of glucose, along with an earlier shift toward lactate consumption, was expected in the SP-HIP-75% cultures compared to the SP-HIP cultures, the profiles observed were remarkably similar. This outcome may be attributed to a metabolic shift in the SP-HIP-75% cultures, where elevated lactate concentrations led to a decrease in lactate production rate and an increase in lactate consumption, even in the presence of glucose. Such metabolic shifts have been previously documented for batch and fed-batch CHO cultures (Altamirano et al., 2004; Dorai et al., 2009; Lao & Toth, 1997; Li et al., 2012).

6.3.2 Evaluation of the ranking

Two strategies were employed and compared for the ranking of cell clones. Previous studies at the mL-scale have demonstrated that clone ranking is often based on a single productivity parameter (Bielser et al., 2019; Markert et al., 2019). In batch and fed-batch operations, accumulated end-point titre is commonly used as the basis for ranking. However, in this work, two distinctly different operation modes, FB and SP, were compared. Therefore, a suitable parameter was required to account for both the product accumulation in FB operations and the product removal through medium exchange in SP. The cell-specific production rate, q_P, which has been suggested for early-stage screening at low cell concentrations to avoid the early exclusion of clones (Markert et al., 2019), was chosen as the ranking parameter. The calculation of q_P in this work incorporated the variable flow rates of both FB and SP, ensuring a fair comparison between the operation modes.

Initially, a clone ranking based on q_P was conducted. For mAb1, the ranking of clones for SP-CD CHO and SP-HIP was nearly identical with only minor differences observed for lower-performing clones ranked in positions #6 to #8. This suggested that the medium had little impact on the ranking outcome. However, a comparison between operation modes (FB vs SP-HIP) revealed more pronounced differences. Some clones were ranked significantly higher or lower depending on the mode, although the top clone remained consistent across both operation modes. Notably, some clones shifted positions by more than two ranks (e.g., mAb1_C6). Similar observations were made when comparing different perfusion rates (SP-HIP vs SP-HIP-75%), with the top-ranked clone for SP-HIP-75% dropping to position #4 in SP-HIP cultures. These findings on clone ranking based on q_P led to the hypothesis that both (i) the operation mode and (ii) the perfusion rate impact clone rankings. Consequently, the selection of clone candidates for transfer to perfusion bioreactors for further selective screening may differ depending on the chosen method (operation mode) and the type of workflow (manual vs automated perfusion rate).

In a complementary study, the bspAb1 cell clone ranking between FB and SP showed more changes in ranking positions compared to the mAb1 cell line. For instance, bspAb1_C2 performed considerably worse in SP culture (#5) compared to FB culture (#2). Notably, the rankings comparing SP-CD CHO and SP-HIP (1 RV d^{-1}) showed some differences in the better performing clones, in contrast to the worst-performing clones observed in the mAb1 ranking. It is important to note that this discrepancy could be attributed to the smaller number of clones evaluated for bspAb1.

When comparing the rankings for SP cultures with total and partial medium exchanges (1 RV d^{-1} vs 0.75 RV d^{-1}), the ranking differences for top performing clones were similar to those observed

in the mAb1 clones. Despite the smaller number of clones studied for bspAb1, a trend emerged suggesting that both the operation mode and the perfusion rate influenced the cell clone ranking.

However, these results also prompted a re-evaluation of the medium's impact on the ranking outcomes. While the exact compositions of the commercially available media (Thermo Fisher Scientific) are proprietary, it is stated that the HIP medium has a higher native concentration of several components compared to a standard FB medium (e.g., CD CHO), which is designed to be paired with a feed for optimal performance (Thermo Fisher Scientific, 2024).

Further studies, incorporating additional media types and larger clone panels, would provide more insights into the media's role in influencing clone rankings. However, based on the current findings, it is likely that the impact of media composition is minor in comparison to the impact of operation mode and perfusion rate.

Additionally, glucose access should be considered in future investigations. A preliminary clone screening, which included glucose supplementation in the perfusion-specific HIP medium and total medium exchange, was conducted with the mAb1 clones (referred to as SP-HIP20; see **Appendix Section A.2**). This investigation revealed only minor differences in the single parameter ranking between conditions with and without glucose supplementation, similar to the variations observed between different media. However, significant differences remained between the operation modes. Given these results, glucose-limited conditions were chosen for this study, as real-time glucose control is generally not feasible at this scale during cell clone screening. Medium optimisation is typically addressed in subsequent studies focused on lead clones, conducted at bioreactor scale, where glucose concentrations will be monitored, measured, and controlled in real-time to maintain a predetermined range.

The small working volume of well plates in initial cell clone screenings often limits the range of parameters that can be studied, typically restricting assessments to VCCs and titre. However, the increasing demand for greater predictability and process robustness has driven the development of high-throughput analytical technologies, which require less volume per individual analysis, thereby enabling the assessment of additional parameters such as metabolites. While the process operation in well-plate systems often differs from that in larger-scale bioreactor operations (e.g., orbital shaking vs. stirring), early insights into growth, metabolic behaviour, and process performance can still provide valuable information for process development and clone selection.

Previous studies have demonstrated a strong correlation between MWP and a perfusion bioreactor in terms of growth and production performance (Tregidgo et al., 2023). To further assess the applicability of MWP systems for clone screening, comparability studies were conducted for three of the eight clones, comparing MWP data (1 RV d^{-1}) with historical data for

7L perfusion bioreactors (1.2 RV d^{-1}). These showed consistently good comparability for both growth and productivity metrics (data not shown).

The MWP methods used in this work facilitated the collection of sufficient material to measure several key parameters of growth (i.e. VCC, viability), productivity (i.e. titre), and metabolism. From these measurements, additional parameters such as cell-specific rates were derived. Some studies have incorporated growth parameters (e.g. VCC or growth rate) into their clone ranking by assigning scores to each parameter and determining ranks based on an overall score, calculated using equally weighted parameters (Gagliardi et al., 2019). However, this approach is typically performed manually and is limited to a small number of clones and parameters, making it impractical for large-scale screenings.

In industrial cell clone screening processes, several hundred candidates are often assessed in MWPs. Therefore, the manual evaluation of each parameter, assignment of scores, and determination of ranks for all clones would be an impractical and time-consuming task. To address this challenge, Goldrick et al., (2023) developed the manufacturability index (MI_{CL}), a new tool designed to summarise cell clone performance. The MI_{CL} combines multiple parameters into a single numerical value, considering both the ranking within each parameter and the relative importance of each parameter through weighted values.

Next, the MI_{CL} approach was adapted for investigations in MWPs to compare different operation modes and another clone ranking based on the MI_{CL} was performed. The parameters selected for this ranking included yields and cell-specific rates among other and were carefully chosen after extensive discussions with industry collaborators to account for variations in feeding and medium exchange protocols, which can cause metabolite and product accumulation or dilution. At the same time, the number of parameters was kept consistent across both operation modes to ensure a fair comparison between FB and SP cultures. A total of ten parameters were selected, with lactate concentration included as the only volumetric parameter impacted by differences in feed and medium exchange protocols. This decision was based on the dual role of lactate as both a toxic by-product that can inhibit cell growth and as a potential carbon source when metabolism shifts from lactate production to consumption (Luo et al., 2021; Mulukutla et al., 2012; Pereira et al., 2018). Importantly, parameter selection can be tailored for individual projects based on specific requirements. Future rankings for perfusion candidates may incorporate additional metrics that capture critical factors such as genetic stability and long-term process performance. In addition, data from cell-arrest stages, obtained through parallel screenings of clones at different temperatures, could provide valuable insights into clone manufacturability at large scale. Finally, in this case study, all parameters were weighted equally (weight = 1); however, users may assign

higher or lower weights to individual parameters as needed, allowing flexibility in prioritising project-specific objectives.

The ranking obtained using the MI_{CL} strategy showed a similar overall outcome as the ranking based on the q_P with regard to differences between operation modes and between perfusion rates (for both panels of cell lines). These results emphasise that the chosen methods (FB vs SP) at MWP scale impact the candidate selection for further screening in larger scales. Specifically, this might lead to the exclusion of clones more suited for perfusion processes while including clones more appropriate for fed-batch cultivation.

The comparison across ranking methods (q_P vs MI_{CL}) provided valuable insights. For example, the ranking for FB using either the single parameter q_P or the MI_{CL} metric was identical for both cell line panels, suggesting that for FB cultures the q_P is a good enough indicator for early stage ranking at MWP scale where availability of data is limited. However, the same cannot be said for SP cultures, as notable differences between the ranking methods (q_P vs MI_{CL}) were observed. A prominent example of this discrepancy was mAb1_C7 in SP-CD CHO, which ranked low (#6) for q_P but on top position for MI_{CL} ranking. The most likely explanation for this finding was the better growth observed for mAb1_C7 in SP-CD CHO, where viabilities were high throughout and the highest maximum VCCs was achieved, compared to FB, SP-HIP, or SP-HIP-75%. Another possible explanation is that medium composition influences ranking, a hypothesis supported by ranking differences for bspAb1 clones, where variations between SP-CD CHO and SP-HIP were evident in both q_P-based rankings and MI_{CL} rankings for SP-HIP20 under higher glucose concentrations. Another interesting example was clone mAb1_C6, which ranked overall better in SP cultures compared to FB, including SP-HIP-75% where it had ranked much lower for the q_P based ranking. This observation also highlighted an interesting aspect when comparing the ranking methods (q_P vs MI_{CL}) for SP cultures. The MI_{CL} strategy appeared to provide more consistent ranking results across SP cultures, regardless of the medium or perfusion rate. With few exceptions, the same mAb1 clones clustered into either higher or lower ranks, with mAb1_C1 acting as a "barrier" in the middle. For bspAb1, the greater ranking differences observed can likely be attributed to the smaller number of clones, but even so, a clustering of clones at lower-ranking positions was evident. This finding supports the hypothesis that the MI_{CL} strategy yields a more consistent ranking across different perfusion rates and media for SP cultivations.

6.3.3 Evaluation of the reproducibility

Lastly, to assess the reproducibility of the results, particular emphasis was placed on the SP screening, where previous analyses had shown that clone rankings differed between ranking strategies. To further investigate the statistical variability, the SP-HIP-75% condition was selected for a repeat experiment using the mAb1 clone panel.

The comparison of the two runs showed a close similarity of growth and metabolic performance, even though the second run showed slightly slower growth. A possible reason for this could be that Run 2 (P16) was initiated at a later passage number than Run 1 (P10). However, previous studies found no significant impairment of performance for passage numbers up to P20 (Kaur et al., 2023; Qian et al., 2020). Another likely cause is the manual operation of the clone screening workflow, which is inherently more susceptible to operator error and day-to-day variability. These factors may affect the precision of medium exchanges or cause unintentional disturbance of the cell pellet, potentially influencing clone performance. Automating this workflow would likely reduce such variability and improve both reproducibility and process robustness.

The clone ranking of both runs using the single parameter strategy based on the q_P is reported in **Table 6.1** and showed that 4 out of 8 clones were ranked at identical positions including the two top clones. Among the remaining four, two clones showed moderate rank shifts of two positions (e.g. from #3 to #5 and vice versa), while the other two clones exhibited larger changes. These variations may be partially explained by the growth differences between the runs. For instance, clones mAb1_C2 and mAb1_C6 achieved higher VCCs in Run 1, which would typically indicate higher productivity. While this was reflected in the ranking of mAb1_C2 (dropping from #3 in Run 1 to #5 in Run 2), mAb1_C6 demonstrated the opposite trend, improving from #6 to #4, suggesting that other factors beyond growth contributed to the ranking shift.

As shown in **Section 6.2.1.4**, the comparison of ranking strategies within Run 1 (q_P vs MI_{CL}) revealed significant differences in rank positions for some clones. While the top two clones remained unchanged, others such as mAb1_C2 were ranked lower, and clones like mAb1_C6 ranked higher using the MI_{CL} strategy. A similar pattern was observed for Run 2. For example, mAb1_C2 dropped from #5 in the q_P-based ranking to #8 in the MI_{CL}-based ranking.

When comparing MI_{CL}-based rankings across both runs, only the top-ranked clone remained the same. Although the exact rank positions for the other clones differed, a clear clustering pattern emerged: clones mAb1_C4, mAb1_C6, and mAb1_C8 consistently ranked "high," whereas the remaining clones ranked "low." Interestingly, several clones appeared in positional pairs across runs—for example, mAb1_C1 and mAb1_C3 consistently occupied the #5 and #6 positions, albeit with minor variation. These small differences—limited to one ranking position in most cases—can likely be attributed to the variability inherent in manual operation.

In summary, although the q_P-based ranking resulted in more identical ranks across runs (four clones), it also showed greater variation in rank shifts, with several clones moving two or more positions. In contrast, the MI_{CL}-based strategy yielded a more consistent overall ranking pattern, with changes typically limited to a single position—except for mAb1_C8, which shifted by two

positions. These findings reinforce the earlier hypothesis (**Sections 6.3.2**) that MI_{CL}-based rankings offer improved consistency and robustness across SP conditions.

6.4 Concluding remarks

The objective of the work presented in this chapter was to investigate more representative approaches for cell line screening in the context of perfusion bioprocesses, where fed-batch methodology remains the industry standard despite its limited relevance to continuous operation modes. Current early-stage clone selection practices may not adequately reflect the demands of perfusion processes, and more suitable methodologies are needed to close this gap.

This work demonstrated the impact of operational mode on early clone evaluation by comparing fed-batch and semi-perfusion cultures across 14 clones producing two different therapeutic proteins at MWP scale. Growth and metabolic performance were assessed, followed by clone ranking using two strategies: a traditional single-parameter approach based on specific productivity (q_P), and a multi-parameter approach using the Manufacturability Index (MI_{CL}). The observed differences in productivity and growth between operation modes led to shifts in clone rankings, indicating that fed-batch screening alone may overlook clones better suited for perfusion. These findings underscore the importance of aligning screening conditions with the intended production environment, even at small scale.

The MI_{CL} strategy further demonstrated the value of incorporating multiple performance parameters into clone evaluation, providing a more holistic view of manufacturability than single-metric approaches. While this study was conducted using a limited number of clones due to manual handling constraints, the consistency of observed trends across both products reinforces the robustness of the approach. Scaling up future work to include larger clone libraries and automation will be essential to validate and expand upon these findings.

In addition, the integration of digital tools such as multivariate data analysis (MVDA) and machine learning holds significant promise for enhancing clone selection. These technologies can facilitate real-time monitoring and data-driven decision-making, supporting a more efficient and informed screening process. Although factors such as product quality and genetic stability are not typically assessed at this stage, advances in analytical techniques may enable earlier evaluation of these attributes in the future.

By employing screening methods that reflect the final production mode and incorporating multi-parameter assessment strategies like MI_{CL}, this work contributes to more predictive and efficient cell line development workflows. Ultimately, this approach has the potential to accelerate biopharmaceutical development and improve the identification of clones best suited for intensified, perfusion-based manufacturing processes.

Chapter 7: Scale-down of semi-perfusion methodology to 96-well deep well plate: early platform characterisation and application to clone screening

7.1 Introduction

Building on the platform characterisation of the 24-well micro-well plate (MWP) system, described in **Chapters 3** to **5**, and its application to a cell clone screening use case in **Chapter 6**, this chapter focuses on the miniaturisation of the semi-perfusion methodology to a 96-well deep-well plate (DWP) format. This step, if successful, might support the introduction of the semi-perfusion operation mode earlier in the cell line development process and aligns the methodology more closely with high-throughput automated workflows, commonly based on fed-batch operations in the same geometry. These workflows are already supported by established hardware configurations, automation scripts, and user expertise. Introducing semi-perfusion at this earlier stage—prior to the 24-well scale—may further enhance the robustness of clone screening workflows and improve the predictability of clone performance in large-scale perfusion processes, as previously demonstrated for batch and fed-batch screening scenarios (Markert et al., 2019). In addition, increasing throughput at this scale enables the screening of more clones under conditions more representative of the target manufacturing process, potentially reducing the risk of excluding clones better suited for perfusion-based production.

While most studies focus on 96-well plate-based cultures operated in batch or fed-batch mode, only a few have explored the application of semi-perfusion at this scale. Notably, Bielser et al., 2019 investigated the feasibility of using semi-perfusion in 96-well DWPs to evaluate the predictiveness of key perfusion parameters, such as the minimum cell-specific perfusion rate (CSPR). Their work demonstrated the method's sensitivity to clone-to-clone differences relevant to perfusion development, though the study did not aim to identify top-producing or fast-growing clones through a full screening campaign.

The aim of this chapter is to assess the feasibility and performance of translating the semi-perfusion methodology to the 96-well DWP format. This miniaturised scale-down builds on the

semi-perfusion platform established in earlier chapters and serves as a foundation for future development and potential technology transfer. To achieve this aim, the first objective is to evaluate key operational considerations for implementing the semi-perfusion method at the 96-well scale, including working volume limitations, oxygen transfer capacity, and practical handling requirements. These parameters are benchmarked against the previously characterised 24-well MWP system to assess scalability and consistency. The second objective is to conduct a pilot clone screening study using a selection of monoclonal antibody (mAb1)-producing clones. Performance is evaluated using two established ranking strategies to determine growth, productivity, and selection outcomes. The third objective is to assess the consistency of clone rankings across the 96-well and 24-well formats, thereby evaluating cross-platform comparability and the reproducibility of the screening approach.

7.2 Results

The results are presented in this section, followed by a discussion in **Section 7.3**. **Section 7.2.1** which aims to provide an initial characterisation of the 96-well DWP platform, with a focus on working volume constraints and an evaluation of cellular performance in comparison to the previously established 24-well MWP system. **Section 7.2.2** presents the results of a cell clone screening study performed in the 96-well DWP format, including the analysis of growth and productivity metrics. The resulting clone rankings are then compared to those obtained using the 24-well MWP platform to assess the consistency and predictive alignment of clone performance across the two scales. The **Section 7.2.1** uses the CHO cobra cell line, while the mAb1 cell line is used for the cell clone screening in **Section 7.2.2**.

7.2.1 CHO cobra cell line in 96-well DWP

7.2.1.1 Investigation of the influence of working volume on growth and productivity performance

The translation of the semi-perfusion methodology to the 96-well DWP format was guided by insights gained from the development of the 24-well MWP system, as described in previous chapters, and further informed by relevant literature. The 24-well MWP method utilised in this work relies on centrifugation-based cell retention and employs either partial or total medium exchanges, shaken at 250 rpm. In contrast, an existing study demonstrated the feasibility of semi-perfusion in 96-well DWPs using automated medium exchange systems based on sedimentation-driven cell retention, employing a partial medium exchange rate of 0.5 RV d^{-1} (Bielser et al., 2019). For general cultivation in 96-well DWPs—regardless of operation mode—the literature reports working volumes between 350 and 450 µL, agitation rates in the range of 320 to 350 rpm (Bielser et al., 2019; Wang, Albanetti, Miro-Quesada, et al., 2018), and orbital shaking diameters of up to 25 mm.

For the semi-perfusion methodology in 96-well DWP presented and evaluated in this section, a centrifugation-based cell retention strategy was adopted in combination with a daily partial medium exchange at 0.75 RV d^{-1}. The 96-well DWP was operated at 300 rpm, the maximum agitation speed permitted by the available shaker platform in an effort to select conditions in line with values reported in literature (Bielser et al., 2019; B. Wang, Albanetti, Miro-Quesada, et al., 2018). Given that the agitation rate was lower than what is typically reported in the literature, which may influence mixing efficiency and mass transfer, a range of working volumes between 200 to 400 µL was evaluated. This range was chosen to encompass and extend below the reported volumes in order to ensure an adequate oxygen transfer rate is achieved through the surface. The lower boundary of this range was selected to ensure that sufficient sample volume would be available to enable VCC and product titre quantification using the analytical methods at hand. Throughout this section, experimental conditions are denoted using the format XX_yyy_Rz, where XX indicates the medium composition—HIP for the perfusion-specific base medium alone, and HIP30 for the base medium supplemented with 30% Feed B. The yyy component refers to the working volume (200, 300, 350, or 400 µL), and Rz denotes the replicate number corresponding to independent experimental runs.

Figure 7.1 presents the growth and STY dynamics for four different working volumes (200, 300, 350 and 400 µL), evaluated in the 96-well DWP semi-perfusion methodology in HIP medium. To assess reproducibility two technically independent runs were performed for each condition.

Sustained cell growth was observed at the lower working volumes of 200 and 300 µL (**Figure 7.1**, **Row 1, Table 7.1**). Following a lag-phase of 1 - 2 days, cells grew exponentially, culminating in maximum VCCs around day 6 reaching between 24 and 30 × 10^6 cells mL^{-1}. The highest VCC was observed for HIP_200_R1, achieving 29.7±0.5 × 10^6 cells mL^{-1}. After peaking, a moderate decline in VCC was observed between days 7 and 10. Notably, cultures at 300 µL exhibited a pronounced drop in VCC between days 9 and 10. Viability showed some initial fluctuation, dropping below 90% during the first two days. However, all cultures recovered to above 95% by day 4, maintaining high viability until maximum cell density was reached (**Figure 7.1**, **Row 1**). Thereafter, a gradual decline in viability occurred in parallel with the decrease in VCC, reaching between 60% and 70% by day 10 in most cases. An exception was noted for HIP_300_R1, where viability dropped more sharply, falling below 50% by day 10.

In contrast, cultures operated at higher working volumes of 350 µL and 400 µL exhibited poor growth performance (**Figure 7.1**, **Row 1**). VCCs remained below 2 × 10^6 cells mL^{-1} until day 3 throughout the first three days of cultivation, during which cultures at lower working volumes had already entered exponential growth. Viability dropped below 90% as early as day 1, a result which is consistent with the initial trends observed for the lower working volumes. However,

unlike the rapid recovery observed at 200 µL and 300 µL, viability in the 350 µL condition remained between 80% and 90%, while cultures at 400 µL showed a more pronounced decline, falling to approximately 70% within the same timeframe (**Figure 7.1**, **Row 1**). Due to the combination of limited cell growth and declining viability—particularly when compared to the more favourable outcomes at lower working volumes—the 350 µL and 400 µL cultures were terminated on day 3.

STY was selected as the dynamic productivity metric instead of absolute titre measurements, due to the nature of the partial medium exchange process, which results in product retention and accumulation over time (**Figure 7.1**, **Row 2, Table 7.1**). Early-stage product formation was minimal, with titre values approaching the detection limit of the analytical method. However, as VCC increased, STY values also rose, reaching peak levels on day 9, with values ranging from 0.06 to 0.1 g L^{-1} across the 200 µL and 300 µL conditions. The highest STY values were observed in the 200 µL cultures. Although titre and STY were also measured in the 350 µL and 400 µL conditions, the values remained near the lower detection limit, indicating negligible productivity under these conditions (**Figure 7.1**, **Row 2**).

In a subsequent experiment, cultivations at 200 µL and 300 µL working volumes were repeated using the optimal medium composition previously identified at the 24-well MWP scale: a perfusion-specific base medium supplemented with 30% Feed B (referred to as HIP30). The inclusion of Feed B was intended to enhance both cell growth and productivity. The resulting growth and productivity data are presented in **Figure 7.2** and are compared to the results from the initial HIP medium conditions discussed earlier.

For the HIP30 conditions, overall growth and viability dynamics were broadly similar to those previously described for cultures in the HIP medium. However, several notable differences were observed (**Figure 7.2**, **Row 1**). At the 200 µL working volume, cultures in HIP30 exhibited a more prolonged and slightly slower growth phase, reaching maximum VCCs on day 9 compared to day 6 in the HIP condition. However, the peak VCCs achieved under HIP30 were slightly higher, ranging between 32 and 33 × 10^6 cells mL^{-1}. Additionally, the initial decline in viability observed during the lag phase for HIP_200_R1 and HIP_200_R2 was not present in the HIP30_200_R1 and HIP30_200_R2 cultures, indicating improved cell viability in the early culture phase. At the 300 µL working volume, HIP30_300_R1 demonstrated slightly slower growth, reaching a maximum VCC of 18.8±3.9 × 10^6 cells mL^{-1} on day 7. In contrast, HIP30_300_R2 followed a similar growth trajectory to the corresponding HIP condition, although the maximum VCC of 27.9±7.5 × 10^6 cells mL^{-1} was reached on day 8 rather than day 6 (**Figure 7.2**, **Row 1, Table 7.1**). However, viabilities began to decline slightly earlier, around day 6.

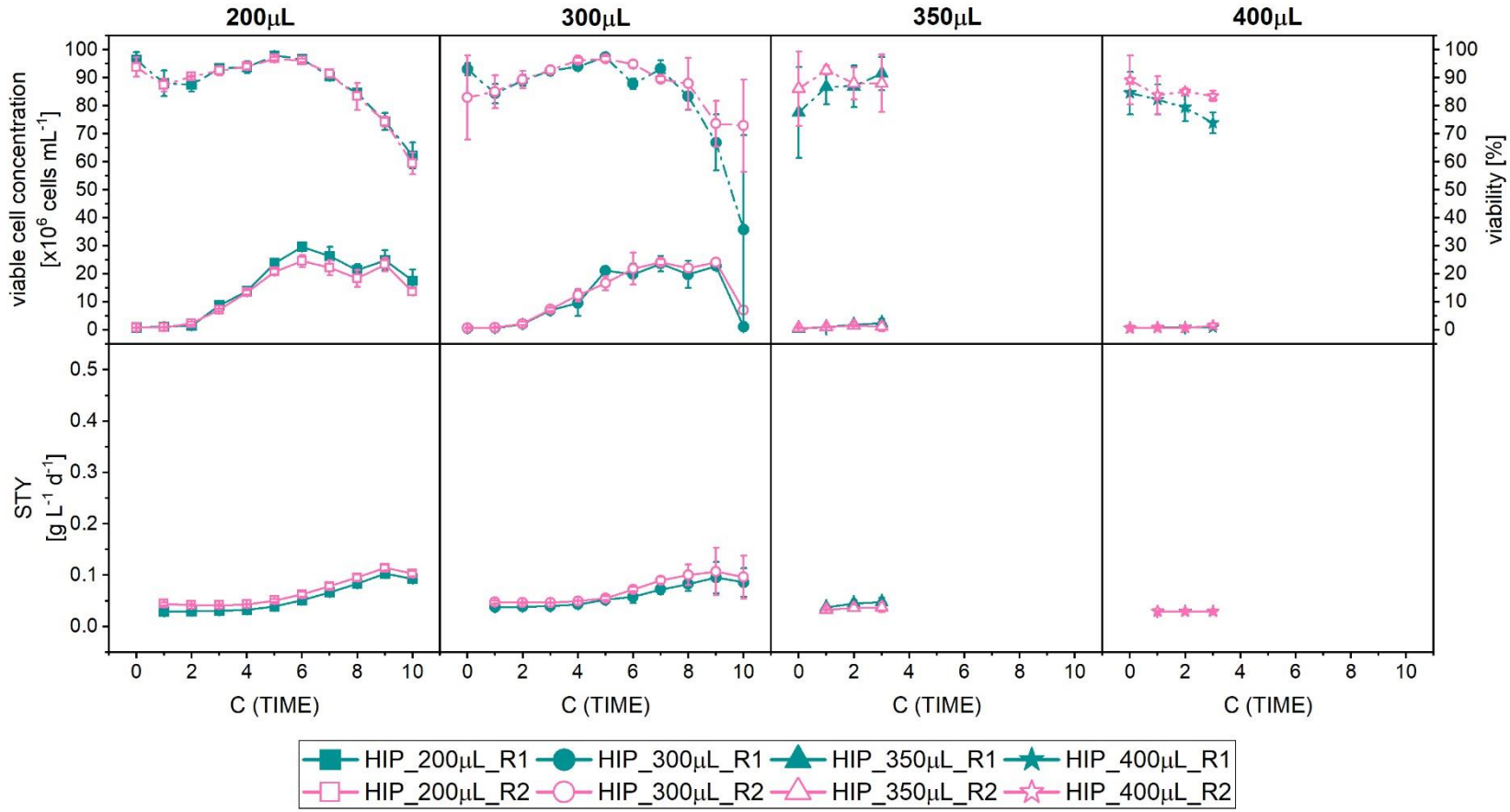

Figure 7.1: Overview of growth and productivity performance of the CHO cobra cell line in 96-well DWPs using semi-perfusion methodologies at four different working volumes. Cells were inoculated at 1 × 10^6 cells mL^{-1} into four working volumes of 200 µL (■), 300 µL (●), 350 µL (▲) and 400 µL (★) and cultivated in HIP medium. For each condition 2 technically independent runs were performed: R1 (closed, ■), R2 (open, ■). A perfusion rate of 0.75 RV d^1 was used from day 1 to day 10. Row 1: viable cell concentration (straight) and viability (dashed), Row 2: Space-Time-Yield (STY). Mean of N = 3 wells. Error bars indicate standard deviation.

Table 7.1: Cellular performance values for CHO cobra cell line in 96-well DWPs using semi-perfusion methodologies at two working volumes and two media compositions.

	96-well DWP							
Medium	**HIP**				**HIP30**			
Working volume	**200 µL**		**300 µL**		**200 µL**		**300 µL**	
Number of Run	**R1**	**R2**	**R1**	**R2**	**R1**	**R2**	**R1**	**R2**
Perfusion rate [RV d^{-1}]	0.75	0.75	0.75	0.75	0.75	0.75	0.75	0.75
max. VCC [x 10^6 cells mL^{-1}]	29.71±0.5	24.6±2.1	23.6±2.8	24.1±1.1	32.4±6.0	29.8±1.7	18.4±3.9	27.9±7.6
q_P [pg $cell^{-1}$ d^{-1}]	17.3±2.3	27.0±6.3	24.7±3.7	28.6±5.3	19.2±2.3	24.7±4.2	21.8±4.5	21.7±6.5
STY [g L^{-1} d^{-1}]#	0.10±0.01	0.11±0.01	0.10±0.03	0.11±0.05	0.21±0.01	0.09±0.02	0.23±0.05	0.15±0.03

Cells were cultivated in HIP medium supplemented with 0% Feed B (HIP) or 30 % Feed B (v/v) (HIP30).
#maximum value
Productivity values are given as average and standard deviation of N = 3 wells over the entire culture duration of 8 days.
CCD: conventional cell density; RV: reactor volume; VCC: viable cell concentration; STY: space-time-yield; q_p: cell specific productivity

Table 7.2: Cellular performance values for CHO cobra cell line in 24-well MWP and 6-well DWPs using semi-perfusion methodologies.

	24-well MWP		6-well DWP	
Working volume	**1.2 mL**	**1.2 mL**	**30 mL**	**30 mL**
Number of Run	**R1**	**R2**	**R1**	**R1**
Inoculation	CCD	HCD	CCD	HCD
max. VCC [x 10^6 cells mL^{-1}]	32.4±1.5	72.9±6.4	34.4±2.86	49.9±5.3
q_P [pg $cell^{-1}$ d^{-1}]	20.8±5.9	27.9±1.6	22.4±2.3	16.9±1.7
STY [g L^{-1} d^{-1}]#	0.03±0.01	0.73±0.02	0.56±0.03	0.94±0.07

Cells were cultivated in HIP medium supplemented with 30 % Feed B (v/v) and the perfusion rate was 1 RV d^{-1}.
#maximum value
Productivity values are given as average and standard deviation of N = 3 wells over the entire culture duration of 8 days.
CCD: conventional cell density; HCD: high cell density; RV: reactor volume; VCC: viable cell concentration; STY: space-time-yield; q_p: cell specific productivity

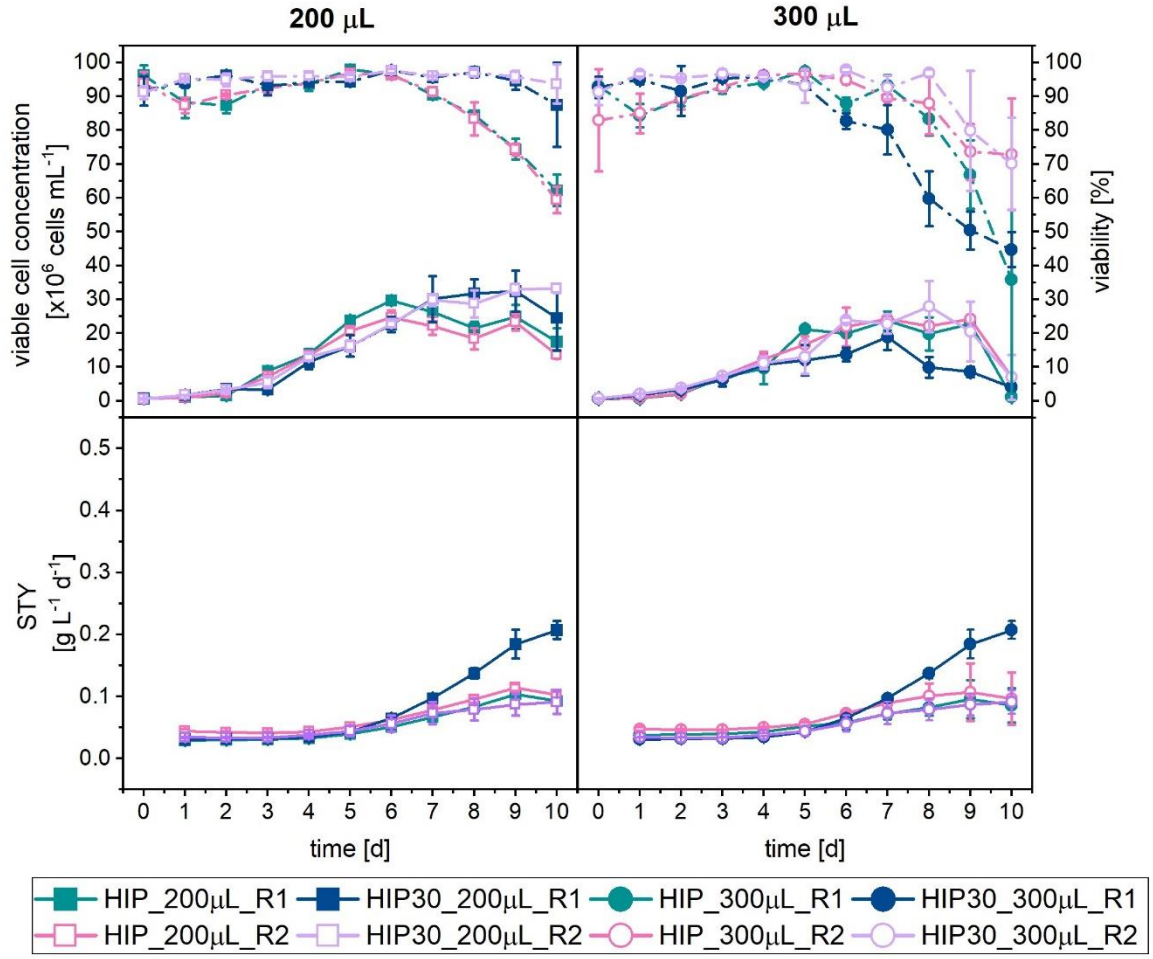

Figure 7.2: Overview of growth and productivity performance of the CHO cobra cell line in 96-well DWPs using semi-perfusion methodologies at two different working volumes and with two different media compositions. Cells were inoculated at 1 × 10^6 cells mL^{-1} into two working volumes of 200 µL (■) and 300 µL (●). Cultures were maintained in HIP medium supplemented with 0% (HIP ■/■) and 30% Feed B (HIP30 ■/■), which each were performed in 2 technically independent runs: R1 (closed), R2 (open). A perfusion rate of 0.75 RV d^1 was used from day 1 to day 10. Row 1: viable cell concentration (straight) and viability (dashed), Row 2: Space-Time-Yield (STY). Mean of N = 3 wells. Error bars indicate standard deviation.

The comparison of STY profiles revealed largely similar results between the HIP conditions and the second HIP30 runs for both working volumes (**Figure 7.2**), with maximum values of approximately 0.09 and 0.1 g L^{-1} d^{-1} achieved on day 10 for 200 µL and 300 µL, respectively. In contrast, the first HIP30 runs exhibited consistently higher STY values, diverging from the typical trend around day 7 and reaching peak levels of 0.2 and 0.22 g L^{-1} d^{-1} for 200 µL and 300 µL, respectively.

7.2.1.2 Comparison between well plate scales – 96-well DWP vs 24-well MWP

In the second stage of this study, results from the initial characterisation of the 96-well DWP semi-perfusion system were compared with previously obtained data from the 24-well MWP and 6-well DWP systems, as presented in Chapter 4 and summarised in **Table 7.2** and **Figure 7.3**. It is important to note that while the 24-well MWP and 6-well DWP experiments were conducted at a

perfusion rate of 1 RV d^{-1}, the 96-well DWP experiments were operated at a slightly lower rate of 0.75 RV d^{-1}.

Across all three systems, when inoculated at a CCD, the maximum VCCs were comparable, with peak values around 30 × 10^6 cells mL^{-1} (**Table 7.1**, **Table 7.2**). Cultures maintained in HIP medium consistently achieved slightly higher VCCs, whereas those in HIP30 displayed marginally lower values. The overall VCC range spanned from 23.6 to 34.4 × 10^6 cells mL^{-1}, with viability trends showing comparable behaviour across platforms (**Table 7.1**, **Table 7.2**). However, for cultures inoculated at a HCD, the results were more variable, with one MWP condition achieving markedly higher VCCs, while the corresponding 6-well DWP cultures remaining within the same VCC range as those inoculated at CCD (**Table 7.1**, **Table 7.2**).

In addition to cell concentration, productivity was evaluated using cell-specific productivity (q_P) and STY, rather than titre alone, to account for differences in perfusion rates across platforms. As shown in **Figure 7.3**, q_P values were largely consistent across all three systems, regardless of medium type or inoculation density, with values ranging from 16 to 28 pg $cell^{-1}$ d^{-1} (**Figure 7.3**, **Table 7.1**, **Table 7.2**). Although some variability was observed, those were largely within the range of error and no significant difference was found. In contrast, STY exhibited more pronounced variation, with notably higher values observed at larger scales in the 24-well MWP and 6-well DWP systems compared to the 96-well DWP (**Table 7.1**, **Table 7.2**).

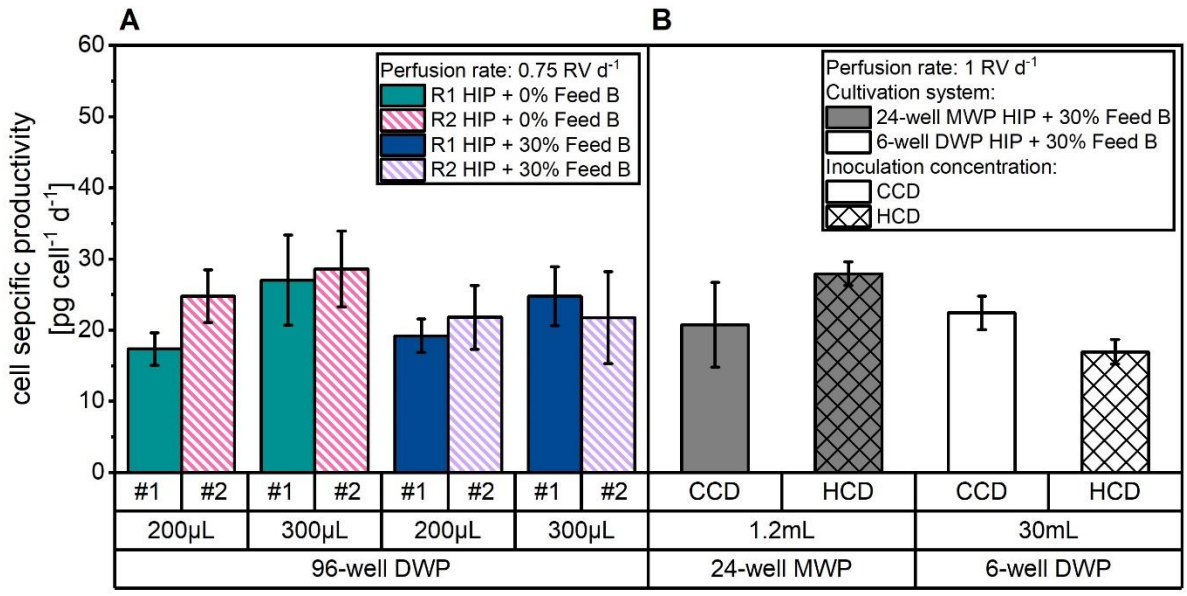

Figure 7.3: Comparison of productivity performance of the CHO cobra cell line in 96-well DWPs, 24-well MWP and 6-well DWP using semi-perfusion methodologies. Cells were inoculated at 1 × 10^6 cells mL^{-1} for 96-well DWP, 24-well MWP (A) 96-well DWP cultures were maintained in HIP medium supplemented with 0% (green and pink) and 30% Feed B (blue and violet) for a culture duration of 10 days. For each condition 2 technically independent runs were performed: R1 (empty), R2 (striped). A perfusion rate of 0.75 RV d^1 was used from day 1 to day 10. (B) For 24-well MWP (grey) and 6-well DWP (white) cultures, cells were inoculated at 1 × 10^6 cells mL^{-1} (CCD, empty) and 10-20 × 10^6 cells mL^{-1} (HCD, cross-striped). Cultures were maintained in HIP medium supplemented with 30% Feed B for a culture duration of 8 and 10 days for 24-well MWP and 6-well DWP, respectively. A perfusion rate of 1 RV d^1 was used from day 1 to day 10. Error bars indicate standard deviation.

7.2.2 mAb1 cell line in 96-well DWP

7.2.2.1 Clone screening with two working volumes

Following the successful translation of the semi-perfusion method to the 96-well DWP format and the identification of suitable working volumes, a clone screening study was conducted using eight mAb1-producing cell clones. Growth performance and STY data for all clones cultured at the two validated working volumes (200 µL and 300 µL) are presented in **Figure 7.4**.

Overall, cultures in both working volumes exhibited highly comparable growth dynamics (**Figure 7.4**, **Row 1**). In some cases, slightly improved performance was observed at the 200 µL volume, as reflected by a prolonged maintenance of higher VCCs following the achievement of such levels. In contrast, cultures at 300 µL often showed an earlier decline in VCC post-peak. Clones mAb1_C3 and mAb1_C4 are representative examples of this trend. Despite the general similarity in growth behaviour across the two volumes, variability between clones was evident. Maximum VCCs ranged from 7.0 – 32.6 $\times 10^6$ cells mL^{-1} for cultures at 200 µL, and from 5.3 - 34.9 $\times 10^6$ cells mL^{-1} for those at 300 µL. Clone mAb1_C7 consistently achieved the highest maximum VCCs across both volumes, while mAb1_C1 showed the lowest performance. The majority of clones—namely mAb1_C2, mAb1_C3, mAb1_C4, mAb1_C5, and mAb1_C8—achieved maximum VCCs within the range of 7 and 10 × 10^6 cells mL^{-1} under both working volume conditions. While mAb1_C7 showed a slightly higher peak VCC at 300 µL, a general trend was observed where clones reached higher maximum VCCs in the 200 µL working volume. This observation is consistent with the findings reported in the previous section for the CHO cobra cell line.

Viability profiles were also largely comparable between the two volumes. However, a more pronounced decline in viability was observed in 300 µL cultures, particularly in the later stages of cultivation. When considered alongside the earlier VCC decline observed under the same conditions, these findings suggest that cultures at 300 µL may experience inhibitory effects that limit sustained growth and viability maintenance.

The evaluation of the STY revealed generally similar dynamics between the two working volumes, with both exhibiting nearly identical developmental trends. After an initial lag phase, STY gradually increased, reaching maximum values ranging from 0.04 to 0.14 g L^{-1} d^{-1}. Two exceptions to this pattern were observed for clones mAb1_C5 and mAb1_C6. For mAb1_C5, the STY in the 300 µL culture was notably higher, initially rising before stabilising at approximately 0.1g L^{-1} d^{-1} whereas in the 200 µL culture, STY showed a gradual increase, peaking at around 0.08 g L^{-1} d^{-1}. Conversely, mAb1_C6 demonstrated a relatively constant STY of approximately 0.09 g L^{-1} d^{-1} in the 200 µL culture, while the 300 µL culture exhibited the typical increasing trend observed in other clones. The observed discrepancies may be attributed to limitations in HPLC-based protein quantification, as indicated by the larger standard deviations associated with these analytical

measurements. While a detailed investigation into their origin was beyond the scope of this study, it is worth noting that previous datasets have demonstrated high consistency with this method, supporting its general reliability under standard conditions.

7.2.2.2 Comparison between well plate scales – 96-well DWP vs 24-well MWP

Following the screening performed in the 96-well DWP, the results were compared with those from the previously conducted screening in the 24-well MWP. This comparison utilised the two available runs of the 24-well MWP screening operated at a perfusion rate of 0.75 RV d^{-1} from the reproducibility study detailed in Chapter 6. The primary focus of the comparison was on cell-specific productivity (q_P) analysis and clone ranking outcomes based on the two strategies described earlier.

It is important to note that cell growth in the 24-well MWP cultures consistently achieved higher maximum concentrations, ranging between 28 and 38 × 10^6 cells mL^{-1} (**Chapter 6, Section 6.2.1.4 – Reproducibility**). Despite this difference in growth performance, q_P values demonstrated strong comparability across both scales (**Figure 7.*5***). In the 24-well MWP screening, raw q_P values ranged from 16.46 to 46.57 pg $cell^{-1}$ d^{-1} in Run 1 and 12.21 to 40.98 pg $cell^{-1}$ d^{-1} in Run 2 (**Table 7.4**). For the 96-well DWP screening, q_P values ranged from 7.4 to 32.2 pg $cell^{-1}$ d^{-1} at 200 µL working volume and 8.2 to 50.61 pg $cell^{-1}$ d^{-1} at 300 µL (**Table 7.4**). Across all experiments and scales, clone mAb1_C5 consistently exhibited the highest q_P, while clone mAb1_C7 showed the lowest q_P values.

Given these largely comparable q_P profiles, similar clone rankings were anticipated when applying a single parameter ranking strategy based on q_P alone. The results of this ranking are summarised in **Table 7.3**, with a colour code used to visually distinguish each clone, ranging from violet (mAb1_C1) to dark red (mAb1_C8). For the 96-well DWP screening, both working volumes (200 µL and 300 µL) yielded consistent rankings, with mAb1_C5 identified as the top-performing clone in both cases. Additionally, mAb1_C6 and mAb1_C2 were consistently ranked in the second and third positions, albeit with their positions swapped between the two volumes. At the lower end of the ranking, most clones either maintained the same position or shifted by only one rank. For example, mAb1_C7 was consistently identified as the lowest-performing clone, while mAb1_C4 improved slightly from position #5 (q_P: 23.18±12.13 pg $cell^{-1}$ d^{-1}) in the 200 µL culture to #4 (q_P: 38.30±13.89 pg $cell^{-1}$ d^{-1}) in the 300 µL culture. The only notable changes were observed for mAb1_C8, which dropped from #4 to #7 position between the two volumes (q_P: 25.47±3.86 and 23.41±8.11 pg $cell^{-1}$ d^{-1}, respectively), and mAb1_C1, which improved from #7 to #5 (q_P: 21.53±2.22 and 29.64±4.00 pg $cell^{-1}$ d^{-1}, respectively).

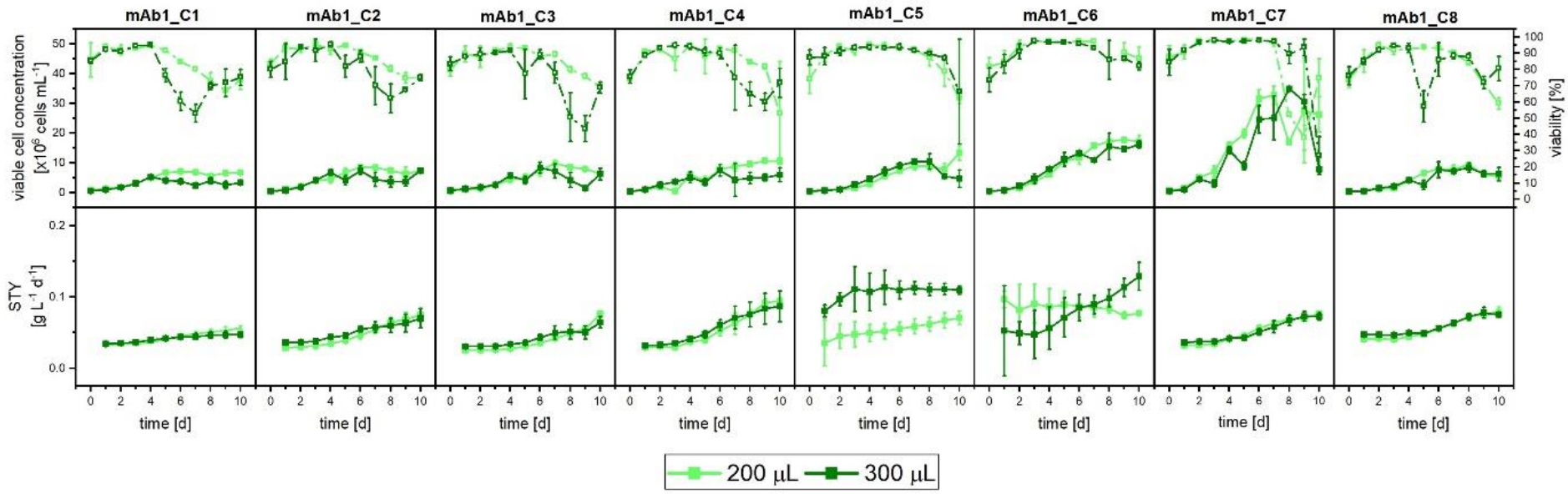

Figure 7.4: Overview of growth and productivity performance of the mAb1 CHO cell clone screening in 96-well DWPs using semi-perfusion methodologies. Cells were inoculated at 1 × 10^6 cells mL^{-1} into two working volumes of 200 µL (■), and 300 µL (■), and cultivated in HIP medium. A perfusion rate of 0.75 RV d^1 was used from day 1 to day 10. Row 1: viable cell concentration (closed, straight) and viability (open, dashed), Row 2: Space-Time-Yield (STY). Mean of N = 3 wells. Error bars indicate standard deviation.

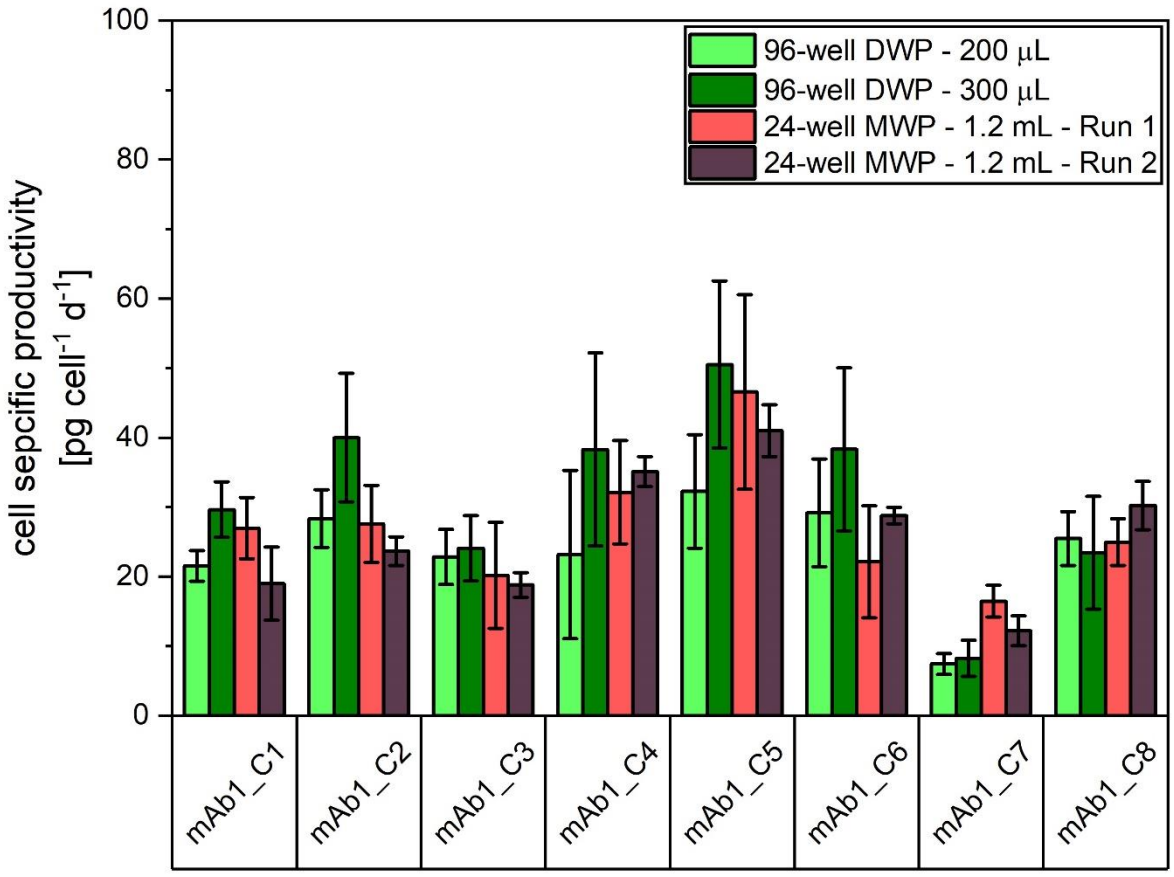

Figure 7.5: Comparison of cell specific productivity of the mAb1 CHO cell clone screening in 96-well DWPs and 24-well MWPs using semi-perfusion methodologies. Cells were inoculated at 1 × 10^6 cells mL^{-1} and cultivated in HIP medium. A perfusion rate of 0.75 RV d^1 was used in all systems and medium exchange was initiated on fay 1 for 96-well DWP and day 3 for 24-well MWP and lasted till the end of culture on day 10. For 24-well MWP cultures. Error bars indicate standard deviation.

Table 7.3: Rankings of 8 mAb1 CHO cell clones based on cell specific productivity for semi-perfusion operation in 96-well DWP and 24-well MWP with partial medium exchanges using a perfusion rate of 0.75 RV d^{-1} in HIP medium. Ranking from top to bottom considered best to worst performing.

Ranking position	96-well DWP		24-well MWP	
	SP-HIP-75%	SP-HIP-75%	SP-HIP-75%	SP-HIP-75%
	200 µL	300 µL	1.2 mL	1.2 mL
	-	-	Run 1	Run 2
#1	mAb1_C5	mAb1_C5	mAb1_C5	mAb1_C5
#2	mAb1_C6	mAb1_C2	mAb1_C4	mAb1_C4
#3	mAb1_C2	mAb1_C6	mAb1_C2	mAb1_C8
#4	mAb1_C8	mAb1_C4	mAb1_C1	mAb1_C6
#5	mAb1_C4	mAb1_C1	mAb1_C8	mAb1_C2
#6	mAb1_C3	mAb1_C3	mAb1_C6	mAb1_C1
#7	mAb1_C1	mAb1_C8	mAb1_C3	mAb1_C3
#8	mAb1_C7	mAb1_C7	mAb1_C7	mAb1_C7

Colour code to simplify the ranking visually.

When comparing rankings across scales, mAb1_C5 remained the top performer (#1) in all experiments (q_P ranges between 32.27±8.18 and 50.52±12.03 pg cell^{-1} d^{-1}). However, greater variability was observed in the rankings of other clones. Some clones performed better in the 96-well DWP, while others showed improved performance in the 24-well MWP. For instance, mAb1_C4 ranked in mid-range positions (#5 and #4 with q_P values of 23.18 ± 12.13 and 38.30±13.89 pg cell^{-1} d^{-1}) in the 96-well DWP, yet achieved second place in both 24-well MWP runs (q_P: 32.14±7.44 and 35.13±2.15 pg cell^{-1} d^{-1}). Conversely, mAb1_C6 performed better in the 96-well format, ranking second and third, compared to rankings on positions #7 and #4 in the 24-well MWP (q_P: 22.13±8.04 and 35.13±2.15 pg cell^{-1} d^{-1}). Overall, although the same top-ranking clone was identified across scales, the q_P-based ranking revealed notable differences in the relative positions of the remaining clones between the 96-well DWP and 24-well MWP.

One of the key outcomes from the cell clone screening and ranking presented in **Chapter 6** was that incorporating multiple parameters through the manufacturability index (MI_{CL}) resulted in a more consistent and robust assessment of clone performance. Therefore, the MI_{CL} metric was also applied to rank clones in the 96-well DWP format. However, due to the limited working volume in the 96-well system, only growth and productivity parameters could be quantified, resulting in a reduced set of parameters for the MI_{CL} calculation. Specifically, five parameters were included: VCC, viability, growth rate, STY, and q_P. In contrast, the MI_{CL} rankings for the 24-well MWP included a total of ten parameters, comprising the same five growth and productivity parameter, supplemented by five metabolite-related parameters, as described in **Chapter 6** and **Chapter 2, Section 2.7.2**.

The raw MI_{CL} values are reported in **Table 7.4**. The observed MI_{CL} ranges were as follows: 0.18–1.00 for 96-well DWP at 200 µL, 0.29–1.00 for 96-well DWP at 300 µL, and 0.43–1.00 for both 24-well MWP runs (previously referred to as SP-HIP-75% Run 1 and Run 2). Notably, the 96-well DWP exhibited the wider MI_{CL} ranges than the 24-well MWP.

The MI_{CL}-based rankings are presented in **Figure 7.*6***, using the same colour-coding scheme previously applied for the q_P-based ranking, ranging from violet (mAb1_C1) to dark red (mAb1_C8). Comparison of the rankings in the 96-well DWP format revealed only minor differences between the two working volumes, with strong overall consistency. Although the top-ranked clone differed, the same three clones—mAb1_C5, mAb1_C6, and mAb1_C8—consistently occupied the top three positions, albeit in different orders. Additionally, mAb1_C2 ranked in the mid-range at positions #5 and #4 in the 200 µL and 300 µL cultures (MI_{CL}: 0.23 (0.018–1.00) and 0.46 (0.29–1.00)), respectively, while mAb1_C1 was consistently identified as the lowest-performing clone in both working volumes (MI_{CL}: 0.18 and 0.29, respectively for 200 µL and 300 µL cultures).

A comparison of the clone rankings generated by the two strategies—q_P-based and MI_{CL}-based—revealed notable shifts for several clones. For instance, clones such as mAb1_C7 and mAb1_C8 achieved higher rankings when evaluated using the MI_{CL} strategy. In contrast, mAb1_C2, which performed well under the single-parameter q_P-based ranking, dropped to lower positions in the MI_{CL}-based ranking. Despite these differences, certain clones demonstrated consistent performance across both strategies. Notably, mAb1_C5 and mAb1_C6 consistently ranked among the top-performing clones, while mAb1_C1 and mAb1_C3 were consistently positioned at the lower end of the rankings, regardless of the strategy applied.

When comparing the MI_{CL}-based rankings across the 96-well DWP and 24-well MWP formats, several consistent trends and noteworthy differences were observed. Clone mAb1_C5 emerged as the top-performing clone in three of the four conditions and ranked second in the remaining one. Furthermore, clones mAb1_C4, mAb1_C5, mAb1_C6, and mAb1_C8 consistently ranked within the top four positions in the 96-well DWP at 200 µL and both runs of the 24-well MWP. For the 96-well DWP at 300 µL, three of these four clones remained in the top positions, except mAb1_C4, which dropped to sixth place. In contrast, clones mAb1_C1 and mAb1_C3 ranked lowest in the 96-well DWP experiments (#6–#8) yet occupied mid-level positions in the 24-well MWP rankings (#5 and #6). Conversely, clones mAb1_C7 and mAb1_C2 were ranked lowest in the 24-well MWP but showed improved rankings in the 96-well DWP. Nevertheless, these four clones (mAb1_C1, mAb1_C2, mAb1_C3, and mAb1_C7) were predominantly ranked within the lower tier across all conditions—except mAb1_C2, which reached fourth place in the 96-well DWP at 300 µL.

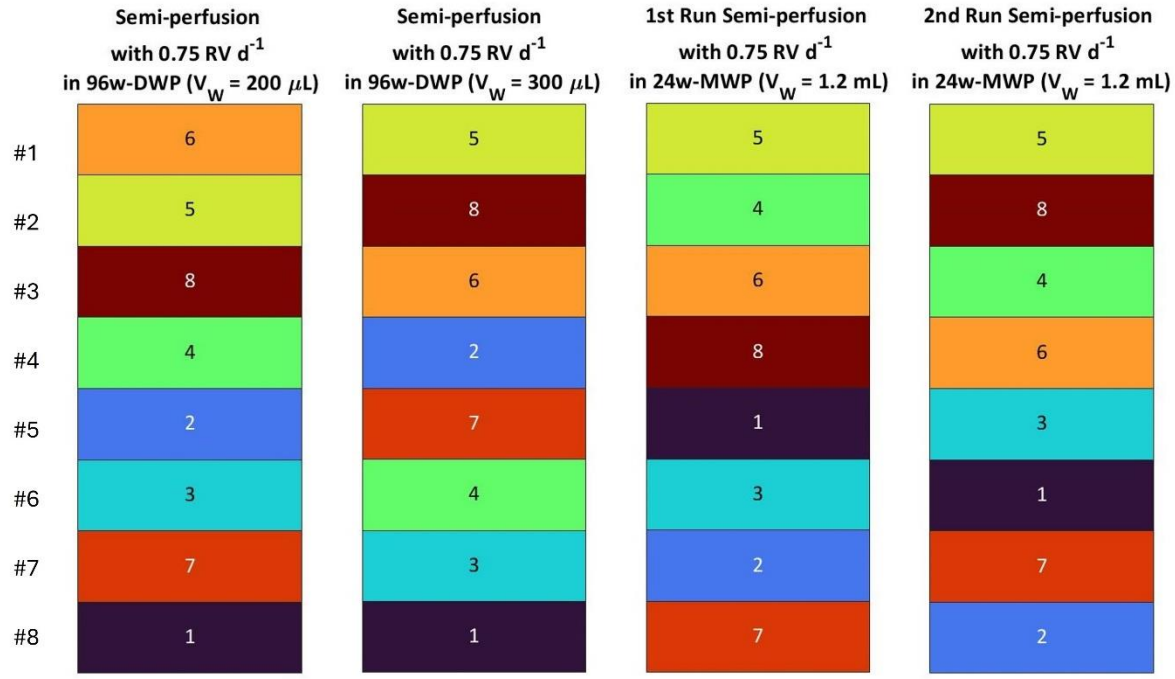

Figure 7.6: Rankings of 8 mAb1 CHO cell clones based on manufacturability index for semi-perfusion operation in 96-well DWP and 24-well MWP with partial medium exchanges using a perfusion rate of 0.75 RV d^{-1} in HIP medium. Ranking from top to bottom considered best to worst performing.

Table 7.4: Summary of cell specific productivities and manufacturability index values of 8 mAb1 clones for semi-perfusion operations with partial medium exchanges in 24-well MWP and 96-well DWP

Clones	q_P [pg cell^{-1} d^{-1}]				MI_{CL}			
	96-well DWP		24-well MWP		96-well DWP		24-well MWP	
	200µL	300µL	Run 1	Run 2	200µL	200µL	Run 1	Run 2
mAb1_C1	21.53±2.22	29.64±4.00	26.98±4.41	18.99±5.25	0.18	0.29	0.69	0.57
mAb1_C2	28.33±4.15	40.00±9.25	27.58±5.53	23.66±2.09	0.23	0.46	0.63	0.43
mAb1_C3	22.83±3.94	24.08±4.70	20.18±7.62	18.81±1.78	0.21	0.31	0.68	0.65
mAb1_C4	23.18±12.13	38.30±13.89	32.14±7.44	35.13±2.15	0.29	0.33	0.89	0.82
mAb1_C5	32.27±8.18	50.52±12.03	46.57±13.98	40.98±3.73	0.75	1.00	1.00	1.00
mAb1_C6	29.16±7.75	38.31±11.75	22.13±8.04	28.77±1.18	1.00	0.63	0.75	0.746
mAb1_C7	7.44±1.49	8.24±2.59	16.46±2.29	12.21±2.15	0.19	0.34	0.43	0.54
mAb1_C8	25.47±3.86	23.41±8.11	24.94±3.37	24.94±3.37	0.67	0.77	0.69	0.86

Productivity values are given as average and standard deviation of N = 3 wells over 8 days from day 3 to day 10 for 24-well MWP and over 10 days from day 1 to 10 for 96-well DWP.
q_p: cell specific productivity; MI_{CL}: cell line manufacturability index

7.3 Discussion

In this chapter, the translation of the semi-perfusion method to 96-well DWP was investigated. The approach was informed by the established methodology in 24-well MWP and supported by insights from literature covering various operation modes in 96-well DWP systems. The evaluation focused on assessing the impact of working volume on cellular growth and productivity, with results benchmarked against previously discussed 24-well MWP cultures from Chapter 4. Building on this foundation, a cell clone screening was conducted to assess growth and productivity performance. Clones were subsequently ranked using both single-parameter and multi-parameter strategies, and the outcomes were compared to those obtained during the 24-well MWP-based clone screening presented in Chapter 6.

7.3.1 96-well DWP semi-perfusion methodology

The adoption of the 96-well DWP format was primarily motivated by the need to increase experimental throughput while maintaining robust and reproducible data quality, particularly during early-stage cell line screening. However, miniaturisation of culture systems is not without challenges; scaling down can introduce variability and necessitates additional characterisation to ensure confidence in the results obtained. To address these considerations, an initial feasibility study was conducted using the CHO Cobra cell line, which was used in previous platform development studies and could therefore support realistic comparisons.

This preliminary investigation does not aim to present a fully optimised ultra-small-scale system but rather serves as a foundational step toward establishing a workable methodology at this scale. The study also aims to identify key operational parameters, highlight critical limitations, and outline areas for future investigation.

A review of the literature revealed a broad range of culture conditions reported for 96-well DWP systems, particularly for orbital diameter, agitation speed, and working volume. Parameter selection for this study was informed by these reports but ultimately constrained by the hardware available. Specifically, the shaker platform used had a fixed orbital diameter of 19 mm and a maximum agitation speed of 300 rpm—substantially lower than those typically reported in the literature (Bielser et al., 2019; Wang, Albanetti, Miro-Quesada, et al., 2018). Consequently, this initial study focused on assessing the effect of working volume on cell performance under these fixed agitation conditions.

The experimental results indicated that lower working volumes (200 and 300 µL) supported sustained cell growth achieving peak VCCs of approximately 24 – 30 × 10^6 cells mL^{-1}. In contrast, higher working volumes (350 and 400 µL) exhibited with poor growth and reduced viability.

These observations are likely attributable to suboptimal mass transfer and mixing at higher fill volumes, particularly given the limited agitation speed.

Currently, there is a lack of data in the literature on mass transfer performance in 96-well DWP systems operated at relatively low shaking speeds (300 rpm) and at relatively large orbital diameter of 19 mm. One relevant study investigated oxygen transfer rates (OTRs) in DWPs under shaking conditions comparable in speed (300 rpm), but with larger orbital diameters of 25 mm and 50 mm, using bacterial cultures (Duetz et al., 2000). This study demonstrated a strong dependence of OTR on both orbital diameter and fill volume: higher working volumes were associated with reduced OTRs. Furthermore, reducing the orbital diameter from 50 mm to 25 mm resulted in a threefold decrease in OTR. These findings indicate that both smaller orbital diameters and higher fill volumes can significantly impair oxygen transfer.

Although the present work employed slightly lower working volumes, the smaller orbital diameter of 19 mm may have introduced additional oxygen transfer limitations. This could plausibly explain the reduced growth and viability observed at the higher working volumes. However, this hypothesis remains speculative. Further investigations are required to characterise the oxygen transfer dynamics under the specific conditions used in this study—namely, 300 rpm agitation and a 19 mm orbital diameter in 96-well DWPs—to confirm whether mass transfer constraints are indeed responsible for the observed performance trends.

The experiments demonstrated good reproducibility between two independent runs using the same medium composition. Unexpectedly, medium supplementation did not have a statistically significant impact on overall culture performance. Although the HIP30 medium formulation (base medium supplemented with 30% Feed B) improved early cell viability, reduced variability in lag phase duration, and marginally increased peak VCCs, previous studies conducted in 24-well MWPs reported more pronounced improvements when comparing base media to blended formulations independent of media used (Lucas et al., 2024). It is possible that a more targeted and comprehensive medium optimisation study—such as one employing a Design of Experiments (DoE) approach—would reveal similar performance enhancements in the 96-well format as those observed in the 24-well system. Preliminary evidence supporting this hypothesis is suggested by the modest improvement in space-time yield (STY) observed under certain conditions with the HIP medium supplemented with 30% Feed B, indicating a potential trend toward enhanced culture performance.

The comparison across scales with the results presented in the previous chapters demonstrated that maximum VCCs were comparable for conventional cell density (CCD) inoculations, reaching approximately 30×10^6 cells mL^{-1}. This suggests that miniaturisation to the 96-well DWP format is feasible without compromising cell growth potential. Cell-specific productivity (q_P) remained

consistent across all scales, underscoring the robustness of the clone's production performance irrespective of culture volume and across both HCD and CCD inoculated cultures. In contrast, STY exhibited greater variability, with larger-scale systems outperforming the 96-well DWP format. This outcome is consistent with previous observations comparing SDMs to larger bioreactor systems, which generally benefit from improved mass transfer and more precise process control. In the present study, the superior performance at larger scales may be attributed to both enhanced oxygen transfer capabilities, and higher perfusion rates (1 RV d^{-1} in 24-well MWP and 6-well DWP compared to 96-well DWP).

7.3.2 Cell clone screening in 96-well DWP

Following an initial characterisation of the 96-well DWP format for semi-perfusion, the feasibility of conducting clone screening under ultra-high-throughput perfusion-like conditions was assessed. Overall, cultures maintained at a 200 µL working volume demonstrated superior peak VCC and sustained viability compared to those at 300 µL. This trend is consistent with earlier observations from experiments using the CHO cobra cell line, where higher working volumes were associated with increased variability and signs of potential oxygen limitation.

While STY profiles followed similar overall trends across volumes, individual deviations were noted for certain clones (e.g., mAb1_C5 and mAb1_C6). These anomalies were likely attributable to analytical variability stemming from limited sampling volumes, which impacted the accuracy of protein quantification using the applied HPLC method. Although HPLC is generally a highly precise method, particularly at low sample volumes where peak sharpness improves, though very low protein concentrations or minimal sample volumes can result in values approaching the method's limit of detection, thereby reducing measurement reliability. Additionally, the HPLC method employed is not optimised for high-throughput analysis. To enable efficient high throughput evaluations, alternative analytical approaches (e.g. Octet) are needed that not only match but ideally surpass the current method in terms of throughput, and measurement robustness, while also requiring minimal sample volumes, an essential consideration given the limited availability and high value of the material.

Despite these deviations, q_P values were broadly comparable between the two working volumes. Although slightly higher q_P values were observed at 300 µL, potentially due to lower cell growth in those cultures, these differences were not statistically significant and remained within the range of experimental variability. This indicates equivalent productivity performance across the two working volumes. Nonetheless, results obtained from the 300 µL condition in the 96-well DWP should be interpreted with caution, given the slight impairment in growth observed under these conditions.

Furthermore, comparison with the previously reported 24-well MWP clone screening study, operated under partial medium exchange at 0.75 RV d^{-1}, revealed similar q_P dynamics. This was supported by the comparable q_P ranges observed in both formats, with values ranging from 7.4 to 50.61 pg $cell^{-1}$ d^{-1} in the 96-well DWP, and from 12 to 47 pg $cell^{-1}$ d^{-1} in the 24-well MWP. Notably, clone mAb1_C5 consistently achieved the highest q_P values across all scales, while mAb1_C7 consistently showed the lowest productivity. The consistency in q_P ranges as well as trends for high producing and low producing clones suggests that these clones exhibit robust performance across different small-scale systems.

The ranking comparisons revealed interesting patterns. Based on the q_P values, it was expected that top- and low-performing clones would show consistent rankings across scales. While this was true for the highest-ranking (mAb1_C5) and lowest ranking clone (mAb1_C7), which maintained their position across both formats, larger discrepancies were observed for the remaining clones. In the 96-well DWP, the same three clones consistently ranked in the top three positions. However, when compared with the 24-well MWP, only the top-ranking clone remained consistent, while the others shifted to lower positions. Similarly, the second best-performing clone in the 24-well MWP ranked much lower in the 96-well DWP (mAb1_C4). Within the same system (i.e., 96-well DWP at 200 µL vs. 300 µL), a clear trend was observed in the clone ranking, with similar clones consistently occupying high, medium, or low positions. This observation aligns with earlier findings from the 24-well MWP semi-perfusion screening (**Chapter 6**).

As in the previous chapter, clone ranking based on a single parameter (q_P) was expanded to a multi-parameter assessment using the manufacturability index (MI_{CL}). However, unlike the 24-well MWP screening where ten parameters were incorporated into the MI_{CL}, the 96-well DWP format allowed for a more limited set of measurements due to lower working volumes and sampling constraints. Consequently, the MI_{CL} ranking for the DWP was based on five parameters: VCC, viability, growth rate, STY, and qP. In contrast, the 24-well MWP included five additional parameters derived from expanded metabolite profiling, made possible by the slightly higher working volume (**Chapter 2**).

The MI_{CL}-based ranking for the 96-well DWP identified the same three clones—mAb1_C6, mAb1_C5, and mAb1_C8—in the top three positions, although with minor differences in exact rank order. Two of these (mAb1_C5 and mAb1_C6) were also top performers in the q_P-based ranking, whereas mAb1_C2, among the top three performers in q_P, dropped to mid-level positions (#4 and #5) in the MI_{CL}-based assessment. A similar trend was observed in the 24-well MWP, where some clones maintained or improved their position with the MI_{CL}, while others dropped, reflecting how broader performance metrics can shift the prioritisation of clones. Notably, when comparing MI_{CL} rankings between the 96-well DWP and the 24-well MWP, a much stronger

alignment was observed than with q_P-based rankings. The same four clones consistently occupied the top four positions, and the same four clones were found at the bottom across both scales. This contrasts with the q_P-based rankings, where only the top-performing clone (mAb1_C5) was consistently ranked, while others varied significantly between formats.

These findings underscore the value of incorporating multiple parameters into clone evaluation to enhance robustness and predictive power. Despite the limited dataset in the 96-well DWP format, the directionality of the ranking was consistent with that from the more comprehensive MWP assessment. This suggests that adding further parameters in future workflows could reinforce early-stage screening decisions and improve scale-up predictability.

7.4 Concluding remarks

The objective of the work presented in this chapter was to investigate the miniaturisation of the semi-perfusion methodology from the 24-well MWP format to the 96-well DWP format. In the context of cell line development, achieving the highest possible throughput while maintaining robust and reliable data quality is a critical requirement. Introducing the semi-perfusion approach at the 96-well plate screening stage—prior to an eventual scale-up to 24-well MWP—offers a strategic advantage in meeting this need. This transition is further supported by the opportunity to leverage existing infrastructure: many high-throughput screening platforms are already built around 96-well DWP formats, with established hardware, software, and user expertise. As such, adapting the semi-perfusion methodology to this format enhances its industrial applicability and streamlines integration into current workflows.

This study demonstrated that working volume has a significant impact on cell performance in the 96-well DWP format, even at fixed agitation conditions. These findings highlight the importance of carefully optimising key parameters such as working volume, shaking diameter, and agitation speed to ensure suitable culture conditions. They also underscore the need for further optimisation to balance the trade-off between maximising material availability for parameter analysis and maintaining high cell performance.

The successful implementation of a semi-perfusion protocol in the 96-well DWP enabled the performance of a high-throughput cell clone screening. The results confirmed that the methodology is sufficiently sensitive to distinguish performance differences among individual clones. Clone ranking outcomes using both single-parameter (q_P) and multi-parameter (MI_{CL}) strategies demonstrated good concordance with previous rankings obtained in the 24-well MWP format. Notably, rankings based on the MI_{CL} approach—which integrates multiple growth and productivity parameters—showed greater consistency across scales and working volumes, underscoring its value as a more robust selection tool.

Overall, this work establishes that the semi-perfusion methodology can be effectively miniaturised to a 96-well DWP format, enabling high-throughput screening with meaningful biological outcomes and cross-scale comparability. This represents a significant step towards streamlined and scalable clone evaluation workflows compatible with existing industrial screening infrastructure.

Chapter 8: Conclusions

8.1 The present contribution

The objective of this research work was to develop a high-throughput, small-scale methodology suitable for intensified cell culture processes, with a specific focus on applications in cell clone screening and selection. The motivation for this work stems from the increasing industrial demand for intensified bioprocesses and the corresponding need to align early-stage screening systems with the operational modes intended for manufacturing. Traditional fed-batch screening approaches may fail to capture clone performance under intensified conditions, resulting in suboptimal clone selection. Therefore, this study aimed to establish a semi-perfusion microwell-based platform capable of supporting high-density cultures in a scalable and parallelised format.

The primary focus of the work was the further development of an existing semi-perfusion strategy using 24-well microwell plates (MWPs). The platform was expanded through the implementation of cell bleed strategies and the evaluation of varying perfusion rate profiles, with the goal of enhancing process understanding and evaluating platform robustness. While the application of cell bleeds has previously been explored in spin tube-based models, their implementation at the microwell plate scale remains largely unaddressed in the literature. Additionally, the use of CSPR-based perfusion rate—commonly employed in perfusion bioreactor systems—was introduced and evaluated within the well-plate context, representing a novel approach to aligning small-scale, high-throughput models with industry-relevant operational strategies.

In parallel, larger-scale deep well plate formats, with working volumes of approximately 30 mL, were explored as intermediate scale-up. These formats retain key operational features of the MWP platform while enabling greater culture volumes and facilitating handling practices similar to those used in shake flask experiments. Selected conditions were subsequently translated to a 250 mL perfusion bioreactor system to assess methodological scalability and the feasibility of transferring defined operating strategies to larger-scale, controlled bioreactor environments.

To evaluate the applicability of the developed platform in an industrially relevant context, the 24-well MWP methodology was tested with a cell clone screening application. Conventional fed-batch

conditions were compared with semi-perfusion modes across multiple media formulations and perfusion strategies. Two panels of production clones—expressing either a monoclonal antibody or a bispecific antibody—were assessed to demonstrate the applicability and versatility of the platform across different recombinant protein formats.

In addition, clone ranking strategies were investigated by comparing a conventional single-parameter approach based on cell-specific productivity (q_P) with a multi-parameter framework incorporating a manufacturability index (MI_{CL}). The comparison was applied across both fed-batch and semi-perfusion conditions to examine potential differences in clone evaluation methodologies.

Finally, efforts were made to further miniaturise the methodology to a 96-well deepwell plate format. The impact different working volumes on key performance indicators—including cell growth, viability, and productivity—was systematically evaluated to determine the feasibility of operating intensified cultures at ultra-small scales.

8.2 Main findings of the investigation

The characterisation of the MWP platform was based on previous work by Tregidgo et al. (2023), who developed a semi-perfusion methodology for 24-well MWPs using centrifugation-based cell retention and a medium exchange rate of 1 RV d^{-1} identified as the most feasible option for manual operation.

Building on literature that explored the use of cell bleed strategies in spin tubes as scale-down models for the optimisation of stable perfusion bioreactor processes (Mayrhofer et al., 2021; Wolf et al., 2020; Wolf et al., 2018, 2019), the existing MWP workflow was adapted to incorporate a cell bleed step while maintaining a perfusion rate of 1 RV d^{-1}. This adapted workflow was evaluated across four experimental conditions, reflecting the used target cell concentrations reported in the literature. The introduction of a cell bleed enabled stable average cell densities across all target concentrations (10 – 40 × cells mL^{-1}), while maintaining high viability and stable profiles for key process parameters such CSPRs, metabolite concentrations, and STYs.

A scale-up of two of the four conditions to a 6-well DWP in comparison to 125 mL shake flask cultures showed great comparability between all three systems and scales. The results demonstrated that high cell concentrations could be maintained at defined setpoints, leading to a stabilised culture environment indicative of “quasi steady-state” conditions. Importantly, this strategy proved to be scalable to DWP and SF, with performance metrics showing good agreement with alternative SDMs and perfusion bioreactor data up to 40 L reported in the literature regarding growth, productivity and metabolite dynamics. Furthermore, the DWP format showed

improved sustainability metrics and operational efficiency compared to shake flasks, which require additional consumables for centrifugation and pose a higher risk of contamination.

Following the implementation of the cell bleed while maintaining a total medium exchange once per day, the focus was shifted towards varying the perfusion rate while aiming for maximum growth (i.e. no cell bleed step). Therefore, a CSPR-based control strategy was implemented to more closely mimic conditions used in perfusion bioreactor systems, in addition to the standard fixed-rate approach of 1 RV d^{-1}. Three distinct CSPR setpoints were investigated and compared against a control condition using fixed medium exchanges, with experiments conducted across different initial seed concentrations to assess their interaction with the perfusion strategy.

The comparative analysis revealed that seed concentration played a critical role in determining the maximum achievable cell density, with higher inoculation levels enabling cultures to reach and sustain elevated cell concentrations—up to 74×10^6 cells mL^{-1} for cultures operated at 1 RV d^{-1}, and up to 45×10^6 cells mL^{-1} for CSPR-based cultures seeded at high densities. Notably, the use of CSPR-based perfusion facilitated the stabilisation of cultures at distinct cell density setpoints over multiple days. For cultures seeded at conventional densities, stabilisation occurred around 30×10^6 cells mL^{-1}, whereas cultures initiated at higher seed concentrations stabilised around 50×10^6 cells mL^{-1}. In both cases, cell viability remained high, and the process environment was characterised by consistent nutrient and metabolite profiles over the stabilisation period. These findings were in contrast to results from control cultures, which upon reaching maximum cell concentration showed a drastic reduction in cell concentration together with a moderate reduction of viability. Furthermore, CSPR-based cultures showed enhanced productivity, with cell-specific productivity reaching up to two-fold higher than in RV d^{-1}-based controls, particularly under CCD inoculation.

To further evaluate the findings in MWP, selected conditions were scaled up to the 6-well DWP as well as a 250 mL perfusion bioreactor. For the scale up to the DWP the two better performing CSPR conditions were selected - 15 and 20 pL $cell^{-1}$ d^{-1} – and both seed densities were investigated. The results closely mirrored those observed in the MWP experiments. Across both CCD and HCD inoculation strategies, CSPR-cultures maintained stable VCCs successfully replicating the stabilisation profiles established in MWP. Cell-specific productivity remained nearly two-fold higher in CSPR-cultures than in RV d^{-1}-based controls and key metabolites exhibited early and sustained stabilisation during the culture period. Furthermore, actual perfusion rates closely aligned with the target CSPRs, highlighting effective perfusion control and reduced variability compared to fixed-rate operations. Collectively, these findings confirm the scalability of the CSPR strategy, with consistent culture behaviour and performance achieved across both MWP and DWP platforms.

In a final step of the CSPR-based perfusion rate integration, the CSPR condition targeting 20 pL cell d^{-1} was transferred to a 250 mL perfusion bioreactor, initiated at a low seed density. While the continuous medium exchange was approximated in the well plate formats through discrete, batch-wise daily medium exchanges, the bioreactor system employed a pump-based setup to enable continuous medium exchange, with manual rate adjustments performed once daily as required. At this larger scale, the CSPR-based strategy successfully reproduced key performance characteristics observed in the MWP and DWP formats, maintaining stable VCCs and consistently high viabilities throughout the culture period. Cell-specific productivity remained consistent across all three systems – MWP, DWP, and bioreactor – at approximately 40 pg $cell^{-1}$ d^{-1}. Additionally, a modest increase in STY was observed in the bioreactor relative to the well plate formats, indicating improved volumetric productivity under continuous operation. Metabolic profiles in the bioreactor aligned closely with those recorded in smaller-scale formats, with efficient nutrient utilisation and limited metabolite accumulation throughout the run. These results collectively demonstrate the scalability and operational robustness of the CSPR-based perfusion approach across multiple cell culture formats.

In the final phase of the platform characterisation, the previously implemented cell bleed and CSPR-based perfusion rate strategies were combined to assess their synergistic impact on culture performance. Experiments conducted in 24-well MWP plate demonstrated that this integrated approach successfully maintained the viable cell concentration at a defined setpoint of 20×10^6 cells mL^{-1} across three CSPR targets (15, 20, and 30 pL $cell^{-1}$ day^{-1}). CSPR-cultures exhibited stable metabolite profiles, with lactate concentrations consistently lower or comparable to controls, despite reduced media turnover. This was a recurring observation across all CSPR-based experiments and is in alignment with literature which showed that controlling nutrient supply relative mitigates toxic metabolite accumulation. Cell-specific productivity was significantly enhanced in CSPR-based cultures, reaching 36.0 pg $cell^{-1}$ day^{-1} compared to 24.6 pg $cell^{-1}$ day^{-1} in controls. While space-time yield remained comparable across conditions, peaking at approximately 0.2 g L^{-1} day^{-1}, the higher q_P in CSPR-cultures highlights the potential for improved product output per cell. Notably, while cultures under CSPR conditions exhibited slower growth rates, overall productivity was not compromised, indicating suitability for prolonged culture durations. Media consumption was also substantially reduced, with savings of up to 53% depending on the CSPR target, representing a notable improvement in process efficiency.

To evaluate the scalability of the approach, selected CSPR conditions (15 and 20 pL $cell^{-1}$ day^{-1}) were transferred to 6-well deepwell plates. While average VCCs were slightly lower in DWPs than in MWPs, the cultures showed similar growth and viabilities dynamics. The oscillatory cell growth patterns characteristic of CSPR cultures were preserved, indicating robust control across scale.

Metabolite profiles in DWPs mirrored those observed in MWPs, with comparable or slightly lower concentrations of key metabolites in CSPR conditions. Cell-specific productivity was again elevated in CSPR cultures, particularly at the lowest CSPR target.

Taken together, these findings confirm that the integrated CSPR and cell bleed strategy supports consistent culture performance across scales. Compared to controls, the CSPR-based approach maintained similar growth and metabolic profiles while improving productivity and significantly reducing media consumption—achieving reductions between 60% and 74% in DWPs.

Following the characterisation of the 24-well MWP platform and the establishment of its capabilities in semi-perfusion operation, the methodology was applied to a cell line screening context. This application was driven by the biopharmaceutical industry's growing transition from traditional fed-batch processes toward intensified and continuous biomanufacturing strategies. Despite this shift, current cell line screening workflows typically rely on fed-batch operation at small scale, while perfusion-based evaluation is reserved for later stages at bench or pilot scale. This discrepancy introduces a risk that cell lines selected under fed-batch conditions may perform sub-optimally in perfusion processes at manufacturing scale.

To address this limitation, a comparative study was undertaken using two panels of production cell lines, comprising a total of 14 clones. Each clone was evaluated under both fed-batch and semi-perfusion conditions in parallel, using the MWP platform. This investigation represents the first reported application of parallelised fed-batch and semi-perfusion cultures in microwell plates for the purpose of clone screening.

The results revealed that clone performance and relative ranking varied markedly between the two process modes. In several instances, clones demonstrating strong performance under fed-batch conditions exhibited reduced performance under semi-perfusion, and vice versa. These findings highlight the significant influence of process mode and perfusion rate on clone behaviour, and consequently, selection outcomes.

In addition to evaluating performance differences, efforts were made to improve the clone ranking strategy employed during screening. Conventionally, clone selection is often based on a single performance parameter—typically a productivity value such as measured endpoint titre in case of fed-batch operation —while other critical parameters such as growth characteristics and metabolite profiles are disregarded. To address this limitation, two ranking strategies were compared: a conventional single-parameter approach here based on the cell specific productivity value (to accommodate different feeding and medium exchange protocols), and a multi-parameter approach using the manufacturability index, which integrates multiple criteria relevant to process performance and robustness.

For fed-batch cultures, both ranking strategies produced identical results, indicating that q_P alone may be a sufficient indicator of overall performance under these conditions. However, in semi-perfusion cultures, the two approaches yielded significantly different rankings. Notably, the manufacturability index provided more consistent and reproducible rankings across independent experimental runs. These findings suggest that, under semi-perfusion conditions, a multi-parameter assessment is essential to capture the complex interplay between growth, productivity, metabolic behaviour and other parameters. Overall, the manufacturability index was found to be a more robust and reliable metric for clone ranking in intensified culture processes. Its implementation in semi-perfusion clone screening could enhance the identification of high-performing clones with favourable manufacturing characteristics, ultimately supporting a more effective and predictive cell line development strategy.

This research highlights the importance of aligning early-stage screening conditions with the intended production process. Incorporating semi-perfusion operation at microwell scale enables more representative evaluation of clone performance under intensified conditions. This approach may support more robust selection decisions and improve the likelihood of identifying high-performing clones suitable for continuous, perfusion-based manufacturing.

In the final exploration of this thesis, the semi-perfusion methodology was further miniaturised and adapted for use in 96-well deep-well plates (DWPs). This extension aimed to assess the feasibility of high-throughput screening under intensified culture conditions at an even smaller scale. Initial experiments were conducted using a single cell line (CHO Cobra) to evaluate the impact of working volume on culture performance, particularly in the context of the limited maximum agitation speed of 300 rpm.

Unlike the manual 24-well MWP approach, which used daily total medium exchanges (1 RV d^{-1}), the 96-well format employed a simplified semi-perfusion protocol based on a fixed partial perfusion rate of 0.75 RV d^{-1}.

Initial investigations focused on the effects of the working volume on the cell culture performance, for which four conditions ranging from 200 µL to 400 µL were tested. These initial cultures were maintained using a perfusion base medium supplemented only with GlutaMAX™ and HT supplement—standard additives to sustain CHO cell growth. At the maximum agitation speed of 300 rpm, cell growth was sustained only in the 200 µL and 300 µL conditions. In contrast, cultures operated at 350 µL and 400 µL failed to maintain growth beyond day 3, likely due to inadequate mixing and oxygen transfer at higher volumes under the given agitation constraints.

To further evaluate the influence of medium composition on performance in the 96-well format, additional experiments were performed at 200 and 300 µL working volume using a previously

optimised medium blend, established in 24-well MWP studies to support high productivity. This blend consisted of perfusion base medium supplemented with 30% Feed B. The aim was to compare performance outcomes in the 96-well system with those previously observed in both 24-well MWP and 6-well DWP formats using the same medium formulation. However, no significant differences in cell growth or productivity were observed between the two media compositions across the working volumes tested in the 96-well DWP. Furthermore, although growth performance was generally superior at larger scales, the cell-specific productivity values were comparable across the three plate formats, indicating good consistency of productivity measurements irrespective of scale.

Subsequently, a semi-perfusion cell clone screening study was performed in the 96-well DWP format using a panel of 8 CHO cell clones expressing a monoclonal antibody. Cultures were conducted at both 200 µL and 300 µL working volumes. For each clone, growth dynamics and STY were largely comparable between the two volumes, although performance differences were observed between individual clones. When compared to previous experiments in 24-well MWPs using the same perfusion rate and medium composition, the trends in cell-specific productivity were maintained—clones with high q_P in the MWP format also demonstrated high q_P in the 96-well DWP format, and vice versa. This consistency represents an initial indication of scalability between the two small-scale well plate systems.

Clone ranking outcomes were also assessed using both previously established strategies: one based solely on cell-specific productivity and the other on the manufacturability index, which integrates multiple performance parameters. The q_P-based ranking identified the same top-performing clone across scales; however, the remaining ranking positions varied more substantially between working volumes and between scales. In contrast, rankings based on the manufacturability index showed higher consistency across working volumes and well plate formats, with the same four clones repeatedly ranking among the top performers. These findings suggest that the manufacturability index provides a more robust and reliable metric for clone selection, particularly in the context of small-scale semi-perfusion screening.

8.3 Recommendations for future work

The results presented in this thesis demonstrate the feasibility and utility of using well plates as scale-down models for semi-perfusion operation. The characterisation of the platform, as described in **Chapters 3** to **5**, confirmed scalability from 24-well MWP to 6-well DWP and included preliminary investigations into 250 mL perfusion bioreactors. Nevertheless, additional validation in larger perfusion systems would strengthen confidence in the predictive power of small-scale models and support their application in industrial process development.

Comparisons with the literature data on spin tubes and perfusion bioreactors with the presented cell bleed strategies in MWP and DWP formats showed promising alignment. However, differences in cell lines and medium compositions between studies limit direct comparability. Furthermore, the implementation of CSPR-based perfusion control and its combination with cell bleeding warrants longer-term cultivation studies. Such experiments would enable evaluation of "quasi steady-state" hypotheses and the scalability of key culture parameters, including metabolite concentrations. This is particularly relevant for lactate, which is known to accumulate in scale-down models and often does not scale linearly with bioreactor processes. Furthermore, long-term studies would allow the alignment and verification of MWP data for specific phases of a perfusion bioreactor from the exponential growth phase to the intended steady-state production phase.

To further enhance and refine the methodology, integration of real-time or at-line sensors for parameters such as biomass, key metabolites (e.g., glucose, lactate), pH, and DO should be considered. These tools could support more precise control strategies, facilitate early detection of culture stress, and provide richer datasets for clone and process evaluation. Miniaturised sensor technologies or non-invasive spectroscopic approaches may be particularly well suited to the well plate format. These could fit well together with the industrial vision of using all available data for decision making, thus generating as much data as early as possible in the process development chain is of great interest. This aligns with drivers to include machine learning approaches to model and predict process or clone performance across scales using multiparametric data, including manufacturability metrics. Looking ahead, the methodology could also be extended to explore the application to other host cell lines such as HEK293 for viral vector production and product type such as difficult-to-express molecules will be important to assess broader applicability. This includes the evaluation of cell lines producing more complex molecules or those used in emerging therapeutic areas such as gene and cell therapy.

The expansion of the semi-perfusion methodology to include additional data measurements is a critical next step for increasing its robustness and industrial relevance. Equally important is the automation of the workflow. Implementing a liquid handling system for medium exchange would not only enhance throughput but also reduce operator variability, making the approach more suitable for high-throughput screening applications.

To generate initial comparative data and assess feasibility, this thesis explored partial medium exchange strategies and the miniaturisation of the workflow to 96-well DWP. As this plate format is already established as the industry standard for fed-batch operations, this transition offers the advantage of leveraging existing hardware and operator expertise. Adapting the semi-perfusion

workflow to this format could therefore accelerate its adoption and integration into current development pipelines.

With a specific focus on cell clone screening as the primary application, scalability to bench-top scale perfusion bioreactors and the investigation of production-relevant conditions remain critical considerations in evaluating any high-throughput screening model. While this study demonstrated good agreement in cell clone screening trends across the 96-well and 24-well formats, it was limited to two small panels of clones due to manual handling constraints. Therefore, further validation using larger clone panels and screening in more representative perfusion systems—such as the ambr®250 or benchtop bioreactors—is necessary. These expanded studies would provide crucial insights into long-term culture stability and productivity under continuous operation, thereby enhancing the predictive power and industrial relevance of small-scale screening platforms.

The manufacturability index further developed and applied in this work proved to be a more holistic and reliable ranking metric, particularly under semi-perfusion conditions. Future studies should aim to refine this index by incorporating additional process-relevant parameters comprising online and off-line data as development advances. Moreover, there is significant potential to leverage machine learning techniques to analyse these multi-parametric datasets. Such models could facilitate early prediction of clone performance and accelerate cell line selection, thereby further streamlining the overall development workflow.

In summary, the findings presented in this thesis lay a strong foundation for the development of miniaturised, high-throughput semi-perfusion screening platforms. Continued methodological refinement, automation, and data integration could significantly enhance early-stage cell line development and better align it with the demands of modern biomanufacturing strategies.

Chapter 9: Research Impact and Implementation

9.1 Introduction

This chapter covers the academic, economic or societal impact of the research presented in this thesis. For Engineering Doctorate (EngD) candidate, such reflections are essential as EngD projects are designed based on industry priorities and practical applications. This EPSRC-funded project was conducted within the AstraZeneca–UCL Centre of Excellence (AZ–UCL CoE), an initiative focused on enhancing predictability and efficiency in biopharmaceutical manufacturing. The Centre leverages high-throughput experimentation, data analytics, and process economics to identify opportunities for improving process performance and decision-making across the development lifecycle.

One of the key challenges currently faced by AstraZeneca and the broader biopharmaceutical industry is the transition from traditional batch-based manufacturing towards integrated continuous biomanufacturing (ICB). Continuous processes have the potential to offer significantly higher productivity, improved product quality, enhanced process robustness, and superior economic and environmental sustainability when compared to fed-batch operations. A fully integrated continuous process requires the upstream and downstream operations to be connected in a seamless, uninterrupted flow. For upstream processes, this typically involves the use of perfusion bioreactors, where fresh medium is continuously supplied while waste and product are removed at a steady rate.

Despite its advantages and growing interest over the past decade, the widespread adoption of continuous biomanufacturing is hindered by several persistent challenges. Perfusion operations—while conceptually well-established since the 1990s for labile biologics—pose practical issues such as increased medium consumption and greater process complexity. A critical bottleneck remains the lengthy development timeline for both product and process development, often extending 10 to 15 years. The absence of scalable, high-throughput, and automatable scale-down models that are essential for the rapid optimisation of perfusion processes contribute to this bottleneck.

This thesis directly addresses that gap by advancing a well plate–based scale-down platform designed to mimic key features of perfusion while being compatible with both automation and miniaturisation. The platform supports semi-perfusion operation at high cell densities, with stable, "quasi–steady-state" conditions maintained through controlled bleed and medium exchange strategies. This approach significantly accelerates early-stage process development and enables more efficient, data-rich experimentation—critical factors in the industrial push toward continuous biomanufacturing.

Furthermore, the work contributes to advancing methodologies for cell line and clone screening, a foundational activity in upstream development. While fed-batch remains the gold standard in this space, it is poorly suited to identifying clones optimised for perfusion-based manufacturing. This thesis investigates how operational mode influences clone performance and ranking, offering new insights into aligning early screening strategies with the needs for intensified processes.

In the following sections the relevant scientific, industrial, and societal impacts of this work are discussed in greater detail, outlining how this research contributes to shaping the future of bioprocess development and manufacturing.

9.2 Scientific and academic impact

The research conducted in this thesis builds upon previous work to develop a well-plate-based scale-down model (SDM) capable of mimicking perfusion processes for automated, high-throughput screening applications. Building on that foundation, this study advances the semi-perfusion methodology in 24-well MWP by integrating a cell bleed strategy and systematically exploring perfusion rate strategies commonly employed in large-scale bioreactors. Using a semi-perfusion approach—comprising daily medium exchange, centrifugation-based cell retention, and controlled cell bleed—this platform supports the cultivation of stable, high-density cultures over extended time periods, achieving "quasi steady-state" operation.

This capability significantly expands the utility of the platform for early-stage process development, enabling the systematic screening of critical process parameters, such as medium exchange volume and bleed rate. These features are essential for the rational selection of operational conditions suitable for scale-up and continuous manufacturing. By providing an automatable and miniaturised alternative to traditional benchtop bioreactors, shake flasks, or spin tubes—which are often resource-intensive and incompatible with high-throughput workflows—this platform fills a critical gap in upstream process development.

To demonstrate its practical applicability, the semi-perfusion methodology was applied to a use case focused on cell clone screening. Two panels of antibody-producing CHO cell clones were

evaluated and ranked under both semi-perfusion and fed-batch conditions using well plate formats. The fed-batch approach was adapted from established literature. This comparative study challenges the conventional use of fed-batch operations during early clone selection, revealing that operational mode strongly influences clone performance and ranking outcomes—and may even lead to the exclusion of clones better suited for perfusion processes.

Overall, this work addresses the limited understanding of the MWP platform's ability to replicate perfusion-like conditions at low working volumes. It confirms the feasibility of achieving high cell densities, implementing cell bleed strategies, and exploring perfusion rates in a scalable, automatable format. Furthermore, by assessing how operational differences affect early-stage clone selection, this study highlights limitations of fed-batch-based screening and positions the semi-perfusion SDM as a more representative alternative for perfusion-focused development. The incorporation of the manufacturability index (MI_{CL}) further enhances the robustness of clone ranking by incorporating multiple performance criteria, ultimately offering new insights into optimising cell line development for intensified and continuous biomanufacturing.

In addition to the core research work, this EngD project encompassed a wide range of academic activities including conference participation, oral and poster presentations, and knowledge dissemination, all of which contributed to strengthening academic–industry collaboration. The scientific outputs of this research have found strong resonance within the bioprocessing community and were presented at several high-impact conferences, including Integrated Continuous Biomanufacturing (ICB) Conferences V and VI, ESACT Frontiers, Single-Use Technology (SUT) Conference VII, and the 7th High Throughput Process Development (HTPD) meeting. Presentations at these fora enabled direct engagement with leading researchers and practitioners in the field of intensified biomanufacturing.

The research has also been shared through multiple internal presentations at UCL and AstraZeneca, ensuring effective knowledge transfer to relevant stakeholders across academia and industry.

Importantly, the outcomes of this project were disseminated through three peer-reviewed, open-access publications, enhancing accessibility and impact. Two of these publications focus on the development and characterisation of the MWP platform for semi-perfusion operation, while the third presents the application of the platform for cell clone screening and the implementation of a multi-parameter clone ranking strategy. Additional manuscripts are currently in preparation to further expand on the platform's capabilities and applications.

Beyond formal publications, the research has sparked ongoing dialogue with industry professionals, particularly around the challenges and opportunities identified in the published

work. These conversations have led to discussions on potential future directions, including integration of sensors technologies and data-rich monitoring tools including additional offline assays to support robust process control and to enable comprehensive process understanding through the application of big data and predictive analytics.

9.3 Industrial Relevance and Application

This research delivers a platform that directly addresses several unmet needs in the biopharmaceutical industry, particularly in the context of process intensification and the transition toward continuous biomanufacturing. The in-depth characterisation of the MWP platform using a semi-perfusion methodology builds confidence in its robustness and repeatability, establishing it as a reliable tool for early-stage process development.

By demonstrating the feasibility of operating well plates under "quasi–steady-state" conditions—achieved through controlled medium exchange and cell bleed strategies—this work introduces a practical, miniaturised alternative to conventional fed-batch clone screening. This is particularly significant given the current industry reliance on fed-batch approaches during early cell line development (CLD), which may not capture the performance potential of clones under perfusion-like conditions.

The research also integrates a manufacturability index (MI_{CL}) into the screening workflow, enabling multi-criteria assessment of clones and refining selection based not only on productivity but also on operational suitability. This offers a more strategic approach to clone selection aligned with continuous biomanufacturing goals, supporting improved scalability, robustness, and overall efficiency in process optimisation.

Although the current semi-perfusion set-up in well plates involves manual handling, efforts are underway to automate the workflow. To support this transition, experimental work included the evaluation of partial medium exchanges in low-volume formats, particularly in the 24-well MWP. For application in cell clone screening, proof-of-concept studies were extended to a 96-well DWP format to leverage existing automation infrastructure, thereby facilitating faster adoption within industrial settings. This adaptation improves compatibility with automated liquid handling systems and aligns with broader trends in the digitalisation of bioprocess laboratories.

The ability to simultaneously assess multiple process parameters using miniaturised volumes offers considerable time and cost advantages. These efficiencies are particularly valuable to cell line development (CLD) teams aiming to accelerate development timelines, reduce material consumption, and make more informed early-stage decisions regarding clone selection under manufacturing-relevant conditions.

The practical value of this platform is already evident. The semi-perfusion methodology and clone screening strategy are in the process of being tech-transferred to AstraZeneca sites in both the UK and US, where efforts toward full automation are underway. Industry engagement has highlighted the platform's relevance for improving early decision-making, particularly by demonstrating the influence of operation mode, perfusion intensity, and ranking strategy on clone selection outcomes. This is encouraging a shift toward adopting manufacturing-representative conditions earlier in development pipelines, supporting more predictive and streamlined workflows.

9.4 Broader Impact and Societal Implications

The development of a miniaturised, scalable, and automation-compatible platform for semi-perfusion culture has implications that extend beyond technical innovation in bioprocess development to societal and economic impact. By enabling earlier and more representative screening of cell clones and process parameters, this research contributes to more efficient and predictable manufacturing of biologics—ultimately supporting faster development of therapeutic products.

Accelerating early-stage process development can significantly shorten the timeline for bringing new biopharmaceuticals to clinical trials and, ultimately, to market. This not only enhances patient access to critical therapies but also reduces the cost of goods by enabling the selection of high-productivity clones tailored to the intended manufacturing process. Lower production costs can translate into more affordable commercial therapeutics, particularly in areas with high unmet medical need. Additionally, by miniaturising experimental formats and enabling high-throughput experimentation, the platform reduces resource consumption—including media, consumables, and lab space—thereby contributing to a smaller environmental footprint. This aligns with the growing emphasis on sustainable manufacturing practices in biopharmaceutical development.

The platform's compatibility with automation and digital tools also supports broader trends in smart process development, smart manufacturing and Industry 4.0. As data-driven decision-making becomes integral to biopharmaceutical development, tools that generate rich, reproducible datasets early in the development lifecycle can facilitate better process understanding, enhance regulatory confidence, and contribute to the creation of more robust and flexible production systems.

Finally, increased accessibility to high-density, perfusion-mimicking screening tools in well-plate format can help democratise advanced bioprocessing techniques. Even in a manual setup, these platforms offer cost advantages by reducing consumable use, medium consumption, and overall resource demands. This makes them especially valuable for smaller biotech companies and academic laboratories, providing a low-cost entry point into continuous biomanufacturing research and innovation.

References

Altamirano, C., Berrios, J., Vergara, M., & Becerra, S. (2013). Advances in improving mammalian cells metabolism for recombinant protein production. *Electronic Journal of Biotechnology*, *16*(3). https://doi.org/ARTN 2 10.2225/vol16-issue3-fulltext-2

Altamirano, C., Illanes, A., Casablancas, A., Gamez, X., Cairo, J. J., & Godia, C. (2001). Analysis of CHO cells metabolic redistribution in a glutamate-based defined medium in continuous culture. *Biotechnol Prog*, *17*(6), 1032–1041. https://doi.org/10.1021/bp0100981

Altamirano, C., Paredes, C., Cairo, J. J., & Godia, F. (2000). Improvement of CHO cell culture medium formulation: Simultaneous substitution of glucose and glutamine. *Biotechnol Prog*, *16*(1), 69–75. https://doi.org/10.1021/bp990124j

Altamirano, C., Paredes, C., Illanes, A., Cairó, J. J., & Gòdia, F. (2004). Strategies for fed-batch cultivation of t-PA producing CHO cells: Substitution of glucose and glutamine and rational design of culture medium. *Journal of Biotechnology*, *110*(2), 171–179. https://doi.org/10.1016/j.jbiotec.2004.02.004

Arnold, L., Lee, K., Rucker-Pezzini, J., & Lee, J. H. (2019). Implementation of Fully Integrated Continuous Antibody Processing: Effects on Productivity and COGm. *Biotechnol J*, *14*(2), e1800061. https://doi.org/10.1002/biot.201800061

Bausch, M., Schultheiss, C., & Sieck, J. B. (2019). Recommendations for Comparison of Productivity Between Fed-Batch and Perfusion Processes. *Biotechnology Journal*, *14*(2), 1700721. https://doi.org/10.1002/biot.201700721

Betts, J. I., & Baganz, F. (2006). Miniature bioreactors: Current practices and future opportunities. *Microb Cell Fact*, *5*(1), 21. https://doi.org/10.1186/1475-2859-5-21

Bielser, J. M., Domaradzki, J., Souquet, J., Broly, H., & Morbidelli, M. (2019). Semi-continuous scale-down models for clone and operating parameter screening in perfusion bioreactors. *Biotechnol Prog*, *35*(3), e2790. https://doi.org/10.1002/btpr.2790

Bielser, J. M., Wolf, M., Souquet, J., Broly, H., & Morbidelli, M. (2018). Perfusion mammalian cell culture for recombinant protein manufacturing—A critical review. *Biotechnol Adv*, *36*(4), 1328–1340. https://doi.org/10.1016/j.biotechadv.2018.04.011

Bielser, J.-M. (2019). *Development of perfusion cell culture processes for the manufacturing of therapeutic recombinant proteins*. https://www.research-

collection.ethz.ch/bitstream/handle/20.500.11850/368475/JBSthesis.pdf?isAllowed=y&sequence=1

Bielser, J.-M., Chappuis, L., Xiao, Y., Souquet, J., Broly, H., & Morbidelli, M. (2019). Perfusion cell culture for the production of conjugated recombinant fusion proteins reduces clipping and quality heterogeneity compared to batch-mode processes. *Journal of Biotechnology*, *302*, 26–31. https://doi.org/10.1016/j.jbiotec.2019.06.006

Caso, S., Aeby, M., Jordan, M., Guillot, R., & Bielser, J.-M. (2022). Effects of pyruvate on primary metabolism and product quality for a high-density perfusion process. *Biotechnology and Bioengineering*, *119*(4), 1053–1061. https://doi.org/10.1002/bit.28033

Charalambidou, A.-D., Wyrobnik, T. A., Micheletti, M., & Ducci, A. (2024). Investigation of the impact of probes and internals on power and flow in stirred tank reactors. *Chemical Engineering Science*, *286*, 119683. https://doi.org/10.1016/j.ces.2023.119683

Chatterjee, S. (2012). *FDA Perspective on Continuous Manufacturing*. https://gmpua.com/Process/ContinuousManufacturing/ContinuousManufacturing.pdf

Chen, C., Le, K., Le, H., Daris, K., Soice, N., Stevens, J., & Goudar, C. T. (2020). Methods for Estimating the Probability of Clonality in Cell Line Development. *Biotechnology Journal*, *15*(2), 1900289. https://doi.org/10.1002/biot.201900289

Chen, C., Wong, H. E., & Goudar, C. T. (2018). Upstream process intensification and continuous manufacturing. *Current Opinion in Chemical Engineering*, *22*, 191–198. https://doi.org/10.1016/j.coche.2018.10.006

Chen, Y. J., Yang, O., Sampat, C., Bhalode, P., Ramachandran, R., & Ierapetritou, M. (2020). Digital Twins in Pharmaceutical and Biopharmaceutical Manufacturing: A Literature Review. *Processes*, *8*(9), 1088–1088. https://doi.org/ARTN 1088 10.3390/pr8091088

Chong, L., Saghafi, M., Knappe, C., Steigmiller, S., Matanguihan, C., & Goudar, C. T. (2013). Robust on-line sampling and analysis during long-term perfusion cultivation of mammalian cells. *Journal of Biotechnology*, *165*(2), 133–137. https://doi.org/10.1016/j.jbiotec.2013.03.008

Chong, Z. X., Yeap, S. K., & Ho, W. Y. (2021). Transfection types, methods and strategies: A technical review. *PeerJ*, *9*(e11165), e11165. https://doi.org/10.7717/peerj.11165

Chotteau, V. (2015). Perfusion Processes. In M. Al-Rubeai (Ed.), *Animal Cell Culture* (pp. 407–443). Springer International Publishing. https://doi.org/10.1007/978-3-319-10320-4_13

Chotteau, V., Schwarz, H., & Mäkinen, M. (2023). Continuous Bioprocessing for Upstream Process: Perfusion Process. In R. Pörtner (Ed.), *Biopharmaceutical Manufacturing: Progress, Trends and Challenges* (pp. 113–158). Springer International Publishing. https://doi.org/10.1007/978-3-031-45669-5_4

Clincke, M. F., Molleryd, C., Samani, P. K., Lindskog, E., Faldt, E., Walsh, K., & Chotteau, V. (2013). Very high density of Chinese hamster ovary cells in perfusion by alternating tangential flow or tangential flow filtration in WAVE Bioreactor-part II: Applications for antibody

production and cryopreservation. *Biotechnol Prog*, *29*(3), 768–777. https://doi.org/10.1002/btpr.1703

Clincke, M. F., Molleryd, C., Zhang, Y., Lindskog, E., Walsh, K., & Chotteau, V. (2013). Very high density of CHO cells in perfusion by ATF or TFF in WAVE bioreactor. Part I. Effect of the cell density on the process. *Biotechnol Prog*, *29*(3), 754–767. https://doi.org/10.1002/btpr.1704

Coffman, J., Brower, M., Connell-Crowley, L., Deldari, S., Farid, S. S., Horowski, B., Patil, U., Pollard, D., Qadan, M., Rose, S., Schaefer, E., & Shultz, J. (2021). A common framework for integrated and continuous biomanufacturing. *Biotechnol Bioeng*, *118*(4), 1721–1735. https://doi.org/10.1002/bit.27690

Coolbaugh, M. J., Varner, C. T., Vetter, T. A., Davenport, E. K., Bouchard, B., Fiadeiro, M., Tugcu, N., Walther, J., Patil, R., & Brower, K. (2021). Pilot-scale demonstration of an end-to-end integrated and continuous biomanufacturing process. *Biotechnol Bioeng*, *118*(9), 3287–3301. https://doi.org/10.1002/bit.27670

Coulet, M., Kepp, O., Kroemer, G., & Basmaciogullari, S. (2022). Metabolic Profiling of CHO Cells during the Production of Biotherapeutics. *Cells*, *11*(12), 1929. https://doi.org/10.3390/cells11121929

Crescioli, S., Kaplon, H., Chenoweth, A., Wang, L., Visweswaraiah, J., & Reichert, J. M. (2024). Antibodies to watch in 2024. *mAbs*, *16*(1), 2297450. https://doi.org/10.1080/19420862.2023.2297450

Croughan, M. S., Konstantinov, K. B., & Cooney, C. (2015). The future of industrial bioprocessing: Batch or continuous? *Biotechnol Bioeng*, *112*(4), 648–651. https://doi.org/10.1002/bit.25529

Dorai, H., Kyung, Y. S., Ellis, D., Kinney, C., Lin, C., Jan, D., Moore, G., & Betenbaugh, M. J. (2009). Expression of anti-apoptosis genes alters lactate metabolism of Chinese Hamster Ovary cells in culture. *Biotechnology and Bioengineering*, *103*(3), 592–608. https://doi.org/10.1002/bit.22269

Dorn, M., Klottrup-Rees, K., Lee, K., & Micheletti, M. (2024). Platform development for high-throughput optimization of perfusion processes—Part I: Implementation of cell bleeds in microwell plates. *Biotechnology and Bioengineering*, *121*(6), 1759–1773. https://doi.org/10.1002/bit.28682

Dorn, M., Lucas, C., Klottrup-Rees, K., Lee, K., & Micheletti, M. (2024). Platform development for high-throughput optimization of perfusion processes—Part II: Variation of perfusion rate strategies in microwell plates. *Biotechnology and Bioengineering*, *121*(6), 1774–1788. https://doi.org/10.1002/bit.28685

Dowd, J. E., Jubb, A., Kwok, K. E., & Piret, J. M. (2003). Optimization and control of perfusion cultures using a viable cell probe and cell specific perfusion rates. *Cytotechnology*, *42*(1), 35–45. https://doi.org/10.1023/A:1026192228471

Drobnjakovic, M., Hart, R., Kulvatunyou, B. (Serm), Ivezic, N., & Srinivasan, V. (2023). Current challenges and recent advances on the path towards continuous biomanufacturing. *Biotechnology Progress*, *39*(6), e3378. https://doi.org/10.1002/btpr.3378

Ducommun, P., Ruffieux, P. A., Kadouri, A., Von Stockar, U., & Marison, I. W. (2002). Monitoring of temperature effects on animal cell metabolism in a packed bed process. *Biotechnology and Bioengineering*, *77*(7), 838–842. https://doi.org/10.1002/bit.10185

Duetz, W. A., Rüedi, L., Hermann, R., O'Connor, K., Büchs, J., & Witholt, B. (2000). Methods for Intense Aeration, Growth, Storage, and Replication of Bacterial Strains in Microtiter Plates. *Applied and Environmental Microbiology*, *66*(6), 2641–2646. https://doi.org/10.1128/aem.66.6.2641-2646.2000

Farid, S. S., Baron, M., Stamatis, C., Nie, W., & Coffman, J. (2020). Benchmarking biopharmaceutical process development and manufacturing cost contributions to R&D. *mAbs*, *12*(1), 1754999. https://doi.org/10.1080/19420862.2020.1754999

Fisher, A. C., Kamga, M. H., Agarabi, C., Brorson, K., Lee, S. L., & Yoon, S. (2019). The Current Scientific and Regulatory Landscape in Advancing Integrated Continuous Biopharmaceutical Manufacturing. *Trends Biotechnol*, *37*(3), 253–267. https://doi.org/10.1016/j.tibtech.2018.08.008

Frye, C., Deshpande, R., Estes, S., Francissen, K., Joly, J., Lubiniecki, A., Munro, T., Russell, R., Wang, T., & Anderson, K. (2016). Industry view on the relative importance of "clonality" of biopharmaceutical-producing cell lines. *Biologicals*, *44*(2), 117–122. https://doi.org/10.1016/j.biologicals.2016.01.001

Fu, T., Zhang, C., Jing, Y., Jiang, C., Li, Z., Wang, S., Ma, K., Zhang, D., Hou, S., Dai, J., Kou, G., & Wang, H. (2016). Regulation of cell growth and apoptosis through lactate dehydrogenase C over-expression in Chinese hamster ovary cells. *Appl Microbiol Biotechnol*, *100*(11), 5007–5016. https://doi.org/10.1007/s00253-016-7348-4

Gagliardi, T. M., Chelikani, R., Yang, Y., Tuozzolo, G., & Yuan, H. (2019). Development of a novel, high-throughput screening tool for efficient perfusion-based cell culture process development. *Biotechnol Prog*, *35*(4), e2811. https://doi.org/10.1002/btpr.2811

Gagnon, M., Nagre, S., Wang, W., & Hiller, G. W. (2018). Shift to high-intensity, low-volume perfusion cell culture enabling a continuous, integrated bioprocess. *Biotechnol Prog*, *34*(6), 1472–1481. https://doi.org/10.1002/btpr.2723

Genzel, Y. (2015). Designing cell lines for viral vaccine production: Where do we stand? *Biotechnol J*, *10*(5), 728–740. https://doi.org/10.1002/biot.201400388

Godawat, R., Konstantinov, K., Rohani, M., & Warikoo, V. (2015). End-to-end integrated fully continuous production of recombinant monoclonal antibodies. *Journal of Biotechnology*, *213*, 13–19. https://doi.org/10.1016/j.jbiotec.2015.06.393

Goldrick, S., Alosert, H., Lovelady, C., Bond, N. J., Senussi, T., Hatton, D., Klein, J., Cheeks, M., Turner, R., Savery, J., & Farid, S. S. (2023). Next-generation cell line selection methodology

leveraging data lakes, natural language generation and advanced data analytics. *Frontiers in Bioengineering and Biotechnology*, *11*. https://doi.org/10.3389/fbioe.2023.1160223

Gomez, N., Ambhaikar, M., Zhang, L., Huang, C. J., Barkhordarian, H., Lull, J., & Gutierrez, C. (2017). Analysis of Tubespins as a suitable scale-down model of bioreactors for high cell density CHO cell culture. *Biotechnol Prog*, *33*(2), 490–499. https://doi.org/10.1002/btpr.2418

Gomez, N., Barkhordarian, H., Lull, J., Huh, J., GhattyVenkataKrishna, P., & Zhang, X. (2019). Perfusion CHO cell culture applied to lower aggregation and increase volumetric productivity for a bispecific recombinant protein. *Journal of Biotechnology*, *304*, 70–77. https://doi.org/10.1016/j.jbiotec.2019.08.001

Goudar, C., Biener, R., Boisart, C., Heidemann, R., Piret, J., de Graaf, A., & Konstantinov, K. (2010). Metabolic flux analysis of CHO cells in perfusion culture by metabolite balancing and 2D [13C, 1H] COSY NMR spectroscopy. *Metabolic Engineering*, *12*(2), 138–149. https://doi.org/10.1016/j.ymben.2009.10.007

Granicher, G., Coronel, J., Trampler, F., Jordan, I., Genzel, Y., & Reichl, U. (2020). Performance of an acoustic settler versus a hollow fiber-based ATF technology for influenza virus production in perfusion. *Appl Microbiol Biotechnol*, *104*(11), 4877–4888. https://doi.org/10.1007/s00253-020-10596-x

Granicher, G., Tapia, F., Behrendt, I., Jordan, I., Genzel, Y., & Reichl, U. (2021). Production of Modified Vaccinia Ankara Virus by Intensified Cell Cultures: A Comparison of Platform Technologies for Viral Vector Production. *Biotechnol J*, *16*(1), e2000024. https://doi.org/10.1002/biot.202000024

Hansen, H. A., & Emborg, C. (1994). Influence of ammonium on growth, metabolism, and productivity of a continuous suspension Chinese hamster ovary cell culture. *Biotechnology Progress*, *10*(1), 121–124. https://doi.org/10.1021/bp00025a014

Hassell, T., Gleave, S., & Butler, M. (1991). Growth inhibition in animal cell culture. *Applied Biochemistry and Biotechnology*, *30*(1), 29–41. https://doi.org/10.1007/bf02922022

Hein, M. D., Chawla, A., Cattaneo, M., Kupke, S. Y., Genzel, Y., & Reichl, U. (2021). Cell culture–based production of defective interfering influenza A virus particles in perfusion mode using an alternating tangential flow filtration system. *Applied Microbiology and Biotechnology*, *105*(19), 7251–7264. https://doi.org/10.1007/s00253-021-11561-y

Hong, J. K., Lakshmanan, M., Goudar, C., & Lee, D.-Y. (2018). Towards next generation CHO cell line development and engineering by systems approaches. *Current Opinion in Chemical Engineering*, *22*, 1–10. https://doi.org/10.1016/j.coche.2018.08.002

Hosseini, S. S., Khalili, S., Baradaran, B., Bidar, N., Shahbazi, M.-A., Mosafer, J., Hashemzaei, M., Mokhtarzadeh, A., & Hamblin, M. R. (2021). Bispecific monoclonal antibodies for targeted immunotherapy of solid tumors: Recent advances and clinical trials. *International Journal of Biological Macromolecules*, *167*, 1030–1047. https://doi.org/10.1016/j.ijbiomac.2020.11.058

Janoschek, S., Schulze, M., Zijlstra, G., Greller, G., & Matuszczyk, J. (2019). A protocol to transfer a fed-batch platform process into semi-perfusion mode: The benefit of automated small-scale bioreactors compared to shake flasks as scale-down model. *Biotechnol Prog*, *35*(2), e2757. https://doi.org/10.1002/btpr.2757

Jarasch, A., Koll, H., Regula, J. T., Bader, M., Papadimitriou, A., & Kettenberger, H. (2015). Developability assessment during the selection of novel therapeutic antibodies. *J Pharm Sci*, *104*(6), 1885–1898. https://doi.org/10.1002/jps.24430

Jin, L., Wang, Z. S., Cao, Y., Sun, R. Q., Zhou, H., & Cao, R. Y. (2021). Establishment and optimization of a high-throughput mimic perfusion model in ambr((R)) 15. *Biotechnol Lett*, *43*(2), 423–433. https://doi.org/10.1007/s10529-020-03026-5

Karst, D. J., Scibona, E., Serra, E., Bielser, J.-M., Souquet, J., Stettler, M., Broly, H., Soos, M., Morbidelli, M., & Villiger, T. K. (2017). Modulation and modeling of monoclonal antibody N-linked glycosylation in mammalian cell perfusion reactors. *Biotechnology and Bioengineering*, *114*(9), 1978–1990. https://doi.org/10.1002/bit.26315

Karst, D. J., Steinebach, F., Soos, M., & Morbidelli, M. (2017). Process performance and product quality in an integrated continuous antibody production process. *Biotechnol Bioeng*, *114*(2), 298–307. https://doi.org/10.1002/bit.26069

Kaur, R., Jain, R., Budholiya, N., & Rathore, A. S. (2023). Long term culturing of CHO cells: Phenotypic drift and quality attributes of the expressed monoclonal antibody. *Biotechnology Letters*, *45*(3), 357–370. https://doi.org/10.1007/s10529-023-03346-2

Kim, B. J., Diao, J., & Shuler, M. L. (2012). Mini-scale bioprocessing systems for highly parallel animal cell cultures. *Biotechnology Progress*, *28*(3), 595–607. https://doi.org/10.1002/btpr.1554

Kim, T. K., & Eberwine, J. H. (2010). Mammalian cell transfection: The present and the future. *Anal Bioanal Chem*, *397*(8), 3173–3178. https://doi.org/10.1007/s00216-010-3821-6

Konstantinov, K., Goudar, C., Ng, M., Meneses, R., Thrift, J., Chuppa, S., Matanguihan, C., Michaels, J., & Naveh, D. (2006). The 'push-to-low' approach for optimization of high-density perfusion cultures of animal cells. *Adv Biochem Eng Biotechnol*, *101*, 75–98. https://doi.org/10.1007/10_016

Kreye, S., Stahn, R., Nawrath, K., Goralczyk, V., Zoro, B., & Goletz, S. (2019). A novel scale-down mimic of perfusion cell culture using sedimentation in an automated microbioreactor (SAM). *Biotechnol Prog*, *35*(5), e2832. https://doi.org/10.1002/btpr.2832

Labrijn, A. F., Janmaat, M. L., Reichert, J. M., & Parren, P. W. H. I. (2019). Bispecific antibodies: A mechanistic review of the pipeline. *Nature Reviews Drug Discovery*, *18*(8), 585–608. https://doi.org/10.1038/s41573-019-0028-1

Lao, M. S., & Toth, D. (1997). Effects of Ammonium and Lactate on Growth and Metabolism of a Recombinant Chinese Hamster Ovary Cell Culture. *Biotechnology Progress*, *13*(5), 688–691. https://doi.org/10.1021/bp9602360

Leong, J., Tang, W. Q., Chng, J., Ler, W. X., Manan, N. A., Sim, L. C., Zheng, Z. Y., Zhang, W., Walsh, I., Zijlstra, G., Pennings, M., & Ng, S. K. (2024). Biomass specific perfusion rate as a control lever for the continuous manufacturing of biosimilar monoclonal antibodies from CHO cell cultures. *Biotechnology Journal*, *19*(7), 2400092. https://doi.org/10.1002/biot.202400092

Li, F., Vijayasankaran, N., Shen, A. (Yijuan), Kiss, R., & Amanullah, A. (2010). Cell culture processes for monoclonal antibody production. *mAbs*, *2*(5), 466–477. https://doi.org/10.4161/mabs.2.5.12720

Li, J., Wong, C. L., Vijayasankaran, N., Hudson, T., & Amanullah, A. (2012). Feeding lactate for CHO cell culture processes: Impact on culture metabolism and performance. *Biotechnol Bioeng*, *109*(5), 1173–1186. https://doi.org/10.1002/bit.24389

Lin, H., Leighty, R. W., Godfrey, S., & Wang, S. B. (2017). Principles and approach to developing mammalian cell culture media for high cell density perfusion process leveraging established fed-batch media. *Biotechnology Progress*, *33*(4), 891–901. https://doi.org/10.1002/btpr.2472

Lin, P.-C., Chan, K. F., Kiess, I. A., Tan, J., Shahreel, W., Wong, S.-Y., & Song, Z. (2019). Attenuated glutamine synthetase as a selection marker in CHO cells to efficiently isolate highly productive stable cells for the production of antibodies and other biologics. *mAbs*, *11*(5), 965–976. https://doi.org/10.1080/19420862.2019.1612690

Lucas, C., Blackman, M., Rayat, A., Mainwaring, D., & Micheletti, M. (2024). Two scale-down tools for the optimization of perfusion bioreactors for the manufacture of biopharmaceuticals. *Journal of Advanced Manufacturing and Processing*, *n/a*(n/a), e10180. https://doi.org/10.1002/amp2.10180

Luo, Y., Kurian, V., & Ogunnaike, B. A. (2021). Bioprocess systems analysis, modeling, estimation, and control. *Current Opinion in Chemical Engineering*, *33*, 100705–100705. https://doi.org/ARTN 100705 10.1016/j.coche.2021.100705

Mahal, H., Branton, H., & Farid, S. S. (2021). End-to-end continuous bioprocessing: Impact on facility design, cost of goods, and cost of development for monoclonal antibodies. *Biotechnol Bioeng*, *118*(9), 3468–3485. https://doi.org/10.1002/bit.27774

Malm, M., Saghaleyni, R., Lundqvist, M., Giudici, M., Chotteau, V., Field, R., Varley, P. G., Hatton, D., Grassi, L., Svensson, T., Nielsen, J., & Rockberg, J. (2020). Evolution from adherent to suspension: Systems biology of HEK293 cell line development. *Sci Rep*, *10*(1), 18996. https://doi.org/10.1038/s41598-020-76137-8

Markert, S., Musmann, C., Hülsmann, P., & Joeris, K. (2019). Automated and enhanced clone screening using a fully automated microtiter plate-based system for suspension cell culture. *Biotechnology Progress*, *35*(2), e2760. https://doi.org/10.1002/btpr.2760

Martinelle, K., & Häggström, L. (1993). Mechanisms of ammonia and ammonium ion toxicity in animal cells: Transport across cell membranes. *Journal of Biotechnology*, *30*(3), 339–350. https://doi.org/10.1016/0168-1656(93)90148-G

Mayrhofer, P., Castan, A., & Kunert, R. (2021). Shake tube perfusion cell cultures are suitable tools for the prediction of limiting substrate, CSPR, bleeding strategy, growth and productivity behavior. *Journal of Chemical Technology & Biotechnology*, *96*(10), 2930–2939. https://doi.org/10.1002/jctb.6848

Mertz, L. (2021). *New Vaccine-Manufacturing Methods Are Moving Away From the Egg*.

Mordor, I. (2024). *Biopharmaceuticals Industry | Market Growth, Overview, Size*.

Moreira, A. S., Silva, A. C., Sousa, M. F. Q., Hagner-McWhirterc, A., Ahlenc, G., Lundgren, M., Coroadinha, A. S., Alves, P. M., Peixoto, C., & Carrondo, M. J. T. (2020). Establishing Suspension Cell Cultures for Improved Manufacturing of Oncolytic Adenovirus. *Biotechnol J*, *15*(4), e1900411. https://doi.org/10.1002/biot.201900411

Moses, S., Manahan, M., Ambrogelly, A., & Ling, W. L. W. (2012). Assessment of AMBRTM as a model for high-throughput cell culture process development strategy. *Advances in Bioscience and Biotechnology*, *3*(7), Article 7. https://doi.org/10.4236/abb.2012.37113

Müller, D., Klein, L., Lemke, J., Schulze, M., Kruse, T., Saballus, M., Matuszczyk, J., Kampmann, M., & Zijlstra, G. (2022). Process intensification in the biopharma industry: Improving efficiency of protein manufacturing processes from development to production scale using synergistic approaches. *Chemical Engineering and Processing - Process Intensification*, *171*, 108727. https://doi.org/10.1016/j.cep.2021.108727

Mulukutla, B. C., Gramer, M., & Hu, W. S. (2012). On metabolic shift to lactate consumption in fed-batch culture of mammalian cells. *Metab Eng*, *14*(2), 138–149. https://doi.org/10.1016/j.ymben.2011.12.006

Munro, T. P., Le, K., Le, H., Zhang, L., Stevens, J., Soice, N., Benchaar, S. A., Hong, R. W., & Goudar, C. T. (2017). Accelerating patient access to novel biologics using stable pool-derived product for non-clinical studies and single clone-derived product for clinical studies. *Biotechnology Progress*, *33*(6), 1476–1482. https://doi.org/10.1002/btpr.2572

Narayanan, H., Sponchioni, M., & Morbidelli, M. (2022). Integration and digitalization in the manufacturing of therapeutic proteins. *Chemical Engineering Science*, *248*, 117159–117159. https://doi.org/10.1016/j.ces.2021.117159

Nasr, M. M., Krumme, M., Matsuda, Y., Trout, B. L., Badman, C., Mascia, S., Cooney, C. L., Jensen, K. D., Florence, A., Johnston, C., Konstantinov, K., & Lee, S. L. (2017). Regulatory Perspectives on Continuous Pharmaceutical Manufacturing: Moving From Theory to Practice: September 26-27, 2016, International Symposium on the Continuous Manufacturing of Pharmaceuticals. *Journal of Pharmaceutical Sciences*, *106*(11), 3199–3206. https://doi.org/10.1016/j.xphs.2017.06.015

Nikolay, A., Bissinger, T., Granicher, G., Wu, Y., Genzel, Y., & Reichl, U. (2020). Perfusion Control for High Cell Density Cultivation and Viral Vaccine Production. *Methods Mol Biol*, *2095*, 141–168. https://doi.org/10.1007/978-1-0716-0191-4_9

Ozturk, S. S. (1996). Engineering challenges in high density cell culture systems. *Cytotechnology*, *22*(1), 3–16. https://doi.org/10.1007/BF00353919

Pappenreiter, M., Schwarz, H., Sissolak, B., Jungbauer, A., & Chotteau, V. (2024). Product sieving of mAb and its high molecular weight species in different modes of ATF and TFF perfusion cell cultures. *Journal of Chemical Technology & Biotechnology*, *n/a*(n/a). https://doi.org/10.1002/jctb.7386

Pereira, S., Kildegaard, H. F., & Andersen, M. R. (2018). Impact of CHO Metabolism on Cell Growth and Protein Production: An Overview of Toxic and Inhibiting Metabolites and Nutrients. *Biotechnol J*, *13*(3), e1700499. https://doi.org/10.1002/biot.201700499

Pincus, S., Sadowski, C., Reyes, E., & Madsen, J. (2018). A Suspension Vero Cell Line for Production of Viral Vaccines and Viral Therapeutics. *BioProcessing Journal*, *17*. https://doi.org/10.12665/J17OA.Pincus

Portela, R. M. C., Varsakelis, C., Richelle, A., Giannelos, N., Pence, J., Dessoy, S., & von Stosch, M. (2021). When Is an In Silico Representation a Digital Twin? A Biopharmaceutical Industry Approach to the Digital Twin Concept. *Adv Biochem Eng Biotechnol*, *176*, 35–55. https://doi.org/10.1007/10_2020_138

Puck, T. T. (1957). The genetics of somatic mammalian cells. *Adv Biol Med Phys*, *5*, 75–101. https://doi.org/10.1016/b978-1-4832-3111-2.50006-7

Qian, Y., Sowa, S. W., Aron, K. L., Xu, P., Langsdorf, E., Warrack, B., Aranibar, N., Tremml, G., Xu, J., McVey, D., Reily, M., Khetan, A., Borys, M. C., & Li, Z. J. (2020). New insights into genetic instability of an industrial CHO cell line by orthogonal omics. *Biochemical Engineering Journal*, *164*, 107799. https://doi.org/10.1016/j.bej.2020.107799

Qin, Y., Ma, R., Li, Y., Li, Y., Chen, G., & Zhou, W. (2022). Productivity and quality improvement for a symmetric bispecific antibody through the application of intensified perfusion cell culture. *Antib Ther*, *5*(2), 111–120. https://doi.org/10.1093/abt/tbac009

Radhakrishnan, D., Wells, E. A., & Robinson, A. S. (2018). Strategies to enhance productivity and modify product quality in therapeutic proteins. *Current Opinion in Chemical Engineering*, *22*, 81–88. https://doi.org/10.1016/j.coche.2018.09.005

Rathore, A. S., Thakur, G., & Kateja, N. (2023). Continuous integrated manufacturing for biopharmaceuticals: A new paradigm or an empty promise? *Biotechnology and Bioengineering*, *120*(2), 333–351. https://doi.org/10.1002/bit.28235

Romann, P., Kolar, J., Chappuis, L., Herwig, C., Villiger, T. K., & Bielser, J.-M. (2023). Maximizing yield of perfusion cell culture processes: Evaluation and scale-up of continuous bleed recycling. *Biochemical Engineering Journal*, *193*, 108873. https://doi.org/10.1016/j.bej.2023.108873

Rouiller, Y., Bielser, J.-M., Brühlmann, D., Jordan, M., Broly, H., & Stettler, M. (2016). Screening and assessment of performance and molecule quality attributes of industrial cell lines across different fed-batch systems. *Biotechnology Progress*, *32*(1), 160–170. https://doi.org/10.1002/btpr.2186

Samaras, J. J., Micheletti, M., & Ding, W. (2022). Transformation of Biopharmaceutical Manufacturing Through Single-Use Technologies: Current State, Remaining Challenges,

and Future Development. *Annual Review of Chemical and Biomolecular Engineering*, *13*(Volume 13, 2022), 73–97. https://doi.org/10.1146/annurev-chembioeng-092220-030223

Sandner, V., Pybus, L. P., McCreath, G., & Glassey, J. (2019). Scale-Down Model Development in ambr systems: An Industrial Perspective. *Biotechnology Journal*, *14*(4), 1700766. https://doi.org/10.1002/biot.201700766

Sartorius Stedim Biotech, Zoro, B., & McHugh, K. (2020). Scale-Down Models to Support Process Characterization. *BioProcessing Journal*, *19*. https://doi.org/10.12665/J19OA.Zoro

Schwarz, H., Gomis-Fons, J., Isaksson, M., Scheffel, J., Andersson, N., Andersson, A., Castan, A., Solbrand, A., Hober, S., Nilsson, B., & Chotteau, V. (2022). Integrated continuous biomanufacturing on pilot scale for acid-sensitive monoclonal antibodies. *Biotechnol Bioeng*, *119*(8), 2152–2166. https://doi.org/10.1002/bit.28120

Schwarz, H., Lee, K., Castan, A., & Chotteau, V. (2023). Optimization of medium with perfusion microbioreactors for high density CHO cell cultures at very low renewal rate aided by design of experiments. *Biotechnology and Bioengineering*, *n/a*(n/a). https://doi.org/10.1002/bit.28397

Schwarz, H., Zhang, Y., Zhan, C., Malm, M., Field, R., Turner, R., Sellick, C., Varley, P., Rockberg, J., & Chotteau, V. (2020). Small-scale bioreactor supports high density HEK293 cell perfusion culture for the production of recombinant Erythropoietin. *J Biotechnol*, *309*, 44–52. https://doi.org/10.1016/j.jbiotec.2019.12.017

Sewell, D. J., Turner, R., Field, R., Holmes, W., Pradhan, R., Spencer, C., Oliver, S. G., Slater, N. K., & Dikicioglu, D. (2019). Enhancing the functionality of a microscale bioreactor system as an industrial process development tool for mammalian perfusion culture. *Biotechnol Bioeng*, *116*(6), 1315–1325. https://doi.org/10.1002/bit.26946

Silk, N. J., Denby, S., Lewis, G., Kuiper, M., Hatton, D., Field, R., Baganz, F., & Lye, G. J. (2010). Fed-batch operation of an industrial cell culture process in shaken microwells. *Biotechnology Letters*, *32*(1), 73–78. https://doi.org/10.1007/s10529-009-0124-0

Singh, N., Vayer, P., Tanwar, S., Poyet, J.-L., Tsaioun, K., & Villoutreix, B. O. (2023). Drug discovery and development: Introduction to the general public and patient groups. *Frontiers in Drug Discovery*, *3*. https://doi.org/10.3389/fddsv.2023.1201419

Sinharoy, P., Aziz, A. H., Majewska, N. I., Ahuja, S., & Handlogten, M. W. (2020). Perfusion reduces bispecific antibody aggregation via mitigating mitochondrial dysfunction-induced glutathione oxidation and ER stress in CHO cells. *Sci Rep*, *10*(1), 16620. https://doi.org/10.1038/s41598-020-73573-4

Szkodny, A. C., & Lee, K. H. (2022). Biopharmaceutical Manufacturing: Historical Perspectives and Future Directions. *Annual Review of Chemical and Biomolecular Engineering*, *13*(Volume 13, 2022), 141–165. https://doi.org/10.1146/annurev-chembioeng-092220-125832

Tapia, F., Vázquez-Ramírez, D., Genzel, Y., & Reichl, U. (2016). *Bioreactors for high cell density and continuous multi-stage cultivations: Options for process intensification in cell culture-based viral vaccine production*. Springer Verlag.

ThermoFisher Scientific. (2024). *High-Intensity Perfusion CHO Medium*. https://www.thermofisher.com/order/catalog/product/A4230201

Tihanyi, B., & Nyitray, L. (2020). Recent advances in CHO cell line development for recombinant protein production. *Drug Discovery Today: Technologies*, *38*, 25–34. https://doi.org/10.1016/j.ddtec.2021.02.003

Tjio, J. H., & Puck, T. T. (1958). Genetics of somatic mammalian cells. II. Chromosomal constitution of cells in tissue culture. *J Exp Med*, *108*(2), 259–268. https://doi.org/10.1084/jem.108.2.259

Tregidgo, M., Dorn, M., Lucas, C., & Micheletti, M. (2023). Design and characterization of a novel perfusion reactor for biopharmaceuticals production. *Chemical Engineering Research and Design*, *194*, 344–357. https://doi.org/10.1016/j.cherd.2023.04.066

Tregidgo, M., Lucas, C., Dorn, M., & Micheletti, M. (2023). Development of mL-scale Pseudo-Perfusion Methodologies for High-Throughput Early Phase Development Studies. *Biochemical Engineering Journal*, *195*, 108906. https://doi.org/10.1016/j.bej.2023.108906

Trinh, K., Garcia-Briones, M., Chalmers, J. J., & Hink, F. (1994). Quantification of damage to suspended insect cells as a result of bubble rupture. *Biotechnol Bioeng*, *43*(1), 37–45. https://doi.org/10.1002/bit.260430106

Tripathi, N. K., & Shrivastava, A. (2019). Recent Developments in Bioprocessing of Recombinant Proteins: Expression Hosts and Process Development. *Front Bioeng Biotechnol*, *7*, 420. https://doi.org/10.3389/fbioe.2019.00420

Vazquez-Ramirez, D., Genzel, Y., Jordan, I., Sandig, V., & Reichl, U. (2018). High-cell-density cultivations to increase MVA virus production. *Vaccine*, *36*(22), 3124–3133. https://doi.org/10.1016/j.vaccine.2017.10.112

Vazquez-Ramirez, D., Jordan, I., Sandig, V., Genzel, Y., & Reichl, U. (2019). High titer MVA and influenza A virus production using a hybrid fed-batch/perfusion strategy with an ATF system. *Appl Microbiol Biotechnol*, *103*(7), 3025–3035. https://doi.org/10.1007/s00253-019-09694-2

Villiger-Oberbek, A., Yang, Y., Zhou, W., & Yang, J. (2015). Development and application of a high-throughput platform for perfusion-based cell culture processes. *J Biotechnol*, *212*, 21–29. https://doi.org/10.1016/j.jbiotec.2015.06.428

Voisard, D., Meuwly, F., Ruffieux, P.-A., Baer, G., & Kadouri, A. (2003). Potential of cell retention techniques for large-scale high-density perfusion culture of suspended mammalian cells. *Biotechnology and Bioengineering*, *82*(7), 751–765. https://doi.org/10.1002/bit.10629

Walls, P. L. L., McRae, O., Natarajan, V., Johnson, C., Antoniou, C., & Bird, J. C. (2017). Quantifying the potential for bursting bubbles to damage suspended cells. *Sci Rep*, *7*(1), 15102. https://doi.org/10.1038/s41598-017-14531-5

Walsh, G. (2018). Biopharmaceutical benchmarks 2018. *Nat Biotechnol*, *36*(12), 1136–1145. https://doi.org/10.1038/nbt.4305

Walsh, G., & Walsh, E. (2022). Biopharmaceutical benchmarks 2022. *Nature Biotechnology*, *40*(12), 1722–1760. https://doi.org/10.1038/s41587-022-01582-x

Walther, J., Lu, J., Hollenbach, M., Yu, M., Hwang, C., McLarty, J., & Brower, K. (2019). Perfusion Cell Culture Decreases Process and Product Heterogeneity in a Head-to-Head Comparison With Fed-Batch. *Biotechnology Journal*, *14*(2), 1700733. https://doi.org/10.1002/biot.201700733

Wang, B., Albanetti, T., Miro-Quesada, G., Flack, L., Li, L., Klover, J., Burson, K., Evans, K., Ivory, W., Bowen, M., Schoner, R., & Hawley-Nelson, P. (2018). High-throughput screening of antibody-expressing CHO clones using an automated shaken deep-well system. *Biotechnol Prog*, *34*(6), 1460–1471. https://doi.org/10.1002/btpr.2721

Wang, B., Albanetti, T., Miro-Quesada, G., Flack, L., Li, L., Klover, J., Burson, K., Evans, K., Ivory, W., Bowen, M., Schoner, R., & Hawley-Nelson, P. (2018). High-throughput screening of antibody-expressing CHO clones using an automated shaken deep-well system. *Biotechnology Progress*, *34*(6), 1460–1471. https://doi.org/10.1002/btpr.2721

Wang, S. B., Lee-Goldman, A., Ravikrishnan, J., Zheng, L., & Lin, H. (2018). Manipulation of the sodium-potassium ratio as a lever for controlling cell growth and improving cell specific productivity in perfusion CHO cell cultures. *Biotechnology and Bioengineering*, *115*(4), 921–931. https://doi.org/10.1002/bit.26527

Warikoo, V., Godawat, R., Brower, K., Jain, S., Cummings, D., Simons, E., Johnson, T., Walther, J., Yu, M., Wright, B., McLarty, J., Karey, K. P., Hwang, C., Zhou, W., Riske, F., & Konstantinov, K. (2012). Integrated continuous production of recombinant therapeutic proteins. *Biotechnol Bioeng*, *109*(12), 3018–3029. https://doi.org/10.1002/bit.24584

Wolf, M., Bielser, J. M., & Morbidelli, M. (2020). Design and Optimisation of Mammalian Cell Perfusion Cultures. *Perfusion Cell Culture Processes for Biopharmaceuticals: Process Development, Design, and Scale-Up*, 67–99. https://doi.org/Book_Doi 10.1017/9781108847209

Wolf, M. K. F. (2018). *Development and Optimization of Mammalian Cell Perfusion Cultures for Continuous Biomanufacturing*.

Wolf, M. K. F., Lorenz, V., Karst, D. J., Souquet, J., Broly, H., & Morbidelli, M. (2018). Development of a shake tube-based scale-down model for perfusion cultures. *Biotechnol Bioeng*, *115*(11), 2703–2713. https://doi.org/10.1002/bit.26804

Wolf, M. K. F., Muller, A., Souquet, J., Broly, H., & Morbidelli, M. (2019). Process design and development of a mammalian cell perfusion culture in shake-tube and benchtop bioreactors. *Biotechnol Bioeng*, *116*(8), 1973–1985. https://doi.org/10.1002/bit.26999

Wong, H. E., Chen, C., Le, H., & Goudar, C. T. (2021). From chemostats to high-density perfusion: The progression of continuous mammalian cell cultivation. *Journal of Chemical Technology & Biotechnology*, *97*(9), 2297–2304. https://doi.org/10.1002/jctb.6841

Wu, Y., Bissinger, T., Genzel, Y., Liu, X., Reichl, U., & Tan, W. S. (2021). High cell density perfusion process for high yield of influenza A virus production using MDCK suspension cells. *Appl Microbiol Biotechnol*, *105*(4), 1421–1434. https://doi.org/10.1007/s00253-020-11050-8

Wurm, F. (2013). CHO Quasispecies—Implications for Manufacturing Processes. *Processes*, *1*(3), 296–311. https://doi.org/10.3390/pr1030296

Wurm, F. M. (2004). Production of recombinant protein therapeutics in cultivated mammalian cells. *Nat Biotechnol*, *22*(11), 1393–1398. https://doi.org/10.1038/nbt1026

Xu, W.-J., Lin, Y., Mi, C.-L., Pang, J.-Y., & Wang, T.-Y. (2023). Progress in fed-batch culture for recombinant protein production in CHO cells. *Applied Microbiology and Biotechnology*, *107*(4), 1063–1075. https://doi.org/10.1007/s00253-022-12342-x

Zhang, L., Schwarz, H., Wang, M., Castan, A., Hjalmarsson, H., & Chotteau, V. (2021). Control of IgG glycosylation in CHO cell perfusion cultures by GReBA mathematical model supported by a novel targeted feed, TAFE. *Metab Eng*, *65*, 135–145. https://doi.org/10.1016/j.ymben.2020.11.004

Zhang, Y. P., Sun, J., & Ma, Y. (2017). Biomanufacturing: History and perspective. *J Ind Microbiol Biotechnol*, *44*(4–5), 773–784. https://doi.org/10.1007/s10295-016-1863-2

Zobel-Roos, S., Schmidt, A., Mestmäcker, F., Mouellef, M., Huter, M., Uhlenbrock, L., Kornecki, M., Lohmann, L., Ditz, R., & Strube, J. (2019). Accelerating Biologics Manufacturing by Modeling or: Is Approval under the QbD and PAT Approaches Demanded by Authorities Acceptable Without a Digital-Twin? *Processes*, *7*(2), 94–94. https://doi.org/10.3390/pr7020094

A. Appendix

A.1 Chapter 2: Cell culture and cell culture analytics

Additional information related to cell culture and cell culture analytics is compiled below. This includes settings for cell concentration and metabolite measurements, as well as the cell culture expansion scheme used to prepare cells for experimental work.

Table A.1: Cell expansion in shake flasks

Shake flask type [mL]	culture volume [mL]
125	12 - 25
250	25 - 50
500	50 - 100
1000	100 – 200
2000	200 - 400

Table A.2: Vi-CELL™ XR measurement settings

Settings	Values
Cell type	CHO (HY2)
Diameter [µm]	6.00 – 50.0
Minimum circularity	0.0
Cell brightness [%]	75
Cell sharpness	100
Viable cell spot brightness [%]	75
Viable cell spot area [%]	5.00
Decluster degree	Medium
Image size [pixels]	x
Aspirate cycles	1
Trypan blue mixing cycles	3

Table A.3: Validated range of CuBian VC culture biochemical analyzer for metabolite analysis

Solution	Validated area [mmol L^{-1}]
Glucose	0.6 – 22.20
Lactate	0.2 - 62
Ammonium	0.1 - 10

A.2 Chapter 6: Cell clone screening

An additional cell clone screening was performed to investigate the impact of glucose depletion on the cell clone performance. Therefore, HIP medium was supplemented with 20% CHO CD Efficient Feed™ B Liquid Nutrient Supplement (Gibco®, Thermo Fisher Scientific, Massachusetts, USA), in the following referred to as Feed B. According to the manufacturer, Feed B is a serum- and animal-free, chemically defined, glucose-rich liquid nutrient supplement. The experiment is referred to as SP-HIP20.

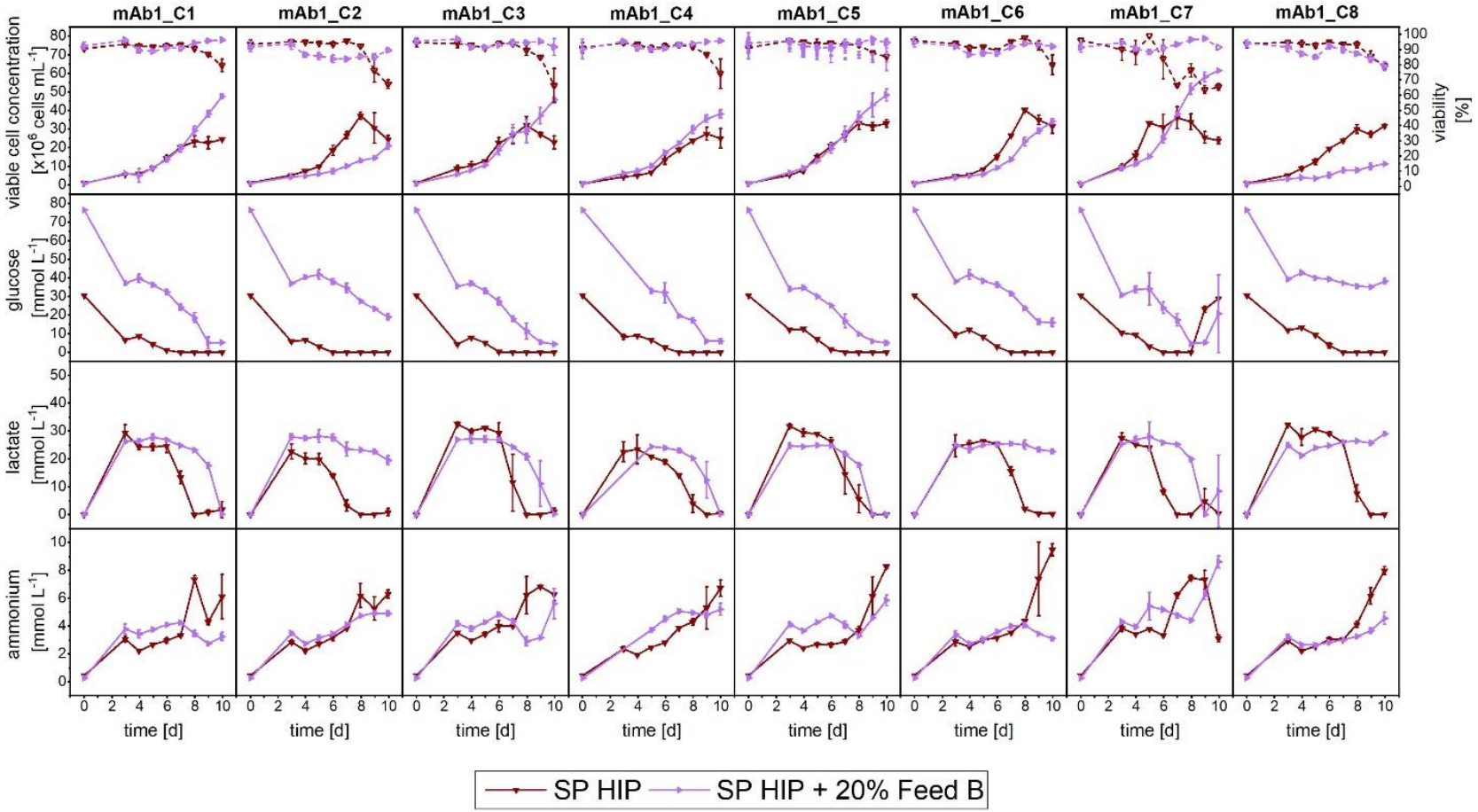

Figure A.1: Overview of growth and metabolites for mAb1 CHO cell clone screening in MWPs using semi-perfusion methodologies. Cells were inoculated at 1 x 10^6 cells mL^{-1} and cultivated in HIP medium (▼) and HIP medium supplemented with 20% Feed B (►). Row 1: viable cell concentration (closed, straight) and viability (open, dashed), Row 2: glucose concentration; Row 3: lactate concentration; Row 4: ammonium concentration. Columns display the eight individual clones. Mean of N = 3 wells. Error bars indicate standard deviation.

Table A.4: Ranking of eight mAb1 CHO cell clones based on average cell specific productivity values for semi-perfusion operation with total medium exchanges in HIP medium and HIP medium supplemented with 20% Feed B. Ranking from top to bottom considered best to worst performing.

Ranking position	SP-HIP	SP-HIP20
	1 RV d^{-1}	1 RV d^{-1}
#1	mAb1_C4	mAb1_C8
#2	mAb1_C6	mAb1_C5
#3	mAb1_C1	mAb1_C4
#4	mAb1_C5	mAb1_C6
#5	mAb1_C2	mAb1_C2
#6	mAb1_C3	mAb1_C3
#7	mAb1_C8	mAb1_C1
#8	mAb1_C7	mAb1_C7

Colour code to simplify the ranking visually.

Clones in SP-HIP20 conditions performed largely similar to clones of SP-HIP. The main differences identified were slightly higher growth for mAb1_C7, while mAb1_C8 showed significantly reduced growth. This reduced growth was evaluated as the main contributor to the top rank of mAb1_C8 in the SP-HIP20 condition due to the calculation of the q_P. While some differences were observable these were evaluated as minor compared to the differences between operation modes.

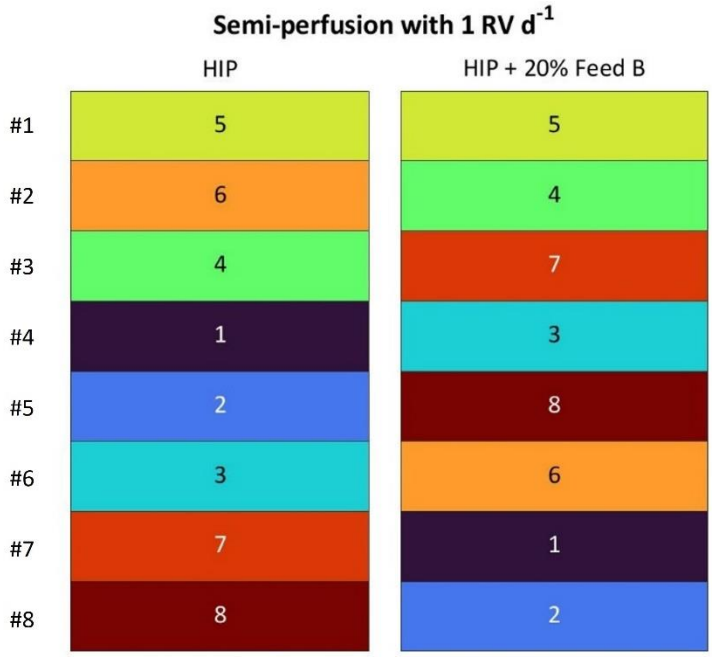

Figure A.2: Ranking of eight mAb1 CHO cell clones based on manufacturability index for semi-perfusion operation with total medium exchanges in HIP medium and HIP medium + 20% Feed B. Ranking from top to bottom considered best to worst performing.